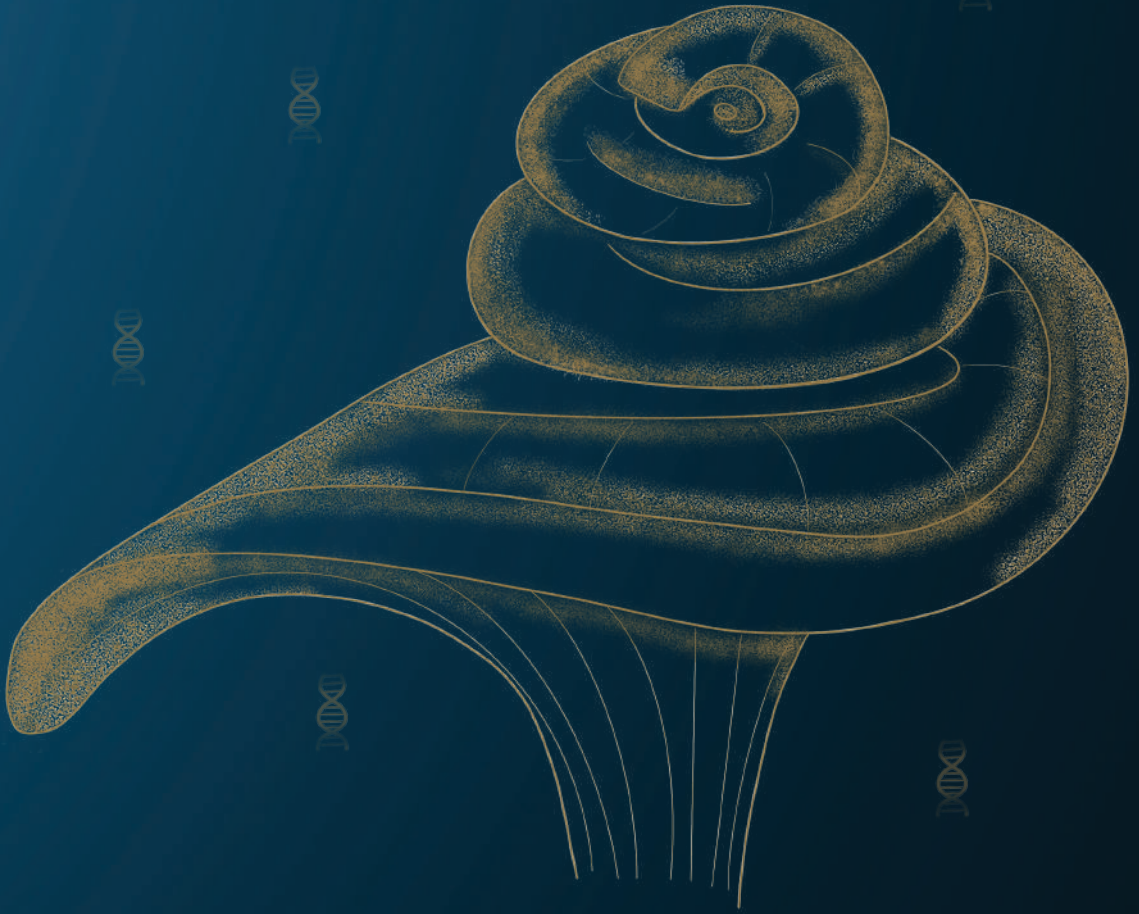


Hereditary Hearing loss



About the known
and unknown

Jeroen Smits

Hereditary hearing loss

About the known and unknown

Jeroen Jules Smits

The work presented in this thesis was carried out within the Donders Institute for Brain Cognition and Behaviour and within Hearing and Genes, at the department of Otorhinolaryngology and the department of Human Genetics of the Radboud university medical center in Nijmegen, the Netherlands.

The printing of this thesis was generously supported by Advanced Bionics, Phonak, PENTAX Medical, Viatrix, Daleco Pharma, MED-EL, Beter Horen, MediTop, ALK, Schoonenberg HoorSupport, Oticon Medical, ChipSoft, Cochlear, KNO-winkel.nl/DOS Medical, and the Radboud university medical center.

ISBN: 978-94-6416-891-4

Provided by thesis specialist Ridderprint, ridderprint.nl

Printing: Ridderprint
Cover design: Yasmin Katlich, persoonlijkproefschrift.nl
Lay-out: Jules Verkade, persoonlijkproefschrift.nl

© 2021, Jeroen Smits

All rights reserved. No part of this publication may be reproduced, stored in a retrieval system, or transmitted in any form or by any means, electronic, mechanical, photocopying, recording or otherwise, without prior permission.

Hereditary hearing loss

About the known and unknown

Proefschrift

ter verkrijging van de graad van doctor
aan de Radboud Universiteit Nijmegen
op gezag van de rector magnificus prof. dr. J.H.J.M. van Krieken,
volgens besluit van het college voor promoties
in het openbaar te verdedigen op
vrijdag 25 maart 2022
om 12:30 uur precies

door

Jeroen Jules Smits
geboren op 28 januari 1992
te Zwolle

Promotor

Prof. dr. J.M.J. Kremer

Copromotoren

Dr. R.J.E. Pennings

Dr. ir. C.P. Lanting

Manuscriptcommissie

Prof. dr. M.A.A.P. Willemsen (voorzitter)

Prof. dr. R.J. Stokroos (Universitair Medisch Centrum Utrecht)

Prof. dr. V. Van Rompaey (Universiteit Antwerpen, België)

Carpe Diem

Voor Omi

TABLE OF CONTENTS

Chapter 1	General introduction	9
Chapter 2	A novel COCH mutation affects the vWFA2 domain and leads to a relatively mild DFNA9 phenotype <i>Otology & Neurotology 2021</i>	29
	Genotype-phenotype correlations of pathogenic COCH variants in DFNA9: a HuGE systematic review and audiometric meta-analysis <i>Submitted</i>	53
Chapter 3	Exploring the missing heritability in subjects with hearing loss, enlarged vestibular aqueducts, and a single or no pathogenic SLC26A4 variant <i>Human Genetics, 2021</i>	91
Chapter 4	De novo and inherited loss-of-function variants of ATP2B2 are associated with rapidly progressive hearing impairment <i>Human Genetics, 2019</i>	135
	A RIPOR2 in-frame deletion is a frequent and highly penetrant cause of adult-onset hearing loss <i>Journal of Medical Genetics, 2020</i>	165
	Cochlear supporting cells require GAS2 for cytoskeletal architecture and hearing <i>Developmental Cell, 2021</i>	209
Chapter 5	General discussion	257
Summaries	English summary	278
	Nederlandse samenvatting	281
Appendices	Abbreviations	288
	Research data management	291
	PhD portfolio	292
	List of publications	294
	Curriculum vitae	296
	Dankwoord	297



INTRODUCTION

Sound and communication

Since the dawn of mankind, sound plays a vital role in human life. This role varies from the auditory perception of the environment and its threats to a tool for communication. A sound is a vibration distributed as a longitudinal acoustic wave through a medium, be it solid, gas or liquid. The properties of the medium; namely the density, pressure, viscosity, and movement of the medium itself, influence the behavior of the wave. Four generic properties characterize sounds; frequency, amplitude, propagation velocity (through the medium), and direction. Sounds can be a simple phenomenon, for example, a single pure tone, but may also merge together in complex patterns such as speech.

The auditory system enables humans to gather, process, and interpret sounds. This system can distinguish sounds that differ only 0.2% in frequency, ranging from 20 to 20,000 Hz.^{1,2} Moreover, it can handle a wide range of sound loudness, ranging from a sound that elicits an eardrum vibration of one picometer, up to the tremendous vibrations produced by aircraft engines, a trillion-fold in acoustic power.^{3,4} Furthermore, the ability of the auditory system to locate sounds (in the horizontal plane or azimuth) is an important feature that can mainly be attributed to binaural hearing. For localization in the vertical plane (or elevation) monaural cues can be used.⁵ Due to these extensive properties of the auditory system, hearing is one of the most important senses to perceive our surrounding world.

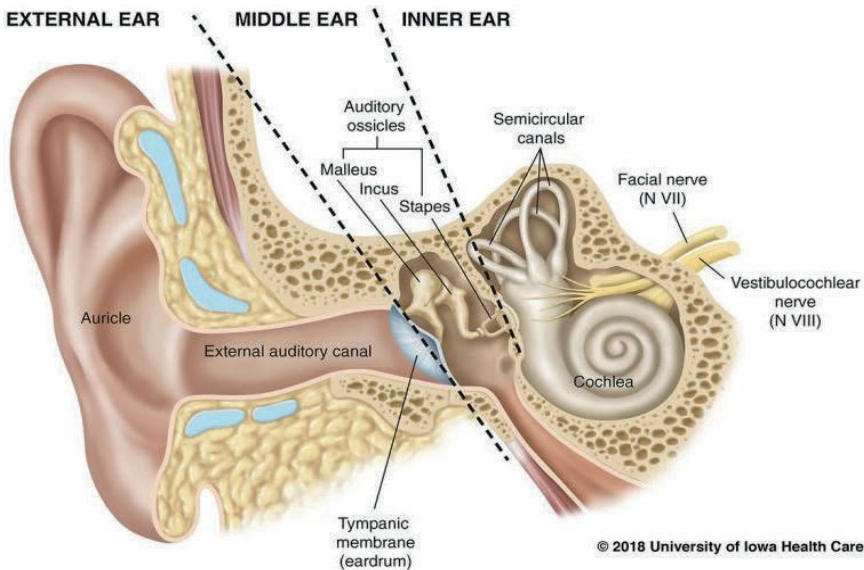


Figure 1 Anatomical parts of the external, middle and inner ear. Figure used with permission from the University of Iowa.

Anatomy and physiology of the hearing organ

The human ear consists of three main parts, the external, middle, and inner ear (**Figure 1**). All three parts play an important role in the process of hearing and can be affected by disease.

The external ear consists of the auricle, or pinna, and the external auditory canal. Sounds are first received by the auricle. The distinct shape of the auricle is essential for localization in the vertical plane and amplification of sounds – especially those with frequencies important for speech detection – and the conduction of sound waves to the external auditory canal.⁶ At the end of the external auditory canal, the sound waves set the tympanic membrane in motion (**Figure 2a**).

Medial to the tympanic membrane is the middle ear cavity, which is closely connected to the mastoid air cells. This cavity harbors the ossicular chain, that consists of the malleus, incus, and stapes, named after the objects they resemble in shape. The malleus is connected to the tympanic membrane. The stapes footplate, on the other hand, is attached to the oval window of the cochlea. The ossicular chain transmits sound vibrations from the tympanic membrane to the cochlea and simultaneously can amplify them. The bilateral human cochleae are mirror-shaped, coiled, fluid-filled bony tubes, situated in the petrous pyramids of the temporal bones (**Figure 2a**).⁸ The energy of the movement of the stapes footplate at the oval window is transduced to the fluid-filled scala vestibuli. At the cochlear helicotrema, the scala vestibuli connects to the scala tympani, which terminates at the round window. The scala media is situated between these scalae and is separated from the scala vestibuli by Reissner's membrane and from the scala tympani by the basilar membrane (**Figure 2b**). The scala tympani and scala vestibuli contain perilymph, a sodium-rich fluid that connects with the cerebrospinal fluid through the cochlear aqueduct. The scala media contains a potassium-rich fluid, the endolymph, which resembles the cytoplasm. The electrolyte difference between endolymph and perilymph results in an electric potential of +80 microvolts, the endocochlear potential.⁷

The organ of Corti

The organ of Corti is located on the basilar membrane and runs 33-34 mm (SD ± 2.28 mm) along the spiral-shaped cochlea (**Figure 2c**).⁹ The organ of Corti contains hair cells, supporting cells, and border cells.¹⁰ One of the most distinguishable components of the organ of Corti are the hair cells with stereocilia that are anchored at their apical surface. The interlinked stereocilia protrude into the endolymph and are organized in rows of decreasing height. Hair cells come in two types; inner and outer hair cells (**Figure 2c**). The single row of ~3,500 inner hair cells (IHC) are the sensory receptors that translate sound vibrations into electrochemical signals.^{11,12} These are transmitted at the ribbon synapses to the afferent nerve fibers and via the spiral ganglion cell bodies further to the cochlear

nucleus of the brainstem.⁷ In contrast, the three rows of ~12,000 outer hair cells (OHC) are mainly stimulated by efferent nerve fibers and do not provide any sensory information. The OHCs have a role as cochlear amplifiers in the biomechanical properties of the organ of Corti, thereby enhancing sensitivity, frequency tuning, and determine the dynamic range of sound perception.^{11,12}

Adjacent to the hair cells, several different types of supporting cells play an important role in the cochlea. From lateral to medial, these are Hensen's cells, Deiters' cells, pillar cells, inner phalangeal cells, and border cells. These cells each have distinct morphologies and overlapping roles in development, structural integrity, ion homeostasis, and mechanosensitivity of the organ of Corti.^{13,14} The organ of Corti is covered by a gelatinous extracellular matrix, the tectorial membrane. The tectorial membrane is in direct physical contact with the stereocilia of the OHCs and is thought to be involved in the longitudinal propagation of energy in the intact cochlea.¹⁵ Recent research has shown that the membrane also controls hearing sensitivity by acting as a cochlear calcium storage.¹⁶

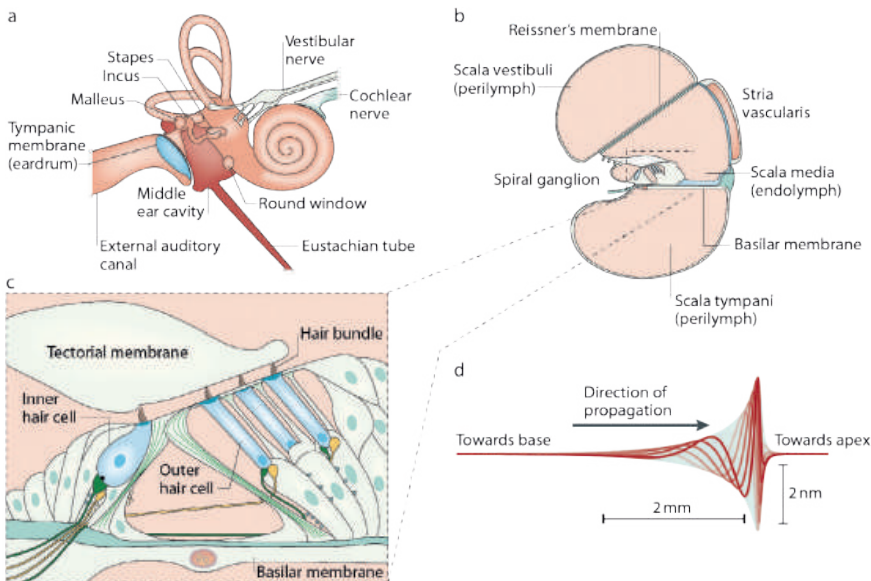


Figure 2 (a) The inner ear consists of the cochlea and the vestibular organ. (b) A cross-section of the cochlea, which shows the three liquid-filled compartments, the scalae vestibuli, media and tympani. These are separated by two elastic partitions; Reissner's membrane and the basilar membrane. (c) The organ of Corti is located on the basilar membrane, within the scala media. The single row of inner hair cells and three rows of outer hair cells are surrounded by supporting cells. (d) When the cochlea is excited by sound, the motion of the stapes produces alternate increases and decreases in the pressure of the liquid at the base of the scala vestibuli. The pressure difference across the basilar membrane elicits a series of travelling waves that progress along the membrane. Figure from Hudspeth (2014)⁷ with permission from the Nature Publishing group.

Sound waves set the fluids in the scalae in a wave-like motion, causing the basilar membrane to move (**Figure 2d**). As a result, the stereocilia deflect in a synchronized manner against the tectorial membrane and mechano-electrical transduction channels at the stereociliary tips open. This leads to an influx of K^+ from the endolymph into the stereocilia. The depolarization caused by this process results in a receptor potential that opens voltage-gated Ca^{2+} channels at the basal side of the plasma membrane of the hair cells. The influx of Ca^{2+} induces the release of the neurotransmitter glutamate at the synapse with the nerve fibers of the spiral ganglion.^{7,17,18} This triggers action potentials and these signals are transmitted through the cochlear nerve to the cochlear nucleus in the brainstem and ultimately the auditory cortex.

The mammalian cochlea is tonotopically organized, which means that higher frequencies, up to 20,000 Hz in humans, are perceived at the cochlear base and lower frequencies, as low as 20 Hz in humans, at the apex (**Figure 3**).

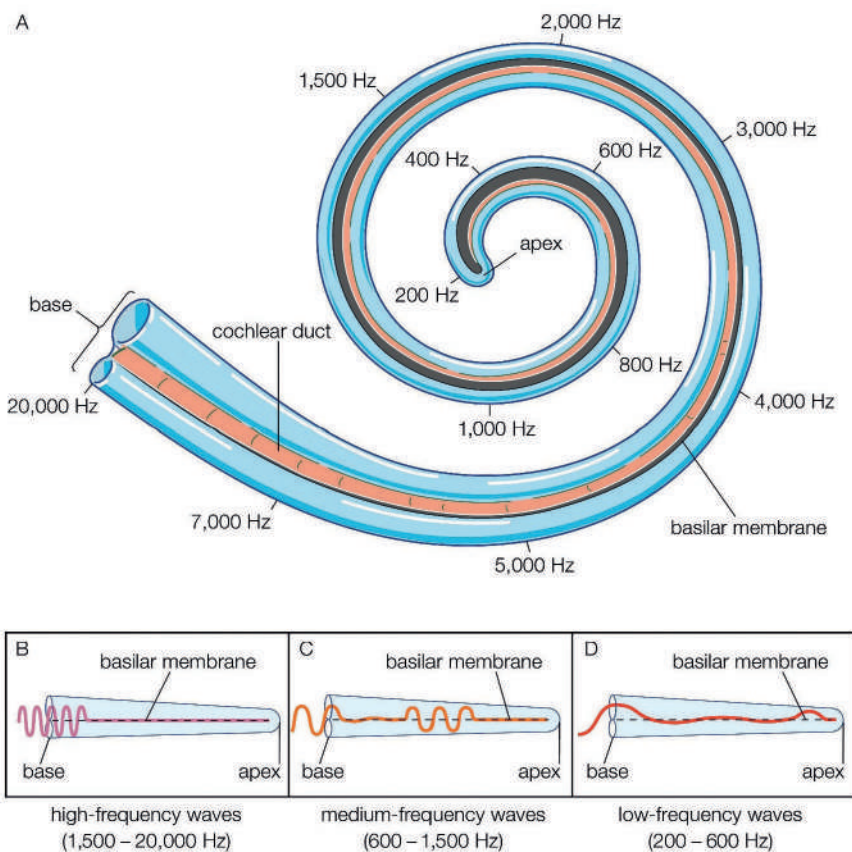


Figure 3 Tonotopic map of the human cochlea. A specific frequency of vibration causes a maximum resonance of the basilar membrane at a specific distance from the base. Figure used with permission from Alamy Limited.

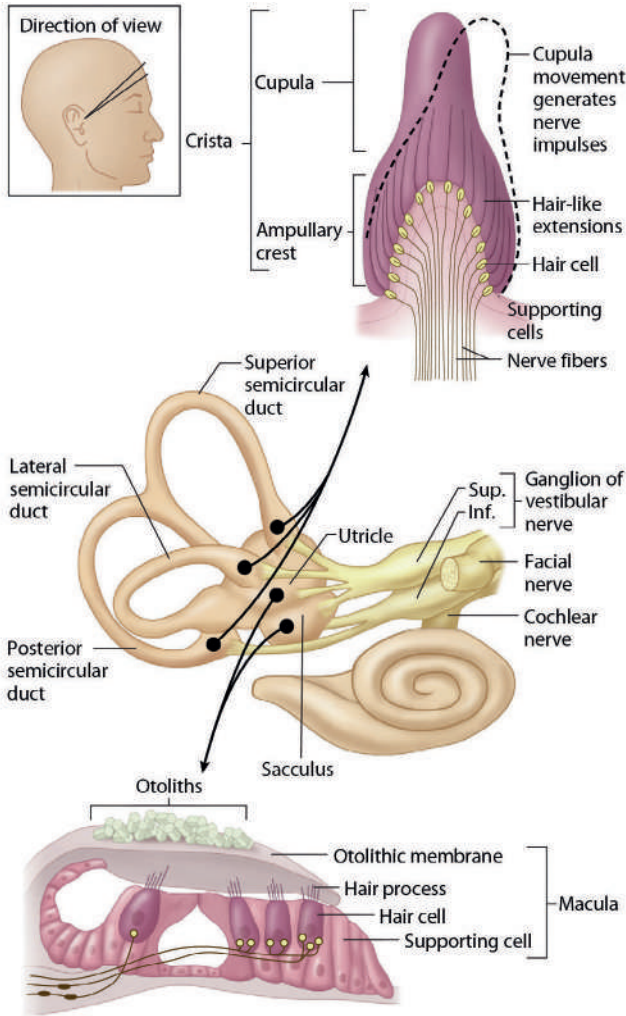


Figure 4 Anatomy and physiology of the vestibular organ. The ampulla of a semicircular canal with the cupula is shown in the uppermost part of the figure. The cupula is displaced by the flow of endolymph when the head moves. As a result, the hair bundles are also displaced. Their movement is exaggerated in the diagram. In the bottom of the figure is a schematic representation of the utricle and saccule, the otolith organs. Hair cells in the epithelium of the utricle and saccule have apical hair bundles that project into the otolithic membrane, a gelatinous mass that is covered by millions of calcium carbonate particles (otoliths). Both the utricle and the saccule provide information about acceleration, in the horizontal and vertical plane respectively. Figure used with permission of Elsevier.

The cochlear tonotopy is achieved by structural and morphological characteristics that display conspicuous base-to-apex gradients in the cochlea. The tectorial and basilar membrane, for example, become wider and thicker towards the apex of the cochlea. In addition, the cell bodies of outer hair cells, Deiters' cells, and pillar cells are longer, and hair

cell stereocilia are fewer and taller.¹³ The stiffness of the basilar membrane decreases, and Deiters' and pillar cell bodies show decreasing amounts of cytoskeletal elements from base to apex.¹³ Together, these characteristics determine the frequency sensitivity at a given point along the cochlear duct.

Anatomy and physiology of the vestibular organ

The vestibular organ, which forms the inner ear together with the cochlea, consists of three semicircular canals and two otolith organs; the utricle and saccule, together called the vestibulum (**Figure 4**).¹⁹

The three semicircular canals, named the superior-, posterior- and horizontal canals are oriented orthogonally to each other and filled with endolymph. The 3D-positioning of the canals is essential for the detection of rotational movements in the axial-, coronal- and sagittal plane and more than one canal is stimulated at once on each side if a head movement is out of those planes (**Figure 4**). The cristae ampullaris are dilatations at the end of each semicircular canal and contain the sensory epithelium, consisting of hair cells and supporting cells. The cupula and stereocilia are embedded in gelatinous masses. Displacement of the endolymph in the direction of the kinocilia will lead to depolarization of the hair cells (**Figure 4**).

The utricle and saccule detect head movements in the horizontal and vertical plane, respectively. They also each have a sensory epithelium, called the macula utriculi and macula sacculi, with hair cells and supporting cells. As in the semicircular canals, stereocilia and a kinocilium protrude from the hair cells into gelatinous masses; the otolithic membranes. These are covered with small calcium carbonate particles called otoconia, or otoliths (**Figure 4**).^{19,20}

Upon rotational acceleration or deceleration of the head, movement of the endolymph in the semicircular canals bends the cupula, which in turn causes stereocilia and kinocilia to deflect. The same occurs in the utricle and saccule upon movement of the otoliths due to linear acceleration (and gravitational forces). The deflection of the stereocilia causes hair cells to depolarize or hyperpolarize. This leads to the transduction of action potentials via the vestibular nerve that are transduced to the the vestibular nuclei and the brainstem.

As the vestibular system is designed to detect movements of the head, these signals to the brainstem are combined with information from proprioceptors and the visual system in order to maintain the balance of the body.^{20,21} The input of these multimodal signals are important for e.g. the vestibulo- and cervico-ocular, responsible for gaze stabilization during head movements.

Hereditary hearing loss

Hearing loss is estimated to be one of the most prevalent disabilities worldwide.^{22,23} Congenital hearing loss and hearing loss with an onset in childhood can often be explained by defects in a single gene, namely up to 49% and 37% of the cases, respectively.²⁴ The percentage of cases that are 'solved' decreases with increasing age of onset of the condition.²⁴ This may, for example, be explained by an increasing contribution of environmental factors affecting hearing (e.g., ototoxicity or noise exposure), or by defects in genes that are not associated (yet) with hearing loss and thus unrecognized. Currently, over 120 genes are known to be associated with monogenic forms of non-syndromic sensorineural hearing loss.²⁵ Proteins encoded by these genes fulfill different roles in the cochlea and vestibulum, for example, structural support, signal transduction, and ion homeostasis. Defects of these genes can cause different audiovestibular phenotypes, depending on the role of the encoded proteins in the process of hearing.

It is estimated that 70-80% of early-onset non-syndromic hereditary hearing loss is inherited in an autosomal recessive and 20-30% in an autosomal dominant manner. X-linked, Y-linked, and mitochondrial inheritance patterns are rare (~1-2% per inheritance pattern).²⁶ A nomenclature system, the so-called DFN-system, was designed for chromosomal loci associated with non-syndromic hearing loss. Now, this is also employed to indicate the condition. DFN stands for DeafNess, and according to the inheritance pattern, a letter and, in order of discovery, a number is added; DFNA[#] (autosomal dominant), DFNB[#] (autosomal recessive), DFNX[#] (X-linked), DFN Y[#] (Y-linked) and DFNM[#] (modifier). Several genes have been associated with both dominantly and recessively inherited types of hearing loss, e.g., *GJB2*; DFNB1 and DFNA3A, or *PTPRQ*; DFNA73 and DFNB84.²⁷⁻³⁰

In addition to these non-syndromic forms of hereditary hearing loss, over 400 syndromic forms of hearing loss are described.³¹ These syndromes are characterized by hearing loss and various other medical complaints, among which eye (Stickler syndrome, Usher syndrome), kidney (branchio-oto-renal syndrome), thyroid gland (Pendred syndrome), and fertility disorders in females (Perrault syndrome).³¹ Several genes are associated with both syndromic and non-syndromic types of hearing loss, e.g., *MYO7A* associated with DFNA11, DFNB2, and Usher syndrome type Ib.³²⁻³⁴

Diagnostic care in hereditary HL

In The Netherlands, medical genetic care for hereditary hearing loss is provided by specialized tertiary care otogenetic teams in academic centers. All are united in a nationwide collaboration called DOOFNL (Diagnostiek en Onderzoek Oto genotype Fenotype Nederland). Within DOOFNL, diagnostic standards and protocols have been aligned.

During a consultation, medical and family history are taken, and a pedigree is drawn. Acquired forms of hearing loss, e.g., perinatal CMV-viral infections, noise exposure, ototoxic medication, and ear infections, are considered and when applicable, further examined.³⁵⁻³⁷ Physical examination consists of a general ENT examination, an evaluation of dysmorphic features, and basic balance tests (e.g., Romberg's and head-impulse-test). Audiometric testing consists of pure tone and speech audiometry³⁸ and if required, measurements of otoacoustic emissions, tympanometry, auditory steady-state response or brainstem evoked response audiometry. In the case of vestibular complaints, a thorough vestibular examination can be performed. This examination typically includes electronystagmography, such as rotary chair testing and caloric irrigation testing, but also video head impulse testing, and measurements of cervical and ocular vestibular evoked myogenic potentials. Additional consultations of other medical specialists and examinations, e.g., CT and MRI scans, CMV PCR, and blood tests, can be performed upon indication.

In the recent past, only single gene tests were employed in medical genetic testing for hearing loss. The choice of the gene was based on the (auditory) phenotype of the patient. However, due to the high degree of genetic heterogeneity and phenotypic overlap in hereditary hearing loss, the diagnostic yield was only 16%.²⁴ The introduction of next-generation sequencing techniques, e.g., whole exome sequencing (WES), had a significant impact on the diagnostic yield for different diseases.³⁹ For hearing loss in the Netherlands, the diagnostic yield increased to ~33.5% with WES²⁴, although it should be noted that the gene panel consisted of 120 genes at that time, associated with both syndromic and non-syndromic types of hereditary hearing loss. Currently, over 230 genes are included in the panel. Other studies achieved similar percentages when applying WES for diagnostic testing of (suspected) hereditary hearing loss.^{40,41}

At this moment, genetic testing in routine diagnostic care is carried out according to a protocol (**Figure 5**) that is developed based on the insights derived from the evaluation of a cohort of 200 patients from the Netherlands.²⁴ First, a primarily phenotype-driven single gene test is considered in all patients based on specific (additional) characteristics, e.g., an enlarged vestibular aqueduct or retinitis pigmentosa. Other indications can be a combination of (non-syndromic) features and a high disease allele frequency (sometimes even regional).^{42,43} If these tests are negative or not indicated, WES with data analysis targeting a panel of genes associated with syndromic and non-syndromic forms of hearing loss can be performed by the Genome Diagnostics centers. Identified variants are classified according to the guidelines of the American College of Medical Genetics and Genomics.⁴⁴ Pathogenic variants that have been reported to be causative for hearing loss are listed in databases such as the Human Gene Mutation Database⁴⁵, the Deafness Variation Database⁴⁶

and Clinvar⁴⁷. As also genes associated with syndromic hearing loss are included in the deafness gene panel, patients or their parents need to be counseled thoroughly prior to testing on the possibility that the hearing loss is part of a syndrome.

The outcome of genetic testing is, upon indication, discussed in a multidisciplinary meeting. If testing revealed a molecular genetic diagnosis, the patient is subsequently counseled on different aspects of the disease. Counseling focuses on potential progression of hearing loss, genetic risks of family members, and potential rehabilitation options, now and in the future. If there are additional symptoms in the context of a syndromic form of hearing loss, this is discussed in detail. If necessary, patients are referred to other medical specialists. Patients with a negative test result can be advised to contact the counselors again in 3-5 years, to reevaluate the data and also address genes that were added to the panel in the meantime.⁴⁸

Psychosocial and emotional consequences of genetic testing for hearing loss

Attention to social-emotional consequences is given during the whole diagnostic trajectory, as testing for hereditary hearing impairment can have several positive and negative implications, even before the start of the diagnostic trajectory. Based on interviews, Lesperance et al. (2018) noted several reasons for declining a genetic evaluation of hearing loss beforehand⁴⁹, such as financial burden, complexity, bad timing, or (parental) distress for a bad diagnosis. During the first consultation, people are counseled on the benefits and potential consequences of genetic testing. Advantages are that a genetic diagnosis can provide clarity about the cause of hearing loss, additional comorbidities and improve hearing rehabilitation.⁵⁰

Depending on the personal situation of an individual, genetic testing for hereditary hearing loss can evoke neutral or even positive feelings.^{50,51} On the other hand, the lack of a genetic diagnosis can cause confusion and uncertainty in some patients or parents about the cause of the hearing loss, especially in families with several affected individuals. If needed, additional aftercare is provided, varying from referring to patient associations to psychological and social support by social workers, especially in cases with severe syndromic forms.

Research on known and unknown deafness genes

Often, the cause of hearing loss in a patient remains elusive in medical genetic testing. A defect in a known deafness gene can be missed, a variant in a gene not associated yet with hearing loss can be identified, or there is no underlying genetic cause for hearing loss.

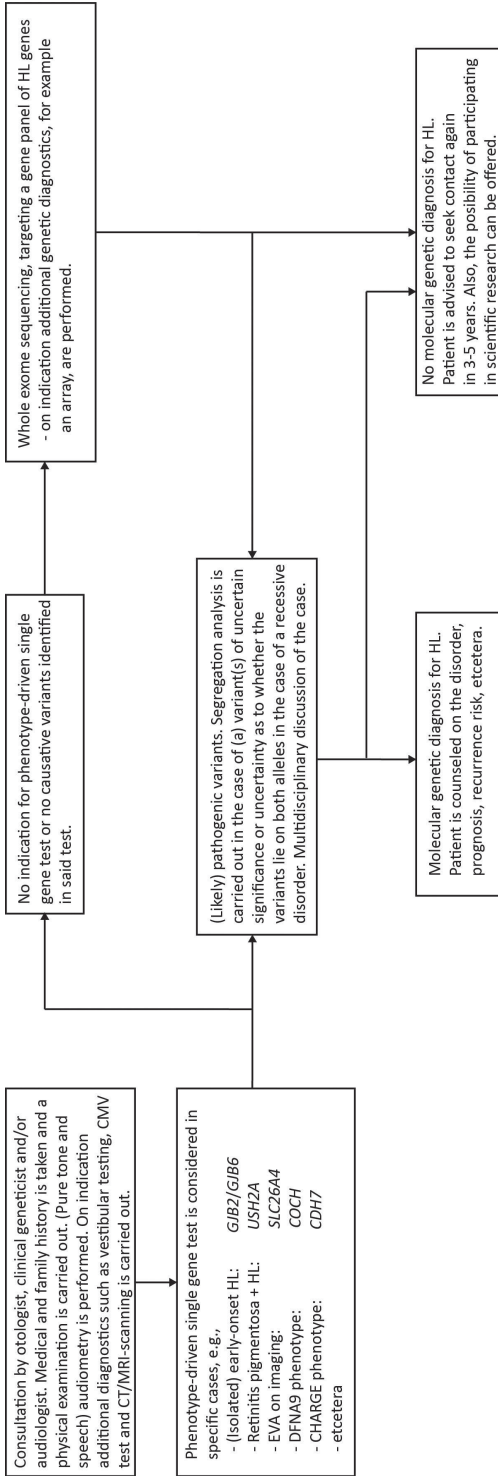


Figure 5 Schematic illustration of the diagnostic protocol used in patients suspected of hereditary hearing loss in the Hearing&Genes outpatient clinic of the Radboudumc, Nijmegen.

Known deafness genes

A pathogenic variant in genes currently associated with hearing loss can be missed due to technical or knowledge gaps, as pointed out by Kremer (2019).⁵² Known defects in intronic (e.g., *DFNA5*) or regulatory sequences (e.g., the noncoding exon 1 of *GJB2*) may, for example, escape detection in whole exome sequencing (WES).⁵² Whole genome sequencing (WGS) allows the detection of variants in non-coding regions of the genome. (Likely) pathogenic variants may also be identified but not considered pathogenic due to a high allele frequency (>1%) or no predicted effect on the protein (silent mutations). The latter type of variants can affect splicing.⁵³ Other reasons for research on known deafness genes are confirming or rejecting the association of a gene with hereditary hearing loss, e.g., if only 1-2 (small) families have been reported, as is the case for *GRAP* or *SPNS2*.^{54,55} Furthermore, additional genotype-phenotype correlation studies can confirm a specific phenotype or expand the phenotype, which is essential for counseling of patients. This is also true for genes where the phenotype displays a lot of variation, for example, *COCH*, *RIPOR2*, or *MYO6*.⁵⁶⁻⁵⁸ It is also important to make a clear distinction between an expected syndromic or non-syndromic phenotype, as is the case for non-syndromic hearing loss type *DFNB12* and Usher syndrome type 1d, which are both caused by pathogenic variants in *CDH23*.⁵⁹ In Usher syndrome type 1, congenital deafness is accompanied by congenital vestibular areflexia and progressive vision loss due retinitis pigmentosa, mostly starting in childhood. In these cases, an unclear diagnosis can cause uncertainty about the future, especially in young children, where no eye phenotype is yet present. Other examples of research into genes already associated with hearing loss are the identification of potential erroneous genotype-disease associations⁶⁰⁻⁶³, natural history studies^{64,65}, and the elucidation of the molecular mechanism as handles for the development of therapeutic strategies.^{66,67}

Unknown deafness genes

A further explanation for the lack of a genetic diagnosis in routine diagnostics is that the hearing loss is caused by a defect in a gene that has not been associated with hearing loss yet. In the past years, many additional genes have been associated with hearing loss in humans²⁵ and large-scale studies of mouse mutants suggest that defects in up to 1,000 genes are likely to cause hearing loss.^{54,68} Several different approaches and techniques can be applied to identify those genes, as summarized by Gillissen et al.⁶⁹ Currently, techniques such as homozygosity mapping and linkage analysis with genome-wide single nucleotide polymorphism arrays are largely being replaced by whole exome sequencing (WES) and whole genome sequencing (WGS).^{69,70} A WES dataset of one subject can consist of over 100,000 variants. Filtering and prioritization strategies are applied to assess the data efficiently. Large-scale population databases (e.g., gnomAD⁷¹) can separate common from rare variants. Lists of

candidate genes for hearing loss in humans, based on studies in animals, such as mice^{54,68,72-75} or expression of certain genes in the cochlea⁷⁶⁻⁷⁸, can highlight interesting genes to be assessed first. *In silico* tools can be used to obtain an indication of a potential deleterious effect of a variant. Examples of tools are PolyPhen-2, SIFT, CADD, and MutationTaster.⁷⁹⁻⁸² If WES data of large cohorts of affected subjects are available, computational algorithms can be applied to identify candidate variants based on their enrichment in cohorts of affected subjects.⁸³ The power of analyzing large datasets underlines the importance of national and international collaborations, such as the Dutch DOOFNL collaboration.^{84,85}

Scope of this thesis

Knowledge in the field of genetics and hereditary hearing loss specifically, has increased significantly in recent decades. Despite this, many questions remain unanswered. The research performed for and described in this thesis aims to enhance the knowledge on hereditary hearing loss and answer some questions.

Chapter 1 serves as an introduction to the research presented in the following chapters. In **chapters 2 and 3** the knowledge on genes already associated with hereditary hearing loss is enhanced. In chapter 2.1, we identified a *COCH* variant, affecting the vWFA2 domain, in a family with an autosomal dominant inheritance pattern of hearing loss. The affected subjects show a relatively mild audiovestibular phenotype, compared to subjects with DFNA9 caused by other variants in *COCH*. The variable phenotype of DFNA9 is further evaluated in a systematic review and audiological meta-analysis in chapter 2.2, which aims to serve as a variant-specific guide for counselling and care in DFNA9. Chapter 3 describes the study of *SLC26A4*, which is associated with recessively inherited hearing loss and enlargement of the vestibular aqueduct. In many cases, only mono-allelic variants in coding and splice site regions of *SLC26A4* are identified. In this chapter, an *SLC26A4*-linked haplotype that is enriched in mono-allelic cases is scrutinized to identify the pathogenic variant of this allele. In **chapter 4**, two novel human deafness genes are presented. A third gene, that was up to now only linked to recessively inherited hearing loss, is also associated with dominantly inherited hearing loss. First, we describe five families in which *de novo* and inherited pathogenic variants in *ATP2B2* cause autosomal dominantly inherited rapidly progressive hearing loss. Secondly, in an international collaboration, we revealed that *GAS2* is essential for hearing in mice and man. Thirdly, an in-frame deletion in *RIPOR2* was identified to also underlie autosomal dominant hearing loss in 12 families of Dutch origin. Based on the allele frequency of the *RIPOR2* variant, it is estimated that in the Netherlands, 13,000 people are at risk to develop hearing loss. And finally, In **chapter 5** the content of this thesis is discussed, and a future outlook is presented towards the identification of novel causes of hereditary hearing loss and the development of (genetic) therapies.

REFERENCES

1. Micheyl, C., Xiao, L. & Oxenham, A.J. Characterizing the dependence of pure-tone frequency difference limens on frequency, duration, and level. *Hear Res* 292, 1-13 (2012).
2. Wier, C.C., Jesteadt, W. & Green, D.M. Frequency discrimination as a function of frequency and sensation level. *J Acoust Soc Am* 61, 178-84 (1977).
3. Dalhoff, E., Turcanu, D., Zenner, H.P. & Gummer, A.W. Distortion product otoacoustic emissions measured as vibration on the eardrum of human subjects. *Proc Natl Acad Sci U S A* 104, 1546-51 (2007).
4. Yost, W. & Killion, M. in *Encyclopedia of Acoustics Vol 3*. (ed. Crocker, M.) 1545-1554 (Wiley-Interscience, 1997).
5. Van Wanrooij, M.M. & Van Opstal, A.J. Sound localization under perturbed binaural hearing. *J Neurophysiol* 97, 715-26 (2007).
6. Middlebrooks, J.C. & Green, D.M. Sound localization by human listeners. *Annu Rev Psychol* 42, 135-59 (1991).
7. Hudspeth, A.J. Integrating the active process of hair cells with cochlear function. *Nat Rev Neurosci* 15, 600-14 (2014).
8. Rask-Andersen, H. *et al.* Human cochlea: anatomical characteristics and their relevance for cochlear implantation. *Anat Rec (Hoboken)* 295, 1791-811 (2012).
9. Miller, J.D. Sex differences in the length of the organ of Corti in humans. *J Acoust Soc Am* 121, EL151-5 (2007).
10. Ten Donkelaar HJ, E.K., Fritzsche B, Kachlik D, Carlson M, Isaacson B, Topsakal V, Broman J, Tubbs RS, Baud R. An Updated Terminology for the Internal Ear with Combined Anatomical and Clinical Terms. *Journal of Phonetics & Audiology* (2020).
11. Lim, D.J. Cochlear anatomy related to cochlear micromechanics. A review. *J Acoust Soc Am* 67, 1686-95 (1980).
12. Jahan, I., Pan, N., Kersigo, J. & Fritzsche, B. Beyond generalized hair cells: molecular cues for hair cell types. *Hear Res* 297, 30-41 (2013).
13. Raphael, Y. & Altschuler, R.A. Structure and innervation of the cochlea. *Brain Res Bull* 60, 397-422 (2003).
14. Wan, G., Corfas, G. & Stone, J.S. Inner ear supporting cells: rethinking the silent majority. *Semin Cell Dev Biol* 24, 448-59 (2013).
15. Meaud, J. & Grosh, K. The effect of tectorial membrane and basilar membrane longitudinal coupling in cochlear mechanics. *J Acoust Soc Am* 127, 1411-21 (2010).
16. Strimbu, C.E., Prasad, S., Hakizimana, P. & Fridberger, A. Control of hearing sensitivity by tectorial membrane calcium. *Proc Natl Acad Sci U S A* 116, 5756-5764 (2019).
17. Vollrath, M.A., Kwan, K.Y. & Corey, D.P. The micromachinery of mechanotransduction in hair cells. *Annu Rev Neurosci* 30, 339-65 (2007).
18. LeMasurier, M. & Gillespie, P.G. Hair-cell mechanotransduction and cochlear amplification. *Neuron* 48, 403-15 (2005).
19. Kingma, H. & van de Berg, R. Anatomy, physiology, and physics of the peripheral vestibular system. *Handb Clin Neurol* 137, 1-16 (2016).
20. Khan, S. & Chang, R. Anatomy of the vestibular system: a review. *NeuroRehabilitation* 32, 437-43 (2013).

21. Purves D, A.G., Fitzpatrick, et al. The vestibular system. in *Neuroscience* 343–362. (Sinauer Associates, Inc, Sunderland, MA, 2008).
22. World Health Organisation. The global burden of disease: 2004 update. (Geneva: World Health Organization, 2008).
23. World Health Organisation. Deafness and hearing loss: Key facts 2019 update. (Geneva: World Health Organization, 2019).
24. Zazo Seco, C. *et al.* The diagnostic yield of whole-exome sequencing targeting a gene panel for hearing impairment in The Netherlands. *Eur J Hum Genet* 25, 308-314 (2017).
25. Van Camp, G. & Smith, R. Hereditary Hearing Loss Homepage.
26. Mahboubi, H., Dwabe, S., Fradkin, M., Kimonis, V. & Djalilian, H.R. Genetics of hearing loss: where are we standing now? *Eur Arch Otorhinolaryngol* 269, 1733-45 (2012).
27. Kelsell, D.P. *et al.* Connexin 26 mutations in hereditary non-syndromic sensorineural deafness. *Nature* 387, 80-3 (1997).
28. Morle, L. *et al.* A novel C202F mutation in the connexin26 gene (GJB2) associated with autosomal dominant isolated hearing loss. *J Med Genet* 37, 368-70 (2000).
29. Schraders, M. *et al.* Mutations in PTPRQ are a cause of autosomal-recessive nonsyndromic hearing impairment DFN84 and associated with vestibular dysfunction. *Am J Hum Genet* 86, 604-10 (2010).
30. Eisenberger, T. *et al.* A C-terminal nonsense mutation links PTPRQ with autosomal-dominant hearing loss, DFNA73. *Genet Med* 20, 614-621 (2018).
31. Toriello H.V., Reardon W., Gorlin R.J. & editors. *Hereditary Hearing Loss and its Syndromes.*, (Oxford University Press, New York, 2004).
32. Liu, X.Z. *et al.* Mutations in the myosin VIIA gene cause non-syndromic recessive deafness. *Nat Genet* 16, 188-90 (1997).
33. Liu, X.Z. *et al.* Autosomal dominant non-syndromic deafness caused by a mutation in the myosin VIIA gene. *Nat Genet* 17, 268-9 (1997).
34. Weil, D. *et al.* Defective myosin VIIA gene responsible for Usher syndrome type 1B. *Nature* 374, 60-1 (1995).
35. Zahnert, T. The differential diagnosis of hearing loss. *Dtsch Arztebl Int* 108, 433-43; quiz 444 (2011).
36. Riga, M., Korres, G., Chouridis, P., Naxakis, S. & Danielides, V. Congenital cytomegalovirus infection inducing non-congenital sensorineural hearing loss during childhood; a systematic review. *Int J Pediatr Otorhinolaryngol* 115, 156-164 (2018).
37. Korver, A.M. *et al.* DECIBEL study: Congenital cytomegalovirus infection in young children with permanent bilateral hearing impairment in the Netherlands. *J Clin Virol* 46 Suppl 4, S27-31 (2009).
38. Bosman, A.J. & Smoorenburg, G.F. Intelligibility of Dutch CVC syllables and sentences for listeners with normal hearing and with three types of hearing impairment. *Audiology* 34, 260-84 (1995).
39. Neveling, K. *et al.* A post-hoc comparison of the utility of sanger sequencing and exome sequencing for the diagnosis of heterogeneous diseases. *Hum Mutat* 34, 1721-6 (2013).
40. Sheppard, S. *et al.* Utility and limitations of exome sequencing as a genetic diagnostic tool for children with hearing loss. *Genet Med* 20, 1663-1676 (2018).
41. Likar, T. *et al.* Diagnostic outcomes of exome sequencing in patients with syndromic or non-syndromic hearing loss. *PLoS One* 13, e0188578 (2018).

42. Fransen, E. *et al.* A common ancestor for COCH related cochleovestibular (DFNA9) patients in Belgium and The Netherlands bearing the P51S mutation. *J Med Genet* 38, 61-5 (2001).
43. Chan, D.K. & Chang, K.W. GJB2-associated hearing loss: systematic review of worldwide prevalence, genotype, and auditory phenotype. *Laryngoscope* 124, E34-53 (2014).
44. Wallis, Y. *et al.* Practice Guidelines for the Evaluation of Pathogenicity and the Reporting of Sequence Variants in Clinical Molecular Genetics. . *ACGS/VGKL* (2013).
45. Cooper, D.N. & Krawczak, M. Human Gene Mutation Database. *Hum Genet* 98, 629 (1996).
46. Azaiez, H. *et al.* Genomic Landscape and Mutational Signatures of Deafness-Associated Genes. *Am J Hum Genet* 103, 484-497 (2018).
47. Landrum, M.J. *et al.* ClinVar: improving access to variant interpretations and supporting evidence. *Nucleic Acids Res* 46, D1062-D1067 (2018).
48. Sun, Y. *et al.* Increased diagnostic yield by reanalysis of data from a hearing loss gene panel. *BMC Med Genomics* 12, 76 (2019).
49. Lesperance, M.M., Winkler, E., Melendez, T.L. & Yashar, B.M. "My Plate is Full": Reasons for Declining a Genetic Evaluation of Hearing Loss. *J Genet Couns* 27, 597-607 (2018).
50. Withrow, K.A. *et al.* Impact of genetic advances and testing for hearing loss: results from a national consumer survey. *Am J Med Genet A* 149A, 1159-68 (2009).
51. Oonk, A.M.M. *et al.* Psychological impact of a genetic diagnosis on hearing impairment-An exploratory study. *Clin Otolaryngol* 43, 47-54 (2018).
52. Kremer, H. Hereditary hearing loss; about the known and the unknown. *Hear Res* 376, 58-68 (2019).
53. Collin, R.W. *et al.* Mid-frequency DFNA8/12 hearing loss caused by a synonymous TECTA mutation that affects an exonic splice enhancer. *Eur J Hum Genet* 16, 1430-6 (2008).
54. Ingham, N.J. *et al.* Mouse screen reveals multiple new genes underlying mouse and human hearing loss. *PLoS Biol* 17, e3000194 (2019).
55. Li, C. *et al.* Dysfunction of GRAP, encoding the GRB2-related adaptor protein, is linked to sensorineural hearing loss. *Proc Natl Acad Sci U S A* 116, 1347-1352 (2019).
56. Bae, S.H. *et al.* Identification of pathogenic mechanisms of COCH mutations, abolished cochlin secretion, and intracellular aggregate formation: genotype-phenotype correlations in DFNA9 deafness and vestibular disorder. *Hum Mutat* 35, 1506-13 (2014).
57. de Bruijn, S.E. *et al.* A RIPOR2 in-frame deletion is a frequent and highly penetrant cause of adult-onset hearing loss. *J Med Genet* (2020).
58. Oonk, A.M.M. *et al.* Progressive hereditary hearing impairment caused by a MYO6 mutation resembles presbycusis. *Hearing Research* 299, 88-98 (2013).
59. Bork, J.M. *et al.* Usher syndrome 1D and nonsyndromic autosomal recessive deafness DFNB12 are caused by allelic mutations of the novel cadherin-like gene CDH23. *Am J Hum Genet* 68, 26-37 (2001).
60. Donaudy, F. *et al.* Multiple mutations of MYO1A, a cochlear-expressed gene, in sensorineural hearing loss. *Am J Hum Genet* 72, 1571-7 (2003).
61. Eisenberger, T. *et al.* Targeted and genomewide NGS data disqualify mutations in MYO1A, the "DFNA48 gene", as a cause of deafness. *Hum Mutat* 35, 565-70 (2014).

62. Delmaghani, S. *et al.* Defect in the gene encoding the EAR/EPTP domain-containing protein TSPEAR causes DFNB98 profound deafness. *Hum Mol Genet* 21, 3835-44 (2012).
63. Bowles, B. *et al.* TSPEAR variants are primarily associated with ectodermal dysplasia and tooth agenesis but not hearing loss: A novel cohort study. *Am J Med Genet A* (2021).
64. Mey, K., Bille, M., Rye Rasmussen, S.H., Tranebjaerg, L. & Caye-Thomasen, P. The Natural History of Hearing Loss in Pendred Syndrome and Non-Syndromic Enlarged Vestibular Aqueduct. *Otol Neurotol* 40, e178-e185 (2019).
65. Mullen, A.L., Moghissi, A.A., Stanley, R.E., Lloyd, S.R. & Fort, P.A. Biological half-life of tritium in chickens and eggs. *Health Phys* 30, 310-1 (1976).
66. Minoda, R., Miwa, T., Ise, M. & Takeda, H. Potential treatments for genetic hearing loss in humans: current conundrums. *Gene Ther* 22, 603-9 (2015).
67. Zhang, W. *et al.* Cochlear Gene Therapy for Sensorineural Hearing Loss: Current Status and Major Remaining Hurdles for Translational Success. *Front Mol Neurosci* 11, 221 (2018).
68. Bowl, M.R. *et al.* A large scale hearing loss screen reveals an extensive unexplored genetic landscape for auditory dysfunction. *Nat Commun* 8, 886 (2017).
69. Gilissen, C., Hoischen, A., Brunner, H.G. & Veltman, J.A. Disease gene identification strategies for exome sequencing. *Eur J Hum Genet* 20, 490-7 (2012).
70. Vona, B., Nanda, I., Hofrichter, M.A., Shehata-Dieler, W. & Haaf, T. Non-syndromic hearing loss gene identification: A brief history and glimpse into the future. *Mol Cell Probes* 29, 260-70 (2015).
71. Karczewski, K.J. *et al.* The mutational constraint spectrum quantified from variation in 141,456 humans. *Nature* 581, 434-443 (2020).
72. Brown, S.D., Hardisty-Hughes, R.E. & Mburu, P. Quiet as a mouse: dissecting the molecular and genetic basis of hearing. *Nat Rev Genet* 9, 277-90 (2008).
73. Friedman, L.M., Dror, A.A. & Avraham, K.B. Mouse models to study inner ear development and hereditary hearing loss. *Int J Dev Biol* 51, 609-31 (2007).
74. de Angelis, M.H. *et al.* Analysis of mammalian gene function through broad-based phenotypic screens across a consortium of mouse clinics. *Nat Genet* 47, 969-978 (2015).
75. Bowl, M.R. & Brown, S.D.M. Genetic landscape of auditory dysfunction. *Hum Mol Genet* 27, R130-R135 (2018).
76. Shen, J., Scheffer, D.I., Kwan, K.Y. & Corey, D.P. SHIELD: an integrative gene expression database for inner ear research. *Database (Oxford)* 2015, bav071 (2015).
77. Schrauwen, I. *et al.* A comprehensive catalogue of the coding and non-coding transcripts of the human inner ear. *Hear Res* 333, 266-274 (2016).
78. Mullen, R.J., Eicher, E.M. & Sidman, R.L. Purkinje cell degeneration, a new neurological mutation in the mouse. *Proc Natl Acad Sci U S A* 73, 208-12 (1976).
79. Vaser, R., Adusumalli, S., Leng, S.N., Sikic, M. & Ng, P.C. SIFT missense predictions for genomes. *Nat Protoc* 11, 1-9 (2016).
80. Kircher, M. *et al.* A general framework for estimating the relative pathogenicity of human genetic variants. *Nat Genet* 46, 310-5 (2014).

81. Schwarz, J.M., Cooper, D.N., Schuelke, M. & Seelow, D. MutationTaster2: mutation prediction for the deep-sequencing age. *Nature Methods* 11, 361-362 (2014).
82. Adzhubei, I.A. *et al.* A method and server for predicting damaging missense mutations. *Nat Methods* 7, 248-9 (2010).
83. Lelieveld, S.H. *et al.* Meta-analysis of 2,104 trios provides support for 10 new genes for intellectual disability. *Nat Neurosci* 19, 1194-6 (2016).
84. Kaplanis, J. *et al.* Evidence for 28 genetic disorders discovered by combining healthcare and research data. *Nature* 586, 757-762 (2020).
85. Wells, H.R.R. *et al.* GWAS Identifies 44 Independent Associated Genomic Loci for Self-Reported Adult Hearing Difficulty in UK Biobank. *Am J Hum Genet* 105, 788-802 (2019).



Chapter 2.1

A novel *COCH* mutation affects the vWFA2 domain and leads to a relatively mild DFNA9 phenotype

Jeroen J. Smits, Eline van Beelen, Nicole J.D. Weegerink, Jaap Oostrik, Patrick L.M. Huygen, Andy J. Beynon, Cornelis P. Lanting, Henricus P.M. Kunst, Margit Schraders, Hannie Kremer, Erik de Vrieze and Ronald J.E. Pennings

Otology & Neurotology 42, e399-e407 (2021)

ABSTRACT

DFNA9 is a globally occurring hereditary disorder, characterized by progressive hearing loss and with or without (major) vestibular deterioration. *COCH* consist of several domains, among which a LCCL domain and two vWFA domains. The majority of *COCH* mutations has been reported in parts encoding for the LCCL domain. In this study genetic analysis was performed using linkage analysis, variable number of tandem repeats analysis and molecular inversion probes. Audiovestibular data was collected and analyzed. Regression analysis was performed on pure tone audiometry and speech recognition scores and correlated with the age and/or level of hearing loss. We identified a novel mutation in *COCH*, c.1312C>T p.(Arg438Cys) which co-segregates with hearing loss and a variable degree of vestibular (dys)function in this family. The reported mean age of onset of hearing loss is 33 years (range: 18-49 years). Hearing loss primarily affects higher frequencies and its progression is relatively mild (0.8 dB/year). Speech perception is remarkably well preserved in affected family members when compared to other DFNA9 families with different *COCH* mutations. These findings expand the genotypic and phenotypic spectrum of DFNA9. The c.1312C>T mutation, which affects the vWFA2 domain, causes a relatively mild audiovestibular phenotype when compared to other *COCH* mutations.

INTRODUCTION

Nonsyndromic hereditary hearing loss (HL) is a highly heterogeneous disorder for which causative mutations in more than 115 genes have been reported.¹ The *COCH* gene is one of these and mutations within *COCH* lead to DFNA9, which is one of the more prevalent types of dominantly inherited causes of nonsyndromic HL. In general, DFNA9 is characterized by progressive high-frequency HL with an onset in adulthood and often includes deterioration of vestibular function. Furthermore, mutations in *COCH* are also associated with autosomal recessive HL.²

Families with DFNA9 have been identified on four continents across different populations, e.g. American, Dutch, Belgian, Italian, Australian, South Korean and Japanese, see Bae et al. and references therein.³ To date, about 25 different mutations have been reported to be causative for DFNA9 (Human Gene Mutation Database, 2019.2, Deafness Variation Database⁴ ClinVar⁵). Most of the reported mutations have only been described in one or two families. The c.151C>T (p.(Pro51Ser)) substitution is an exception to this and is a frequently identified founder mutation in the Netherlands and Belgium.⁶

COCH is mapped to chromosome 14 and encodes the cochlin protein.⁷ Cochlin consists of among others a Limulus factor C, Cochlin, and Lgl1 (LCCL) domain and two von Willebrand factor A-like (vWFA) domains, the latter two bind to extracellular matrix components. Cochlin is expressed in human fetal cochlear and vestibular tissues, but also in other tissues (e.g. eye and muscle).^{8,9} The exact function has yet to be elucidated, but Jung et al. reported a role for cleaved cochlin in the local immune system.¹⁰ The majority of mutations have been reported in parts of the gene that encode the LCCL domain.³ This paper describes the clinical characteristics of DFNA9 in a large Dutch family caused by a novel *COCH* mutation that affects the vWFA2 domain of cochlin.

MATERIALS AND METHODS

Subjects and audiovestibular examination

This study was approved by the medical ethics committee of the Radboudumc and was carried out according to the Declaration of Helsinki. Written informed consent was obtained from all participants or their legal representatives. The GENDEAF guidelines were applied for the description of the auditory phenotype.¹¹ Medical history was obtained from all subjects by anamnesis and a clinical questionnaire. Pure tone audiometry was performed in a sound-attenuated booth and thresholds were determined from 250 Hz to 8 kHz, according to current standards. Previously performed pure tone and speech audiometry were retrieved. The International Organisation for Standardization standard 7029:2017 was used to derive

the 95th percentile thresholds for individual hearing thresholds for each frequency at a certain age. A subject was considered affected when the best hearing ear showed thresholds worse than the 95th percentile for at least three frequencies.

To evaluate cross-sectional progression of HL in this family, age-related typical audiograms (ARTA) were calculated according to a previously described method.¹² In addition, individual progression of HL was determined by the average progression of the pure tone average for the frequencies 0.5 to 4 kHz ($PTA_{0.5-4\text{kHz}}$) between the first and last audiogram of each subject. This was only determined when the follow-up after onset of HL was at least 10 years. Speech audiometry was performed with a phonetically balanced standard Dutch consonant-vowel-consonant word list.¹³ Average speech scores of both ears were used for all calculations. Speech recognition scores were evaluated by cross-sectional non-linear regression analysis of maximum phoneme recognition scores plotted against $PTA_{1-4\text{kHz}}$ values and age, by fitting a 2-parameter sigmoidal function $Y = 100\% \left(1 - \frac{1}{1 + e^{-a(X-b)}} \right)$ where Y is the phoneme score (%), X is either age (years) or $PTA_{1-4\text{kHz}}$ kHz (dB), a is the slope factor, and b the point on the X-axis where Y equals 50%. Data from earlier published speech recognition scores¹⁴⁻¹⁸ on other *COCH* mutations and presbycusis were recalculated with above mentioned function. Calculations and statistical analyses were performed by using Prism 5, Python 3.8.1 with NumPy 1.18.1 and a Jupyter notebook with Seaborn 0.10.0. Vestibular function was evaluated by oculomotor tests, caloric measurements and rotational chair testing, as described previously.¹⁹

Genetic analyses

Blood samples were taken from 23 family members (**Figure 1**, marked with an *) and DNA was extracted according to standard procedures. DNA samples were genotyped using the Illumina HumanCoreExome v1.1 array according to the manufacturer's protocol. In order to select independent single nucleotide polymorphisms (SNPs), pruning ($r^2 = 0.025$) was performed with PLINK.²⁰ Superlink online SNP 1.1 software was employed for approximate linkage analysis using the Morgan *lm_linkage* program.^{21,22} Default settings with a window size of 20 SNPs were used. To confirm the results of the suggestive linkage and to determine the segregation of the disease-associated haplotype, genotype analysis of variable number tandem repeat (VNTR) markers (D14S1021, D14S54 and D14S257) was performed.²³ All coding exons and exon-intron boundaries of *COCH* (NM_004086.2) were amplified with PCR for the index patient and subsequently analyzed by Sanger sequencing as described.²⁴ Primer sequences and PCR conditions are available upon request. Segregation analysis of the c.1312C>T variant in *COCH* exon 11 was carried out by PCR amplification followed by *FokI* restriction digestion according to the manufacturer's protocol. Restriction fragments

were analyzed on a 2% agarose gel. The c.1312C>T variant removes a *FokI* restriction site in exon 11 of *COCH*.

To exclude other known genes associated with hereditary HL, targeted DNA sequencing was performed for subjects IV.1, III.9 and III.13 using Molecular Inversion Probes (MIPs). MIPs were designed to cover exons and exon-intron boundaries of a panel of 89 HL genes (Table S1).^{25,26} For each targeted region, an average coverage of 163 (IV.1), 999 (III.9), and 685 (III.13) reads was obtained. A coverage of >20 reads/target was reached for 93.3% of the MIPs. Variants were evaluated according to the criteria described in the supplemental methods section.

RESULTS

Family study

The index case of family W08-2035 (subject III.4) presented himself at our out-patients clinic with progressive sensorineural HL. The pedigree (Figure 1) of his family suggested a dominant inheritance pattern of HL. In routine molecular genetic diagnostics *KCNQ4* (exons 1, 5, 6 and 7; DFNA2), *GJB2*, (exons 1 and 2; DFNA3A), *GJB6* (exon 3; DFNA3B), *GSDME* (3' 110 base pairs of intron 7 were sequenced and the presence of c.991-15_991-13delTTC mutation evaluated; DFNA5), *COCH* (exons 4 and 5; DFNA9) and *POU4F3* (exons 1 and 2; DFNA15) were sequenced, which did not unveil a causative variant. Therefore, it was decided to conduct a family study to identify a potential underlying genetic defect. A total of 42 family members consented to participate in this study. After questionnaires, consultations and audiometric testing, a total of 15 living family members were identified as (possibly) affected. Deceased family members were considered affected based on hetero-anamnesis.

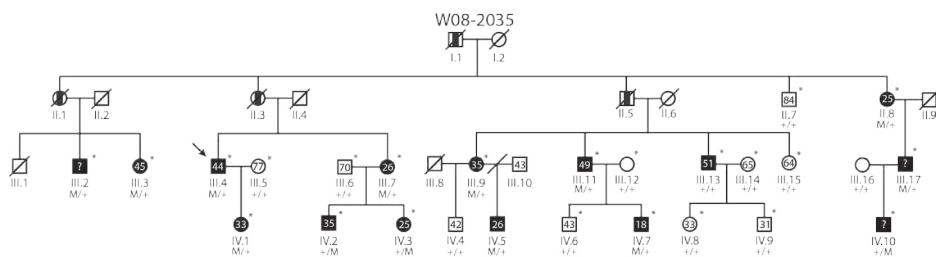


Figure 1. Pedigree of family W08-2035 and segregation of *COCH* mutation c.1312C>T The onset age of hearing impairment is shown for all affected subjects and the age at the most recent audiometric evaluation in unaffected subjects. Subjects who did not report an age of onset are indicated with a question mark. Subjects included in the linkage analysis are marked with an asterisk. M, c.1312C>T *COCH* mutation; +, wildtype; square, male; circle, female; open symbol, clinically unaffected; filled symbol, clinically affected; slash through symbol, deceased; slash through line, divorced; arrow, index case; vertical black bar through symbol, subject determined to be affected by heteroanamnesis. Note III.13, who is considered a phenocopy.

Identification of the c.1312C>T variant in COCH

Genome-wide approximate linkage analysis, assuming an autosomal dominant mode of inheritance with a disease-allele frequency of 0.001 and a penetrance of 95%, did not reveal any regions with suggestive linkage. The linkage analysis was repeated allowing for phenocopies by adjusting the penetrance for the normal genotype to 0.001. This resulted in a single region with suggestive linkage (LOD-score >2) (**Figure S1**). The region is located on chromosome 14q12, and reached a maximum LOD-score of 2.01. Suggestive linkage was confirmed by VNTR marker genotyping (**Figure S2**) which also revealed that affected individual III.13 does not carry the disease allele. The identified linkage region harbours the *COCH* gene, which is associated with DFNA9. Sequence analysis of *COCH* (NM_004086.2) in individual III.4 revealed a heterozygous variant in exon 11: c.1312C>T, p.(Arg438Cys). This missense variant is expected to affect the vWFA2 domain of cochlin. The variant is reported only once in heterozygous state in the Genome Aggregation Database (gnomAD, version 2.1.1, 125,748 exomes) and absent from HGMD, Deafness Variation Database and ClinVar. Importantly, the variant is predicted to be deleterious according to PolyPhen-2 (score of 0.974, range 0–1) and MutationTaster (probability of 1, range 0–1).^{27,28} The SIFT-score is 0.05, scores of <0.05 are considered deleterious.²⁹ See also **Table S2**.

The c.1312C>T variant was found to co-segregate with HL in 14 of the 15 hearing impaired family members; the variant was not identified in individual III.13, as was expected from VNTR marker analysis. This subject reported an estimated onset age of HL of about 51 years, which is relatively late compared to the family members with the c.1312C>T *COCH* variant (mean 33, range 18-49 years). *COCH* sequencing was repeated for confirmation. Furthermore, results of VNTR marker analysis of his children did not provide any indication for an erroneous swap of blood samples. To address the option that a variant in other genes associated with HL underlies the condition in the family, MIPs analysis was performed in subjects IV.1, III.9, and III.13. They did not share any other (likely) pathogenic variants in known deafness genes. Therefore, it was concluded that the c.1312C>T variant is the cause of HL in this family and that subject III.13 is a phenocopy.

Table 1. Individual results of otoscopic examination, audiometry, imaging and progression of HL

Subject	Age of onset (y)	Otoscopic examination	Clinical remarks	Imaging	Subject age (y)		Audiometry				Progression of HI		General remarks/	
					PTA	SRT	Maximum SRS (%)	Progression rate (dB/y)	YOF (y)					
				MRI	R	L	R	L	R	L	R	L		
II.8	25	NT	NR		72	70	NT	NT	NT	NT	NA	NA	0	
III.2	U	N	T		33	38	37	35	84	93	NA	NA	0	
III.3	45	N	T		30	30	37	38	100	100	NA	NA	0	
III.4	44	N			52	55	52	57	95	90	1.6	1.6	24	
III.7	26	N	V		63	70	65	69	100	95	1.5	1.5	11	
III.9	35	N	T, V, O		48	45	48	52	95	95	0.3	0.3	14	
III.11	49	N			40	38	44	41	92	100	1.3	1.3	11	
III.17	NR	NT	NR		23	25	NT	NT	NT	NT	NA	NA	0	BERA: normal
IV.1	33	NT	T		7	7	NR	15	100	95	NA	NA	5	
IV.2	35	N			18	17	14	19	100	100	NA	NA	0	
IV.3	25	unilateral myringosclerosis, retraction pocket	O, V	N	37	40	37	38	100	95	NA	NA	8	
IV.5	26	N	T		12	18	NT	NT	NT	NT	NA	NA	8	
IV.7	18	N	T, V, O		10	10	9	11	100	100	0.8	0.8	15	
IV.12	NR	NT	NR		7	7	NT	NT	NT	NT	NA	NA	0	
III.13	51	N			32	37	37	40	100	100	1.4	1.4	19	Phenacopy

Age of onset is the age of onset in years as reported by the subjects. Subject age is the age at which the audiometric data of column 7 to 12 were obtained. If there was no speech audiometric data measured during the latest audiometry, the penultimate audiogram was selected. Progression rate of HL, calculated as described in the methods section, when there was at least a follow-up duration of 10 years. Subjects II.8, III.17 and IV.12 were living abroad during the study. Only audiometric data and DNA samples were available. y, years; PTA, pure tone average (mean of 0.5, 1 and 2 kHz air conduction thresholds); R, right; L, left; SRT, speech reception threshold; SRS, speech recognition score in %; YOF, years of follow up; NR, age of onset of HL not reported; NT, not tested; N, no abnormalities; T, Tinnitus; O, recurrent otitis; V, vestibular complaints; NA, not applicable.

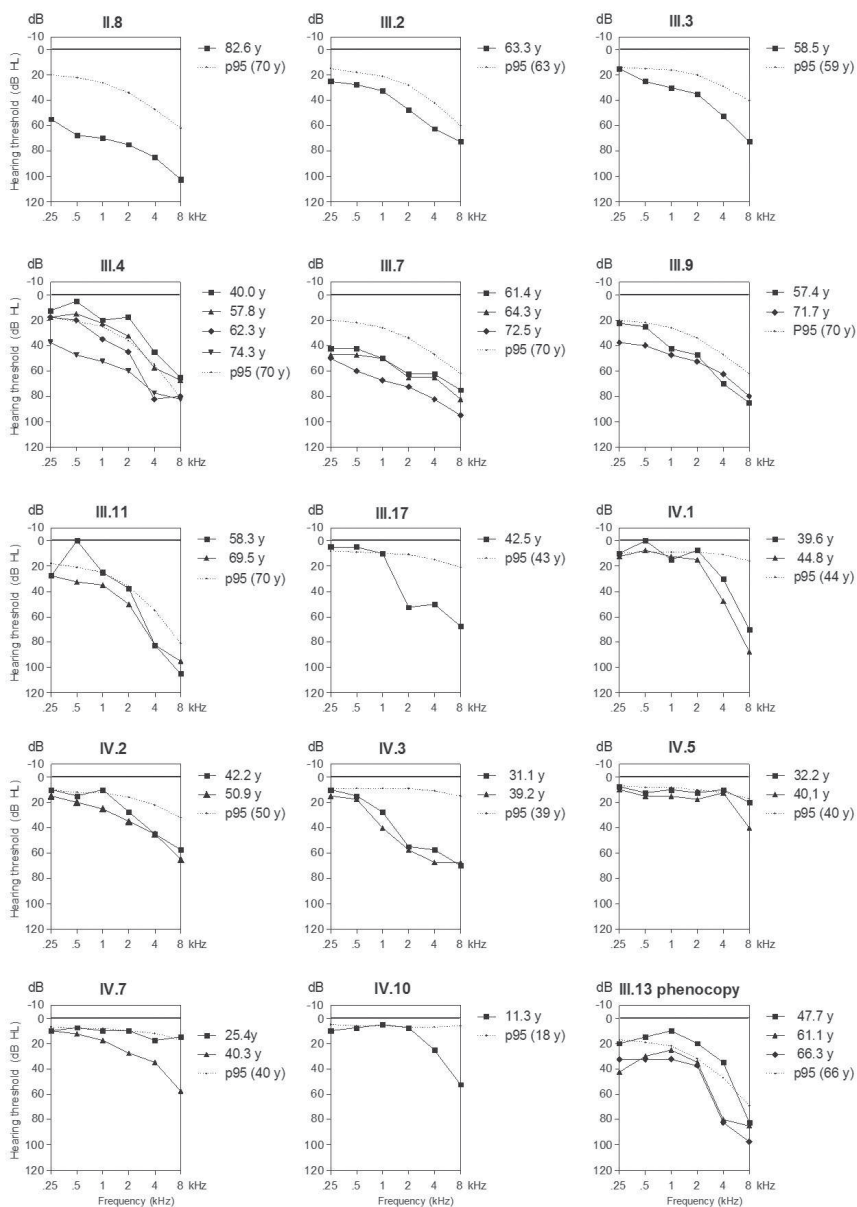


Figure 2. Audiometry Air conduction thresholds of all subjects with the c.1312C>T *COCH* mutation and of the phenocopy are depicted. The p95 values are matched to the individuals' sex and age at the most recent audiometry, according to the ISO 7029:2017 standard. The age range for which the ISO 7029:2017 can be applied is 18 to 70 years. y, age in years; R, right; L, left; dB HL, decibel hearing level; kHz, kilohertz.

Audio-vestibular testing shows a mildly progressive HL with variable vestibular dysfunction

A total number of 25 affected and unaffected subjects underwent audiometric evaluations. The 14 affected subjects with the c.1312C>T mutation in *COCH* reported a mean and median onset age of HL of 33 years (range: 18-49 years; see **Table 1** for subject characteristics). There were no indications for acquired HL in the affected subjects. Their audiograms showed bilateral symmetric sensorineural high-frequency HL without air-bone gaps (**Figure 2**).

Ten subjects had normal hearing for their age (i.e. within the 95th percentile) and, as mentioned previously, subject III:13 was a phenocopy. **Figure 3** shows the age-related typical audiograms (ARTA), which display an average progression of HL of about 0.8 dB/year. Progression was significant for all frequencies (*F*-test, deviation from zero, *p*-value: ≤ 0.0011)

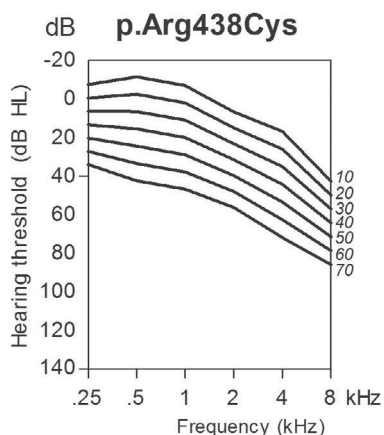


Figure 3. Age-Related Typical Audiograms (ARTA) of c.1312C>T, p.(Arg438Cys) DFNA9 subjects ARTA is derived from cross-sectional linear regression analysis of last visit audiograms of affected subjects with the c.1312C>T *COCH* mutation. *y*, age in years; dB HL, decibel hearing level; kHz, kilohertz.

Five subjects had sufficient audiometric data to calculate individual progression of HL, which varied between 0.3 to 1.6 dB per year (**Table 1**). Speech audiometry was performed in 10 of 14 affected family members with the c.1312C>T mutation. **Figure 4** shows the maximum phoneme scores of these individuals plotted against age (left panel) and PTA_{1-4kHz} (right panel), and was compared to speech perception scores of subjects with presbycusis or other *COCH* mutations. The latter comparison shows that speech perception is remarkably preserved in this family, at high age as well as at higher PTA levels.

Vestibular history showed that subjects III.7, III.9, IV.3 and IV.7 complained about their balance. Vestibular testing was carried out in subjects III.4, III.9, IV.2, IV.3, IV.5, IV.7 and the phenocopy (III.13). **Table 2** displays results for vestibular history and examinations. Affected subjects III.4, III.9, IV.3 and IV.7 showed (severe) vestibular hyporeflexia. Subjects IV.2 and IV.5 had normal vestibular function at the age of 50 and 40 years, respectively.

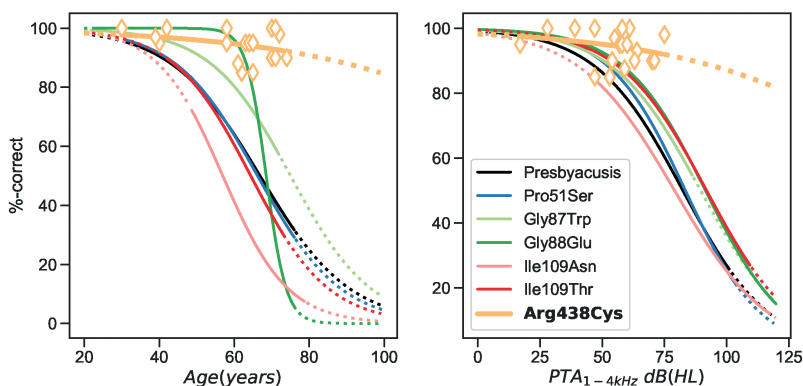


Figure 4. Speech audiometry of DFNA9 subjects Left panel: binaural mean phoneme scores plotted against the subjects' age. Right panel: phoneme scores plotted against the binaural mean pure tone average at 1, 2 and 4 kHz (PTA_{1-4kHz}). The black line represents normal values for a given age, as described in the Material and Methods section. Data for other mutations in *COCH* (noted as amino acid substitutions in figure legend) obtained from families published in Bom et al. 2001 (14), Kemperman et al. 2005 (15), Pauw et al. 2011 (16) and Pauw et al. 2007 (17, 18).

DISCUSSION

In this study, we describe the identification of a novel missense mutation (c.1312C>T, p.(Arg438Cys)) in *COCH*, which is associated with DFNA9. This mutation affects the vWFA2 domain of cochlin. Affected subjects have progressive HL with an average onset at 33 years and an annual deterioration rate of 0.8 dB/year. Vestibular test results vary from normal to vestibular dysfunction. Speech perception scores of subjects with the c.1312C>T *COCH* mutation are remarkably preserved when compared to those of subjects with other *COCH* mutations.

The onset age of auditory complaints in patients with DFNA9 varies between the 2nd and 5th decade of life.³ This is also true for the present family, in which the reported ages of onset of HL ranged from 18 to 49 years. This variation may be, in part, related to the fact that a self-reported age of onset of a disease is prone to inaccuracy, as was previously shown for depression.³⁰ Nevertheless, the variation in age of onset in the present family is clearly objectified in the audiograms. Subjects IV.5 and IV.7 display mild HL around the age of 30 years, while subject IV.3 has severe high frequency HL at the age of 31 years. Subject IV.10 already has moderate HL at the age of 11 years (this subject did not report an age of onset of HL) for which we could not identify an additional acquired explanation. An early onset of HL has, however, been associated with mutations affecting the vWFA2 domain³, and intrafamilial variation in onset age of dominantly inherited HL has also been reported for mutations in several other genes than *COCH*, e.g. *MYO6*, *POU4F3* and *OSBPL2*.³¹⁻³⁴

All affected subjects in this study had symmetric hearing loss. The ARTA show a down-sloping high-frequency HL, with an average progression of 0.8 dB/year. Additional individual longitudinal analyses in five subjects showed individual progression of HL of about 0.3-1.6 dB/year. This rate of progression is relatively mild compared to the progression observed in individuals with most of the other reported mutations in *COCH*. Progression is, for example, 2-7 dB/year for the c.151C>T (p.Pro51Ser), 1.0-2.8 dB/y for the c.326C>T (p.Ile109Thr) and 3.6-4.6 dB/year for the c.263G>A (p.Gly88Glu) mutation.^{15,35,36} These mutations all affect the LCCL domain of cochlin. To our knowledge, there are currently no other data in literature available on progression of HL for *COCH* mutations that affect the vWFA1 and vWFA2 domains of cochlin. Maximum phoneme scores plotted against age and PTA_{1-4kHz} show a remarkable better performance in the present family compared to families with DFNA9 caused by other *COCH* mutations or to presbycusis, even at an advanced age. Speech recognition scores in the latter two groups are comparable. The present c.1312C>T mutation affects the vWFA2 domain, whereas all other reported speech recognition scores are derived from patients with *COCH* mutations that affect the LCCL domain. Whether speech recognition is indeed better in DFNA9 cases with a *COCH* mutation that affects the vWFA2 domain needs to be confirmed in other families.

Vestibular function assessment in six subjects showed a variable vestibular phenotype associated with the c.1312C>T mutation, ranging from normal function (n=2) to (severe) hypofunction (n=4). It has to be noted that two out of four subjects with vestibular dysfunction passed the age of 70, meaning that an age-related component could also contribute to the vestibular phenotype³⁷. Nevertheless, these results are in line with other reports of vestibular hypofunction in subjects with *COCH* mutations affecting the vWFA2 domain.³⁸⁻⁴¹ In contrast, mutations that affect the LCCL domain of cochlin (e.g. p.Pro51Ser and p.Gly87Trp) appear to be associated with a more severe vestibular phenotype. To illustrate this, all patients above the age of 60 years with the c.151C>T (p.Pro51Ser) mutation have vestibular areflexia.^{35,42} It needs, however, to be emphasized, that the number of vestibular assessed subjects in most studies with mutations affecting the vWFA domain are relatively small (1- 6 subjects)³⁸⁻⁴¹, compared to those affecting the LCCL domain, e.g. the c.151C>T (p.Pro51Ser) mutation.^{35,42} Based on these results, we hypothesize that mutations that affect the LCCL domain lead to a more severe vestibular phenotype, compared to those affecting the vWFA2 domain. Further vestibular assessments on fully genotyped DFNA9 families with mutations affecting these domains are needed to confirm or reject this hypothesis.

As discussed above, phenotypical differences in terms of progression of HL, speech understanding and vestibular function appear to exist between the identified c.1312C>T

mutation affecting the vWFA2 domain and mutations that affect the LCCL domain of cochlin.^{3,43,44} These differences have been considered previously in several reports and have been the starting point for developing several hypotheses relating to pathophysiological mechanisms underlying DFNA9, and are based on differences in cochlin function at cellular and molecular levels.^{3,10,45} While the role of cochlin in the inner ear is not completely understood, evidence suggests that cochlin proteins undergo proteolytic cleavage between the LCCL domain and the downstream vWFA domains.^{10,46} This cleavage results in an N-terminal peptide containing the LCCL domain, which is secreted into the perilymphatic space.^{10,46} The C-terminal peptide that contains both vWFA domains is assumed to interact with collagen in the extracellular matrix.^{47,48} Bae et al. extensively studied the pathogenic mechanisms of *COCH* mutations affecting the LCCL and vWFA domains and correlated these with the respective audiovestibular phenotypes. They summarized that subjects with mutations affecting the vWFA1 and vWFA2 domains had a relatively early onset of HL and less vestibular dysfunction compared to those with mutations affecting the LCCL domain. Upon overexpression in cultured cells they showed that mutations that affected either of the vWFA domains resulted in the formation of high-molecular-weight cochlin aggregates, whereas, mutations affecting the LCCL domain led to the formation of cochlin dimers.^{3,41} Furthermore, Bae et al. reported that mutations that affect the vWFA domains result in a higher amount of accumulated cochlin within a cell and correlated this with the significantly earlier average age of onset of HL.³ In addition, Jung et al. reported that LCCL domain-containing cochlin peptides have an intracochlear immunomodulatory role.¹⁰ We hypothesize that HL after bacterial infection can differ between DFNA9 patients with mutations that affect the LCCL domain, and with mutations in the vWFA domains.

The presently studied c.1312C>T mutation affects the vWFA2 domain and is associated with a relatively early, although variable age, of onset of HL and in addition presents with relatively mild audiovestibular characteristics. This is in agreement with previously reported genotype-phenotype correlations.^{3,38,49} However, this does not explain the relatively mild progression of HL and remarkably good speech perception scores that subjects with the identified c.1312C>T *COCH* mutation display. Speech perception was never before investigated in DFNA9 patients with mutations affecting the vWFA domains. It, therefore, is too early to conclude that mutations that affect this domain have little effect on speech perception. It is also important to realize that genetic modifiers and environmental factors can contribute to phenotypic differences, even between family members affected by the same mutation. Further studies on the molecular disease mechanism are required and can also explore possibilities for therapeutic strategies.

In conclusion, this report expands the genotypic and phenotypic spectrum of DFNA9. The novel c.1312C>T *COCH* mutation is associated with a dominantly inherited mildly progressive high frequency HL with a variable age of onset. Speech perception and vestibular function are mildly affected. The remarkably preserved speech perception scores at higher age in this study warrant further audiovestibular investigation of families with DFNA9 caused by *COCH* mutations affecting the vWFA2 domain.

ACKNOWLEDGEMENTS

This study was financially supported by a grant of the Heinsius-Houbolt foundation [to R.J.E.P. and H.K].

REFERENCES

1. Van Camp, G. & Smith, R. Hereditary Hearing Loss Homepage. (<https://hereditaryhearingloss.org/>).
2. JanssensdeVarebeke, S.P.F. *et al.* Bi-allelic inactivating variants in the *COCH* gene cause autosomal recessive prelingual hearing impairment. *Eur J Hum Genet* 26, 587-591 (2018).
3. Bae, S.H. *et al.* Identification of pathogenic mechanisms of *COCH* mutations, abolished cochlin secretion, and intracellular aggregate formation: genotype-phenotype correlations in DFNA9 deafness and vestibular disorder. *Hum Mutat* 35, 1506-13 (2014).
4. Azaiez, H. *et al.* Genomic Landscape and Mutational Signatures of Deafness-Associated Genes. *Am J Hum Genet* 103, 484-497 (2018).
5. Landrum, M.J. *et al.* ClinVar: improving access to variant interpretations and supporting evidence. *Nucleic Acids Res* 46, D1062-D1067 (2018).
6. Fransen, E. *et al.* A common ancestor for *COCH* related cochleovestibular (DFNA9) patients in Belgium and The Netherlands bearing the P51S mutation. *J Med Genet* 38, 61-5 (2001).
7. Manolis, E.N. *et al.* A gene for non-syndromic autosomal dominant progressive postlingual sensorineural hearing loss maps to chromosome 14q12-13. *Hum Mol Genet* 5, 1047-50 (1996).
8. Robertson, N.G., Khetarpal, U., Gutierrez-Espeleta, G.A., Bieber, F.R. & Morton, C.C. Isolation of novel and known genes from a human fetal cochlear cDNA library using subtractive hybridization and differential screening. *Genomics* 23, 42-50 (1994).
9. Robertson, N.G. *et al.* Mapping and characterization of a novel cochlear gene in human and in mouse: a positional candidate gene for a deafness disorder, DFNA9. *Genomics* 46, 345-54 (1997).
10. Jung, J. *et al.* Cleaved Cochlin Sequesters *Pseudomonas aeruginosa* and Activates Innate Immunity in the Inner Ear. *Cell Host Microbe* 25, 513-525 e6 (2019).
11. M. Mazzoli, G.V.C., V. Newton, N. Giarbini, F. Declau, A. Parving. Recommendations for the description of genetic and audiological data for families with nonsyndromic hereditary hearing impairment. (2003).
12. Huygen, P.L.M., Pennings, R.J.E. & Cremers, C.W. Characterizing and distinguishing progressive phenotypes in nonsyndromic autosomal dominant hearing impairment. in *audiological medicine 1* Vol. 1 37-46 (2003).
13. Bosman, A.J. & Smoorenburg, G.F. Intelligibility of Dutch CVC syllables and sentences for listeners with normal hearing and with three types of hearing impairment. *Audiology* 34, 260-84 (1995).
14. Bom, S.J. *et al.* Speech recognition scores related to age and degree of hearing impairment in DFNA2/KCNQ4 and DFNA9/COCH. *Arch Otolaryngol Head Neck Surg* 127, 1045-8 (2001).
15. Kemperman, M.H. *et al.* Audiometric, vestibular, and genetic aspects of a DFNA9 family with a G88E *COCH* mutation. *Otol Neurotol* 26, 926-33 (2005).
16. Pauw, R.J., Huygen, P.L., Colditz, G.M. & Cremers, C.W. Phenotype analysis of an Australian DFNA9 family with the 1109N *COCH* mutation. *Ann Otol Rhinol Laryngol* 120, 414-21 (2011).
17. Pauw, R.J. *et al.* Clinical characteristics of a Dutch DFNA9 family with a novel *COCH* mutation, G87W. *Audiol Neurootol* 12, 77-84 (2007).
18. Pauw, R.J. *et al.* Phenotype description of a novel DFNA9/COCH mutation, I109T. *Ann Otol Rhinol Laryngol* 116, 349-57 (2007).
19. Onk, A.M. *et al.* Vestibular function and temporal bone imaging in DFNB1. *Hear Res* 327, 227-34 (2015).

20. Purcell, S. *et al.* PLINK: a tool set for whole-genome association and population-based linkage analyses. *Am J Hum Genet* 81, 559-75 (2007).
21. Silberstein, M. *et al.* A system for exact and approximate genetic linkage analysis of SNP data in large pedigrees. *Bioinformatics* 29, 197-205 (2013).
22. Tong, L. & Thompson, E. Multilocus lod scores in large pedigrees: combination of exact and approximate calculations. *Hum Hered* 65, 142-53 (2008).
23. Zazo Seco, C. *et al.* Allelic Mutations of KITLG, Encoding KIT Ligand, Cause Asymmetric and Unilateral Hearing Loss and Waardenburg Syndrome Type 2. *Am J Hum Genet* 97, 647-60 (2015).
24. Wesdorp, M. *et al.* MPZL2, Encoding the Epithelial Junctional Protein Myelin Protein Zero-like 2, Is Essential for Hearing in Man and Mouse. *Am J Hum Genet* 103, 74-88 (2018).
25. Hardenbol, P. *et al.* Multiplexed genotyping with sequence-tagged molecular inversion probes. *Nature Biotechnology* 21, 673 (2003).
26. Khandelwal, K.D. *et al.* Novel IRF6 Mutations Detected in Orofacial Cleft Patients by Targeted Massively Parallel Sequencing. *Journal of Dental Research* 96, 179-185 (2016).
27. Adzhubei, I.A. *et al.* A method and server for predicting damaging missense mutations. *Nature methods* 7, 248-249 (2010).
28. Schwarz, J.M., Cooper, D.N., Schuelke, M. & Seelow, D. MutationTaster2: mutation prediction for the deep-sequencing age. *Nature Methods* 11, 361 (2014).
29. Vaser, R., Adusumalli, S., Leng, S.N., Sikic, M. & Ng, P.C. SIFT missense predictions for genomes. *Nature Protocols* 11, 1 (2015).
30. Lindsay A.Farrer, Louis P.Florio, Martha L.Bruce, Philip J.Leaf & Myrna M.Weissman. Reliability of self-reported age at onset of major depression. *Journal of Psychiatric Research* 23, 35-47 (1989).
31. Sampaio-Silva, J. *et al.* Exome Sequencing Identifies a Novel Nonsense Mutation of MYO6 as the Cause of Deafness in a Brazilian Family. *Ann Hum Genet* 82, 23-34 (2018).
32. Thoenes, M. *et al.* OSBPL2 encodes a protein of inner and outer hair cell stereocilia and is mutated in autosomal dominant hearing loss (DFNA67). *Orphanet J Rare Dis* 10, 15 (2015).
33. Sanggaard, K.M. *et al.* A novel nonsense mutation in MYO6 is associated with progressive nonsyndromic hearing loss in a Danish DFNA22 family. *Am J Med Genet A* 146A, 1017-25 (2008).
34. Pauw, R.J. *et al.* Audiometric characteristics of a Dutch family linked to DFNA15 with a novel mutation (p.L289F) in POU4F3. *Arch Otolaryngol Head Neck Surg* 134, 294-300 (2008).
35. JanssensdeVarebeke, S., Topsakal, V., Van Camp, G. & Van Rompaey, V. A systematic review of hearing and vestibular function in carriers of the Pro51Ser mutation in the COCH gene. *Eur Arch Otorhinolaryngol* 276, 1251-1262 (2019).
36. Verhagen, W.I. *et al.* Hereditary cochleovestibular dysfunction due to a COCH gene mutation (DFNA9): a follow-up study of a family. *Clin Otolaryngol Allied Sci* 26, 477-83 (2001).
37. Zalewski, C.K. Aging of the Human Vestibular System. *Semin Hear* 36, 175-96 (2015).
38. Yuan, H.J. *et al.* Novel mutations in the vWFA2 domain of COCH in two Chinese DFNA9 families. *Clin Genet* 73, 391-4 (2008).
39. Faletta, F., Pirastu, N., Athanasakis, E., Somaschini, A., Pianigiani, G and Gasparini, P. A novel mutation in the vWFA2 domain of the COCH gene in an Italian DFNA9 family. *Audiological Medicine*, 4-7 (2011).

40. Street, V.A. *et al.* A novel DFNA9 mutation in the vWFA2 domain of COCH alters a conserved cysteine residue and intrachain disulfide bond formation resulting in progressive hearing loss and site-specific vestibular and central oculomotor dysfunction. *Am J Med Genet A* 139A, 86-95 (2005).
41. Cho, H.J. *et al.* A novel COCH mutation associated with autosomal dominant nonsyndromic hearing loss disrupts the structural stability of the vWFA2 domain. *J Mol Med (Berl)* 90, 1321-31 (2012).
42. Bischoff, A.M. *et al.* Vestibular deterioration precedes hearing deterioration in the P51S COCH mutation (DFNA9): an analysis in 74 mutation carriers. *Otol Neurotol* 26, 918-25 (2005).
43. Tsukada, K. *et al.* Detailed hearing and vestibular profiles in the patients with COCH mutations. *Ann Otol Rhinol Laryngol* 124 Suppl 1, 100S-105 (2015).
44. Kim, B.J. *et al.* Distinct vestibular phenotypes in DFNA9 families with COCH variants. *Eur Arch Otorhinolaryngol* 273, 2993-3002 (2016).
45. Jung, J., Kim, H.S., Lee, M.G., Yang, E.J. & Choi, J.Y. Novel COCH p.V123E Mutation, Causative of DFNA9 Sensorineural Hearing Loss and Vestibular Disorder, Shows Impaired Cochlin Post-Translational Cleavage and Secretion. *Hum Mutat* 36, 1168-75 (2015).
46. Ikezono, T. *et al.* Identification of the protein product of the Coch gene (hereditary deafness gene) as the major component of bovine inner ear protein. *Biochim Biophys Acta* 1535, 258-65 (2001).
47. Nagy, I., Trexler, M. & Patthy, L. The second von Willebrand type A domain of cochlin has high affinity for type I, type II and type IV collagens. *FEBS Lett* 582, 4003-7 (2008).
48. Robertson, N.G. *et al.* Mutations in a novel cochlear gene cause DFNA9, a human nonsyndromic deafness with vestibular dysfunction. *Nat Genet* 20, 299-303 (1998).
49. Wang, Q. *et al.* Different Phenotypes of the Two Chinese Proband with the Same c.889G>A (p.C162Y) Mutation in COCH Gene Verify Different Mechanisms Underlying Autosomal Dominant Nonsyndromic Deafness 9. *PLoS One* 12, e0170011 (2017).

SUPPLEMENTARY METHODS

Annotated variants were filtered, based on a population allele frequency of $\leq 0.05\%$ in the gnomAD exome and genome database V.2.1 (<https://gnomad.broadinstitute.org/>) and our in-house exome database (containing ~15.000 alleles). Variants in coding and splice site regions (-14/+14 nt) were analyzed. Interpretation of missense variants was performed using the in silico pathogenicity prediction tools CADD-PHRED (≥ 15)¹, SIFT (≤ 0.05)², PolyPhen-2 (PPH2, ≥ 0.450)³ and MutationTaster (deleterious)⁴. Only those called variants were considered that had a quality-by-depth >150 and that were associated with an autosomal dominant inherited type of HI. Shared variants in the MIPs data of the selected subjects were analyzed. To address the possible existence of one or more phenocopies, shared variants between two subjects (IV.1 with III.9, IV.1 with III.13 and III.9 with III.13) were also analyzed separately. Variants were considered if a pathogenic effect was predicted by at least two different tools. Potential effects on splicing of missense and synonymous variants were evaluated using five algorithms (SpliceSiteFinder, MaxEntScan, NNSPLICE, GeneSplicer and Human Splicing Finder) via the AlamutVisual software (V.2.10, Interactive Biosoftware). A change of $\geq 5\%$ in splice site scores predicted by at least two algorithms was considered significant.

SUPPLEMENTARY TABLES

Table S1. Hearing loss genes covered by MIPS panel

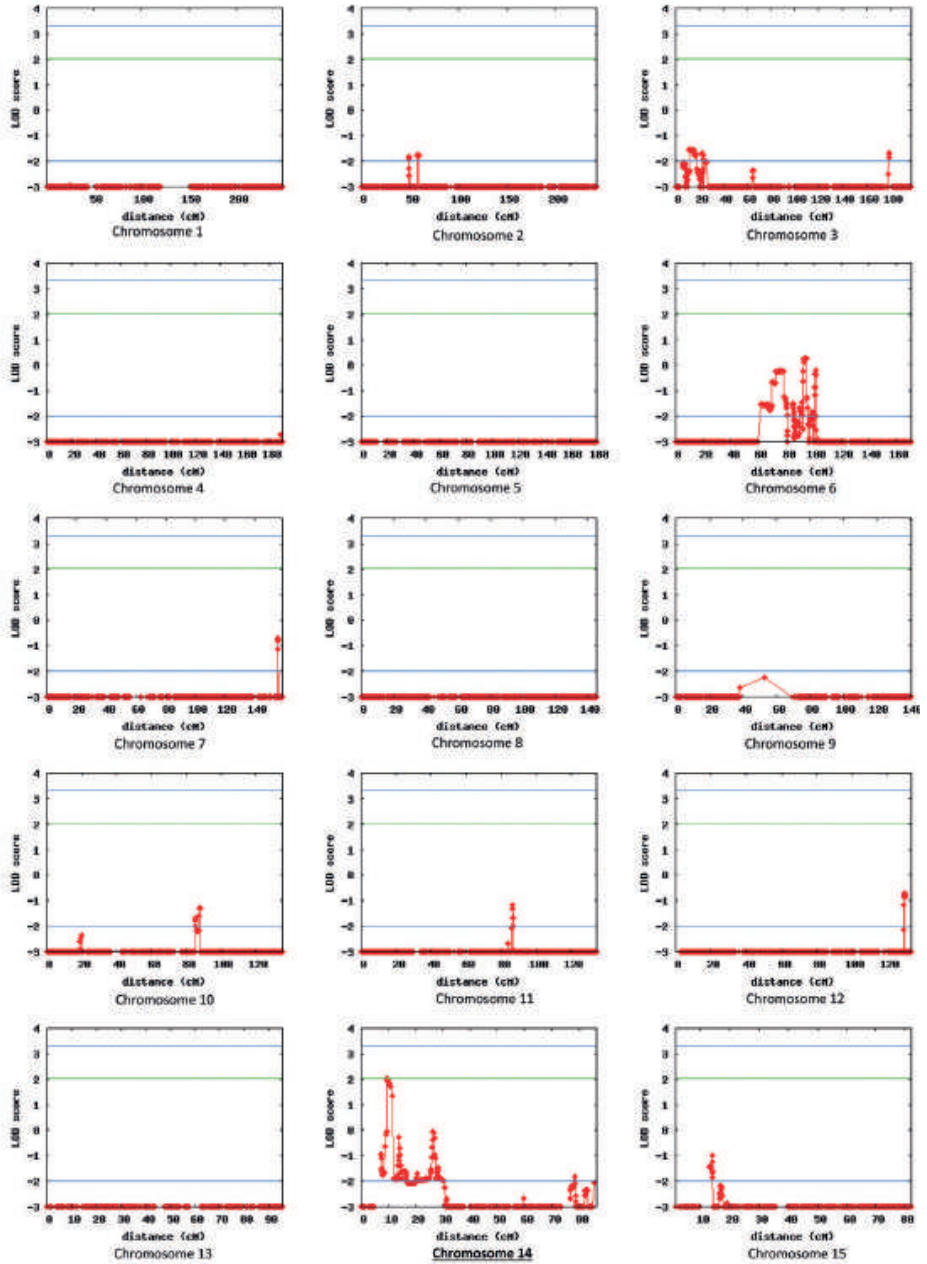
<i>ACTG1</i>	<i>GRM7</i>	<i>PTPRQ</i>
<i>ADCY1</i>	<i>GRM8</i>	<i>RDX</i>
<i>BDP1</i>	<i>GRXCR1</i>	<i>RIPOR2</i>
<i>BSND</i>	<i>GRXCR2</i>	<i>SERPINB6</i>
<i>CABP2</i>	<i>HGF</i>	<i>SIX1</i>
<i>CCDC50</i>	<i>ILDR1</i>	<i>SLC17A8</i>
<i>CDH23</i>	<i>KARS</i>	<i>SLC26A4</i>
<i>CEACAM16</i>	<i>KCNQ4</i>	<i>SLC26A5</i>
<i>CIB2</i>	<i>LHFPL5</i>	<i>SMPX</i>
<i>CLDN14</i>	<i>LOXHD1</i>	<i>STRC</i>
<i>CLIC5</i>	<i>LRTOMT</i>	<i>SYNE4</i>
<i>COCH</i>	<i>MARVELD2</i>	<i>TBC1D24</i>
<i>COL11A2</i>	<i>MIR96</i>	<i>TECTA</i>
<i>COL4A6</i>	<i>MSRB3</i>	<i>TJP2</i>
<i>CRYM</i>	<i>MYH14</i>	<i>TMC1</i>
<i>DCDC2</i>	<i>MYH9</i>	<i>TMEM132E</i>
<i>GSDME</i>	<i>MYO15A</i>	<i>TMIE</i>
<i>DFNB31</i>	<i>MYO3A</i>	<i>TMPRSS3</i>
<i>DFNB59</i>	<i>MYO6</i>	<i>TNC</i>
<i>DIABLO</i>	<i>MYO7A</i>	<i>TPRN</i>
<i>DIAPH1</i>	<i>NAT2</i>	<i>TRIOBP</i>
<i>ELMOD3</i>	<i>OSBPL2</i>	<i>TSPEAR</i>
<i>EPS8</i>	<i>OTOA</i>	<i>USH1C</i>
<i>ESPN</i>	<i>OTOF</i>	<i>USH1G</i>
<i>ESRRB</i>	<i>OTOG</i>	
<i>EYA4</i>	<i>OTOGL</i>	
<i>GIPC3</i>	<i>P2RX2</i>	
<i>GJB2</i>	<i>PCDH15</i>	
<i>GJB3</i>	<i>PNPT1</i>	
<i>GJB6</i>	<i>POU3F4</i>	
<i>GPSM2</i>	<i>POU4F3</i>	
<i>GRHL2</i>	<i>PRPS1</i>	

Table S2. Detailed information on *COCH*, cochlin and pathogenicity predictions on the identified *COCH* variant.

Gene symbol	Genomic positions <i>COCH</i>	RefSeq <i>COCH</i> transcript	RefSeq cochlin protein	Genomic change	cDNA change	Protein change	GnomAD EAF (%)	GnomAD GAF (%)	CADD PHRED	SIFT	PPH2	Mutation Taster	PhyloP	GERP	REVEL
<i>COCH</i>	chr14:31,343,741-31,359,822	NM_004086.2	NP_004077.1	g.31,355,353C>T	c.1312C>T	p.Arg438Cys	3.98E-06	-	23.9	0.05	0.974	Disease causing	1.388	4.06	0.697

Scores that meet the thresholds for a possibly deleterious effect are indicated in red. Thresholds are: CADD-PHRED (≥ 15); SIFT (< 0.05); PolyPhen-2 (≥ 0.450)³ and MutationTaster (disease causing)⁴; PhyloP (≥ 2.7)⁵; GERP (≥ 2)⁶ and REVEL (> 0.5)⁷. Genomic positions *COCH* according to GRCh37/hg19; GnomAD_EAF and GnomAD_GAF, allele frequencies in gnomAD total exome database and genome database, respectively; CADD_PHRED, Combined Annotation Dependent Depletion PHRED score; SIFT, Scale-Invariant Feature Transform; PPH2, PolyPhen-2 score; PhyloP, phylogenetic *P*-values; GERP, Genomic Evolutionary Rate Profiling; REVEL, Rare Exome Variant Ensemble Learner -, frequency not available.

SUPPLEMENTARY FIGURES



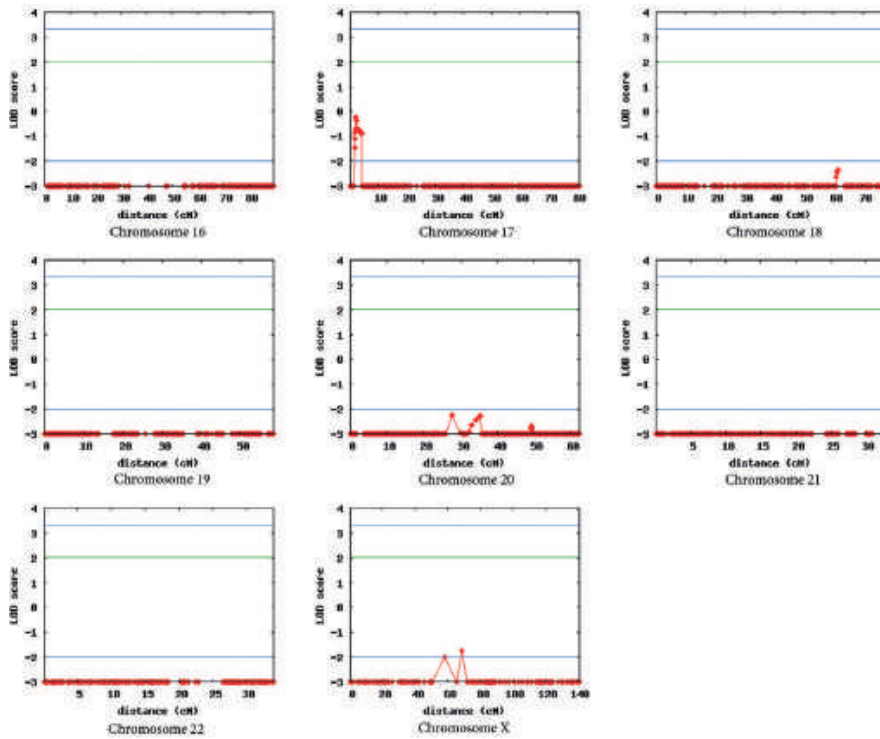


Figure S1 Linkage analysis. The blue lines define the customary LOD score range. The green line demonstrates the maximum LOD score measured genome-wide in this experiment.

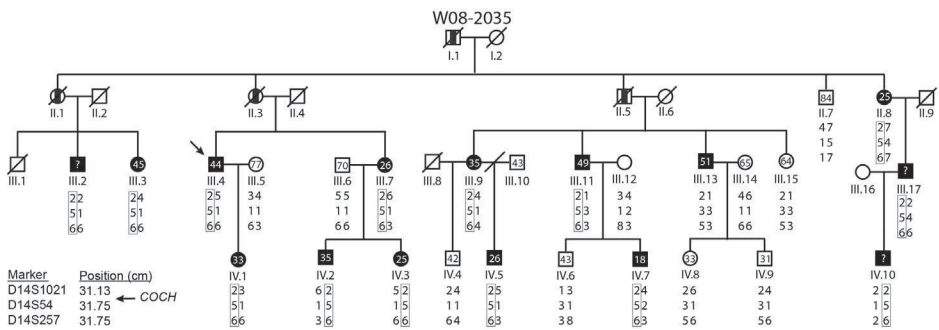


Figure S2 Results of VNTR marker genotyping. Affected individual III.13 does not carry the disease allele. The shared haplotype is boxed. The c.1312C>T *COCH* variant is located between the markers D14S1021 and D14S54. cM, centimorgan.

SUPPLEMENTARY REFERENCES

1. Kircher, M. *et al.* A general framework for estimating the relative pathogenicity of human genetic variants. *Nature genetics* 46, 310-315 (2014).
2. Vaser, R., Adusumalli, S., Leng, S.N., Sikic, M. & Ng, P.C. SIFT missense predictions for genomes. *Nature Protocols* 11, 1 (2015).
3. Adzhubei, I.A. *et al.* A method and server for predicting damaging missense mutations. *Nature methods* 7, 248-249 (2010).
4. Schwarz, J.M., Cooper, D.N., Schuelke, M. & Seelow, D. MutationTaster2: mutation prediction for the deep-sequencing age. *Nature Methods* 11, 361 (2014).
5. Pollard, K.S., Hubisz, M.J., Rosenbloom, K.R. & Siepel, A. Detection of nonneutral substitution rates on mammalian phylogenies. *Genome Res* 20, 110-21 (2010).
6. Cooper, G.M. *et al.* Distribution and intensity of constraint in mammalian genomic sequence. *Genome Res* 15, 901-13 (2005).
7. Ioannidis, N.M. *et al.* REVEL: An Ensemble Method for Predicting the Pathogenicity of Rare Missense Variants. *Am J Hum Genet* 99, 877-885 (2016).



Chapter 2.2

Genotype-phenotype correlations of pathogenic *COCH* variants in DFNA9: a HuGE systematic review and audiometric meta-analysis

Sybren M.M. Robijn*, Jeroen J. Smits*, Kadriye Sezer, Patrick L.M. Huygen, Andy J. Beynon, Erwin van Wyk, Hannie Kremer, Erik de Vrieze, Cornelis P. Lanting~ and Ronald J.E. Pennings~ (*~ gelijke bijdrage)

Submitted

Abstract

Pathogenic missense variants in *COCH* are associated with DFNA9, an autosomal dominantly inherited type of progressive sensorineural hearing loss with or without vestibular dysfunction. This study presents a systematic review and meta-analysis of all known DFNA9-associated *COCH* variants and their associated phenotypes with use of the PRISMA and HuGENet guidelines. The literature search yielded 48 studies describing the audiovestibular phenotypes of 27 DFNA9-associated variants in *COCH*. A meta-analysis of audiometric data was performed by constructing age-related typical audiograms and by performing analyses on the age of onset and progression of hearing loss. We present a detailed overview of genotype-phenotype correlations of all currently known pathogenic *COCH* variants associated with DFNA9. Significant differences were found between the calculated ages of onset and progression of the audiovestibular phenotypes of subjects with pathogenic variants affecting either the LCCL domain of cochlin, or the vWFA2 and Ivd1 domains. We conclude that the audiovestibular phenotypes associated with DFNA9 are highly variable. Variants affecting the LCCL domain of cochlin generally lead to more progression of hearing loss when compared to variants affecting the other domains. This review serves as a reference for prospective natural history studies in preparation of future therapeutic interventions.

INTRODUCTION

Hearing loss (HL) is one of the most common sensory impairments and is estimated to affect 432 million people worldwide.¹ Congenital or childhood-onset sensorineural HL is caused by genetic conditions in more than half of the cases. Adult-onset HL is, however, a much more complex disorder and is caused by a combination of environmental and genetic (risk) factors.² Despite this, a growing number of dominantly inherited types of HL is associated with an adult-onset; e.g., DFNA10 (*EYA4*, MIM: 601316), DFNA15 (*POU3F4*, MIM: 602459), DFNA21 (*RIPOR2*, MIM: 607017), and DFNA22 (*MYO6*, MIM: 606346).³⁻⁶

DFNA9 is another example of an adult-onset type of dominantly inherited HL and is caused by missense variants in *COCH*. It is characterized by progressive high-frequency HL, often accompanied by a variable degree of vestibular dysfunction as opposed to homozygous loss of function mutations which lead to autosomal recessive, early onset and severe hearing loss (DFNB110).⁷ The exact prevalence of pathogenic missense variants in *COCH* is unknown, but DFNA9 has been reported in numerous families on four continents.⁸ More than 25 different *COCH* variants have been reported to be causative of DFNA9 (Human Gene Mutation Database, 2020.4). *COCH* encodes cochlin, which is expressed in, among other tissues, the human inner ear.⁹ Cochlin is an extracellular matrix protein, but its exact role in the inner ear remains elusive. The protein is predicted to contain the following functional domains: an LCCL domain (Limulus factor C, Cochlin and Late gestation lung protein Lgl1), two vWFA domains (von Willebrand Factor A-like 1 and 2), and two Ivd domains (short intervening domains 1 and 2). Several studies have shown that the LCCL domain of cochlin plays a role in the local innate immune system of the cochlea.¹⁰⁻¹² Based on these findings, it was hypothesized that the inner ear of subjects with DFNA9 might be more susceptible to infections.¹¹ Studies corroborating this hypothesis have not yet been published.

Many studies have investigated the role of DFNA9-associated mutations on post-translational processing and cleavage of cochlin (reviewed by Verdoodt et al.¹³). Several of these studies have suggested that variants affecting the individual cochlin domains lead to distinctly different phenotypes.^{8,13} A concise systematic review and meta-analysis of all pathogenic *COCH* variants and their corresponding phenotypes is, however, still missing. This study aims to fill that gap and presents a systematic review of current DFNA9 literature and a meta-analysis of the available audiometric data to formulate robust genotype-phenotype correlations for DFNA9 to improve variant-specific counseling. The results from this study are also essential to define outcome measures that evaluate the effectiveness of future variant-specific (genetic) therapies.

MATERIALS AND METHODS

Systematic review

The systematic review was performed according to the HuGENet recommendations for systematic reviews.¹⁴ In addition, the Cochrane Handbook¹⁵, the Centre for Reviews and Disseminations guidance for undertaking reviews in health care¹⁶, and the PRISMA statement¹⁷ were applied in the review process. A review protocol was created and prospectively registered in PROSPERO (registration number CRD42018108199).

A search was conducted in relevant databases (PubMed, NCBI's Gene database, EMBASE, the Cochrane Library and Web of Science) focusing on DFNA9 genotype-phenotype correlation studies (last search update January 20th, 2021). For a comprehensive search of '*COCH*' and '*DFNA9*', all available MeSH terms were combined with free text words of all known synonyms: '*COCH*', '*Cochlin*', '*coagulation factor C homolog*', '*Coch5B2*', '*COCH-5B2*' and '*DFNA9*' (**Table S1**). In addition, grey literature was searched to identify relevant missing reports. No restrictions were applied during the search process. After duplicate removal, the remaining studies were screened by title and abstract. Reference lists of these publications were scanned forward and backward for additional reports. **Figure 1** shows a flowchart of the selection and filtering process. Two reviewers independently performed title and abstract screening, full-text screening, and final selection of eligible studies. Only studies published in either English or Dutch were included, however none of the excluded studies in other languages appeared to contain audiovestibular examinations of DFNA9 patients. Studies on animal models were excluded. No restrictions were placed on the methods that evaluated the genotype, phenotype, sample size, or publication date. After each phase of screening, the reviewers met to reach consensus.

Both reviewers used standardized forms (available upon request) to extract data and assess the risk of bias for each included study. Data on the self-reported age of onset, symptoms of vestibular dysfunction, and results of audiovestibular examinations were extracted for each underlying pathogenic *COCH* variant (**Table S2**). When available, normative test results for vestibular function (i.e., normal, hypofunction, or areflexia) were extracted. These were based on rotary chair tests, calorics, and video Head Impulse Tests (vHIT). Only data of subjects with a genetically confirmed DFNA9 diagnosis were included in this study. Corresponding authors were contacted to supply missing data. In addition, data were combined and deduplicated when multiple studies described the same individuals. Finally, disagreements were resolved by discussion and consultation of a third and fourth reviewer.

Some of the previous studies reported on phenotypic differences between variants affecting different domains of cochlin.^{8,13} To further assess this, subjects were pooled based on their identified pathogenic variant into three different cochlin domain groups: the LCCL, Ivd1, and vWFA2 domain groups. RefSeq NM_004086.2 was used to describe all *COCH* variants.

Meta-analysis

Original audiometric data were extracted and retrieved from the forty-eight included studies in the systematic review and used in the meta-analysis. Eleven of the included studies were performed on families previously diagnosed in our hospital.¹⁸⁻²⁷ We did not add additional hearing-impaired family members that were not previously reported in literature. Cross-sectional linear regression analyses were performed on bilateral averaged hearing thresholds to evaluate the progression of HL. For each variant, Age-Related Typical Audiograms (ARTA) were constructed in order to visualize progression of hearing loss.^{20,28} ARTA were only constructed for a *COCH* variant when individual audiograms of at least eight different subjects of different ages were available.

To assess potential differences in the progression of HL, the annual threshold deterioration (ATD) across the different *COCH* variants was calculated using cross-sectional non-linear regression analyses of hearing thresholds as a function of age. We first determined the pure-tone average across 0.5-4.0 kHz ($PTA_{0.5-4\text{ kHz}}$) for each subject. A two-parameter logistic function was used to fit the data, i.e. $PTA_{0.5-4\text{ kHz}} \sim \frac{130}{1+e^{(-scale \cdot (age-age_{mid})}}$, similar to Pauw et al.²⁹ The parameter age_{mid} describes the value at which the hearing thresholds are halfway between 0 dB and the asymptotic value (fixed at 130 dB), and $scale$ represents the slope of the function at this midpoint, which we use as an estimate for the ATD. In contrast to the self-reported age of onset that was recorded in the systematic review, we also calculated the age of onset in the meta-analysis. The calculated age of onset was defined as the age at which the calculated hearing threshold exceeds 25 dB, as the WHO classifies this as abnormal hearing, and subjects could benefit from amplification.¹ The calculated age of onset was determined by interpolating the function fit using the parameters age_{mid} and $scale$.

The logistic function was fitted to the audiometric data per domain group. The regression coefficients and their confidence intervals were assessed to test for differences between domains. For this, we constructed a null-model by pooling all data across the three domains and successively adding grouping parameters using analysis of variance (ANOVA) testing and comparing the conditional likelihoods with the null model. The calculated age of onset and the ATD were obtained for each domain. We further obtained a fit describing progression over time for each variant with at least five data points and assessed the 95% confidence intervals of the calculated age of onset and progression of HL. All analyses were conducted using R statistical programming language version 3.6.2 using packages *dplyr*, *tidyr*, *nls*, *nls.multstart* for analyses and data handling and *ggplot2* for visualization. Code available at <https://zenodo.org/badge/latestdoi/359572523>.

RESULTS

Systematic review

The total yield of the search strategy was 2,016 studies. After full-text screening, 48 studies met the eligibility criteria and together reported on 27 different *COCH* variants (**Figure 1**). Thirty-seven of these studies were retrospective family studies, describing the (audiovestibular) phenotype of *COCH* variants.^{18-27,29-55} Eleven of the included studies were not primarily designed as genotype-phenotype studies but as validation studies of genetic analyses or histopathological studies.^{9,56-65} Most of the selected studies were judged to have a high risk of bias on one or more domains (**Figure 2 and Table S3**), and only two studies had an overall low risk of bias.^{32,48} Bias mostly related to selective reporting and selective loss to follow-up. No restrictions were placed on the inclusion of articles based on bias. Articles describing homozygous loss-of-function variants in *COCH* that lead to DFNB110,^{7,66-68} were excluded from further analysis, additional study details can be found in **Table S4**. We also decided to exclude the c.266C>A; p.(Pro89His) *COCH* variant, previously reported by Dodson et al. (2012), from this study (**see Table S4**). They identified this variant in a child who presented with congenital profound unilateral HL and an ipsilateral enlarged vestibular aqueduct (EVA).⁶⁹ In contrast with the authors, we deem this variant non-pathogenic as an EVA has not been associated with DFNA9 in literature^{34,43} and is a plausible explanation for the unilateral HL in this case. In addition, we identified this variant in two unrelated adult subjects with bilateral HL seen in our institute. In both cases, the variant segregated to a normal hearing parent (unpublished results).

The 48 included studies reported on subjects predominantly from the Netherlands and Belgium, followed by the USA, China, Korea, Australia, Japan, Canada, Italy, Austria, Poland, and Hungary. Several studies reported on the same individuals or families, and deduplication was performed.^{9,18-21,23,29,33,35,37,42,56,59,61} After deduplication and removal of subjects with HL but without a genetic confirmation of DFNA9, a total of 444 subjects with a genetically confirmed DFNA9 diagnosis were identified. An overview of extracted genotype and phenotype characteristics is given in **Table S2**. A majority of studies (n=46) used a self-reported age of onset of HL and/or vestibular symptoms (**Figure 3**). In general, HL presented with ages of onset that ranged from the 2nd to 7th decade. Four studies calculated the age of onset through (non)linear regression analyses on available audiometric results as an attempt to objectify this outcome (**Table S2**).^{18,20,22,35} Two of these studies, both on subjects with the p.(Pro51Ser variant), compared the self-reported ages of onset with those calculated by linear regression. Bom et al. (1999) described a self-reported age of onset ranging from 36 to 63 years and a calculated onset range of 34 to 51 years¹⁸, whereas Bischoff et al. (2005) described a different family and reported these ranges as 18 to 51 and 38 to 49, respectively.²²

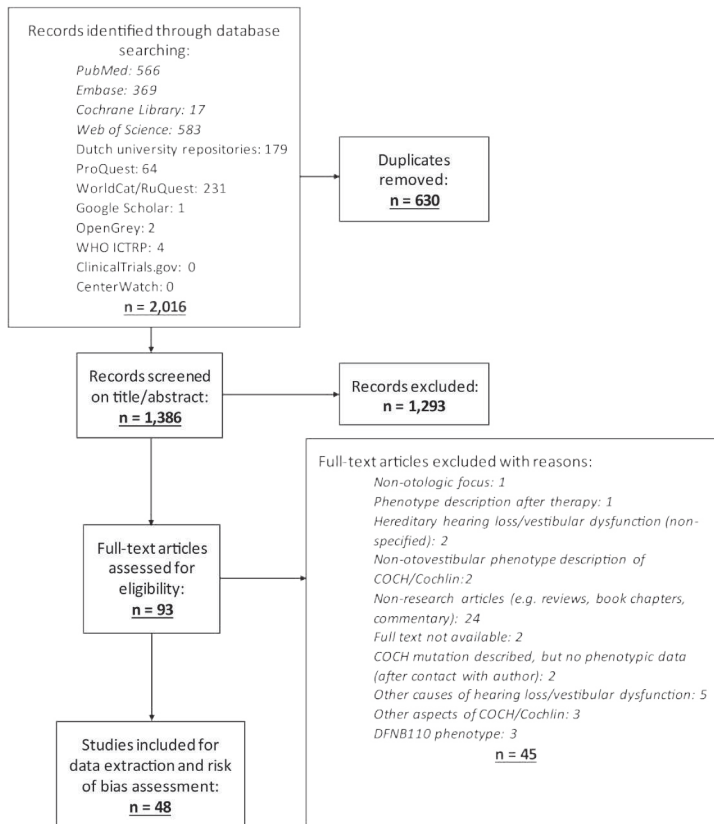


Figure 1. Flowchart of literature search Systematic identification and inclusion of relevant studies on genotype-phenotype correlations in DFNA9.

Twenty studies compared the age of onset of HL with the age of onset of vestibular impairment (**Figure 3**). Most of these studies ($n=12$, among six on p.(Pro51Ser)) concluded that vestibular symptoms manifested at approximately the same age as HL. Eight studies presented a self-reported age of onset of vestibular dysfunction after the onset of HL, as was highlighted in a recent systematic review on subjects with the p.Pro51Ser variant (age of onset of HL: 32.8 years vs. vestibular dysfunction: 34 – 40 years).⁷⁰ In contrast, Bischoff et al. (2005) measured vestibulo-ocular reflexes and concluded that vestibular dysfunction started on average nine years earlier than HL in subjects with this variant. Their study also showed vestibular function to deteriorate more rapidly over time than HL.²² The presence or absence of vestibular symptoms was reported for 26 pathogenic variants. Vertigo was the most frequently mentioned symptom (for 50% of the variants), followed by instability and balance problems, especially in the dark (for 31% of the variants). For nine variants, a lack of vestibular symptoms was specifically reported (see **Table S2**), two variants within the LCC1^{30,58-61}, one in the lvd1⁶⁴ and six in the vWFA2 domain^{41,45-47,51,62}).

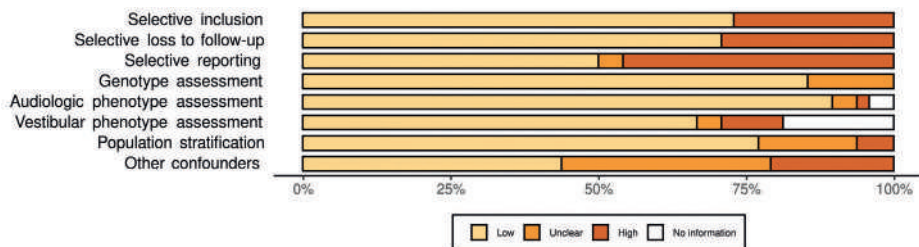
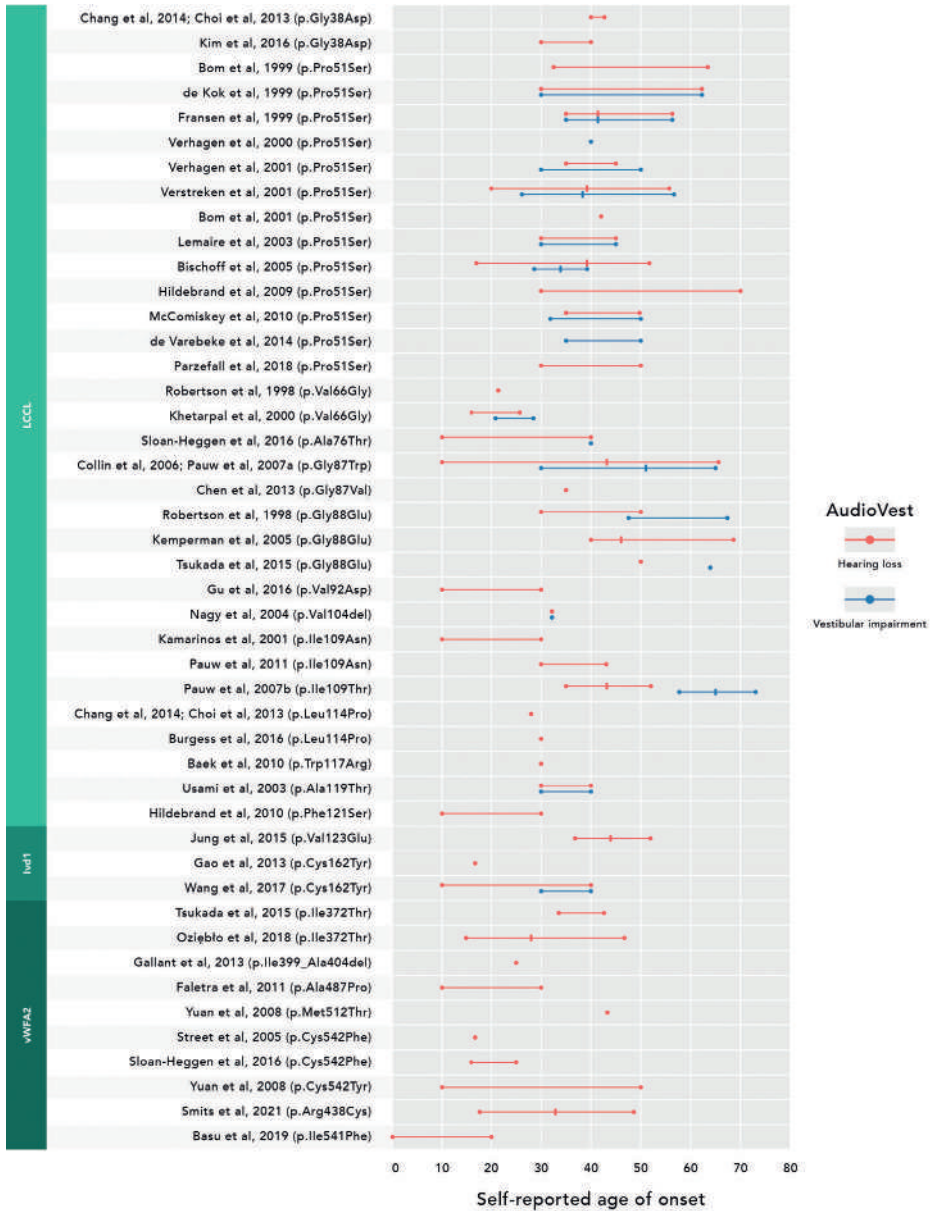


Figure 2. Risk of bias assessment Judgements of two reviewers about each risk of bias item are presented as percentages for all included studies.

All studies reported progression of HL over time. The ATD ranged from 0.7 dB to 7.0 dB/year, whereas the decrease in maximum speech recognition scores ranged from 0.99 to 3%/year (**Table S2**). The raw audiometric data were analyzed in more detail in the meta-analysis. The results of the vestibular examinations varied widely. We extracted 182 vestibular assessments from 160 individual subjects with 17 different pathogenic variants in *COCH*. Eighty subjects carried the p.(Pro51Ser) variant. It is important to note that the type and amount of vestibular function tests varied widely between studies (**Table S2**). Studies on subjects in the LCCL group reported more often vestibular dysfunction to occur in these subjects when compared to the subjects in the vWFA2 or Ivd1 groups (**Table S2**). **Figure S1** shows the severity of vestibular dysfunction in the LCCL group as the percentage of subjects with either normal, hypofunction, or areflexia, as a function of the age in decade steps. No reliable comparison could be made with the other domain groups because of insufficient objective data in these groups.

Some studies reported additional symptoms, including (incomplete segregation of) cardiovascular disease in two families with the p.(Pro51Ser) substitution^{18,23}, memory loss, and night blindness in a family with the p.(Phe121Ser) substitution.³¹ In addition, Bischoff et al. (2007) investigated the presence of ocular abnormalities in DFNA9 subjects hailing from four different families^{22,25,36,71} and concluded that the p.(Pro51Ser) and p.(Gly88Glu) variants were possibly associated with vertical corneal striae and related ocular symptoms as this phenomenon was present in 27 out of 61 affected subjects (and 5 out of 37 unaffected family members).⁷² Three other studies evaluated ocular involvement in 65 subjects with the p.(Pro51Ser)^{37,50} and p.(Ile109Thr)²⁶ substitutions. In only one of these subjects, with the p.(Pro51Ser) substitution, a corneal scratch in one eye was found. Based on the latter studies, it can therefore be concluded that it is unlikely that vertical corneal striae are part of the DFNA9 phenotype.



Twelve studies reported on temporal bone imaging of patients with DFNA9.^{9,22,27,34,37,38,43,50,54,58,64,73} Only two studies reported abnormal radiologic findings in subjects with the p.(Pro51Ser) substitution. Janssens de Varebeke et al. (2014) reported sclerotic lesions and/or narrowing of one or more semicircular canals on CT and MR imaging (n=8)³⁴, and Hildebrand et al. (2009) reported on the presence of bilateral superior semicircular canal dehiscence in one subject.⁴³

Meta-analysis

Figure 4 shows the ARTA that were constructed for 14 *COCH* variants. This was not possible for the other variants due to an insufficient number of subjects for which audiometric data was available. In those cases, individual audiograms of the affected subjects are presented in **Figure S2**. Five variants (p.Val104del⁴⁴, p.Ala119Thr³⁸, p.Ile399_Ala404del⁴⁵, p.Met512Thr⁴¹, p.Cys542Tyr⁴¹) were excluded from the meta-analysis and individual presentation (**Figure S2**) because of a lack of audiometric data, despite attempts to retrieve data via corresponding authors. In general, individual audiograms and ARTA showed progression of HL over all frequencies, although higher frequencies deteriorated earlier and more than lower frequencies (see **Figure 4**).

A total of 744 audiograms, obtained in 297 subjects, could be extracted and were included in the analysis. The majority of the included subjects pertain to the LCCL group (n=249). In contrast, only a relatively small number of subjects belong to the lvd1 or vWFA2 group (n=4 and 44, respectively). Single audiometric assessments were available in 163 subjects. For the remaining 134 subjects, two or more (repeated) measurements were extracted (**Figure S3**).

Figure 5A shows the progression of HL with increasing age for all included DFNA9 subjects across the three domain groups. An ANOVA analysis on the models showed that the data is best modeled by adding both a grouping variable describing the midpoints for the three domains ($F(2,740) = 1,52$ $p = 0.02$) and a separate variable for the ATD ($F(2,738) = 17.09$, $p < 0.001$), each compared to the null-model. The parameter fits indicated a calculated age of onset of 35.3 years for the LCCL group, 17.0 years for the lvd1 group, and 13.0 years for the vWFA2 group (see **Figure 5A**). ATD is visible in all groups, and the estimates vary between 2.06, 2.14, and 0.91 dB/year for the LCCL group, the lvd1 group, and the vWFA2 group, respectively. There are apparent differences in the calculated ages of onset of HL and especially the ATD between subjects in the three affected domain groups (see also **Figure S4**). Subjects in the LCCL group had hearing thresholds varying from near-normal in the first two decades of life to moderate-to-severe around the fifth decade to severe-to-profound from the 7th decade onwards. Hearing thresholds in subjects in the vWFA2 and the lvd1 group, in general, showed higher thresholds in the first two decades. Note however that not

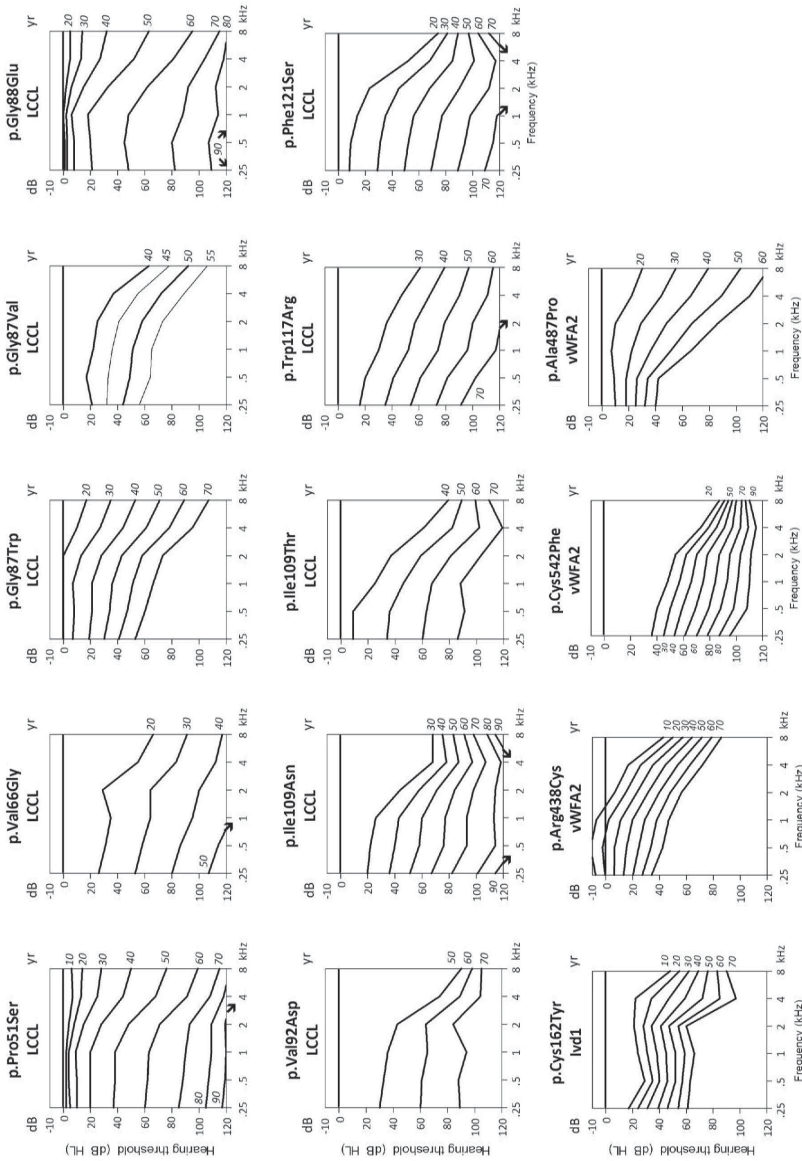


Figure 4. Age-Related Typical Audiograms (ARTA) for fourteen COCH mutations.

ARTA are derived from cross-sectional linear regression analysis of last visit audiograms of affected subjects. Downward arrows indicate either out-of-scale measurements, or underestimation of mean thresholds due to exclusion of such measurements. Yr: age in years, dB HL: decibel hearing level, kHz: kilohertz.

all variants within each domain share the same phenotype; for some variants in the vWFA2 domain, the (calculated) age of onset is higher and the progression of HL over time is much more gradual than for the variants in the *lvd1* and the LCCL domain.²⁷

For 15 variants, we have obtained more than five data points in the analyses allowing for a variant-specific analysis of the age of onset and ATD. **Figure 5B** shows the parameter estimates for the calculated ages of onset (years) and ATD (dB/year) of these variants. Subjects in the vWFA2 domain group have a highly variable calculated age of onset. The variability for the calculated age of onset for variants in the LCCL group ranges between 17.6 – 47.9 years. There is limited data on the *lvd1* domain, but the calculated onset for the single variant with sufficient data is also much earlier than for those in the LCCL group.

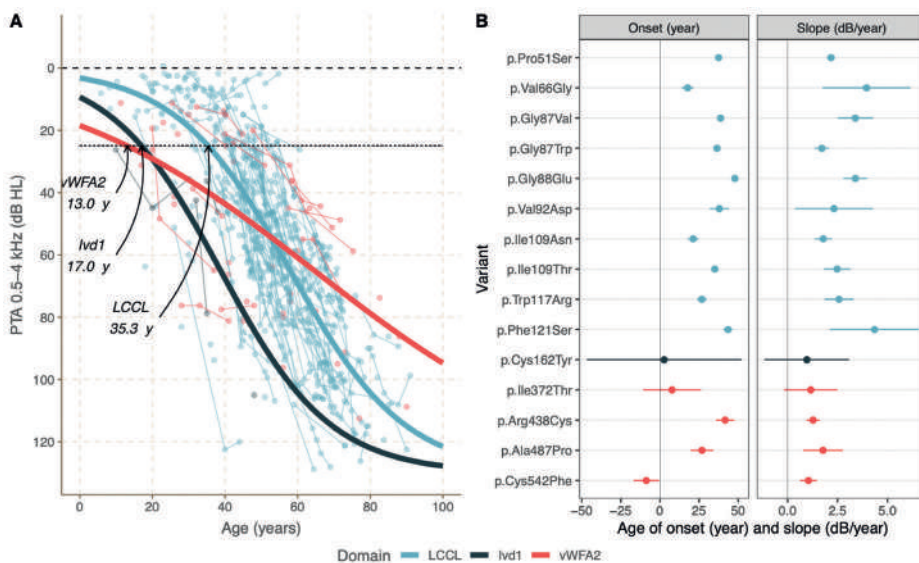


Figure 5. A phenotypic analysis of DFNA9; the calculated age of onset and annual threshold deterioration (ATD) across variants affecting cochlin within the LCCL, the *lvd1*, and the vWFA2 domain. (A) ATD of the pure-tone average across $PTA_{0.5-4kHz}$ with increasing age. Longitudinal data from single subjects are shown as a semi-transparent line between successive time-points. A non-linear logistic fit shows the average PTA over time for the LCCL domain (blue), the *lvd1* domain (black), and the vWFA2 domain (red). **(B)** The parameter estimates and their 95% confidence intervals for the calculated age of onset (arbitrarily set at 25 dB) and the ATD (dB/year) for the various variants within the LCCL domain (blue), the vWFA2 domain (red), and the *lvd1* domain (black). The dashed line shows the averaged calculated onset and ATD across all variants (unweighted for differences between the number of subjects for each variant).

Most data on the ATD are available for subjects in the LCCL domain group. The range varies considerably from 1.7 – 4.3 dB/year (see **Figure 5B** and the fits for the individual variants in **Figure S4**). The ATD in subjects in the *lvd1* group is similar to that of the LCCL

group (**Figure 5A**, pooled across all variants). However, individual variants may exhibit a slower progression of HL (**Figure 5B**). Subjects in the vWFA2 group have, on average, a more gradual ATD, independent from the rather variable calculated age of onset in this group. From this comprehensive analysis can be concluded that substantial phenotypic differences exist between the different *COCH* variants, both within and across domain groups (**Figure 5B**).

DISCUSSION

The systematic review of this study provides a comprehensive overview of the audiovestibular phenotype of all (n=27) currently (01-2021) known variants in *COCH* associated with DFNA9. Age-related typical audiograms were constructed for counseling purposes and display the progression of HL in decade steps per variant when sufficient data were available. A meta-analysis of crude audiometric data showed high phenotypic variability not only between individuals with different *COCH* variants but also between subjects with the same *COCH* variant. Furthermore, variants that affect the LCCL domain are associated with more progression of HL when compared to variants that affect the other cochlin domains. The results of the present study are also important because of recent promising developments in the evolving field of genetic therapies for hereditary hearing loss. The first preclinical study⁷⁴ on the development of such a therapy for DFNA9 was recently published. The results of the present meta-analysis can be used as a baseline to assess the efficacy of such novel therapeutics in future clinical trials.

The age of onset of HL and vestibular dysfunction in DFNA9 is variable and was assessed via self-reported history in the studies included in the systematic review, and calculated from audiometric data in the meta-analysis. The self-reported ages of onset for HL ranged from the 2nd to 7th decade of life and the 3rd to 7th decade for vestibular complaints. A self-reported age of onset is prone to recall bias⁷⁵ and reporting the age of onset in ranges without an average, or in decades (for example used by Parzefall et al.⁵⁴), can lead to over- or underestimation of the actual age of onset. Calculating the age of onset via a simple two-parameter model is a more robust indicator of the actual average age of onset than taking the average self-reported age of onset. Different opinions can be found in literature on whether audiologic or vestibular signs manifest first in subjects with the most-studied pathogenic variant in *COCH*: p.(Pro51Ser). Janssens de Varebeke et al. (2019) showed that subjects with this variant initially presented audiovestibular symptoms, with high variability, between 30 and 50 years of age.⁷⁰ Based on vestibular evaluation, they calculated that vestibular deterioration starts at an average age of 36 years and that vestibular areflexia is always present at 60 years. Additionally, they found that HL began at the age of 32.8 years,

which is slightly earlier than the result from our analysis (37.4 years). Based on their results, Janssens de Varebeke et al. (2019) concluded that vestibular impairment starts later but progresses faster than HL.⁷⁰ Their study, however, contradicts the study by Bischoff et al. (2005), who analyzed objective audiovestibular test results of the largest group of subjects (n=74) studied to date, all of which belong to a single Dutch DFNA9 family in which the p.(Pro51Ser) mutation was identified. Bischoff et al. (2005) showed that vestibular function deteriorated faster but also manifested earlier than HL.^{22,70} Based on our systematic review and the analyses performed in the studies mentioned above, we conclude that there are insufficient reliable studies to draw firm conclusions on whether audiologic or vestibular signs manifest first.

Previous genotype-phenotype correlation studies showed that vestibular dysfunction is most often reported by subjects with variants that affect the LCCL domain. Studies that reported on variants that affect the other cochlin domains, in general, reported a lack of vestibular complaints in their subjects.^{41,45-47,51,62,63} There are, however, also studies that explicitly reported an absence of complaints in the presence of vestibular areflexia.^{40,46} The latter is most likely due to central vestibular compensation, which occurs when subjects use somatosensory and/or visual cues to reweigh their loss of vestibular function.^{24,41,47} We have shown that HL in subjects in the vWFA2 domain group is slowly progressive, especially when compared to subjects in the LCCL domain group that experience much more progression of HL. A similar slower deterioration of vestibular function in the subjects of the vWFA2 domain group might go much more unnoticed since vestibular compensation is easier for subjects with a slow deterioration of vestibular function when compared to those with a faster deterioration or sudden vestibular loss. We, therefore, conclude that vestibular history is an unreliable assessment of vestibular function and that it is essential to include objective measurements of vestibular function in genotype-phenotype correlation studies of any type of hereditary HL. In addition, it is also important to realize that a wide range of objective tests can be used to evaluate vestibular function and that, even when similar tests are used, local calibration or used instruments may vary between different centers. This makes it challenging to review test results from different studies systematically. We, therefore, decided to apply a normative approach to the test results in this study. The majority of the included studies in this systematic review based their vestibular outcomes on calorization and/or rotary chair tests. These tests mainly assess lateral semicircular canal function and might therefore under- or overestimate the severity of vestibular dysfunction. To formulate more complete vestibular genotype-phenotype correlations in the future, we strongly advise to test both otolith organs by ocular and cervical Vestibular Evoked Myogenic Potential (VEMP) tests and to test the separate semicircular canals by video Head Impulse Tests (vHIT) to assess all parts of the vestibular organ.

The results of the present study can support physicians in counseling of DFNA9 patients on audiovestibular progression over time. The developed variant-specific ARTA are a useful tool for this purpose. In many subjects with DFNA9, progression of HL may eventually necessitate cochlear implantation.⁷⁶ The quality of the ARTA is depending on the number of subjects that can be included for each variant. This number varied highly in this study, from only one subject with the p.(Ala119Thr) variant to 208 subjects with the p.(Pro51Ser) variant. The latter variant is a well-studied founder mutation in the Dutch/Belgian population. The number of subjects with other pathogenic variants in *COCH*, and thus the amount of available phenotypic data, is much smaller. The results of audiometric evaluations of these subjects are therefore prone to selection bias, especially because inter- and intrafamilial variation is known to occur in DFNA9.^{23,26,29,35,39,52} In studies with large numbers of included subjects, as is the case for the p.(Pro51Ser) variant, the influence of selection bias decreases. Variation in the phenotype may also be explained by genetic modifiers or the cumulative contribution of environmental factors like the use of ototoxic medication, noise exposure, or chronic ear infections.¹ These confounders are usually not reported in the assessed studies but can significantly impact hearing and distort the clinical phenotype associated with *COCH* variants for which only a few subjects have been reported.

We observed, in line with the literature,¹³ the trend that progression of HL associated with variants within the LCCL domain group is faster than in the other domain groups. The age of onset, however, is highly variable between the cochlin domains, the individual *COCH* variants and even within families. This study identified clear phenotypic outliers that question the previously suggested correlation between the phenotype and affected cochlin domain. Firstly, subjects with the p.(Pro51Ser) or the p.(Val66Gly) variant, both affecting the LCCL domain, have a markedly different calculated age of onset of HL. Secondly, patients having the p.(Arg438Cys) variant that affects the vWFA2 domain show a remarkably high age of onset of HL (41,6 years). In contrast, the HL associated with the p.(Val66Gly) variant that affects the LCCL domain has a relatively early calculated age of onset (17,6 years). Thirdly, although the HL associated with the p.(Cys542Phe) and the p.(Ala487Pro) variants is comparably progressive, the calculated age of onset is much lower for subjects having the p.(Cys542Phe) variant (**Figure 5B**).

Over the last two decades, several studies evaluated the effects of various DFNA9-associated *COCH* variants on intracellular protein transport, post-translational processing, secretion and dimer/oligomer formation of mutant cochlin proteins.^{8,41,64,77-79} In 2014, Bae et al. analyzed the molecular effects of 7 different DFNA9-associated mutations, and observed a negative correlation between the amount of accumulated intracellular mutant cochlin in overexpression studies and the age of onset of HL. For this, they took an average

onset based on the reported range (i.e., $[\text{max-min}]/2$) of the (often self-reported) age of onset in small groups of individuals with the same variant. They correlated an earlier age of onset of HL in individuals with DFNA9-associated variants within the vWFA2 domain to intracellular aggregate formation, affecting intracellular trafficking and secretion of cochlin.⁸ A recent review on DFNA9 pathophysiology by Verdoodt et al.¹³ concluded that pathogenic variants affecting the LCCL domain do not appear to alter intracellular cochlin trafficking and secretion but instead lead to dimerization of cochlin proteins. While the term misfolding is often used for the formation of these dimers, there is no direct evidence that an alteration in folding of the mutant cochlin protein underlies the observed dimerization. We combined the suspected molecular mechanisms of action for the studied *COCH* variants with the calculated age of onset and progression of HL obtained in the meta-analysis (**Table S5**). These data do not provide a satisfactory explanation of the observed phenotypic differences between variants within the same functional domain. Therefore, we conclude that the observed molecular defects upon overexpression of mutant cochlin may indicate variant pathogenicity but that they are less suitable to predict how pathogenic variants in cochlin affect phenotypic outcomes of HL. The expression levels in such assays usually far exceed the physiological levels of cochlin expression. This is important since it is well known that overexpression of proteins can violate the balanced intracellular gene transcription and translation, thereby affecting protein folding, complex assembly, and downstream regulatory pathways. In other words, all of the molecular defects that were previously attributed to mutant cochlin, including defects in post-translational protein processing, protein misfolding, and associated defects in protein cleavage and secretion, have also been reported as so-called overexpression artifacts⁸⁰, and have potentially obscured the precise molecular genotype-phenotype correlation of DFNA9 mutations. Therefore, the observed discrepancies between the outcome of our meta-analysis, and the previously published molecular defects after overexpression of mutant cochlin proteins, advocate for more refined studies, using physiological expression levels and advanced cell culture models or animal models. Only then will we be able to elucidate why some of the variants affecting the LCCL or the vWFA2 domains lead a markedly different phenotype as compared to the majority of variants affecting these domains.

Conclusion

This study presents an extensive overview of HL and vestibular dysfunction associated with different pathogenic variants in *COCH* and is important for variant-specific counseling of individuals with DFNA9 and their relatives. Significant differences in both age of onset and progression of HL and vestibular dysfunction were seen between and within subjects with

different pathogenic variants in *COCH*. The results presented in this study are also essential for evaluating the efficacy of promising targeted genetic therapies in future clinical trials. Despite suggestions in previous studies, we do not find a clear correlation between the affected cochlin domains and the resulting phenotype. Further studies on DFNA9 animal and cell models are needed to elucidate the underlying pathogenic mechanisms.

ACKNOWLEDGEMENTS

This study was financially supported by a grant of the Heinsius-Houbolt foundation [to R.J.E.P. and H.K].

REFERENCES

1. World Health Organization. Deafness and hearing loss. (2018).
2. Tu, N.C. & Friedman, R.A. Age-related hearing loss: Unraveling the pieces. *Laryngoscope Investig Otolaryngol* 3, 68-72 (2018).
3. Oonk, A.M. *et al.* Progressive hereditary hearing impairment caused by a MYO6 mutation resembles presbycusis. *Hear Res* 299, 88-98 (2013).
4. Pauw, R.J. *et al.* Audiometric characteristics of a Dutch family linked to DFNA15 with a novel mutation (p.L289F) in POU4F3. *Arch Otolaryng Head Neck Surg* 134, 294-300 (2008).
5. O'Neill, M.E. *et al.* A gene for autosomal dominant late-onset progressive non-syndromic hearing loss, DFNA10, maps to chromosome 6. *Hum Mol Genet* 5, 853-6 (1996).
6. de Bruijn, S.E. *et al.* A RIPOR2 in-frame deletion is a frequent and highly penetrant cause of adult-onset hearing loss. *J Med Genet* (2020).
7. Janssens de Varebeke, S.P.F. *et al.* Bi-allelic inactivating variants in the *COCH* gene cause autosomal recessive prelingual hearing impairment. *Eur J Hum Genet* 26, 587-591 (2018).
8. Bae, S.H. *et al.* Identification of pathogenic mechanisms of *COCH* mutations, abolished cochlin secretion, and intracellular aggregate formation: genotype-phenotype correlations in DFNA9 deafness and vestibular disorder. *Hum Mutat* 35, 1506-13 (2014).
9. Robertson, N.G. *et al.* Mutations in a novel cochlear gene cause DFNA9, a human nonsyndromic deafness with vestibular dysfunction. *Nat Genet* 20, 299-303 (1998).
10. Boulassel, M.R., Tomasi, J.P., Deggouj, N. & Gersdorff, M. *COCH5B2* is a target antigen of anti-inner ear antibodies in autoimmune inner ear diseases. *Otology & Neurotology* 22, 614-618 (2001).
11. Jung, J. *et al.* Cleaved Cochlin Sequesters *Pseudomonas aeruginosa* and Activates Innate Immunity in the Inner Ear. *Cell Host Microbe* 25, 513-525 e6 (2019).
12. Rhyu, H.J., Bae, S.H., Jung, J. & Hyun, Y.M. Cochlin-cleaved LCCL is a dual-armed regulator of the innate immune response in the cochlea during inflammation. *BMB Rep* 53, 449-452 (2020).

13. Verdoodt, D., Van Camp, G., Ponsaerts, P. & Van Rompaey, V. On the pathophysiology of DFNA9: Effect of pathogenic variants in the COCH gene on inner ear functioning in human and transgenic mice. *Hear Res* 401, 108162 (2021).
14. Little, J. & Higgins, J. *The HuGENet™ HuGE Review Handbook, version 1.0*, (Centers for Disease Control and Prevention, 2006).
15. Higgins, J. & Green, S. *Cochrane Handbook for Systematic Reviews of Interventions Version 5.1.0*, (The Cochrane Collaboration, 2011).
16. York: Centre for Reviews and Dissemination. CRD's guidance for undertaking reviews in health care. . (University of York, 2011).
17. Moher, D., Liberati, A., Tetzlaff, J., Altman, D.G. & PRISMA Group. Preferred reporting items for systematic reviews and meta-analyses: the PRISMA statement. *Ann Intern Med* 151, 264-269 (2009).
18. Bom, S.J. *et al.* Progressive cochleovestibular impairment caused by a point mutation in the COCH gene at DFNA9. *Laryngoscope* 109, 1525-30 (1999).
19. de Kok, Y.J. *et al.* A Pro51Ser mutation in the COCH gene is associated with late onset autosomal dominant progressive sensorineural hearing loss with vestibular defects. *Hum Mol Genet* 8, 361-6 (1999).
20. Bom, S.J., Kemperman, M.H., Huygen, P.L., Luijendijk, M.W. & Cremers, C.W. Cross-sectional analysis of hearing threshold in relation to age in a large family with cochleovestibular impairment thoroughly genotyped for DFNA9/COCH. *Ann Otol Rhinol Laryngol* 112, 280-6 (2003).
21. Bom, S.J. *et al.* Speech recognition scores related to age and degree of hearing impairment in DFNA2/KCNQ4 and DFNA9/COCH. *Arch Otolaryngol Head Neck Surg* 127, 1045-8 (2001).
22. Bischoff, A.M. *et al.* Vestibular deterioration precedes hearing deterioration in the P51S COCH mutation (DFNA9): an analysis in 74 mutation carriers. *Otol Neurotol* 26, 918-25 (2005).
23. Verhagen, W.I. *et al.* Hereditary cochleovestibular dysfunction due to a COCH gene mutation (DFNA9): a follow-up study of a family. *Clin Otolaryngol Allied Sci* 26, 477-83 (2001).
24. Alberts, B., Selen, L.P.J., Verhagen, W.I.M., Pennings, R.J.E. & Medendorp, W.P. Bayesian quantification of sensory reweighting in a familial bilateral vestibular disorder (DFNA9). *J Neurophysiol* 119, 1209-1221 (2018).
25. Collin, R.W. *et al.* Identification of a novel COCH mutation, G87W, causing autosomal dominant hearing impairment (DFNA9). *Am J Med Genet A* 140, 1791-4 (2006).
26. Pauw, R.J. *et al.* Phenotype description of a novel DFNA9/COCH mutation, I109T. *Ann Otol Rhinol Laryngol* 116, 349-57 (2007).
27. Smits, J.J. *et al.* A Novel COCH Mutation Affects the vWFA2 Domain and Leads to a Relatively Mild DFNA9 Phenotype. *Otol Neurotol* 42, e399-e407 (2021).
28. Huygen, P.L.M., Pennings, R.J.E. & Cremers, C. Characterizing and distinguishing progressive phenotypes in nonsyndromic autosomal dominant hearing impairment. *Audiological Medicine* 1, 37-46 (2003).
29. Pauw, R.J., Huygen, P.L., Colditz, G.M. & Cremers, C.W. Phenotype analysis of an Australian DFNA9 family with the 1109N COCH mutation. *Ann Otol Rhinol Laryngol* 120, 414-21 (2011).
30. Kim, B.J. *et al.* Distinct vestibular phenotypes in DFNA9 families with COCH variants. *Eur Arch Otorhinolaryngol* 273, 2993-3002 (2016).
31. Hildebrand, M.S. *et al.* A novel mutation in COCH-implications for genotype-phenotype correlations in DFNA9 hearing loss. *Laryngoscope* 120, 2489-93 (2010).

32. Chen, D.Y., Chai, Y.C., Yang, T. & Wu, H. Clinical characterization of a novel COCH mutation G87V in a Chinese DFNA9 family. *Int J Pediatr Otorhinolaryngol* 77, 1711-5 (2013).
33. Fransen, E. *et al.* High prevalence of symptoms of Meniere's disease in three families with a mutation in the COCH gene. *Hum Mol Genet* 8, 1425-9 (1999).
34. de Varebeke, S.P. *et al.* Focal sclerosis of semicircular canals with severe DFNA9 hearing impairment caused by a P51S COCH-mutation: is there a link? *Otol Neurotol* 35, 1077-86 (2014).
35. Verhagen, W.I. *et al.* Familial progressive vestibulocochlear dysfunction caused by a COCH mutation (DFNA9). *Arch Neurol* 57, 1045-7 (2000).
36. Kemperman, M.H. *et al.* Audiometric, vestibular, and genetic aspects of a DFNA9 family with a G88E COCH mutation. *Otol Neurotol* 26, 926-33 (2005).
37. Verstreken, M. *et al.* Hereditary otovestibular dysfunction and Meniere's disease in a large Belgian family is caused by a missense mutation in the COCH gene. *Otol Neurotol* 22, 874-81 (2001).
38. Usami, S. *et al.* Mutations in the COCH gene are a frequent cause of autosomal dominant progressive cochleo-vestibular dysfunction, but not of Meniere's disease. *Eur J Hum Genet* 11, 744-8 (2003).
39. Lemaire, F.X. *et al.* Progressive late-onset sensorineural hearing loss and vestibular impairment with vertigo (DFNA9/COCH): longitudinal analyses in a Belgian family. *Otol Neurotol* 24, 743-8 (2003).
40. Baek, J.I. *et al.* The Trp117Arg mutation of the COCH gene causes deafness in Koreans. *Clin Genet* 77, 399-403 (2010).
41. Yuan, H.J. *et al.* Novel mutations in the vWFA2 domain of COCH in two Chinese DFNA9 families. *Clin Genet* 73, 391-4 (2008).
42. Luo, J. *et al.* Cardiac Troponin I R193H Mutation Is Associated with Mitochondrial Damage in Cardiomyocytes. *DNA Cell Biol* 40, 184-191 (2021).
43. Hildebrand, M.S. *et al.* Mutation in the COCH gene is associated with superior semicircular canal dehiscence. *Am J Med Genet A* 149A, 280-5 (2009).
44. Nagy, I., Horvath, M., Trexler, M., Repassy, G. & Patthy, L. A novel COCH mutation, V104del, impairs folding of the LCCL domain of cochlin and causes progressive hearing loss. *J Med Genet* 272, 265-265 (2005).
45. Gallant, E. *et al.* Novel COCH mutation in a family with autosomal dominant late onset sensorineural hearing impairment and tinnitus. *Am J Otolaryngol* 34, 230-5 (2013).
46. Tsukada, K. *et al.* Detailed hearing and vestibular profiles in the patients with COCH mutations. *Ann Otol Rhinol Laryngol* 124 Suppl 1, 100S-10S (2015).
47. Street, V.A. *et al.* A novel DFNA9 mutation in the vWFA2 domain of COCH alters a conserved cysteine residue and intrachain disulfide bond formation resulting in progressive hearing loss and site-specific vestibular and central oculomotor dysfunction. *Am J Med Genet A* 139A, 86-95 (2005).
48. Pauw, R.J. *et al.* Clinical characteristics of a Dutch DFNA9 family with a novel COCH mutation, G87W. *Audiol Neurootol* 12, 77-84 (2007).
49. Faletra, F. *et al.* A novel mutation in the vWFA2 domain of the COCH gene in an Italian DFNA9 family. *Audiological Medicine* 9, 4-7 (2010).
50. McComiskey, D.A. Investigation of the Genetic Cause of Hearing Loss in 28 Autosomal Dominant Families within the Newfoundland Founder Population. (Memorial University of Newfoundland (Canada), 2010).

51. Oziębło, D., Tacikowska, G., Skarżyński, H. & Oldak, M. Postlingual sensorineural hearing loss due to a very rare coch pathogenic variant. *J Hear Sci* 8(2018).
52. Wang, Q. *et al.* Different Phenotypes of the Two Chinese Proband with the Same c.889G>A (p.C162Y) Mutation in COCH Gene Verify Different Mechanisms Underlying Autosomal Dominant Nonsyndromic Deafness 9. *PLoS One* 12, e0170011 (2017).
53. Basu, A. *et al.* First Report of Bilateral External Auditory Canal Cochlin Aggregates (“Cochlinomas”) with Multifocal Amyloid-Like Deposits, Associated with Sensorineural Hearing Loss and a Novel Genetic Variant in COCH Encoding Cochlin. *Head Neck Pathol* 14, 808-816 (2020).
54. Parzefall, T. *et al.* Identification of a rare COCH mutation by whole-exome sequencing : Implications for personalized therapeutic rehabilitation in an Austrian family with non-syndromic autosomal dominant late-onset hearing loss. *Wien Klin Wochenschr* 130, 299-306 (2018).
55. Gu, X. *et al.* Massively Parallel Sequencing of a Chinese Family with DFNA9 Identified a Novel Missense Mutation in the LCCL Domain of COCH. *Neural Plast* 2016, 5310192 (2016).
56. Khetarpal, U. DFNA9 is a progressive audiovestibular dysfunction with a microfibrillar deposit in the inner ear. *Laryngoscope* 110, 1379-84 (2000).
57. Kim, B.J. *et al.* Targeted Exome Sequencing of Deafness Genes After Failure of Auditory Phenotype-Driven Candidate Gene Screening. *Otol Neurotol* 36, 1096-102 (2015).
58. Burgess, B.J. *et al.* Histopathology of the Human Inner Ear in the p.L114P COCH Mutation (DFNA9). *Audiol Neurootol* 21, 88-97 (2016).
59. Chang, M.Y. & Choi, B.Y. Strategy for the customized mass screening of genetic sensorineural hearing loss in koreans. *Korean J Audiol* 18, 45-9 (2014).
60. Wei, Q. *et al.* Targeted genomic capture and massively parallel sequencing to identify novel variants causing Chinese hereditary hearing loss. *J Transl Med* 12, 311 (2014).
61. Choi, B.Y. *et al.* Diagnostic application of targeted resequencing for familial nonsyndromic hearing loss. *PLoS One* 8, e68692 (2013).
62. Cho, H.J. *et al.* A novel COCH mutation associated with autosomal dominant nonsyndromic hearing loss disrupts the structural stability of the vWFA2 domain. *J Mol Med* 90, 1321-1331 (2012).
63. Gao, J. *et al.* Whole exome sequencing identifies a novel DFNA9 mutation, C162Y. *Clin Genet* 83, 477-81 (2013).
64. Jung, J., Kim, H.S., Lee, M.G., Yang, E.J. & Choi, J.Y. Novel COCH p.V123E Mutation, Causative of DFNA9 Sensorineural Hearing Loss and Vestibular Disorder, Shows Impaired Cochlin Post-Translational Cleavage and Secretion. *Hum Mutat* 36, 1168-75 (2015).
65. Sloan-Heggen, C.M. *et al.* Comprehensive genetic testing in the clinical evaluation of 1119 patients with hearing loss. *Hum Genet* 135, 441-450 (2016).
66. Mehregan, H. *et al.* Novel Mutations in KCNQ4, LHFPL5 and COCH Genes in Iranian Families with Hearing Impairment. *Arch Iran Med* 22, 189-197 (2019).
67. Danial-Farran, N. *et al.* Homozygote loss-of-function variants in the human COCH gene underlie hearing loss. *Eur J Hum Genet* 29, 338-342 (2021).
68. Booth, K.T. *et al.* Novel loss-of-function mutations in COCH cause autosomal recessive nonsyndromic hearing loss. *Hum Genet* 139, 1565-1574 (2020).

69. Dodson, K.M. *et al.* Etiology of unilateral hearing loss in a national hereditary deafness repository. *Am J Otolaryngol* 33, 590-4 (2012).
70. Janssens de Varebeke, S., Topsakal, V., Van Camp, G. & Van Rompaey, V. A systematic review of hearing and vestibular function in carriers of the Pro51Ser mutation in the COCH gene. *Eur Arch Otorhinolaryngol* 276, 1251-1262 (2019).
71. Bom, S.J., Kunst, H.P., Huygen, P.L., Cremers, F.P. & Cremers, C.W. Non-syndromal autosomal dominant hearing impairment: ongoing phenotypical characterization of genotypes. *Br J Audiol* 33, 335-48 (1999).
72. Bischoff, A.M. *et al.* Vertical corneal striae in families with autosomal dominant hearing loss: DFNA9/COCH. *Am J Ophthalmol* 143, 847-852 (2007).
73. Kemperman, M.H. *et al.* DFNA9/COCH and its phenotype. *Adv Otorhinolaryngol* 61, 66-72 (2002).
74. de Vrieze, E. *et al.* AON-based degradation of c.151C>T mutant COCH transcripts associated with dominantly inherited hearing impairment DFNA9. *Mol Ther Nucleic Acids* 24, 274-283 (2021).
75. Althubaiti, A. Information bias in health research: definition, pitfalls, and adjustment methods. *J Multidiscip Healthc* 9, 211-7 (2016).
76. Vermeire, K. *et al.* Good speech recognition and quality-of-life scores after cochlear implantation in patients with DFNA9. *Otol Neurotol* 27, 44-9 (2006).
77. Grabski, R. *et al.* Mutations in COCH that result in non-syndromic autosomal dominant deafness (DFNA9) affect matrix deposition of cochlin. *Hum Genet* 113, 406-16 (2003).
78. Robertson, N.G., Hamaker, S.A., Patriub, V., Aster, J.C. & Morton, C.C. Subcellular localisation, secretion, and post-translational processing of normal cochlin, and of mutants causing the sensorineural deafness and vestibular disorder, DFNA9. *J Med Genet* 40, 479-86 (2003).
79. Yao, J., Py, B.F., Zhu, H., Bao, J. & Yuan, J. Role of protein misfolding in DFNA9 hearing loss. *J Biol Chem* 285, 14909-19 (2010).
80. Gibson, T.J., Seiler, M. & Veitia, R.A. The transience of transient overexpression. *Nat Methods* 10, 715-21 (2013).

SUPPLEMENTARY TABLES

Table S1. Search strategy

Database	(MeSH) terms
PubMed/Gene database	"COCH protein, human" [Supplementary Concept] OR "Deafness, Autosomal Dominant 9" [Supplementary Concept]
	OR
	COCH [text word (tw)] OR cochlin [tw] OR coagulation factor C homolog [tw] OR Coch5B2 [tw] OR COCH-5B2 [tw] OR DFNA9 [tw]
	OR
	PubMed Links for Gene
EMBASE	Cochlin/
	OR
	(COCH OR cochlin OR coagulation factor C homolog OR Coch5B2 OR COCH-5B2 OR DFNA9)
The Cochrane Library	(Search "All text") COCH OR Cochlin OR "coagulation factor C homolog" OR Coch5B2 OR COCH-5B2 OR DFNA9
Web of Science	(Search on "Topic") COCH OR cochlin OR "Coagulation factor C homolog" OR Coch5B2 OR COCH-5B2 OR DFNA9

PubMed, NCBI's Gene database, EMBASE, the Cochrane Library and Web of Science were searched for relevant studies. All available MeSH terms were combined with free text words of all known synonyms of *COCH* and DFNA9.

Table S2. Study characteristics and overview of the audiovestibular phenotypes

Variant in COCH Protein domain	Author year	Population /ethnicity	Sample size		Clinical evaluation				Self-reported age of onset and complaints				
			Genetically confirmed	Clinically suspected	Audiologic	Vestibular	Additional	Onset of hearing loss	Onset of vestibular complaint	Complaints	Vestibular results		
											Va	Vh	Vn
c.113G>A (p.Gly38Asp) LCCL	Wei et al, 2014	Chinese	13	NA	History, PE, PTA	History, PE	NA	Late-onset	NA	No symptoms			
	Chang et al, 2014	Korean	1	NA	History, PTA	History, VNG, caloric, rotatory	NA	41	NA	No symptoms			
	Choi et al, 2013	Korean	1	NA	History, PTA	History, VNG, caloric, rotatory	NA	41	NA	No symptoms	NA	2	1
	Kim et al, 2016	Korean	6	12	History, PTA	History, PE, caloric, rotatory, EOG	NA	30-40	NA	No symptoms			
c. 151C>T (p.Pro51Ser) LCCL	Bom et al, 1999	Dutch	16	6	History, PE, PTA	History, ENG, caloric, rotatory	History (CVD), PE (neurologi/c)	36 - 63 Calculated: 34 - 51	NA	NA	NA		
	de Kok et al, 1999	Dutch	23	24	History, PE (otologic), PTA	History, EOG, rotatory	PE (neurologi/c)	30 - 62	30 - 62	Instability in the dark, oscillopsia	62	23	17
	Bom et al, 2003	Dutch	34	NA	History, PTA	NA	NA	Calculated: 32,1 - 40,7	NA	NA	NA		

Table S2. (continued)

Variant in COCH Protein domain	Author year	Population /ethnicity	Sample size		Clinical evaluation				Self-reported age of onset and complaints				
			Genetically confirmed	Clinically suspected	Audiologic	Vestibular	Additional	Onset of hearing loss	Onset of vestibular complaint	Complaints	Vestibular results		
										Va	Vh	Vn	
c.151C>T (p.Pro51Ser) LCCL (continued)	Fransen et al, 1999	Belgian	34	13	History, PE, PTA	History, PE, vestibular testing (N/S)	NA	42 (35 – 56)	42 (35 – 56)	Vertigo/no symptoms			
	Verstreken et al, 2001	Belgian	60	13	History, PE, PTA, supraliminary tests*	History, ENG, caloric, rotatory	CT, MR, PE (neurologic, ophthalmic), urine sediment	39 ± 10 (20 – 56)	38 ± 11 (5 – 57)	Instability in the dark, vertigo, tendency to fall, drunken feeling, aural fullness			
	Janssens de Varebeke et al, 2014	Caucasian	9	NA	History, PTA	History, ENG, caloric, rotatory	CT, MR, CBCT	46*	35 – 50	Instability in the dark, vertigo, oscillopsia, aural fullness, dizziness			
	Born et al, 2001	Dutch Flemish	42	NA	PTA, SA	NA	NA	42	NA	NA	62	23	
	Verhagen et al, 2000	NA	4	NA	History, PTA	ENG, caloric rotatory	NA	Calculated: 28	40	Instability in the dark, vertigo, nausea, oscillopsia			
	Bischoff et al, 2005	Dutch	30	14	History, PE, PTA, SA, BAEP	History, ENG, rotatory	CT, MR, PE (neurologic)	39 (18 – 51) Calculated: 43 (38 – 49)	34 (29 – 39)	Vertigo/no symptoms			
	Lemaire et al, 2003	Belgian	16	NA	History, PE, PTA, SA	History, ENG, caloric rotatory	NA	30 – 45	30 - 45	Instability in the dark, vertigo, oscillopsia, aural fullness/no symptoms			

Table S2. (continued)

Variant in COCH Protein domain	Author year	Population /ethnicity	Sample size		Clinical evaluation			Self-reported age of onset and complaints					
			Genetically confirmed	Clinically suspected	Audiologic	Vestibular	Additional	Onset of hearing loss	Onset of vestibular complaint	Complaints	Vestibular results		
										Va	Vh	Vn	
	Verhagen et al, 2001	Dutch	8	8	History, PTA	History, ENG, caloric, rotatory	History (CVD)	35 – 45	4 th – 5 th decade	Instability in the dark, vertigo, nausea, oscillopsia, motion sickness/no symptoms			
	Parzefall et al, 2018	Austrian	5	2	History, PE (otologic), PTA, Freiburger-SA	NA	CT, MR	4 th – 5 th decade	NA	NA			
c.151C>T (p.Pro51Ser) LCCL (continued)	Hildebrand et al, 2009	American	6	10	History, PTA	History	CT	4 th – 7 th decade	NA	Instability in the dark, dizziness, no symptoms	62	23	17
	McComiskey et al, 2010	Canadian	7	5	History, PTA	History	History (ophthalmic), CT	35 – 49	32 – 50	Instability, vertigo, dizziness/no symptoms			
	Alberts et al, 2018	Dutch	16	NA	NA	Rotatory, VEMP, vHIT, velocity step tests, caloric	NA	NA	< 49 ^a	NA			
c.197T>G (p.Val66Gly) LCCL	Robertson et al, 1998	American	16	5	History, PE (ORL, genetic), PTA, SA	Vestibular tests(N/S)	PE (neurologic), MR	20.8	NA	No symptoms			
	Khetarpal et al, 2000	American	3	NA	History, PE (ORL)	History, ENG, SVAR, S/D posturography	PE (neurologic)	16 – 26	21 – 28	NA	3	NA	NA

Table S2. (continued)

Variant in COCH Protein domain	Author year	Population /ethnicity	Sample size		Clinical evaluation			Self-reported age of onset and complaints					
			Genetically confirmed	Clinically suspected	Audiologic	Vestibular	Additional	Onset of hearing loss	Onset of vestibular complaint	Complaints	Vestibular results		
										Va	Vh	Vn	
c.226G>A (p.Ala76Thr) LCCL	Sloan-Heggen et al, 2016	Caucasian	3	NA	History, PE, PTA	History	NA	NA	Teens - 40	40	NA	NA	NA
c.259G>T (p.Gly87Trp) LCCL	Collin et al, 2006 Pauw et al, 2007a	Dutch Dutch	1 17	24 8	History, PTA History, PE, PTA, SA	History, ENG History, ENG, caloric, rotatory	NA PE (ophthalmic)	43 (10 – 66)	51 (30 – 65)	Instability in the dark, vertigo, tendency to fall/no symptoms	2	8	NA
c.260G>T (p.Gly87Val) LCCL	Chen et al, 2013	Chinese	5	3	History, PE, PTA, OAE	History, PE, ENG	NA	Mid – 40s	NA	Vestibular symptoms	NA	1	NA
c.263G>A (p.Gly88Glu) LCCL	Kemperman et al, 2005 Robertson et al, 1998	Dutch American	16 6	13 6	History, PE (otologic) PTA, SA History, PE (ORL, genetic), PTA, SA	History, ENG, caloric, rotatory Vestibular tests(N/5)	History (CVD), CT, MR PE (neurologic), MR	46 (40 – 68) 4 th decade – 5 th decade	Approximately the same age as HI 48 – 67	Instability in the dark, vertigo, tendency to fall/no symptoms Vertigo, oscillopsia, balance problems, dizziness/no symptoms	5	2	6
	Tsukada et al, 2015	Japanese	4	1	History, PTA, SA	History, caloric, VEMP, CDP	NA	Early 50s	64	Vestibular symptoms, dizziness/no symptoms			

Table S2. (continued)

Variant in COCH Protein domain	Author year	Population /ethnicity	Sample size		Clinical evaluation				Self-reported age of onset and complaints				
			Genetically confirmed	Clinically suspected	Audiologic	Vestibular	Additional	Onset of hearing loss	Onset of vestibular complaint	Complaints	Vestibular results		
										Va	Vh	Vn	
c.275T>A (p.Val92Asp) LCCL	Gu et al, 2016	Chinese	7	4	History, PE, PTA	History, ENG, caloric	NA	2 nd – 3 rd decade	NA	Vertigo, dizziness/ no symptoms	NA	5	NA
c.311_313delTAG (p.Val104del) LCCL	Nagy et al, 2005	Hungarian	1	NA	History, PTA	NA	NA	32	32	Vertigo, nausea, vomiting	1	NA	NA
c.326T>A (p.Ile109Asn) LCCL	Pauw et al, 2011	Australian	8	6	History, PTA, SA	History	NA	30-43	After symptoms of HL	Instability in the dark, vertigo, oscillopsia, tendency to fall/no symptoms	NA	NA	NA
	Kamarinos et al, 2001	Australian	13	NA	NA	NA	NA	2 nd – 3 rd decade	By the time of profound HL	Instability in the dark, vertigo, oscillopsia, balance problems	NA	NA	NA
c.326T>C (p.Ile109Thr) LCCL	Pauw et al, 2007b	Dutch	11	2	History, PE, PTA, SA	History, ENG, caloric, rotatory	PE (ophthalmic)	43 (35-52)	65 (58 – 73)	Instability in the dark, vertigo, oscillopsia, tendency to fall/no symptoms	NA	NA	6

Table S2. (continued)

Variant in COCH Protein domain	Author year	Population /ethnicity	Sample size		Clinical evaluation			Self-reported age of onset and complaints					
			Genetically confirmed	Clinically suspected	Audiologic	Vestibular	Additional	Onset of hearing loss	Onset of vestibular complaint	Complaints	Vestibular results		
										Va	Vh	Vn	
	Burgess et al, 2016	American	1	4	History, PTA	History	CT	30	NA	No symptoms			
c.341T>C (p.Leu114Pro) LCCL	Chang et al, 2014	Korean	1	NA	History, PTA	History	NA	28	NA	No symptoms	NA	NA	NA
	Choi et al, 2013	Korean	1	NA	History, PTA	History	NA	28	NA	No symptoms			
c.349T>C (p.Trp117Arg) LCCL	Baek et al, 2010***	Korean	10	2	History, PE, PTA, SA	History, PE, caloric	NA	Early 30s	NA	Dizziness/no symptoms	1	NA	NA
c.355G>A (p.Ala119Thr) LCCL	Usami et al, 2003	Japanese	1	1	History, PTA	History, caloric	CT	4 th decade	4 th decade	Vertigo, dizziness	NA	1	NA
c.362T>C (p.Phe121Ser) LCCL	Hildebrand et al, 2010	American	7	3	PE (otologic & genetic), PTA	ENG, caloric	NA	2 nd – 3 rd decade	NA	Vertigo, positional nystagmus, balance problems, dizziness	NA	NA	NA
c.368T>A (p.Val123Glu) Ivd1	Jung et al, 2015	Korean	3	3	History, PTA, ABR	History, caloric	CT, MR	44.4 ± 6.3 (37 – 52)	NA	No symptoms	NA	NA	1

Table S2. (continued)

Variant in COCH Protein domain	Author year	Population /ethnicity	Sample size		Clinical evaluation				Self-reported age of onset and complaints			
			Genetically confirmed	Clinically suspected	Audiologic	Vestibular	Additional	Onset of hearing loss	Onset of vestibular complaint	Complaints	Vestibular results	
										Va	Vh	Vn
	Kim et al, 2015	Korean	1	5	History, PE (otologic & genetic), PTA	NA	NA	NA	30 ^a	NA	NA	
c.485G>A (p.Cys162Tyr) Ivd1	Wang et al, 2017	Chinese	2	28	History, PTA, tympanometry, TEOAE, DPOAE	History, VNG, ECOG, caloric, VEMP, vHIT	NA	NA	2 nd – 4 th decade	4 th decade	Vertigo, aural fullness/no symptoms	NA
	Gao et al, 2013	Chinese	9	16	History, PTA	History	NA	NA	17	NA	No symptoms	NA
	Kim et al, 2016	Korean	5	1	PTA	History, PE, caloric, rotatory	NA	NA	NA	NA	Vertigo, vomiting, aural fullness, dizziness	NA
c.1115T>C (p.Ile372Thr) vWFA2	Oziębło et al, 2018	Polish	5	2	History, PTA	History, VEMP (cervical and ocular)	NA	NA	28,25 years (15 – 47 years)	NA	No symptoms	2
	Tsukada et al, 2015	Japanese	3	6	History, PTA, SA	History	NA	NA	33-42	NA	No symptoms	1
c.1312C>T (p.Arg438Cys) vWFA2	Smits et al, 2021	Dutch	14	1	History, otoscopy	History	MRI	MRI	33 (18-49)	NA	Balance problems	4
												NA
												10

Table S2. (continued)

Variant in COCH Protein domain	Author year	Population /ethnicity	Sample size		Clinical evaluation				Self-reported age of onset and complaints				
			Genetically confirmed	Clinically suspected	Audiologic	Vestibular	Additional	Onset of hearing loss	Onset of vestibular complaint	Complaints	Vestibular results		
											Va	Vh	Vn
c.119G_12139del18 (p.Ile399_ Ala404del) vWFA2	Gallant et al, 2013	American	3	5	History, PE	NA	MR	Mid to late 20s	NA	No symptoms	NA	NA	NA
c.1459C>G (p.Ala487Pro) vWFA2	Faleria et al, 2011	Italian	9	1	History, PE (ORL), PTA	History, caloric	NA	2 nd - 3 rd decade	NA	Vertigo, dizziness	NA	1	NA
c.1535T>C (p.Met512Thr) vWFA2	Yuan et al, 2008	Chinese	2	NA	History, audiometric testing (N/S)	Oculomotor test, CDP, rotatory, SOT, VEMP	NA	43	NA	No symptoms	NA	NA	2
c.1580T>G (p.Phe527Cys) vWFA2	Cho et al, 2012	Korean	2	4	History, PE, PTA	History, **PE (vestibular) posturography, rotatory	NA	26*	NA	No symptoms	NA	NA	1
c.1621A>T, (p.Ile541Phe) vWFA2	Basu et al, 2019	Caucasian	1	3	History, otoscopy, PTA	NA	CT, autoimmune workup	Childhood	NA	NA	NA	NA	NA
c.1624T>C (p.Cys542Arg) vWFA2	Tsukada et al, 2015	Japanese	1	3	History, PTA, SA	History	NA	Grade school	Grade school	Vertigo	NA	NA	NA

Table S2. (continued)

Variant in COCH Protein domain	Author year	Population /ethnicity	Sample size		Clinical evaluation			Self-reported age of onset and complaints					
			Genetically confirmed	Clinically suspected	Audiologic	Vestibular	Additional	Onset of hearing loss	Onset of vestibular complaint	Complaints	Vestibular results		
										Va	Vh	Vn	
c.1625G>A (p.Cys542Tyr) vWFAZ	Yuan et al, 2008	Chinese	6	NA	History, audiometric testing (N/S)	Oculomotor test, CDP, rotatory, SOT, VEMP	NA	2 nd – 5 th decade	NA	No symptoms	NA	6	NA
c.1625G>T (p.Cys542Phe) vWFAZ	Street et al, 2005	American	16	4	History, PTA, tympanometry	History, oculomotor test (VNG), CDP, EOG, ENG, caloric, rotatory, VEMP	NA	16 – 25	NA	No symptoms	NA	3	NA
	Sloan-Heggen et al, 2016	Caucasian	3	NA	History, PE, PTA	History	NA	NA	NA	NA	NA		

COCH transcript NM_004086.2 was used as reference sequence. Vestibular function assessment (both examination and reports of subjects) varied between and within subjects. Therefore, all findings in a study are reported. NA: not available, ^a: derived from the audiogram, pure tone average or vestibular test(s), Vb, bilateral vestibular dysfunction; Vu, unilateral vestibular dysfunction; Vn, no vestibular dysfunction; PTA, pure tone audiometry; PE, physical examination; OAE, otoacoustic emission; SA, speech audiometry; BAEP, brainstem auditory evoked potential; supraliminary tests*, speech audiometry, tone-decay test, short increment sensitivity index test, impedance audiometry, transient evoked otoacoustic emissions & brainstem auditory responses; TEOAE, transient evoked product otoacoustic emission; DPOAE, distortion product otoacoustic emission; ABR, auditory brainstem response; ECOG, electrocochleography; ENG, electronystagmography; SVAR, sinusoidal vertical axis rotation; S/D posturography, static & dynamic posturography; CDP, computerized dynamic posturography; SOT, sinusoidal oscillation test; VEMP, vestibular evoked myogenic potential, EOG, electrooculography; VNG, videonystagmography; vHIT, video head impulse test, **PE (vestibular: *spontaneous nystagmus, head shaking test, Dix-Hallpike test, positional test*); CT, Computed Tomography; MR, Magnetic Resonance; CBCT, Cone Beam Computed Tomography. ***One family (15) described by Robertson et al. (1998), with the p.Trp117Arg variant, was excluded because of a lack of phenotypic data.⁸

Table S3. Risk of bias summary

	Risk of bias							
	D1	D2	D3	D4	D5	D6	D7	D8
Robertson et al. 1998	+	X	X	+	+	+	+	-
Bom et al. 1999	+	+	X	-	+	+	+	+
De Kok et al. 1999	X	X	X	+	+	+	+	+
Fransen et al. 1999	X	X	X	+	+	+	+	-
Verhagen et al. 2000	+	+	+	+	+	+	X	X
Khetarpal et al. 2000	X	+	X	-	X	+	-	-
Verstreken et al. 2001	X	X	+	+	+	+	X	+
Bom et al. 2001	X	+	+	-	+		-	X
Verhagen et al. 2001	+	+	X	-	+	+	-	+
Kamarinou et al. 2001	+	X	X	+	-	-	+	-
Bom et al. 2003	X	+	-	+	+		+	+
Lemaire et al. 2003	+	X	X	+	+	+	-	+
Usami et al. 2003	+	+	X	+	+	+	+	+
Bischoff et al. 2005	+	+	X	-	+	+	X	+
Kemperman et al. 2005	+	X	+	+	+	+	+	+
Nagy et al. 2005	+	+	X	+	+	-	+	X
Street et al. 2005	+	X	+	+	+	+	+	-
Pauw et al. 2007a	X	+	X	+	+	+	+	+
Pauw et al. 2007b	+	+	+	+	+	+	+	+
Collin et al. 2006	+	X	+	+	+	+	+	-
Yuan et al. 2008	X	+	X	+	+	+	+	X
Hildebrand et al. 2009	+	X	X	-	+	X	-	+
McComiskey et al. 2010	+	+	+	+	+	X	-	+
Baek et al. 2010	+	+	+	+	+	+	+	X
Hildebrand et al. 2010	+	X	X	+	+	+	+	-
Pauw et al. 2011	+	+	+	+	+	X	+	-
Fal.etra et al. 2011	+	+	+	+	+	+	+	X
Cho et al. 2012	+	+	+	+	+	+	+	X

Choi et al. 2013	+	+	X	+	+	●	+	+
Chen et al. 2013	+	+	+	+	+	+	+	+
Gao et al. 2013	+	+	X	+	+	●	+	-
Galant et al. 2013	+	+	X	+	-	●	+	-
Wei et al. 2014	+	+	+	+	+	X	+	-
Chang et al. 2014	+	+	X	+	+	+	+	X
de Varebeke et al. 2014	X	+	+	-	+	+	-	+
Tsukada et al. 2015	+	X	+	+	+	+	+	X
Jung et al. 2015	+	X	X	+	+	+	+	-
Kim et al. 2015	X	+	-	+	+	●	+	+
Kim et al. 2016	+	+	+	+	+	+	+	-
Gu et al. 2016	+	X	X	+	+	+	+	X
Burgess et al. 2016	+	+	+	+	+	●	-	+
SloanHighHeggen et al. 2016	+	+	+	+	+	X	+	+
Wang et al. 2017	X	+	+	+	+	+	+	-
Parzefal et al. 2018	+	+	+	+	+	●	+	-
Alberts et al. 2018	+	+	+	+	●	+	+	-
Ozieblo et al. 2018	X	+	+	+	+	+	+	+
Basu et al. 2019	X	+	X	+	●	●	+	+
Smits et al. 2020	+	+	+	+	+	+	+	-

D1: Selective inclusion
 D2: Selective loss to follow-up
 D3: Selective reporting
 D4: Genotype assessment
 D5: Audiologic phenotype assessment
 D6: Vestibular phenotype assessment
 D7: Population stratification
 D8: Other confounders

Judgement
 X High
 - Unclear
 + Low
 ● Not applicable

Judgements of two reviewers about each risk of bias items for all included studies.

Table S4. Variants in COCH that are not associated with DFNA9

Variant (zygosity)	References	Sample size		Age of onset (in years)		Progression of hearing loss	Vestibular dysfunction		Remarks
		Genetically	Clinically	HL	V		Examination	Reported by subjects	
c.266C>A (p.Pro89His) (heterozygous)	Dodson et al. 2012	1	NA	Birth	NA	NA	NA	NA	Enlarged vestibular Aqueduct; identified in two in-house normal hearing subjects
c.292C>T (p.Arg98X) (homozygous)	Janssens de Varebeke et al. 2018	2	NA	Birth	First decade	1.8 – 2.0 dB/year	Vb / Vn	Vestibular symptoms/no symptoms	DFNB110 phenotype
c.116T>A (p.Leu39X) (homozygous)	Mehregan et al. 2019	3	3	School age	NA	NA	NA	No symptoms	DFNB110 phenotype
c.984_985dup (p.Phe329Leufs*16) (homozygous)	Daniel-Farran et al. 2020	3	NA	Pre-lingual	NA	Yes	NA	NA	DFNB110 phenotype
c.631G>T (p.Glu211Ter) (homozygous)	Booth et al. (2020)	1	NA	Birth	NA	NA	NA	NA	DFNB110 phenotype
c.439A>T (p.Lys147Ter)*	Booth et al. (2020)	1	NA	Birth	NA	NA	NA	NA	DFNB110 phenotype
c.571_572delinsAG (p.Val191Arg) (compound heterozygous)	Booth et al. (2020)	1	NA	Birth	NA	NA	NA	NA	DFNB110 phenotype
c.271C>G (p.Arg91Gly) (homozygous)	Booth et al. (2020)	1	NA	Birth	NA	NA	NA	NA	DFNB110 phenotype
c.1093_1101del (p.Ser365_Asn367del) (homozygous)	Booth et al. (2020)	1	NA	Birth	NA	NA	NA	NA	DFNB110 phenotype

Study characteristics and overview of the audiovestibular phenotype of COCH variants not associated with DFNA9. COCH transcript NM_004086.2 was used as reference sequence. NR, not reported; HL, hearing loss; V, vestibular dysfunction; Vb, bilateral vestibular dysfunction; Vn, no vestibular dysfunction.

Table S5. Suspected mechanisms of action of different pathogenic COCH variants (based on literature) correlated to calculated age of onset and progression of HL.

Variant in Cochlin	Protein Domain	ER to Golgi transport	Cleavage	Secretion	Dimerisation /aggregation	Number of subjects in analysis (number of audiograms in analysis)	Calculated age of onset (years)	Progression (dB/year)
p.Pro51Ser	LCCL	normal	↓	normal	dimerization	130(397)	37,44	2,17
p.Val66Gly	LCCL	normal	↓	normal	dimerization	7(9)	17,63	3,95
p.Gly87Trp	LCCL	normal	N/A	normal	none	28(67)	36,43	1,71
p.Gly87Val	LCCL	normal	N/A	N/A	N/A	5(11)	38,75	3,39
p.Gly88Glu	LCCL	normal	↓↓	normal	dimerization	26(61)	47,88	3,39
p.Val92Asp	LCCL	normal	N/A	N/A	N/A	6(6)	37,92	2,32
p.Ile109Thr	LCCL	normal	↓↓↓	↓↓↓	dimerization	11(34)	35,06	2,48
p.Ile109Asn	LCCL	normal	N/A	N/A	N/A	8(52)	21,24	1,78
p.Trp117Arg	LCCL	normal	↓↓↓	normal	none	10(10)	26,79	2,57
p.Phe121Ser	LCCL	normal	N/A	N/A	N/A	10(18)	43,5	4,35
p.Cys162Tyr	lvd1	ER-retention	↓↓↓	↓↓	oligomerization	3(7)	2,7	0,96
p.Ile372Thr	vWFA2	N/A	N/A	N/A	N/A	4(6)	7,7	1,16
p.Arg438Cys	vWFA2	N/A	N/A	N/A	N/A	14(29)	41,64	1,28
p.Ala487Pro	vWFA2	ER-retention	N/A	↓↓	oligomerization	9(9)	26,85	1,77
p.Cys542Phe	vWFA2	normal	N/A	normal	N/A	14(17)	-8,73	1,04

Table showing the effects of various DFNA9-associated COCH variants on intracellular protein transport, post-translational processing, secretion and dimer/oligomer formation of mutant cochlin proteins in relation to the calculated age of onset and annual progression. Different colors show the relative severity of the annual progression (last column) the calculated age of onset (second to last column), where green indicates slow progression of late onset, and red fast progression or early onset. NP_004077:1 was used as reference. NR: not reported.

SUPPLEMENTARY FIGURES

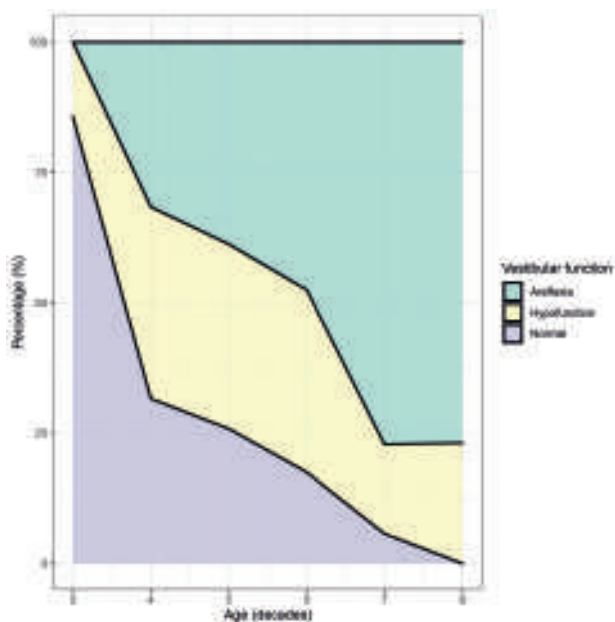


Figure S1. Vestibular function, based on objective vestibular examinations, over decades in percentage of subjects from the LCCL group Figure showing the distribution of vestibular function (Areflexia, Hypofunction, Normal) in percentages over time of patients with pathogenic variants affecting the LCCL domain

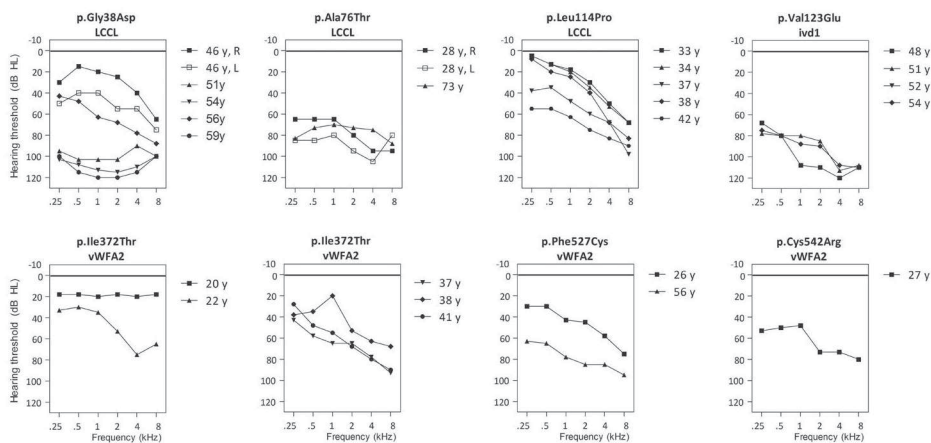
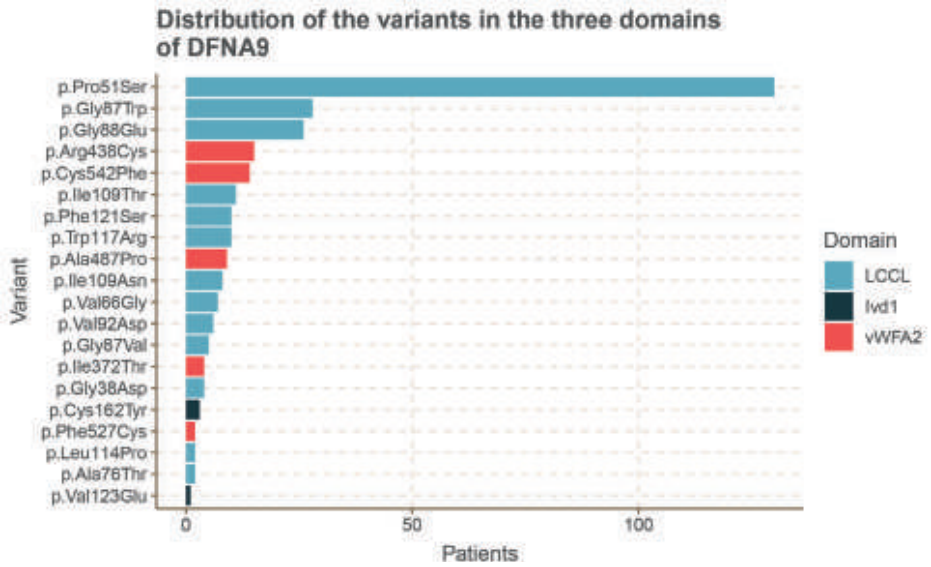
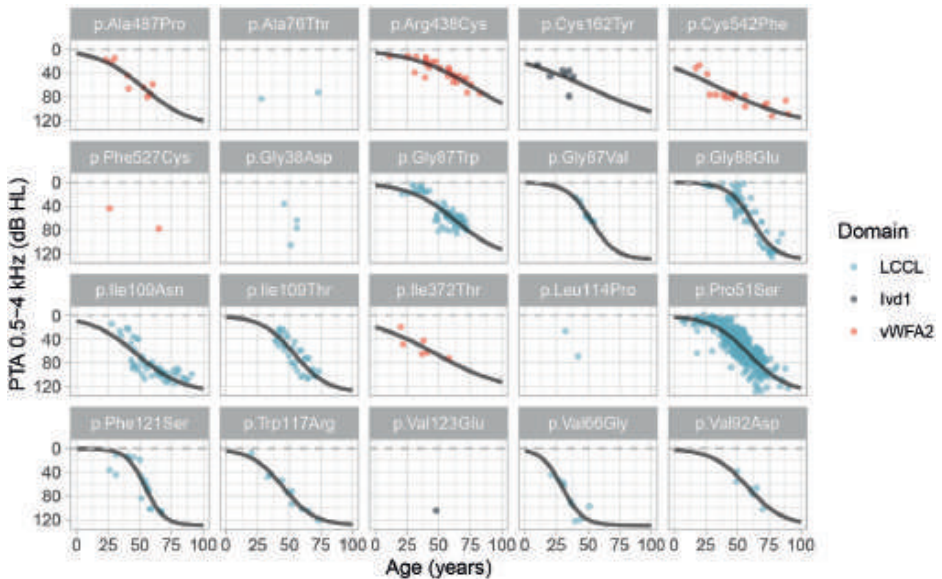


Figure S2. Individual audiograms at various ages of affected subjects of seven COCH variants Air conduction threshold levels are depicted. In the case of asymmetry open symbols were used for the left ear. The audiometric data for p.Ile372Thr has been split in two panels for clarity purposes. R, right ear; L, left ear; dBHL, decibel hearing level; kHz, kilohertz; y, age in years.



2.2

Figure S3. Distribution of subjects The distribution of the number of subjects per variant categorized by affected cochlin domain (LCCL, lvd1 and vWFA2) used in the meta-analysis.





Chapter 3

Exploring the missing heritability in subjects with hearing loss, enlarged vestibular aqueducts, and a single or no pathogenic *SLC26A4* variant

Jeroen J. Smits*, Suzanne E. de Bruijn*, Cornelis P. Lanting, Jaap Oostrik, Luke O’Gorman, Tuomo Mantere, DOOFNL Consortium, Frans P.M. Cremers, Susanne Roosing, Helger G. Yntema, Erik de Vrieze, Ronny Derks, Alexander Hoischen, Sjoert A.H. Pegge, Kornelia Neveling, Ronald J.E. Pennings, and Hannie Kremer
(*gelijke bijdrage)

Human Genetics, in press

ABSTRACT

Pathogenic variants in *SLC26A4* have been associated with autosomal recessive hearing loss (arHL) and a unilateral or bilateral enlarged vestibular aqueduct (EVA). *SLC26A4* is the second most frequently mutated gene in arHL. Despite the strong genotype-phenotype correlation, a significant part of cases remains genetically unresolved. In this study, we investigated a cohort of 28 Dutch index cases diagnosed with HL in combination with an EVA but without (M0) or with a single (M1) pathogenic variant in *SLC26A4*. To explore the missing heritability, we first determined the presence of the previously described EVA-associated haplotype (Caucasian EVA (CEVA)), characterized by 12 single nucleotide variants located upstream of *SLC26A4*. We found this haplotype and a delimited V1-CEVA haplotype to be significantly enriched in our M1 patient cohort (10/16 cases). The CEVA haplotype was also present in two M0 cases (2/12). Short- and long-read whole genome sequencing and optical genome mapping could not prioritize any of the variants present within the CEVA haplotype as the likely pathogenic defect. Short-read whole genome sequencing of the six M1 cases without this haplotype and the two M0/CEVA cases only revealed previously overlooked or misinterpreted splice-altering *SLC26A4* variants in two cases, who are now genetically explained. No deep-intronic or structural variants were identified in any of the M1 subjects. With this study, we have provided important insights that will pave the way for elucidating the missing heritability in M0 and M1 *SLC26A4* cases. For pinpointing the pathogenic effect of the CEVA haplotype, additional analyses are required addressing defect(s) at the RNA, protein, or epigenetic level.

INTRODUCTION

SLC26A4 encodes the transmembrane anion transporter pendrin and is most abundantly expressed in the inner ear, thyroid gland, kidney, and airways epithelia.¹⁻⁵ The 780 amino acid protein is part of the solute carrier family 26 and plays a pivotal role in chloride, bicarbonate and iodine transport. In the inner ear, pendrin functions as a $\text{Cl}^-/\text{HCO}_3^-$ exchanger. The protein is expressed in the epithelial cells of the cochlea (outer sulcus and spindle cells), the vestibular labyrinth (transitional cells), and the endolymphatic duct and sac (mitochondrial-rich cells).^{6,7} Expression of pendrin is essential for the development of the (murine) auditory and vestibular system and for maintaining ion homeostasis in the endolymphatic fluid and the endocochlear potential.^{2,7-9}

Defects in *SLC26A4* are among the most frequent causes (up to 10%) of early-onset autosomal recessive hearing loss (arHL); non-syndromic DFNB4 (MIM: 600791) and Pendred syndrome (MIM: 274600).¹⁰ Individuals carrying biallelic pathogenic *SLC26A4* variants are affected by variable, often progressive and predominantly sensorineural HL with a congenital or childhood-onset.^{11,12} In Pendred syndrome, the HL phenotype is accompanied by an iodine organification defect that can lead to thyroid goiter.¹³ In individuals affected by either syndromic or non-syndromic *SLC26A4*-associated HL, a unilateral or bilateral enlarged vestibular aqueduct (EVA) is observed, which is the most common imaging abnormality in individuals with HL.^{14,15} In some cases, EVA can be part of Mondini dysplasia: an inner ear malformation that includes both EVA and cochlear incomplete partition type II. Although Mondini dysplasia can be observed in both Pendred syndrome and DFNB4 cases, cases with the syndromic type of HL are more likely to present Mondini dysplasia than those with non-syndromic HL.^{16,17}

Pathogenic variants in *SLC26A4* have a loss-of-function effect, leading to malfunctioning of the pendrin ion transporter. Besides the antenatal formation of an EVA, this ultimately leads to acidification of the endolymphatic fluids in the inner ear during embryonic development.^{7,18} Although the exact molecular pathogenic mechanism remains to be elucidated, the lack of pendrin function ultimately leads to degeneration of the sensory cells in the inner ear.⁷

Despite the strong association between defects of *SLC26A4* and HL combined with an EVA, genetic screening of subjects with this combination of defects often does not reveal biallelic pathogenic variants in *SLC26A4* (coined M2). Cohort studies report that 14-31% of the subjects with an EVA and HL carry a monoallelic pathogenic variant in *SLC26A4* (M1), whereas in 10-65% of the subjects, no potentially pathogenic variant in the coding or splice site regions of the gene can be identified (M0).^{16,19,20} Segregation analyses performed in family members of M1 subjects, however, do suggest that in 98% of M1 subjects an

unidentified or unrecognized variant is present on the *trans SLC26A4* allele.^{20,21} In line with this hypothesis, Chattaraj and coworkers reported a haplotype, referred to as the Caucasian EVA (CEVA) haplotype, that was present in 13 of 16 (81%) of the studied M1 families and that was also enriched in M0 subjects.²² The haplotype is defined by the combination of 12 single nucleotide polymorphisms (SNPs; allele frequency (AF) 1.9-4.0%) spanning a 613 kb region. The 12 SNPs are located within a region of linkage disequilibrium that extends from upstream of *PRKAR2B* to intron 3 of *SLC26A4* and are either intergenic or intronic of the genes *SLC26A4*, *BCAP29*, *DUS4L*, *COG5*, *GPR22*, *HBP1*, *PRKAR2B* and *PIK3CG*.²² The true genetic defect of the CEVA allele has not been identified yet, but it cannot be excluded that a potential defect was missed due to the technical limitations of short-read sequencing and other standard-of-care tests. The CEVA haplotype was reported to be associated with a less severe HL phenotype as compared to variants in the protein-coding or splice site regions of *SLC26A4*.²³

We investigated a Dutch cohort of M1 and M0 subjects with HL and a unilateral or bilateral EVA. All subjects were tested for the presence of the CEVA haplotype, and whole genome sequencing (WGS) was performed to detect potentially missed single nucleotide variants (SNVs), structural variants (SVs), and regulatory or deep-intronic variants. Long-read sequencing and optical genome mapping were performed to reveal a potentially missed SV located on the CEVA haplotype. Variants located within the haplotype were subjected to *in silico* analyses to investigate potential effects on the regulation of *SLC26A4* expression or on splicing. With this study, we provided further insights into *SLC26A4*-associated disease.

MATERIAL AND METHODS

Inclusion criteria and clinical evaluation

This study was approved by the medical ethics committee of the Radboud University Medical Center (registration number: NL33648.091.10) and was carried out according to the Declaration of Helsinki. Subjects diagnosed with unilateral or bilateral HL and a unilateral or bilateral EVA on CT or MRI and for whom medical genetic testing only revealed a heterozygous (M1, n=16) or no pathogenic variant (M0, n=12) in *SLC26A4* were eligible to participate in this study. A retrospective cohort of nine subjects with confirmed pathogenic (biallelic) variants in *SLC26A4* was added as a reference cohort (**Table S1**).

Medical history was taken from all participants and special attention was paid to non-genetic causes of HL. Results of pure tone, speech, and brainstem evoked response audiometry, performed in a sound-attenuated booth, were collected. Air and bone conduction pure tone thresholds were determined for frequencies ranging from 0.25 to 8 kHz. Threshold estimates based on brainstem evoked response audiometry were used

when pure tone audiometry was not available. Individuals were considered affected when pure tone thresholds for at least three frequencies were above the frequency-specific 95th percentile of age- and sex-specific thresholds (ISO 7029:2017) for the best hearing ear. In the Netherlands, routine newborn hearing screening is carried out by the detection of transient evoked otoacoustic emissions.²⁴ When available, these data were used to determine whether the HL was congenital.

Previously performed CT and MRI scans were retrieved and reassessed by an experienced neuroradiologist (S.A.H.P.). An EVA was defined as a vestibular aqueduct that measured ≥ 2 mm at the operculum and/or ≥ 1 mm at the midpoint²⁵, in accordance with previously published reports on this topic.^{22,23} Analyses of pair-wise differences between patient groups were performed with R (R Foundation) using multivariate linear regression analysis (using `lsmeans` 2.3.0) with a correction for multiple comparisons using the Holm method.²⁶

Next generation sequencing and variant interpretation

Genomic DNA was isolated from peripheral blood lymphocytes and analyzed by molecular inversion probe (MIP) sequencing, whole exome sequencing (WES) or whole genome sequencing (WGS) (**Table S2**). For WES, exome enrichment was performed using the Agilent SureSelect Human All Exome V4 or V5 kits according to the manufacturer's instructions. Subsequently, sequencing was executed on an Illumina HiSeq system by BGI Europe (Copenhagen, Denmark), with a minimal coverage of 20x for 93.77% of the targets and an average coverage of >100 reads. Read mapping along the hg19 reference genome (GRCh37/hg19) and variant calling was performed using BWA V.0.78²⁷ and GATK HaplotypeCaller V.3.3²⁸, respectively. An in-house developed pipeline was used for variant annotation and copy number variant (CNV) detection was performed using CoNIFER V.0.2.2.3²⁹. WGS was performed by BGI (Hongkong, China) on a BGISEq500 using a 2x 100 bp paired end module, with a minimal median coverage of 30-fold per genome. Read mapping (GRCh37/hg19) and variant calling was performed as described for WES. Structural variants (SVs) were called using the Manta Structural Variant Caller V.1.1.0 (SV detection based on paired end and split read evidence)³⁰ and CNVs using Control-FREEC (CNV detection based on alterations in read depth.³¹ MIP design, sequencing and data analysis were performed as previously described.^{32,33} MIPs were designed to cover exons and exon-intron boundaries of a panel of 120 HL genes (**Table S3**). For each targeted region an average coverage of >500 reads was obtained. A minimal coverage of 20x was reached for 91.78% of the MIPs. CNV detection for *SLC26A4* was performed using a read coverage analysis as previously described.³⁴ Additionally, coding and splice site regions of *FOXI1* and the regions harboring reported pathogenic variants in *EPHA2* were sequenced using Sanger sequencing as previously

described³⁵, since these genes are not included in the MIP panel. Primer sequences and PCR conditions are available upon request.

Variant prioritization was based on an AF of $\leq 0.5\%$ (gnomAD V2.1.1³⁶ and our in-house exome database (~15,000 alleles)), unless specified otherwise. Variant visualization was performed using the IGV software V.2.4 (Broad Institute).³⁷ Interpretation of missense variants was performed using the *in silico* tools CADD-PHRED (≥ 15)³⁸, SIFT (≤ 0.05)³⁹, PolyPhen-2 (≥ 0.450)⁴⁰ and MutationTaster (deleterious)⁴¹ to predict potentially deleterious effects. Variants were prioritized if a deleterious effect was predicted by at least two of these tools. Candidate variants were validated by Sanger sequencing and segregation analysis was performed when DNA of family members was available. Primer sequences and PCR conditions are available upon request. Potential effects on splicing of missense, synonymous and intronic variants were assessed using the deep-learning splice prediction algorithm SpliceAI (≥ 0.1).⁴² The maximum distance between the variant and potential gained or lost splice sites was set to 1000 bp. Predicted splice altering defects were evaluated using an *in vitro* splice assay in HEK293T cells as previously described.⁴³

Detection of the CEVA haplotype

Initial identification of the CEVA haplotype²² was performed with SNP-genotyping by Sanger sequencing in index cases for whom parental DNA was available for segregation analysis. Subsequently, the corresponding VNTR marker haplotype was determined in CEVA-positive families. For additional cases, VNTR marker analysis was performed to enable a fast and cost-effective detection of the CEVA haplotype. For the VNTR marker analysis, DNA segments were amplified by employing touchdown PCR, and subsequent analysis was carried out on an ABI Prism 3730 Genetic Analyzer (Applied Biosystems). Genomic positions of the markers were determined using the UCSC genome browser (GRCh37/hg19).⁴⁴ Alleles were assigned with the GeneMarker software (V.2.6.7, SoftGenetics) according to the manufacturer's instructions. When an individual was suspected of carrying the CEVA haplotype based on VNTR-marker alleles, SNP genotyping by Sanger sequencing was performed to confirm the presence of the twelve SNPs that are located within the haplotype.²² SNP-phasing was performed if DNA samples of family members was available.

Optical genome mapping

Optical genome mapping (Bionano Genomics) was performed as previously described.^{45,46} Ultra-high molecular weight DNA was isolated from whole peripheral blood (collected in EDTA tubes) using the SP Blood & Cell Culture DNA Isolation Kit (Bionano Genomics). CTTAAG labeling was performed using the DLS (Direct Label and Stain) DNA Labeling Kit (Bionano Genomics) and the labeled sample was analyzed using a 3x 1,300 Gb Saphyr chip (G2.3) on

a Saphyr instrument (Bionano Genomics). An effective coverage of 124x was reached, with a label density of 14.63/100 kb and an average N50 of 279 kb. *De novo* assembly (using GRCh37 and GRCh38) and variant annotation were performed using Bionano Solve version 3.4, which includes two separate algorithms for SV and CNV detection. Annotated variants were filtered for rare events as described previously.⁴⁵ In addition, the genomic region spanning the CEVA haplotype was analyzed visually in Bionano Access version 1.4.3.

PacBio long-read sequencing

Genomic DNA was isolated from peripheral blood according to standard procedures and subjected to long-read genome Hi-Fi sequencing using the SMRT sequencing technology (Pacific Biosciences). Library preparation was performed using the SMRTbell™ Template Prep Kit 2.0 (Pacific Biosciences) following manufacturer's instructions. Size selection was performed using a BluePippin DNA size selection system (target fragments ~15-18 kb). Sequence primer V2 and polymerase 2.0 were used for binding. Subsequently, the SMRTbell library was loaded on an 8M SMRTcell and sequencing was performed on a Sequel II system (Pacific Biosciences). Circular consensus sequencing (CCS), Hi-Fi reads, were generated using the CCS (v4.2.0) tool and were aligned to the GRCh37/hg19 reference genome with pbmm2 (v.1.3.0). The unique molecular yield was 93.46 Gb and the post-alignment Hi-Fi- coverage was 12x (Mosdepth v0.3.1⁴⁷). SV calling was performed using PBSV (v2.4.0) and annotation was applied using an in-house SV annotation pipeline.

3

RESULTS

Patient inclusion and genetic prescreening

In this study, we included 28 Dutch index cases diagnosed with a unilateral or bilateral EVA and unilateral or bilateral HL. All individuals were prescreened for pathogenic variants in *SLC26A4* (NM_000441.1) in a diagnostic setting and complete coverage of the coding and splice site (+/- 14 nucleotides) regions of *SLC26A4* was confirmed. In 16 individuals, a heterozygous (likely) pathogenic *SLC26A4* variant was reported and these cases were deemed M1. In the remaining 12 individuals, no potentially pathogenic variants were found in the coding or splice site regions of this gene, and these subjects were therefore considered M0. Causative variants in other genes associated with arHL⁴⁸ were addressed and excluded by analyzing available sequencing data (WES or MIPs-based) or in WGS data obtained in this study (Table S2). This revealed no homozygous or compound heterozygous variants that were known or predicted to be pathogenic, except two compound heterozygous variants in *OTOGL* (NM_173591.3) in individual SLC012 (Table S4). The c.890C>T (p.(Pro297Leu)) variant in *OTOGL* has, however, been reported as (likely) benign in ClinVar⁴⁹ and the Deafness

Variation Database⁵⁰ and is classified as likely benign according to the ACMG guidelines.⁵¹ The c.1369G>T (p.(Val457Leu)) is considered as a variant of unknown significance (ACMG classification). Furthermore, subject SLC012 has progressive high-frequency HL, which differs from the symmetric, moderate, and stable HL associated with *OTOGL* (DFNB84B).^{52,53} Therefore, we considered the identified *OTOGL* variants as non-causative. For none of the cases, (likely) pathogenic variants (UV4/UV5, ClinVar) were identified in genes associated with autosomal dominant HL or syndromic HL.⁴⁸

The CEVA haplotype is enriched in Dutch monoallelic *SLC26A4* cases

In 2017, Chattaraj et al. described the ≥ 613 -kb CEVA haplotype located centromeric of the *SLC26A4* gene to be enriched in M1 *SLC26A4* cases and M0 cases with HL and EVA.²² To investigate whether this haplotype is also enriched in the selected Dutch cohort of M0 and M1 *SLC26A4* cases, we screened for the presence of this haplotype using VNTR marker analysis followed by Sanger sequencing of the 12 CEVA-associated SNPs. The CEVA haplotype was detected in 8 out of 16 (50%) M1 individuals and 2 out of 12 (16.7%) M0 subjects (**Figure 1, Table 1**). In two additional M1 individuals (SLC040 and SLC071), only a partial CEVA haplotype was found, harboring 9/12 SNPs. We will refer to this smaller haplotype as the variant 1-CEVA (V1-CEVA) haplotype.

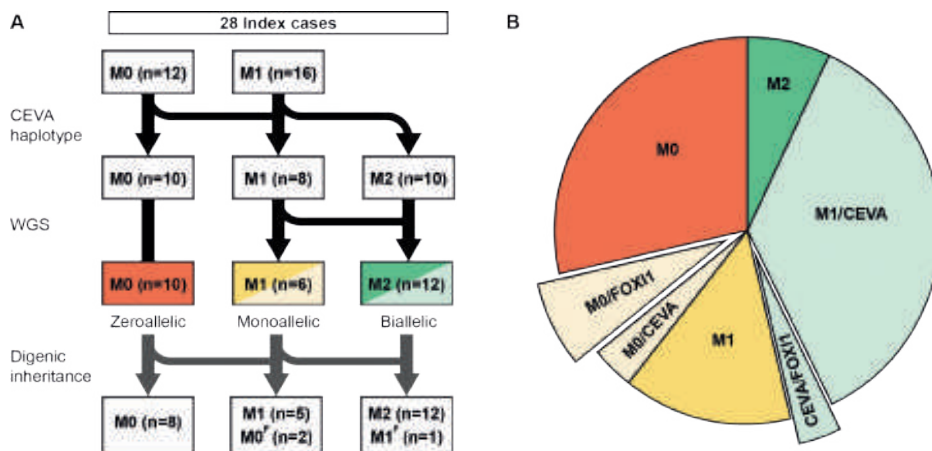


Figure 1. Overview of genetic analyses performed in zeroallelic and monoallelic *SLC26A4* cases. (A-B) To explain the missing heritability in zeroallelic (M0, n=12) and monoallelic (M1, n=16) *SLC26A4* cases, different genetic analyses were performed. Firstly, individuals were screened for the presence of the CEVA haplotype (M0/CEVA, n=2; M1/CEVA, n=10). Secondly, whole genome sequencing (WGS) was performed in all monoallelic cases (M0/CEVA, M1) to identify potential structural, splice (M2, n=2) or regulatory variants. Lastly, sequencing data were screened for potentially pathogenic variants in the *EPHA2*, *FOX11* and *KCNJ10* genes. Digenic inheritance has been previously suggested for variants in these genes and the *SLC26A4* gene. In three cases (M0/FOX11 (M0'), n=2, CEVA/FOX11 (M1'), n=1), a potentially pathogenic variant in *FOX11* (NM_012188.4, c.677C>T) was identified.

The CEVA haplotype has an AF of 2.8% in the 1000G database (28 in 1006 alleles)^{22,54}, and an AF of 3.3% in an in-house control cohort consisting of 322 healthy unrelated individuals (21 in 644 unphased alleles). This implies a significant enrichment of the CEVA haplotype in our M1 cohort (8 in 32 alleles) compared to the 1000G database (p -value 5.419×10^{-6}) and the control cohort (p -value 2.187×10^{-5}) as determined by a two-sided Fisher's exact test). The two M1 cases with the V1-CEVA haplotype were not included in this statistical analysis. Also this V1-CEVA allele is significantly enriched in our M1 cohort as only a single V1-CEVA allele is reported in the 1000G database (1 in 1006 alleles)²² (p -value 0.0027). The CEVA haplotype was not found to be significantly enriched in the M0 cohort (2 in 24 alleles). Although the pathogenicity of the CEVA haplotype is unclear, the significant enrichment of the haplotype within this M1 patient cohort and the patient cohorts (M1 and M0) previously described by Chattaraj and co-workers strongly suggests that a pathogenic defect resides within this haplotype.²² Because of this strong association of the CEVA haplotype with HL and EVA, we considered the M1 individuals carrying the CEVA or the V1-CEVA haplotype as genetically explained (M1/CEVA), and M0 individuals with the CEVA haplotype (M0/CEVA) as monoallelic in further steps of this study. For six M1 individuals, it could not be conclusively determined whether the CEVA haplotype was present *in trans* with the pathogenic *SLC26A4* variant, as the genetic material of family members was not available (**Table 1**).

Whole genome sequencing reveals potential *SLC26A4* splice and regulatory variants in M1 subjects without the CEVA haplotype

To detect any potentially missed coding or unidentified intronic *SLC26A4* variants or variants located *in cis* regulatory elements of the gene, WGS analysis was performed for all six M1 individuals who could not be genetically explained by the presence of the CEVA haplotype. Additionally, WGS analysis was performed for the two M0/CEVA individuals. In none of these eight cases, SVs overlapping with the *SLC26A4* gene were identified by WGS.

To identify any variants with a potential effect on splicing, the deep-learning algorithm SpliceAI was employed.⁴² In two M1 individuals (SLC048 and SLC085), a rare heterozygous potentially splice altering *SLC26A4* variant was identified (**Table 2**). For both variants, the predicted splice defect was investigated using an *in vitro* splice assay performed in HEK293T cells. For SLC048, a canonical splice site variant (c.1342-2A>C), that was overlooked during prescreening efforts, was predicted to remove the splice acceptor site. This variant was previously reported in a study performed by Van Beeck Calkoen and coworkers and in ClinVar.⁵⁵ Indeed, the splice assay revealed loss of the acceptor site and usage of an alternative splice acceptor site located thirteen nucleotides downstream (**Figure S1A**). This leads to the formation of an out-of-frame exon 12 and premature protein truncation (p.(Ser448Leufs*3)). Based on these results, the variant was classified as pathogenic according to the ACMG guidelines.⁵¹

Table 1. Detection of the CEVA haplotype in M1 and M0 individuals

Zeroallelic <i>SLC26A4</i> cases			
Case	Allele 1		Allele 2
	Variant	ACMG	CEVA
SLC014	c.2059G>T; p.(Asp687Tyr)	UV3	
SLC015	-	-	
SLC017	-	-	
SLC039	-	-	<u>ACACATG-GC-C</u> (CEVA)
SLC043	-	-	
SLC052	-	-	
SLC069	-	-	
SLC070	-	-	
SLC073	-	-	
SLC080	-	-	<u>ACACATG-GC-C</u> (CEVA)
SLC084	-	-	
SLC086	-	-	
Monoallelic <i>SLC26A4</i> cases			
SLC002	c.412G>T; p.(Val138Phe)	UV5	
SLC003	c.131dup; p.(Thr45Aspfs*42)	UV5	<u>ACACATG-GC-C</u> (CEVA)
SLC012 ^a	c.707T>C; p.(Leu236Pro)	UV5	<u>ACACATG-GC-C</u> (CEVA)
SLC013	c.1001+1G>A; p.(?)	UV5	<u>ACACATG-GC-C</u> (CEVA)
SLC018	c.349C>T; p.(Leu117Phe)	UV5	
SLC031	c.1001+1G>A; p.(?)	UV5	<u>ACACATG-GC-C</u> (CEVA)
SLC032	c.1334T>G; p.(Leu445Trp)	UV5	
SLC036 ^a	c.1246A>C; p.(Thr416Pro)	UV5	<u>ACACATG-GC-C</u> (CEVA)
SLC040 ^a	c.655_656dup; p.(Phe223Alafs*15)	UV5	<u>GTTCATG-GC-C</u> (V1-CEVA)
SLC045	c.1334T>G; p.(Leu445Trp)	UV5	
SLC048	c.706C>G; p.(Leu236Val)	UV4	
SLC056	c.707T>C; p.(Leu236Pro)	UV5	<u>ACACATG-GC-C</u> (CEVA)
SLC071 ^a	c.1334T>G; p.(Leu445Trp)	UV5	<u>GTTCATG-GC-C</u> (V1-CEVA)
SLC078	c.304G>C; p.(Gly102Arg)	UV4	<u>ACACATG-GC-C</u> (CEVA)
SLC079	c.1001+1G>A; p.(?)	UV5	<u>ACACATG-GC-C</u> (CEVA)
SLC085	c.706C>G; p.(Leu236Val)	UV4	

Presence of the CEVA haplotype was tested in zeroallelic (M0) and monoallelic (M1) *SLC26A4* cases with a unilateral or bilateral enlarged vestibular aqueduct. *SLC26A4* (NM_000441.1) variants reported in ClinVar as (likely) pathogenic (UV4, UV5) were considered causative, whereas variants reported as (likely) benign or of unknown significance were considered non-causative. In ten individuals, the complete CEVA haplotype was detected (ACACATG-GC-C), whereas in two individuals a shorter version of the haplotype was found, consisting of 9/12 CEVA SNPs (GTTCATG-GC-C; V1). For individuals marked with an ^a, it could be conclusively determined that the (V1-)CEVA haplotype is present on the *trans SLC26A4* allele. ACMG, variant classification according to the American College of Medical Genetics and Genomics (ACMG) classification guidelines⁵¹; UV3, uncertain significance; UV4, likely pathogenic; UV5, pathogenic.

In SLC085, a synonymous variant (c.471C>T, classified as likely benign in ClinVar) was identified in exon 5. SpliceAI predicts that this variant strengthens an alternative splice acceptor site (27 nucleotides downstream of the variant). Indeed, an *in vitro* splice assay confirmed that the alternative splice acceptor site is used, which leads to the partial deletion of exon 5 and a truncated protein (p.(Gly139Alafs*6)) (**Figure S1B**). Therefore, this variant is now classified as pathogenic according to the ACMG classification guidelines.⁵¹ The observed splice defect resulting from this synonymous variant underlines the importance of evaluating potential splice effects of all rare variants in coding sequences, using *in silico* prediction splice tools. We considered the two identified splice variants as pathogenic and the HL of the two individuals as genetically explained, thus M2.

To explore variants that are potentially located within a *cis* regulatory element of *SLC26A4*, we extracted all (predicted) human enhancer and promoter elements that are associated with the *SLC26A4* gene from the GeneHancer⁵⁶ and EnhancerAtlas⁵⁷ databases (**Table S5**). GeneHancer V5 is a collection of both predicted and experimentally validated enhancer-to-gene and promoter-to-gene interactions, based on information integrated from multiple resources: ENCODE⁵⁸, Ensembl⁵⁹, FANTOM5⁶⁰, VISTA⁶¹, dbSuper⁶², EPDnew⁶³, UCNEbase⁶⁴ and CraniofacialAtlas⁶⁵. For each regulatory element, a gene interaction score (>7) and element confidence score (>0.7) are provided. The EnhancerAtlas V2 is a database providing enhancer annotations in different species based on experimental datasets determined in several tissues and cell types. WGS data were analyzed for variants located within these elements and two rare potentially regulatory variants (Chr7:107220628C>A, Chr7:107384987C>G) were identified in two M1 individuals (SLC002 and SLC045) (**Table S6**). Both variants are located in a predicted enhancer element of *SLC26A4* according to GeneHancer. We did not find any strong indication of a functional effect for the two variants based on (nucleotide) conservation scores (PhyloP, UCSC genome browser⁴⁴) or loss of transcription factor binding sites (JASPAR database⁶⁶). Therefore, the variants were considered non-pathogenic, although only a reporter assay can completely exclude a potential regulatory effect of the variants on *SLC26A4* expression.

A *FOXI1* missense variant is revealed in three unrelated index cases

Several studies have suggested a potential digenic inheritance for *SLC26A4* variants and variants in *KCNJ10* and *FOXI1*.⁶⁷⁻⁶⁹ Additionally, a more recent study suggested digenic inheritance with pathogenic variants in *EPHA2*.⁷⁰ We screened all remaining genetically unexplained individuals (M1, M0/CEVA and M0) for variants in these genes with an AF ≤5% (gnomAD V2.1.1). In cases for which only MIP sequencing data was available, coding regions and exon-intron boundaries of *FOXI1* and the regions harboring the reported pathogenic variants in *EPHA2* (c.1063G>A; p.(G355R), c.1532C>T; (p.T511M), NM004431.4) were analyzed using Sanger sequencing. In three individuals (SLC039; M0/CEVA, SLC052; M0 and SLC069; M0) a c.677C>T (p.(Thr226Ile)) *FOXI1* (NM_012188.4) missense variant was identified (**Table 3**).

Table 2. WGS revealed two heterozygous splice variants in *SLC26A4*

Case	Class	Genome	cDNA	Protein	In-house AF (%)	gnomAD AF (%)	CADD_PPHRED	SIFT	PPH2	Mutation Taster	SpliceAI	ACMG
SLC048	M1	Chr7:107335064A>C	c.1342-2A>C	p.Ser448Leufs*3	0.00	-	21.7	NA	NA	NA	0.99 (AS loss)	UV5
SLC085	M1	Chr7:107314664C>T	c.471C>T	p.Gly139A1afs*6=	-	0.00	0.725	NA	NA	NA	0.59 (AS gain)	UV5

Whole genome sequencing (WGS) revealed two potentially splice altering variants in *SLC26A4*. Variants are selected based on an allele frequency of $\leq 0.5\%$ in gnomAD and the in-house database. Scores that meet the thresholds for pathogenicity as described in the methods section are indicated in red. The predicted effect on splicing was confirmed in an *in vitro* splice assay that was performed in HEK293T cells (**Figure S1**). Genome; Genomic position according to GRCh37/hg19; In-house AF, allele frequency (%) in an in-house database (~7,500 exomes); GnomAD AF, allele frequency (%) in gnomAD database V.2.1.1; CADD_PPHRED, Combined Annotation Dependent Depletion PHRED score; SIFT, Scale-Invariant Feature Transform; PPH2, PolyPhen-2 score; MutationTaster (prob), MutationTaster score with probability (0-1); spliceAI, splicing prediction score; AS, acceptor site; ACMG, variant classification according to the American College of Medical Genetics and Genomics (ACMG) classification guidelines⁵¹; UV5, pathogenic; NA, not applicable.

Table 3. Rare variants identified in *EPHA2*, *FOX11* and *KCNJ10*

Case	Class	Gene	Transcript	cDNA	Protein	In-house AF (%)	gnomAD AF (%)	CADD_PPHRED	SIFT	PPH2	Mutation Taster	SpliceAI	ACMG
SLC017	M0	<i>EPHA2</i>	NM_004431.4	c.2627G>A	p.(Arg876His)	2.36	1.70	32	0	0.769	NA	0.03	UV2
SLC039	M0/CEVA	<i>FOX11</i>	NM_012188.4	c.677C>T	p.(Thr226Ile)	0.56	0.37	11	0.14	0.109	P	0.03	UV2
SLC052	M0	<i>EPHA2</i>	NM_004431.4	c.1941G>T	p.(Thr647=)	1.09	0.55	7.309	NA	NA	NA	0.05	UV2
SLC052	M0	<i>EPHA2</i>	NM_004431.4	c.1896G>A	p.(Leu632=)	0.76	0.05	3.197	NA	NA	NA	0.05	UV2
SLC052	M0	<i>FOX11</i>	NM_012188.4	c.677C>T	p.(Thr226Ile)	0.56	0.37	11	0.14	0.109	P	0.03	UV2
SLC069	M0	<i>FOX11</i>	NM_012188.4	c.677C>T	p.(Thr226Ile)	0.56	0.37	11	0.14	0.109	P	0.03	UV2

Available sequencing datasets of monoallelic (M1, M0/CEVA) and zeroallelic (M0) individuals were screened for variants in *EPHA2*, *FOX11* and *KCNJ10* with an allele frequency of $\leq 5\%$ in gnomAD (V.2.1.1). Scores that meet the thresholds for pathogenicity as described in the methods section are indicated in red. In-house AF, allele frequency (%) in in-house database (~7,500 exomes); GnomAD AF, allele frequency (%) in gnomAD database V.2.1.1; CADD_PPHRED, Combined Annotation Dependent Depletion PHRED score; SIFT, Scale-Invariant Feature Transform; PPH2, PolyPhen-2 score; MutationTaster (prob), MutationTaster score with probability (0-1); spliceAI, splicing prediction score; ACMG, variant classification according to the American College of Medical Genetics and Genomics (ACMG) classification guidelines⁵¹; UV2, likely benign; NA, not available; P, polymorphism.

The variant was not identified in any of the M1/CEVA or the two M2 cases. *FOXI1* encodes the Forkhead transcription factor FOXI1, a key transcriptional regulator of *SLC26A4*.⁶⁹ Segregation analysis has confirmed that the *FOXI1* variant is not co-inherited with the CEVA allele in individual SLC039, which is in line with digenic inheritance. The Thr226 residue is located outside of the conserved forkhead DNA-binding domain of FOXI1 (amino acids 94-211)⁶⁹ and none of the *in silico* tools used for analysis predicted a deleterious effect of the c.677C>T variant. Nevertheless, the variant is enriched in individuals diagnosed with HL and EVA (3 in 56 alleles in the study cohort versus 165 in 26.590 alleles of the in-house WES cohort, p-value 0.0004), and we consider the c.677C>T *FOXI1* variant as an interesting candidate for functional validation.

In case SLC017, a heterozygous missense variant in *EPHA2* was detected (c.2627G>A (p.(Arg876His))). Although the variant is predicted to be pathogenic by *in silico* prediction tools, it has a relatively high AF of 1.70% (gnomAD) and 2.36% (in-house database) and is classified as likely benign according to the ACMG classification guidelines. Because the variant was only found in an M0 *SLC26A4* case, a potential digenic inheritance of pathogenic *SLC26A4* variants and the newly identified *EPHA2* variant could not be addressed.

To summarize, the CEVA haplotype or a short CEVA haplotype (V1-CEVA) was detected in 12 of the 28 index cases (16 M1, 12 M0) that were included in our study (**Figure 1**). In two individuals (M1), an *SLC26A4* splice variant was identified using WGS. After performing these genetic analyses by which the enrichment of the (V1-)CEVA haplotype in M1 cases was demonstrated, we consider the HL in 12 individuals to be associated with *SLC26A4* defects and these subjects to be genetically explained (2 M2, 10 M1/CEVA), six individuals are considered M1 (4 M1, 2 M0/CEVA), and ten individuals are still considered M0. Additionally, in three individuals (1 M0/CEVA, 2 M0) a potentially pathogenic variant in *FOXI1* was found.

Determination of boundaries of CEVA haplotype

To identify the true pathogenic defect located on the CEVA haplotype, an in-depth analysis of this genomic region was performed. Firstly, the exact boundaries of the genomic region shared by CEVA haplotype carriers were determined using VNTR marker analysis. For two individuals with the complete CEVA haplotype and the two subjects with the V1-CEVA haplotype, DNA samples of family members were available, allowing reliable determination of the marker alleles located within the haplotype. A shared haplotype of 0.89 Mb delimited by markers D7S501 and D7S2459 was identified (**Figure 2** and **Figure S2**). Although the V1-CEVA haplotype shares the marker alleles with the complete CEVA haplotype, the absence of SNPs 1-3 potentially delimits the shared haplotype even more (0.57 Mb, CEVA SNP 3-D7S2459). The remaining eight individuals with the complete CEVA haplotype share identical marker

alleles in the 0.89 Mb-sized region, although they could not be conclusively assigned to the haplotype as no segregation analysis could be performed. For individual SLC003, a deviating repeat length was identified for marker D7S2420. As we cannot exclude a rare event to be responsible for the change in allele length, this marker was still considered part of the shared CEVA haplotype.

Short-read WGS did not reveal a pathogenic defect on the CEVA haplotype

Because of the significant enrichment of the CEVA haplotype in M1 cases, we hypothesized that the subjects with the CEVA haplotype share a yet elusive pathogenic defect. To identify this defect on the CEVA haplotype, short-read WGS was performed in two individuals (SLC012 & SLC036) carrying the CEVA haplotype *in trans* with a pathogenic variant in *SLC26A4* (M1/CEVA). All heterozygous variants with an AF $\leq 5\%$ in gnomAD that were shared between the two individuals and located within the determined boundaries of the CEVA haplotype were analyzed (**Table S7**).

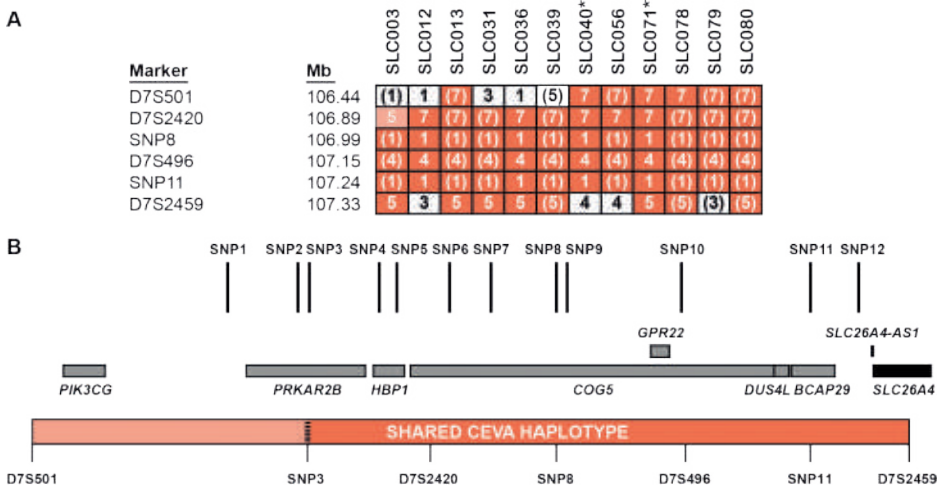


Figure 2. Determination of the boundaries of the shared CEVA haplotype. (A) The CEVA haplotype was detected in 10 individuals, in an additional 2 individuals (SLC040 and SLC071, indicated with *), a smaller haplotype was found, termed V1-CEVA. To determine the boundaries of the CEVA haplotype, VNTR marker analysis was performed. The shared haplotype (0.89 Mb, CEVA; 0.57 Mb V1-CEVA is marked in orange). For marker D7S2420 (light-orange) a deviating CA-repeat length was determined in SLC003. Nevertheless, the marker is still considered to be potentially part of the shared haplotype as a change or repeat length cannot be excluded. Genomic positions (Mb) are according to the UCSC Genome Browser (GRCh37/hg19). (B) A schematic overview of the identified shared CEVA haplotype (D7S501-D7S2459). Positions of the CEVA-associated SNPs and the genes located within the haplotype region (CEVA, D7S501-D7S2459; V1-CEVA, SNP3-D7S2459) have been indicated. All SNPs are located within intronic or intergenic regions. Genomic positions of the CEVA-associated SNPs are provided in **Table S7**. *SLC26A4* (NM_000441.1) is only partially included (exons 10/21) in the shared haplotype.

In total, 20 shared variants remained and included the 12 original SNPs that previously defined the CEVA haplotype.²² Sixteen of the shared variants are located in intronic regions, but for none of them, a significant effect (score ≥ 0.1) on splicing is predicted by SpliceAI. Two variants are located within a *cis* regulatory element of *SLC26A4* according to the GeneHancer database, however, these also show overlap with a long interspersed nuclear element (LINE) repeat element. One variant (CEVA SNP9) has a high nucleotide evolutionary conservation score (PhyloP, 2.769 [range -14, 3]). No SVs or CNVs were detected within or overlapping with the CEVA haplotype and shared by the two individuals.

Regions harboring heterozygous variants with an AF $\leq 5\%$ in gnomAD that were not shared between SLC012 and SLC036 had sufficient coverage to exclude that these variants were only called in one of the subjects but present in both of them. None of the variants identified in either SLC012 or SLC036 were within the *SLC26A4* gene or were obviously deleterious. SVs and CNVs within the CEVA boundaries were analyzed separately for the two subjects which did not reveal any of such variants that were not shared by the two studied subjects. To fully exclude that the CEVA haplotype harbors different pathogenic variants in the studied individuals, a study design including short- and long-read WGS in several nuclear families has to be applied.

Optical genome mapping & long-read sequencing

To investigate the possibility that SVs were missed using short-read sequencing, optical genome mapping (Bionano Genomics) was performed using ultra-high molecular weight DNA isolated from peripheral blood cells of individual SLC012 (M1/CEVA). Optical genome mapping identified a total of 6,565 SVs, of which none were within the CEVA region (D7S501-D7S2459; chr7:106,440,266-107,360,254). Two SV calls (both calling the same 2,196 bp insertion between chr7:107,367,549 and 107,373,585) were located just outside this region (**Figure S3A**). This insertion was also called in 100% of our current optical genome mapping control cohort⁷¹, strongly suggesting that this reflects a reference problem rather than a real SV. Additionally, there were 22 CNV calls, of which none were within the CEVA region.

Subsequently, PacBio long-read sequencing was performed on genomic DNA isolated from individual SLC079 (M1/CEVA; *in trans* status unknown). SV analysis of the long-read sequencing data revealed a total of 55,205 SVs, of which 12 within the CEVA region. After careful interrogation of the SVs, all of them were considered false positives based on SV length, and presence of the SVs in an in-house control dataset. The CEVA haplotype region was also manually inspected in the IGV software, which did not reveal any indications for potential SVs (**Figure S3B**). Interestingly, the insertion event that was detected with optical genome mapping and located just outside the CEVA region was also present in the long-read

sequencing data (chr7:107,370,573, 1,612 bp insertion). This insertion was also present in available in-house control sequencing data, supporting the hypothesis the variant concerns a reference problem and is not a true SV.

A comparable severity of hearing loss in the M1/CEVA and M2 cohorts

As the CEVA haplotype was reported to be associated with a less severe HL phenotype than variants in the protein-coding or splice site regions of *SLC26A4*²³, we addressed genotype-phenotype correlations in our cohort. We were able to retrieve pure tone audiometry of all subjects except for SLC071; for this subject, complete audiometry from only one ear was available (**Figure S2**). The original CT or MRI scans of subjects SLC018 and SLC032 could not be retrieved. However, written reports of the imaging were available. Data on thyroid gland function were not consistently available and were therefore not included in this study. We applied the methods of Chao et al. to compare the severity of HL between four subject groups (M0, M1, M1/CEVA, and M2 **Figure 3, Table 4**).²³ The M1/CEVA group includes the M1/V1-CEVA subjects. Bilateral EVA was present in 7 of 10 (70%) M1/CEVA subjects, in all 4 M1 subjects without the CEVA haplotype, and 7 of 10 (70%) M0 subjects without the CEVA haplotype. All 11 M2 subjects (reference cohort, SLC048 and SLC085) had bilateral EVA. The median pure tone audiometry in the M2 group (85 dB HL, n = 20) was not significantly different from that of the M1/CEVA group (84 dB HL, n = 16) and the M1 group (79.5 dB HL, n = 8) (p-values 0.8300 and 0.7142, respectively, all adjusted for age). Also, no difference was observed between the M1/CEVA group and the M1 group (p = 0.8782). In contrast, when we compare the M2 and M1/CEVA groups with the M0 group, we observed significant differences in the severity of HL (p = 0.0015 and p = 0.0135, respectively). When compared to Chao et al, subjects in our study displayed a similar degree of median HL in the M2 group (86.3 and 85 dB in (23) and the present study, respectively), more severe HL in the M1/CEVA group (47.5 and 84 dB, respectively) and less severe HL in the M0 group (54.4 and 42 dB HL, respectively). Slight age differences were seen between the groups presented in Chao et al. and those in the current study (**Table S8**). Chao and co-workers did not report audiometric data for the M1 group without the CEVA haplotype *in trans*, presumably due to the small sample size. Overall, in contrast to the study by Chao et al., the present study showed that subjects with biallelic pathogenic variants in the coding regions and splice sites of *SLC26A4* have a degree of HL that is similar to that of subjects with a monoallelic *SLC26A4* variant and the CEVA haplotype. Due to the small sample size, we could not test the hypothesis that the CEVA haplotype acts as a modifier in M0 subjects as reported previously.²³

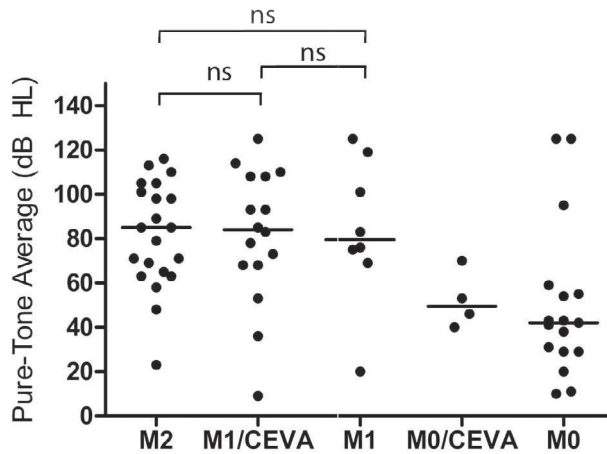


Figure 3. Results of audiometric evaluation in affected individuals. PTA_{0.5-4kHz} for ears with an EVA. Each dot represents the hearing level of an ear with an enlarged vestibular aqueduct, allocated to genotype class (M2, M1/CEVA, M1, M0/CEVA and M0). The M1/CEVA group also includes subjects with an M1/V1-CEVA genotype. For an objective comparison, the same methods as used by Chao et al. (2019) were applied.

DISCUSSION

In this study we investigated 28 genetically unexplained Dutch index cases with HL and a unilateral or bilateral EVA. To elucidate the missing heritability in monoallelic *SLC26A4* cases, who represent 14–31% of subjects with HL and EVA^{16,20}, extensive genomic analyses as well as phenotyping were performed. Important findings in this study were (1) the enrichment of a shared (V1-)CEVA haplotype in M1 *SLC26A4* cases, (2) two *SLC26A4* splice variants and (3) the identification of a *FOXI1* variant in three subjects suggesting a contribution of this variant to the etiology of HL and EVA. Furthermore, the genotype-phenotype analyses revealed that the severity of the HL associated with biallelic variants (M2) in *SLC26A4* is comparable to the HL associated with a monoallelic variant in *SLC26A4* with or without the CEVA haplotype (M1 and M1/CEVA).

For six M1 individuals, it could not be conclusively determined whether the CEVA haplotype was present *in trans* with the (likely) pathogenic *SLC26A4* variant, as no genetic material of family members could be obtained. However, we anticipated that most if not all of the six M1 cases carry the CEVA haplotype *in trans* with the *SLC26A4* variants because it seems highly unlikely that the *SLC26A4* variants all have occurred on an allele with a frequency of <3% in the population.²² Furthermore, the co-occurrence of two partial CEVA haplotypes that together exactly mimic a heterozygous CEVA haplotype in 6 of 16 individuals is highly unlikely as the frequencies of partial CEVA haplotypes in the European population are all (far) below 1%.²² The same holds true for the two M0/CEVA cases for whom we could not determine the phase of the 12 SNPs in the CEVA haplotype.

Table 4. Clinical evaluation of affected individuals

Case	Class	Gender	Age of onset (yr)	Otosopic examination	Newborn hearing screening		Motor development	Imaging		Audiometric evaluation		
					3rd time pass	NA		CT	MRI	Subject age (yr)	PTA (0.5-4kHz)	
SLC014		M	PC	N		3rd time pass	Delayed	BEVA		4	>120	55
SLC015		F	PS	myringosclerosis		N	NR	U EVA R		25	29	66
SLC017		M	PC	N		NA	NR	BEVA		5	10	59
SLC043		F	PC	N		N	NR	U EVA L		17	10	95
SLC052		F	33	N		NA	NR	BEVA		33	20	>120
SLC069	M0	F	15	N		NA	NR	BEVA		19	43	42
SLC070		M	PC	N		NA	N	BEVA		19	43	31
SLC073		M	U	L: atelectatic middle ear, retracted eardrum		NA	NR	U EVA R		12	11	18
SLC084		F	PC	N		3rd time pass	Delayed	BEVA		6	29	38
SLC086		M	PC	N		N	Delayed	BEVA		6	54	41
SLC039	M0/CEVA	F	2-4	N		NA	NR	BEVA		24	46	70
SLC080		F	5	N		N	N	BEVA		6	40	53
SLC002		F	U	N		NA	NR	BEVA		18	83	76
SLC018		M	PC	N		NA	N	BEVA*		16	75	101
SLC032	M1	F	PC	N		NA	NR	BEVA*		59	119	>120
SLC045		F	PC	N		N	N	BEVA		7	20	69
SLC003		M	15	N		NA	NR	U EVA R		17	83	-1
SLC012		M	PC	N		NA	NR	BEVA		17	>120	53
SLC013		F	U	N		NA	NR	BEVA		22	36	9
SLC031	M1/CEVA	M	PS	N		2nd time pass	N	U EVA L		16	0	68
SLC036		F	PC	N		NA	NR	BEVA		20	73	68
SLC040		M	U	N		U	N	U EVA L		7	5	78
SLC056		M	PC	N		NA	NR	BEVA		14	108	93

Table 4. (continued)

Case	Class	Gender	Age of onset (yr)	Otoscopic examination	Newborn hearing screening	Motor development	Imaging		Audiometric evaluation		
							CT	MRI	Subject age (yr)	PTA (0.5-4kHz)	
									R	L	
SLC071		M	PC	N	N	N	BEVA		3	85	NT
SLC078	M1/CEVA (continued)	F	PC	N	NA	U	BEVA		10	114	93
SLC079		F	C	N	R	N	BEVA		2	110	108
SLC048		M	PC	N	NA	NR	BEVA		8	105	71
SLC085		M	C	N	R	N	BEVA		2	23	85
SLC087		F	C	N	R	Delayed		BEVA	5	65	63
SLC088		F	4	N	NA	N		BEVA	17	85	105
SLC089		M	U	N	U	U		BEVA	10	58	98
SLC090	M2	F	3	N	NA	U		BEVA	41	116	110
SLC091		F	2-4	N	N	Delayed		BEVA	12	63	69
SLC092		F	C	N	R	N		BEVA	4	79	48
SLC093		M	PC	N	U	Delayed		BEVA	8	71	98
SLC094		M	PC	sclerotic eardrum L	NA	U		BEVA	37	101	113
SLC095		F	C	N	R	N		BEVA	1	NT	89

Age of onset (AoO), age of onset in years as reported by the subjects. Subject age, the age at which the audiometric data of the last two columns were obtained, in general the last audiogram. Newborn hearing screening was introduced in the Netherlands in 2006. *only written report available. Y, years; PTA, pure tone average, mean of 0.5, 1, 2 and 4 kHz air conduction thresholds; M, male; F, female; R, right; L, left; PC, age of onset of HL is presumably congenital, based on anamnesis; C, age of onset of HL is congenital, based on newborn hearing screening; P5, subject reported onset of HL during primary school, exact age unknown; NR, not reported; NT, not tested; N, no abnormalities; R, refer in newborn hearing screening, failed in test; U, unknown, CT, computed tomography; MRI, magnetic resonance imaging; U EVA L/R, unilateral enlarged vestibular aqueduct in left or right ear; BEVA, bilateral enlarged vestibular aqueduct.

In two cases, the V1-CEVA haplotype was identified. This smaller CEVA haplotype was also reported previously in a single M1 case by Chattaraj and coworkers and likely refines the CEVA haplotype. Alternatively, the V1-CEVA haplotype harbors a different genetic defect. The shared VNTR marker alleles of the V1-CEVA and the CEVA haplotype suggest that V1-CEVA refines the boundaries of the shared genomic region to 0.57 Mb.

We anticipated that a pathogenic variant co-segregates with the CEVA haplotype. Therefore, we subjected the shared genomic region to extensive genomic analyses that included WES, short- and long-read WGS, and optical genome mapping, to reveal any potential variants missed or misinterpreted in earlier studies. None of the applied sequencing or imaging techniques revealed rare SVs that overlap or are present within the CEVA haplotype. In the light of the proven accuracy and efficacy of especially optical genome mapping and long-read sequencing in SV detection⁷², we deem it unlikely that any SVs within the CEVA region escaped detection. Additionally, we evaluated all SNVs with an AF \leq 5% (gnomAD) present within the region for predicted regulatory or splice altering effects but for none of the 20 SNVs a potential effect was predicted by SpliceAI. Two SNVs overlap with a potential regulatory element of *SLC26A4* (GeneHancer, EnhancerAtlas), and one variant is present within the intronic regions of this gene. However, all three variants are located within a highly repetitive element (LINE). Although little is known about the effects of genetic variation within LINE elements, a potential effect on the methylation landscape and consequently gene expression levels has been suggested⁷³ and such an effect can therefore not be excluded for the three indicated variants. For the remaining SNVs, no potential effects on transcript splicing or gene regulation were predicted. Nevertheless, we cannot rule out combinatory effects of the SNVs, since they are all located in *cis*. A thorough experimental (multi-omic) analysis is required to optimally assess the effects of the identified variants. RNA studies can be performed to detect quantitative or qualitative changes affecting the *SLC26A4* transcripts. A defect observed on the RNA level could provide valuable insights that may point towards the true pathogenic defect, and prioritize one, or a combination, of the variants on the CEVA allele. However, *SLC26A4* is not or at extremely low levels expressed in readily accessible patient cell types (e.g., fibroblasts and blood cells). The same holds true for induced pluripotent stem cells or otic progenitor cells.⁷⁴ However, Hosoya and co-workers have successfully developed a protocol that allows the differentiation of otic progenitor cells into outer sulcus-like cells that express *SLC26A4* at high levels. This protocol could potentially be a powerful tool to evaluate the consequences of CEVA haplotype at the RNA level.

SLC26A4 is not the only gene present within the CEVA haplotype, which also spans *BCAP29*, *COG5*, *DUS4L*, *HBP1*, *PIK3CG*, and *PRKAR2B*. For none of these genes, pathogenic variants associated with (syndromic) HL have been reported, nor has a function in the inner ear been described. The majority of the CEVA-associated SNVs (16/20) are located within an

intronic region of these genes, however, for none of these variants a splice altering effect is predicted by SpliceAI.

Since the genetic defect on the CEVA haplotype could not be pinpointed by the genetic analyses, we could not determine whether the AF of the defect is lower than that of the CEVA haplotype and more in line with the expected frequency based on the prevalence of HL (1:1,000 newborns⁷⁵) and the genetic heterogeneity of the condition. Alternatively, the CEVA haplotype could be considered a hypomorphic allele, of which the penetrance depends on the contribution of other co-existing (common) variants.

Not all M0 or M1 *SLC26A4* cases could be genetically explained by the presence of the CEVA haplotype. Therefore, digenic inheritance with variants in *EPHA2*, *FOXI1*, and *KCNJ10* was also explored as a potential explanation for the missing heritability. Digenic inheritance of *SLC26A4* and *EPHA2* has recently been reported in two Japanese Pendred syndrome cases.⁷⁰ A c.1063G>A (p.(Gly355Arg)) and a c.1532C>T (p.(Thr511Met)) variant in *EPHA2* were each found *in trans* with a reported pathogenic variant in *SLC26A4* (Deafness Variation Database⁵⁰). *EPHA2* was identified as a binding partner of pendrin, with a crucial role in regulating pendrin localization.⁷⁰ The identified variants in *EPHA2* were predicted to be pathogenic by several *in silico* predictions tools. However, the c.1532C>T variant has a relatively high allele frequency of 3.03% in the East Asian population, including 11 homozygotes (gnomAD). Yet, in the present study, we did not obtain indications for digenic inheritance of variants in *SLC26A4* and *EPHA2* in subjects with HL and EVA. Besides for *EPHA2*, a digenic mechanism has also been reported and debated for variants in *SLC26A4* and *KCNJ10* or *FOXI1*, with currently no consensus.^{67-69,76,77} *FOXI1* is a transcriptional regulator of *SLC26A4*.⁶⁹ We identified a c.677C>T (p.(Thr226Ile)) *FOXI1* variant in three subjects (2 M0/*FOXI1* and 1 M0/CEVA/*FOXI1*). This variant was previously detected in an individual diagnosed with Pendred syndrome and a monoallelic pathogenic *SLC26A4* variant.⁶⁷ The variant has an allele frequency of 0.71% in non-Finnish Europeans (gnomAD) and affects an amino acid residue located outside the DNA-binding domain but close to the nuclear localization signal (NucPred⁷⁸). Previously reported pathogenic *FOXI1* variants have been shown to affect the DNA-binding properties of the protein.⁷⁹ We speculate that a variant affecting the localization motif of the protein could potentially have a loss of function effect as well. Although the variant is classified as likely benign according to the ACMG classification guidelines, we identified the variant three times in our cohort of genetically unexplained *SLC26A4* cases and combined with the fact that it has been reported in a previous study⁶⁷, this suggests that the variant might actually contribute to the etiology of HL and EVA although not in a monogenic pattern. Interestingly, in *Foxi1*^{-/-} mice, the expansion of the endolymphatic compartment and an audio-vestibular phenotype was observed.⁸⁰ *In situ* hybridization of the endolymphatic duct and sac of these mice revealed complete absence of *Slc26a4* mRNA expression. Functional studies,

among which cellular localizations assays, are warranted to evaluate the effect of the c.677C>T *FOXI1* variant. We did not identify likely pathogenic variants in *KCNJ10* (AF \leq 5%) in our cohort.

WGS did not reveal strong candidate regulatory variants based on data derived from enhancer databases and transcription factor binding site predictions. Nevertheless, interpretation of regulatory variants is still considered complex and is limited by the lack of available epigenetic datasets for the inner ear. Also, no SVs overlapping with *SLC26A4* were detected using WGS, suggesting a limited contribution of SVs to the mutational landscape of *SLC26A4*. This is in line with earlier observations described in literature.^{67,81} For the monoallelic cases (M1, M0/CEVA), no long-read sequencing or optical genome mapping was performed. As it is generally accepted that most SVs could not be accurately detected using short-read sequencing approaches only⁷², it cannot be excluded that causative SVs are present but missed due to technical limitations.

The present study did not confirm that the CEVA allele is associated with a milder HL compared to *SLC26A4* variants affecting the protein-coding sequences, as indicated by Chao et al.²³ They discerned a significantly milder HL in their cohort of M1/CEVA subjects (n=20 ears, median 47.5 dB HL) than we have seen in our cohort of M1/CEVA subjects (n=16 ears, median 84 dB HL). A possible explanation for this discrepancy could be the progression of HL combined with a ~5-year difference in average age between the cohorts (7.5 and 12.8 years, respectively). Progression of HL is seen in up to 39.6% of EVA-ears⁸², with progression rates of ~3.5 – ~5.5 dB/y.^{83,84} On the other hand, the older subjects in our M1/CEVA cohort show less severe HL than the younger subjects, which is questioning the relationship with age. Furthermore, there is also an average age difference of 5 years between the M2 groups in both studies (13.2 years and 18.4 years, respectively), while the severity of HL is comparable (85 and 86.3 dB HL, respectively).

The reported variability of the auditory phenotype associated with EVAs^{18,85,86} may be another explanation for the observed differences in severity of HL in both studies. In literature, many prognostic factors such as genotype, EVA size and morphology, age, head trauma, and gender are reported as underlying explanations for this variability, although some of these studies draw contradicting conclusions.^{82,85,87-91} In the same line, Song et al. reported intrafamilial differences in the severity of hearing loss in siblings with the same biallelic variants in *SLC26A4*.⁹² Larger sample sizes are needed to confirm or reject the hypothesis that the CEVA haplotype is associated with a milder HL phenotype. The significant difference in HL severity between the M2 and M1/CEVA groups versus the M0 group suggests that *SLC26A4* defects have a prognostic value which can be strengthened in the future by the identification of the underlying genetic defects in subjects of the M0 group.

In conclusion, the HL and EVA in 12 of the 28 studied subjects could be associated with *SLC26A4*. In addition, we have identified genetic factors that might (partially) explain the phenotype in four additional subjects. However, we could not pinpoint the genetic defect that is present on the CEVA haplotype. The arrival of third-generation sequencing techniques, the expansion of epigenetic and transcriptomic datasets and the increasing understanding of non-coding, structural, and regulatory variants will aid in solving the missing heritability in *SLC26A4* in the coming years. This is of great importance for counseling patients about the underlying cause and expected prognosis of their HL. Furthermore, as variants in *SLC26A4* are a frequent cause of HL¹⁰, it is an interesting target for the development of a genetic therapy.⁹³ Although the involved molecular defect of the CEVA haplotype is still not resolved, the high prevalence of the CEVA haplotype suggests that a significant portion of monoallelic *SLC26A4* cases can be associated with *SLC26A4* defects by testing for the presence of this haplotype.

ACKNOWLEDGEMENTS

The authors thank Lieke Lamers, Jolinda Put and Evelien Verwoerd for their assistance in genetic analyses and Ronald van Beek, Ellen Kater-Baats, Marcel Nelen and Michiel Oorsprong for technical support. We would like to thank Mieke Wesdorp for including subjects in the study and Galuh D.N. Astuti and Christian Gilissen for their contribution to statistical and bioinformatic analyses. We thank the Radboudumc Genomics Technology Center, Radboud University Medical Center Nijmegen, for their technical assistance. This study was financially supported by a DCMN Radboudumc grant (to H.K. and F.P.M.C.) and by a grant of the Heinsius-Houbolt foundation (to R.J.E.P. and H.K). TM was supported by the Sigrig Jusélius Foundation. This research was part of the Netherlands X-omics Initiative and partially funded by NWO (The Netherlands Organization for Scientific Research; project 184.034.019).

CONSORTIA

DOOFNL consortium: The DOOFNL consortium is a Dutch nationwide collaboration on hereditary hearing loss and consists of M.F. van Dooren, S.G. Kant, H.H.W. de Gier, E.H. Hoefsloot, M.P. van der Schroeff (ErasmusMC, Rotterdam, the Netherlands), L.J.C. Rotteveel, F.G. Ropers (LUMC, Leiden, the Netherlands), J.C.C. Widdershoven, J.R. Hof, E.K. Vanhoutte (MUMC+, Maastricht, the Netherlands), I. Feenstra, H. Kremer, C.P. Lanting, R.J.E. Pennings, H.G. Yntema (Radboudumc, Nijmegen, the Netherlands), R.H. Free and J.S. Klein Wassink-Ruiter (UMCG, Groningen, the Netherlands), R.J. Stokroos, A.L. Smit, M.J. van den Boogaard (UMC, Utrecht, the Netherlands) and F.A. Ebbens, S.M. Maas, A. Plomp, T.P.M. Goderie, P. Merkus and J. van de Kamp (Amsterdam UMC, Amsterdam, the Netherlands).

REFERENCES

1. Everett, L.A., Glaser, B., Beck, J.C., Idol, J.R., Buchs, A., Heyman, M. *et al.* Pendred syndrome is caused by mutations in a putative sulphate transporter gene (PDS). *Nature Genetics* 17, 411-422 (1997).
2. Everett, L.A., Morsli, H., Wu, D.K. & Green, E.D. Expression pattern of the mouse ortholog of the Pendred's syndrome gene (Pds) suggests a key role for pendrin in the inner ear. *Proceedings of the National Academy of Sciences* 96, 9727-9732 (1999).
3. Royaux, I.E., Suzuki, K., Mori, A., Katoh, R., Everett, L.A., Kohn, L.D. *et al.* Pendrin, the protein encoded by the Pendred syndrome gene (PDS), is an apical porter of iodide in the thyroid and is regulated by thyroglobulin in FRTL-5 cells. *Endocrinology* 141, 839-845 (2000).
4. Royaux, I.E., Wall, S.M., Karniski, L.P., Everett, L.A., Suzuki, K., Knepper, M.A. *et al.* Pendrin, encoded by the Pendred syndrome gene, resides in the apical region of renal intercalated cells and mediates bicarbonate secretion. *Proceedings of the National Academy of Sciences* 98, 4221-4226 (2001).
5. Pedemonte, N., Caci, E., Sondo, E., Caputo, A., Rhoden, K., Pfeiffer, U. *et al.* Thiocyanate transport in resting and IL-4-stimulated human bronchial epithelial cells: role of pendrin and anion channels. *Journal of Immunology* 178, 5144-5153 (2007).
6. Wangemann, P., Nakaya, K., Wu, T., Maganti, R.J., Itza, E.M., Sanneman, J.D. *et al.* Loss of cochlear HCO₃⁻ secretion causes deafness via endolymphatic acidification and inhibition of Ca²⁺ reabsorption in a Pendred syndrome mouse model. *American Journal of Physiology - Renal Physiology* 292, f1345-f1353 (2007).
7. Wangemann, P. The role of pendrin in the development of the murine inner ear. *Cellular Physiology and Biochemistry* 28, 527-534 (2011).
8. Dou, H., Xu, J., Wang, Z., Smith, A.N., Soleimani, M., Karet, F.E. *et al.* Co-expression of pendrin, vacuolar H⁺-ATPase alpha4-subunit and carbonic anhydrase II in epithelial cells of the murine endolymphatic sac. *Journal of Histochemistry & Cytochemistry* 52, 1377-1384 (2004).
9. Royaux, I.E., Belyantseva, I.A., Wu, T., Kachar, B., Everett, L.A., Marcus, D.C. *et al.* Localization and functional studies of pendrin in the mouse inner ear provide insight about the etiology of deafness in pendred syndrome. *Journal of the Association for Research in Otolaryngology* 4, 394-404 (2003).
10. Sloan-Heggen, C.M., Bierer, A.O., Shearer, A.E., Kolbe, D.L., Nishimura, C.J., Frees, K.L. *et al.* Comprehensive genetic testing in the clinical evaluation of 1119 patients with hearing loss. *Human Genetics* 135, 441-450 (2016).
11. Lee, H.J., Jung, J., Shin, J.W., Song, M.H., Kim, S.H., Lee, J.H. *et al.* Correlation between genotype and phenotype in patients with bi-allelic SLC26A4 mutations. *Clinical Chemistry* 86, 270-275 (2014).
12. Suzuki, H., Oshima, A., Tsukamoto, K., Abe, S., Kumakawa, K., Nagai, K. *et al.* Clinical characteristics and genotype-phenotype correlation of hearing loss patients with SLC26A4 mutations. *Acta Oto-Laryngologica* 127, 1292-1297 (2007).
13. Fraser, G.R. Association of congenital deafness with goitre (pendred's syndrome): A study of 207 families. *Annals of Human Genetics* 28, 201-249 (1965).
14. van Beeck Calkoen, E.A., Sanchez Aliaga, E., Merkus, P., Smit, C.F., van de Kamp, J.M., Mulder, M.F. *et al.* High prevalence of abnormalities on CT and MR imaging in children with unilateral sensorineural hearing loss irrespective of age or degree of hearing loss. *International Journal of Pediatric Otorhinolaryngology* 97, 185-191 (2017).

15. van Beeck Calkoen, E.A., Merkus, P., Goverts, S.T., van de Kamp, J.M., Mulder, M.F., Sanchez Aliaga, E. *et al.* Evaluation of the outcome of CT and MR imaging in pediatric patients with bilateral sensorineural hearing loss. *International Journal of Pediatric Otorhinolaryngology* 108, 180-185 (2018).
16. Mey, K., Muhamad, A.A., Tranebjaerg, L., Rendtorff, N.D., Rasmussen, S.H., Bille, M. *et al.* Association of SLC26A4 mutations, morphology, and hearing in pendred syndrome and NSEVA. *The Laryngoscope* 129, 2574-2579 (2019).
17. Forli, F., Lazerini, F., Auletta, G., Bruschini, L. & Berrettini, S. Enlarged vestibular aqueduct and Mondini Malformation: audiological, clinical, radiologic and genetic features. *European Archives of Oto-Rhino-Laryngology* 278, 2305-2312 (2021).
18. Griffith, A.J. & Wangemann, P. Hearing loss associated with enlargement of the vestibular aqueduct: mechanistic insights from clinical phenotypes, genotypes, and mouse models. *Hearing Research* 281, 11-17 (2011).
19. Choi, B.Y., Madeo, A.C., King, K.A., Zalewski, C.K., Pryor, S.P., Muskett, J.A. *et al.* Segregation of enlarged vestibular aqueducts in families with non-diagnostic SLC26A4 genotypes. *Journal of Medical Genetics* 46, 856-861 (2009).
20. Azaiez, H., Yang, T., Prasad, S., Sorensen, J.L., Nishimura, C.J., Kimberling, W.J. *et al.* Genotype-phenotype correlations for SLC26A4-related deafness. *Human Genetics* 122, 451-457 (2007).
21. Pryor, S.P., Madeo, A.C., Reynolds, J.C., Sarlis, N.J., Arnos, K.S., Nance, W.E. *et al.* SLC26A4/PDS genotype-phenotype correlation in hearing loss with enlargement of the vestibular aqueduct (EVA): evidence that Pendred syndrome and non-syndromic EVA are distinct clinical and genetic entities. *Journal of Medical Genetics* 42, 159-165 (2005).
22. Chattaraj, P., Munjal, T., Honda, K., Rendtorff, N.D., Ratay, J.S., Muskett, J.A. *et al.* A common SLC26A4-linked haplotype underlying non-syndromic hearing loss with enlargement of the vestibular aqueduct. *Journal of Medical Genetics* 54, 665-673 (2017).
23. Chao, J.R., Chattaraj, P., Munjal, T., Honda, K., King, K.A., Zalewski, C.K. *et al.* SLC26A4-linked CEVA haplotype correlates with phenotype in patients with enlargement of the vestibular aqueduct. *BMC Medical Genetics* 20, 118 (2019).
24. van der Ploeg, C.P., Uilenburg, N.N., Kauffman-de Boer, M.A., Oudesluys-Murphy, A.M. & Verkerk, P.H. Newborn hearing screening in youth health care in the Netherlands: national results of implementation and follow-up. *International Journal of Audiology* 51, 584-590 (2012).
25. Boston, M., Halsted, M., Meinzen-Derr, J., Bean, J., Vijayasekaran, S., Arjmand, E. *et al.* The large vestibular aqueduct: a new definition based on audiologic and computed tomography correlation. *Otolaryngology - Head and Neck Surgery* 136, 972-977 (2007).
26. Lenth, R.V. Least-Squares Means: The R package lsmeans. *Journal of Statistical Software* 69, 1-33 (2016).
27. Li, H. & Durbin, R. Fast and accurate short read alignment with Burrows-Wheeler transform. *Bioinformatics* 25, 1754-1760 (2009).
28. McKenna, A., Hanna, M., Banks, E., Sivachenko, A., Cibulskis, K., Kernysky, A. *et al.* The Genome Analysis Toolkit: a MapReduce framework for analyzing next-generation DNA sequencing data. *Genome Research* 20, 1297-1303 (2010).
29. Krumm, N., Sudmant, P.H., Ko, A., O'Roak, B.J., Malig, M., Coe, B.P. *et al.* Copy number variation detection and genotyping from exome sequence data. *Genome Research* 22, 1525-1532 (2012).

30. Chen, X., Schulz-Trieglaff, O., Shaw, R., Barnes, B., Schlesinger, F., Källberg, M. *et al.* Manta: rapid detection of structural variants and indels for germline and cancer sequencing applications. *Bioinformatics* 32, 1220-1222 (2016).
31. Boeva, V., Popova, T., Bleakley, K., Chiche, P., Cappo, J., Schleiermacher, G. *et al.* Control-FREEC: a tool for assessing copy number and allelic content using next-generation sequencing data. *Bioinformatics* 28, 423-425 (2012).
32. de Bruijn, S.E., Smits, J.J., Liu, C., Lanting, C.P., Beynon, A.J., Blankevoort, J. *et al.* A RIPOR2 in-frame deletion is a frequent and highly penetrant cause of adult-onset hearing loss. *Journal of Medical Genetics* 58, 96 (2021).
33. Neveling, K., Mensenkamp, A.R., Derks, R., Kwint, M., Ouchene, H., Steehouwer, M. *et al.* BRCA testing by single-molecule molecular inversion probes. *Clinical Chemistry* 63, 503-512 (2017).
34. Khan, M., Cornelis, S.S., Pozo-Valero, M.D., Whelan, L., Runhart, E.H., Mishra, K. *et al.* Resolving the dark matter of ABCA4 for 1054 Stargardt disease probands through integrated genomics and transcriptomics. *Genetics in Medicine* 22, 1235-1246 (2020).
35. Wesdorp, M., Murillo-Cuesta, S., Peters, T., Celaya, A.M., Oonk, A., Schraders, M. *et al.* MPZL2, encoding the epithelial junctional protein myelin protein zero-like 2, is essential for hearing in man and mouse. *American Journal of Human Genetics* 103, 74-88 (2018).
36. Karczewski, K.J., Francioli, L.C., Tiao, G., Cummings, B.B., Alfoldi, J., Wang, Q. *et al.* Variation across 141,456 human exomes and genomes reveals the spectrum of loss-of-function intolerance across human protein-coding genes. *bioRxiv*, 531210 (2019).
37. Robinson, J.T., Thorvaldsdóttir, H., Winckler, W., Guttman, M., Lander, E.S., Getz, G. *et al.* Integrative genomics viewer. *Nature Biotechnology* 29, 24-26 (2011).
38. Kircher, M., Witten, D.M., Jain, P., O’Roak, B.J., Cooper, G.M. & Shendure, J. A general framework for estimating the relative pathogenicity of human genetic variants. *Nature Genetics* 46, 310-315 (2014).
39. Vaser, R., Adusumalli, S., Leng, S.N., Sikic, M. & Ng, P.C. SIFT missense predictions for genomes. *Nature Protocols* 11, 1 (2015).
40. Adzhubei, I.A., Schmidt, S., Peshkin, L., Ramensky, V.E., Gerasimova, A., Bork, P. *et al.* A method and server for predicting damaging missense mutations. *Nature Methods* 7, 248-249 (2010).
41. Schwarz, J.M., Cooper, D.N., Schuelke, M. & Seelow, D. MutationTaster2: mutation prediction for the deep-sequencing age. *Nature Methods* 11, 361 (2014).
42. Jaganathan, K., Kyriazopoulou Panagiotopoulou, S., McRae, J.F., Darbandi, S.F., Knowles, D., Li, Y.I. *et al.* Predicting splicing from primary sequence with deep learning. *Cell* 176, 535-548 (2019).
43. Sangermano, R., Khan, M., Cornelis, S.S., Richelle, V., Albert, S., Garanto, A. *et al.* ABCA4 midgenes reveal the full splice spectrum of all reported noncanonical splice site variants in Stargardt disease. *Genome Research* 28, 100-110 (2018).
44. Kent, W.J., Sugnet, C.W., Furey, T.S., Roskin, K.M., Pringle, T.H., Zahler, A.M. *et al.* The human genome browser at UCSC. *Genome Research* 12, 996-1006 (2002).
45. Mantere, T., Neveling, K., Pebrel-Richard, C., Benoist, M., van der Zande, G., Kater-Baats, E. *et al.* Optical genome mapping enables constitutional chromosomal aberration detection. *American Journal of Human Genetics* 108, 1409-1422 (2021).

46. Neveling, K., Mantere, T., Vermeulen, S., Oorsprong, M., van Beek, R., Kater-Baats, E. *et al.* Next-generation cytogenetics: comprehensive assessment of 52 hematological malignancy genomes by optical genome mapping. *American Journal of Human Genetics* 108, 1423-1435 (2021).
47. Pedersen, B.S. & Quinlan, A.R. Mosdepth: quick coverage calculation for genomes and exomes. *Bioinformatics* 34, 867-868 (2018).
48. Van Camp, G. & Smith, R. Hereditary Hearing Loss Homepage. Available from: <https://hereditaryhearingloss.org>.
49. Landrum, M.J., Lee, J.M., Benson, M., Brown, G.R., Chao, C., Chitipiralla, S. *et al.* ClinVar: improving access to variant interpretations and supporting evidence. *Nucleic Acids Research* 46, d1062-d1067 (2018).
50. Azaiez, H., Booth, K.T., Ephraim, S.S., Crone, B., Black-Ziegelbein, E.A., Marini, R.J. *et al.* Genomic landscape and mutational signatures of deafness-associated genes. *American Journal of Human Genetics* 103, 484-497 (2018).
51. Oza, A.M., DiStefano, M.T., Hemphill, S.E., Cushman, B.J., Grant, A.R., Siegert, R.K. *et al.* Expert specification of the ACMG/AMP variant interpretation guidelines for genetic hearing loss. *Human Mutation* 39, 1593-1613 (2018).
52. Yariz, K.O., Duman, D., Zazo Seco, C., Dallman, J., Huang, M., Peters, T.A. *et al.* Mutations in OTOGL, encoding the inner ear protein otogelin-like, cause moderate sensorineural hearing loss. *American Journal of Human Genetics* 91, 872-882 (2012).
53. Oonk, A.M., Leijendeckers, J.M., Huygen, P.L., Schraders, M., del Campo, M., del Castillo, I. *et al.* Similar phenotypes caused by mutations in OTOG and OTOGL. *Ear and Hearing* 35, e84-e91 (2014).
54. Genomes Project Consortium, Auton, A., Brooks, L.D., Durbin, R.M., Garrison, E.P., Kang, H.M. *et al.* A global reference for human genetic variation. *Nature* 526, 68-74 (2015).
55. van Beeck Calkoen, E.A., Engel, M.S.D., van de Kamp, J.M., Yntema, H.G., Goverts, S.T., Mulder, M.F. *et al.* The etiological evaluation of sensorineural hearing loss in children. *European Journal of Pediatrics* 178, 1195-1205 (2019).
56. Fishilevich, S., Nudel, R., Rappaport, N., Hadar, R., Plaschkes, I., Iny Stein, T. *et al.* GeneHancer: genome-wide integration of enhancers and target genes in GeneCards. *Database (Oxford)* 2017, bax028 (2017).
57. Gao, T. & Qian, J. EnhancerAtlas 2.0: an updated resource with enhancer annotation in 586 tissue/cell types across nine species. *Nucleic Acids Research* 48, d58-d64 (2020).
58. Dunham, I., Kundaje, A., Aldred, S.F., Collins, P.J., Davis, C.A., Doyle, F. *et al.* An integrated encyclopedia of DNA elements in the human genome. *Nature* 489, 57-74 (2012).
59. Zerbino, D.R., Wilder, S.P., Johnson, N., Juettemann, T. & Flicek, P.R. The Ensembl regulatory build. *Genome Biology* 16, 56 (2015).
60. Andersson, R., Gebhard, C., Miguel-Escalada, I., Hoof, I., Bornholdt, J., Boyd, M. *et al.* An atlas of active enhancers across human cell types and tissues. *Nature* 507, 455-461 (2014).
61. Visel, A., Minovitsky, S., Dubchak, I. & Pennacchio, L.A. VISTA Enhancer Browser—a database of tissue-specific human enhancers. *Nucleic Acids Research* 35, d88-d92 (2007).
62. Khan, A. & Zhang, X. dbSUPER: a database of super-enhancers in mouse and human genome. *Nucleic Acids Research* 44, d164-d171 (2016).
63. Dreos, R., Ambrosini, G., Cavin Périer, R. & Bucher, P. EPD and EPDnew, high-quality promoter resources in the next-generation sequencing era. *Nucleic Acids Research* 41, d157-d164 (2013).

64. Dimitrieva, S. & Bucher, P. UCNEbase—a database of ultraconserved non-coding elements and genomic regulatory blocks. *Nucleic Acids Research* 41, d101-d109 (2013).
65. Wilderman, A., VanOudenhove, J., Kron, J., Noonan, J.P. & Cotney, J. High-resolution epigenomic atlas of human embryonic craniofacial development. *Cell Reports* 23, 1581-1597 (2018).
66. Fornes, O., Castro-Mondragon, J.A., Khan, A., van der Lee, R., Zhang, X., Richmond, P.A. *et al.* JASPAR 2020: update of the open-access database of transcription factor binding profiles. *Nucleic Acids Research* 48, d87-d92 (2020).
67. Pique, L.M., Brennan, M.L., Davidson, C.J., Schaefer, F., Greinwald, J., Jr. & Schrijver, I. Mutation analysis of the SLC26A4, FOXI1 and KCNJ10 genes in individuals with congenital hearing loss. *PeerJ* 2, e384 (2014).
68. Yang, T., Gurrola, J.G., Wu, H., Chiu, S.M., Wangemann, P., Snyder, P.M. *et al.* Mutations of KCNJ10 together with mutations of SLC26A4 cause digenic nonsyndromic hearing loss associated with enlarged vestibular aqueduct syndrome. *American Journal of Human Genetics* 84, 651-657 (2009).
69. Yang, T., Vidarsson, H., Rodrigo-Blomqvist, S., Rosengren, S.S., Enerback, S. & Smith, R.J. Transcriptional control of SLC26A4 is involved in Pendred syndrome and nonsyndromic enlargement of vestibular aqueduct (DFNB4). *American Journal of Human Genetics* 80, 1055-1063 (2007).
70. Li, M., Nishio, S.-y., Naruse, C., Riddell, M., Sapski, S., Katsuno, T. *et al.* Digenic inheritance of mutations in EPHA2 and SLC26A4 in Pendred syndrome. *Nature Communications* 11, 1343 (2020).
71. Levy-Sakin, M., Pastor, S., Mostovoy, Y., Li, L., Leung, A.K.Y., McCaffrey, J. *et al.* Genome maps across 26 human populations reveal population-specific patterns of structural variation. *Nature Communications* 10, 1025 (2019).
72. Chaisson, M.J.P., Sanders, A.D., Zhao, X., Malhotra, A., Porubsky, D., Rausch, T. *et al.* Multi-platform discovery of haplotype-resolved structural variation in human genomes. *Nature Communications* 10, 1784 (2019).
73. Xie, H., Wang, M., Bischof, J., Bonaldo, M.d.F. & Soares, M.B. SNP-based prediction of the human germ cell methylation landscape. *Genomics* 93, 434-440 (2009).
74. Hosoya, M., Fujioka, M., Sone, T., Okamoto, S., Akamatsu, W., Ukai, H. *et al.* Cochlear cell modeling using disease-specific iPSCs unveils a degenerative phenotype and suggests treatments for congenital progressive hearing loss. *Cell Reports* 18, 68-81 (2017).
75. Morton, C.C. & Nance, W.E. Newborn hearing screening—a silent revolution. *New England Journal of Medicine* 354, 2151-2164 (2006).
76. Landa, P., Differ, A.-M., Rajput, K., Jenkins, L. & Bitner-Glindzicz, M. Lack of significant association between mutations of KCNJ10 or FOXI1 and SLC26A4 mutations in pendred syndrome/enlarged vestibular aqueducts. *BMC Medical Genetics* 14, 85 (2013).
77. Jonard, L., Niasme-Grare, M., Bonnet, C., Feldmann, D., Rouillon, I., Loundon, N. *et al.* Screening of SLC26A4, FOXI1 and KCNJ10 genes in unilateral hearing impairment with ipsilateral enlarged vestibular aqueduct. *International Journal of Pediatric Otorhinolaryngology* 74, 1049-1053 (2010).
78. Brameier, M., Krings, A. & MacCallum, R.M. NucPred—predicting nuclear localization of proteins. *Bioinformatics* 23, 1159-1160 (2007).
79. Enerbäck, S., Nilsson, D., Edwards, N., Heglind, M., Alkanderi, S., Ashton, E. *et al.* Acidosis and deafness in patients with recessive mutations in FOXI1. *Journal of the American Society of Nephrology : JASN* 29, 1041-1048 (2018).

80. Hulander, M., Kiernan, A.E., Blomqvist, S.R., Carlsson, P., Samuelsson, E.J., Johansson, B.R. *et al.* Lack of pendrin expression leads to deafness and expansion of the endolymphatic compartment in inner ears of Foxi1 null mutant mice. *Development* 130, 2013-2025 (2003).
81. Liu, Y.L., Wang, L.L., Wen, J., Mei, L.Y., He, C.F., Jiang, L. *et al.* Application value of high-throughput gene copy number variation detection in the diagnosis of enlarged vestibular aqueduct. *Zhonghua Yi Xue Za Zhi* 101, 103-107 (2021).
82. Alemi, A.S. & Chan, D.K. Progressive hearing loss and head trauma in enlarged vestibular aqueduct: A systematic review and meta-analysis. *Otolaryngology - Head and Neck Surgery* 153, 512-517 (2015).
83. Jackler, R.K. & de la Cruz, A. The large vestibular aqueduct syndrome. *The Laryngoscope* 99, 1238-1243 (1989).
84. Govaerts, P.J., Casselman, J., Daemers, K., De Ceulaer, G., Somers, T. & Offeciers, F.E. Audiological findings in large vestibular aqueduct syndrome. *International Journal of Pediatric Otorhinolaryngology* 51, 157-164 (1999).
85. Gopen, Q., Zhou, G., Whittemore, K. & Kenna, M. Enlarged vestibular aqueduct: review of controversial aspects. *The Laryngoscope* 121, 1971-1978 (2011).
86. Arjmand, E.M. & Webber, A. Audiometric findings in children with a large vestibular aqueduct. *Archives of Otolaryngology-Head & Neck Surgery* 130, 1169-1174 (2004).
87. Archibald, H.D., Ascha, M., Gupta, A., Megerian, C. & Otteson, T. Hearing loss in unilateral and bilateral enlarged vestibular aqueduct syndrome. *International Journal of Pediatric Otorhinolaryngology* 118, 147-151 (2019).
88. Ascha, M.S., Manzoor, N., Gupta, A., Semaan, M., Megerian, C. & Otteson, T.D. Vestibular aqueduct midpoint width and hearing loss in patients with an enlarged vestibular aqueduct. *JAMA Otolaryngology - Head & Neck Surgery* 143, 601-608 (2017).
89. Saeed, H.S., Kenth, J., Black, G., Saeed, S.R., Stivaros, S. & Bruce, I.A. Hearing loss in enlarged vestibular aqueduct: a prognostic factor systematic review of the literature. *Otology & Neurotology* 42, 99-107 (2021).
90. Rah, Y.C., Kim, A.R., Koo, J.-W., Lee, J.H., Oh, S.-h. & Choi, B.Y. Audiologic presentation of enlargement of the vestibular aqueduct according to the SLC26A4 genotypes. *The Laryngoscope* 125, e216-e222 (2015).
91. Miyagawa, M., Nishio, S.-y., Usami, S.-i. & The Deafness Gene Study, C. Mutation spectrum and genotype-phenotype correlation of hearing loss patients caused by SLC26A4 mutations in the Japanese: a large cohort study. *Journal of Human Genetics* 59, 262-268 (2014).
92. Song, M.H., Shin, J.-W., Park, H.-J., Lee, K.-A., Kim, Y., Kim, U.-K. *et al.* Intrafamilial phenotypic variability in families with biallelic SLC26A4 mutations. *The Laryngoscope* 124, e194-e202 (2014).
93. Kim, M.-A., Kim, S.H., Ryu, N., Ma, J.-H., Kim, Y.-R., Jung, J. *et al.* Gene therapy for hereditary hearing loss by SLC26A4 mutations in mice reveals distinct functional roles of pendrin in normal hearing. *Theranostics* 9, 7184-7199 (2019).

SUPPLEMENTARY TABLES

Table S1. Genotype of reference cohort with biallelic pathogenic variants in *SLC26A4*

Case	Allele 1		Allele 2	
	Variant	ACMG	Variant	ClinVar
SLC087	c.1147del; p.(Gln383Argfs*49)	UV5	c.1147del; p.(Gln383Argfs*49)	UV5
SLC088	c.2T>C; p.(Met1?)	UV5	c.707T>C; p.(Leu236Pro)	UV5
SLC089	c.890del; p.(Pro297Glnfs*6)	UV5	c.1246A>C; p.(Thr416Pro)	UV5
SLC090	c.1001+1G>A; p.(?)	UV5	c.1001+1G>A; p.(?)	UV5
SLC091	c.1225C>T; p.(Arg409Cys)	UV5	c.707T>C; p.(Leu236Pro)	UV5
SLC092	c.1694G>A; p.(Cys565Tyr)	UV5	c.707T>C; p.(Leu236Pro)	UV5
SLC093	c.754T>C; p.(Ser252Pro)	UV4	c.1174A>T; p.(Asn392Tyr)	UV5
SLC094	c.2048T>C; p.(Phe683Ser)	UV5	c.707T>C; p.(Leu236Pro)	UV5
SLC095	c.1246A>C; p.(Thr416Pro)	UV5	c.707T>C; p.(Leu236Pro)	UV5

Genotype of a control cohort of nine subjects with two (likely) pathogenic variants in the coding or splice site regions of *SLC26A4* and a Pendred syndrome phenotype. Segregation analysis to confirm biallelic occurrence of the variants could be carried out in all subjects, except for subjects SLC091 and SLC092. ACMG, variant classification according to the American College of Medical Genetics and Genomics (ACMG) classification guidelines; UV4, likely pathogenic; UV5, pathogenic.

Table S2. Details of applied next generation sequencing methods

Case	Sequencing method	Platform	% Reads coverage ≥ 20x	Mean coverage (x reads)
SLC002	WGS	BGISeq500	88.14	36
SLC003	MIPS	NextSeq500	94.78	920
SLC012	WGS	BGISeq500	88.45	37
SLC013	MIPS	NextSeq500	91.78	900
SLC014	MIPS	NextSeq500	92.28	815
SLC015	WES	Illumina HiSeq2000	96.84	115
SLC017	WES	Illumina HiSeq2000	96.70	125
SLC018	WGS	BGISeq500	88.77	39
SLC031	MIPS	NextSeq500	93.31	517
SLC032	WGS	BGISeq500	89.62	43
SLC036	WGS	BGISeq500	89.21	41
SLC039	MIPS	NextSeq500	93.33	676
	WGS	BGISeq500	89.21	41
SLC040	WES	Illumina HiSeq4000	93.50	136
SLC043	WES	Illumina HiSeq2000	94.85	111
SLC045	MIPS	NextSeq500	92.28	590
	WGS	BGISeq500	83.83	30
SLC048	WGS	BGISeq500	88.82	38
SLC052	WES	Illumina HiSeq2000	93.77	103
SLC056	MIPS	NextSeq500	95.21	901
SLC069	WES	Illumina HiSeq2000	96.62	130
SLC070	WES	Illumina HiSeq4000	97.18	118
SLC071	WES	Illumina HiSeq4000	97.33	121
SLC073	MIPS	NextSeq500	94.99	880
SLC078	MIPS	NextSeq500	95.63	1017
SLC079	WES	Illumina HiSeq4000	97.17	101
	LRS	Sequel II PacBio	NA	12
SLC080	WES	Illumina HiSeq4000	97.40	115
	WGS	BGISeq500	85.27	30
SLC084	WES	Illumina HiSeq4000	98.01	123
SLC085	WGS	BGISeq500	80.33	30
SLC086	WES	Illumina HiSeq4000	97.34	123

WES, whole exome sequencing; WGS, short-read whole genome sequencing; MIPS, molecular inversion probe sequencing; LRS, long-read whole genome sequencing; NA, not applicable.

Table S3. Genes analyzed by MIP sequencing

<i>ACTG1</i>	<i>EPS8</i>	<i>LRTOMT</i>	<i>RIPOR2</i>
<i>ADCY1</i>	<i>ESPN</i>	<i>MARVELD2</i>	<i>S1PR2</i>
<i>ADGRV1</i>	<i>ESRRB</i>	<i>MCM2</i>	<i>SERPINB6</i>
<i>AIFM1</i>	<i>EYA1</i>	<i>MIR96</i>	<i>SIX1</i>
<i>ATP1A2</i>	<i>EYA4</i>	<i>MITF</i>	<i>SIX5</i>
<i>BDP1</i>	<i>GIPC3</i>	<i>MPZL2</i>	<i>SLC9A1</i>
<i>BSND</i>	<i>GJB2</i>	<i>MSRB3</i>	<i>SLC17A8</i>
<i>CABP2</i>	<i>GJB3</i>	<i>MYH14</i>	<i>SLC22A4</i>
<i>CCDC50</i>	<i>GJB6</i>	<i>MYH9</i>	<i>SLC26A4</i>
<i>CD164</i>	<i>GPSM2</i>	<i>MYO15A</i>	<i>SLC26A5</i>
<i>CDH23</i>	<i>GRHL2</i>	<i>MYO3A</i>	<i>SMPX</i>
<i>CEACAM16</i>	<i>GRM7</i>	<i>MYO6</i>	<i>SNAI2</i>
<i>CIB2</i>	<i>GRM8</i>	<i>MYO7A</i>	<i>SOX10</i>
<i>CLDN14</i>	<i>GRXCR1</i>	<i>NARS2</i>	<i>STRC</i>
<i>CLIC5</i>	<i>GRXCR2</i>	<i>NAT2</i>	<i>SYNE4</i>
<i>CLPP</i>	<i>GSDME</i>	<i>OSBPL2</i>	<i>TBC1D24</i>
<i>CLRN1</i>	<i>HARS2</i>	<i>OTOA</i>	<i>TECTA</i>
<i>COCH</i>	<i>HGF</i>	<i>OTOF</i>	<i>TJP2</i>
<i>COL11A2</i>	<i>HOMER2</i>	<i>OTOG</i>	<i>TMC1</i>
<i>COL4A6</i>	<i>HSD17B4</i>	<i>OTOGL</i>	<i>TMEM132E</i>
<i>CRYM</i>	<i>ILDR1</i>	<i>P2RX2</i>	<i>TMIE</i>
<i>DCDC2</i>	<i>KARS</i>	<i>PAX3</i>	<i>TMPRSS3</i>
<i>DFNB31</i>	<i>KCNE1</i>	<i>PCDH15</i>	<i>TNC</i>
<i>DFNB59</i>	<i>KCNJ10</i>	<i>PDZD7</i>	<i>TPRN</i>
<i>DIABLO</i>	<i>KCNQ1</i>	<i>PNPT1</i>	<i>TRIOBP</i>
<i>DIAPH1</i>	<i>KCNQ4</i>	<i>POU3F4</i>	<i>TSPEAR</i>
<i>DSPP</i>	<i>KITLG</i>	<i>POU4F3</i>	<i>USH1C</i>
<i>EDN3</i>	<i>LARS2</i>	<i>PRPS1</i>	<i>USH1G</i>
<i>EDNRB</i>	<i>LHFPL5</i>	<i>PTPRQ</i>	<i>USH2A</i>
<i>ELMOD3</i>	<i>LOXHD1</i>	<i>RDX</i>	<i>WFS1</i>

Table S4. Compound heterozygous or homozygous variants in arHL-associated genes

Case	Class	Gene	Transcript	cDNA	Protein	In-house AF (%)	gnomAD AF (%)	CADD_PHRD	SIFT	PPH2	MutationTaster	SpliceAI	ACMG
SLC012	M1	OTOGL	NM_173591.3	c.890C>T	p.(Pro297Leu)	0.09	0.12	22.5	0	1.0	Disease causing	-	UV2
		OTOGL	NM_173591.3	c.1369G>T	p.(Val457Leu)	0.02	0.00	15.4	0	0.683	Disease causing	-	UV3

Homozygous or compound heterozygous variants detected in coding or splice site regions (+/14 nucleotides) of genes associated with autosomal recessive hearing loss (arHL). Variants are selected based on an allele frequency of $\leq 0.5\%$ in gnomAD and the in-house database. Scores that meet the thresholds for pathogenicity as described in the methods section are indicated in red. Thresholds for pathogenicity: CADD-PHRD (≥ 15), SIFT (≤ 0.05), PolyPhen-2 (≥ 0.450), MutationTaster (deleterious) and spliceAI (≥ 0.1). In-house AF, allele frequency (%) in in-house database ($\sim 7,500$ exomes); GnomAD AF, allele frequency (%) in gnomAD database V.2.1.1; CADD_PHRD, Combined Annotation Dependent Depletion PHRED score; SIFT, Scale-Invariant Feature Transform; PPH2, Poly-Phen-2 score; MutationTaster (prob), MutationTaster score with probability (0-1); spliceAI, splicing prediction score; ClinVar, ACMG, variant classification according to the American College of Medical Genetics and Genomics (ACMG) classification guidelines; UV2, likely benign; UV3, uncertain significance.

Table S5. List of *cis* regulatory elements of *SLC26A4*

Gene	Start	End	Source
<i>SLC26A4, SLC26A4-AS1</i>	106740447	106742845	GeneHancer V5.0
<i>SLC26A4, SLC26A4-AS1</i>	106743446	106747050	GeneHancer V5.0
<i>SLC26A4, SLC26A4-AS1</i>	106762501	106763480	GeneHancer V5.0
<i>SLC26A4, SLC26A4-AS1</i>	107103661	107105444	GeneHancer V5.0
<i>SLC26A4, SLC26A4-AS1</i>	107120646	107123445	GeneHancer V5.0
<i>SLC26A4, SLC26A4-AS1</i>	107199656	107223646	GeneHancer V5.0
<i>SLC26A4, SLC26A4-AS1</i>	107219645	107223646	GeneHancer V5.0
<i>SLC26A4, SLC26A4-AS1</i>	107232401	107238444	GeneHancer V5.0
<i>SLC26A4-AS1</i>	107234760	107236310	EnhancerAtlas 2.0
<i>SLC26A4, SLC26A4-AS1</i>	107254046	107255844	GeneHancer V5.0
<i>SLC26A4, SLC26A4-AS1</i>	107262447	107263690	GeneHancer V5.0
<i>SLC26A4, SLC26A4-AS1</i>	107276447	107280445	GeneHancer V5.0
<i>SLC26A4, SLC26A4-AS1</i>	107301300	107302040	EnhancerAtlas 2.0
<i>SLC26A4, SLC26A4-AS1</i>	107301445	107302845	GeneHancer V5.0
<i>SLC26A4, SLC26A4-AS1</i>	107330247	107335644	GeneHancer V5.0
<i>SLC26A4</i>	107334930	107335060	EnhancerAtlas 2.0
<i>SLC26A4</i>	107336480	107338480	EnhancerAtlas 2.0
<i>SLC26A4</i>	107350640	107352980	EnhancerAtlas 2.0
<i>SLC26A4, SLC26A4-AS1</i>	107382558	107387330	GeneHancer V5.0
<i>SLC26A4, SLC26A4-AS1</i>	107495047	107499844	GeneHancer V5.0
<i>SLC26A4, SLC26A4-AS1</i>	107531740	107533640	EnhancerAtlas 2.0
<i>SLC26A4</i>	107564530	107564670	EnhancerAtlas 2.0
<i>SLC26A4, SLC26A4-AS1</i>	107643420	107643550	EnhancerAtlas 2.0
<i>SLC26A4</i>	107743680	107744940	EnhancerAtlas 2.0

List of human *cis* regulatory elements associated with *SLC26A4* or *SLC26A4-AS1* that are collected in the GeneHancer database V5.0² or the EnhancerAtlas 2.0³. Only *cis* regulatory elements with an enhancer score >0.7 and an enhancer-gene interaction score >7 were extracted from Genehancer. For EnhancerAtlas 2.0, all enhancer elements that were experimentally determined in human tissues or cell types were selected. Start and End; Genomic positions on chromosome 7 according to GRCh37/hg19.

Table S6. Heterozygous variants in (predicted) cis regulatory elements of SLC26A4

Case	Class	Variant	gnomAD AF (%)	Regulatory element	Source	Identifier	Enhancer score	Enhancer-gene score	PhyloP
SLC002	M1	Chr7:107220628C>A	-1	Chr7:107219645-107223646	GeneHancer V5	GH07J107579	2.05	10.54	-1.143
SLC045	M1	Chr7:107384987C>G	0.19	Chr7:107382558-107387330	GeneHancer V5	GH07J107742	2.25	10.63	0.183

A list of potential cis regulatory elements of SLC26A4 (GeneHancer V5³ and EnhancerAtlas V2³) was screened for the presence of rare heterozygous variants (allele frequency £0.5%) in available whole genome sequencing datasets. For none of the variants, the loss of a transcription factor binding site (TFBS) is predicted (JASPAR database⁴, >80% TFBS confidence score and a delta score of >10%), gnomAD AF, allele frequency (%) in gnomAD database V2.1.1; Regulatory element, genomic position of regulatory element according to GRCh37/hg19; Identifier; unique identifier of regulatory element as accessible in GeneCards⁵; Enhancer score and Enhancer-gene score of regulatory element as provided by the GeneHancer database; PhyloP⁶; nucleotide evolutionary conservation score.

Table S7. Rare genetic variants located within the CEVA haplotype

Genome	RefSNP	Location	gnomAD AF (%)	SpliceAI	PhyloP	Repeatmasker	Regulatory element
Chr7:106622156T>A	rs6961007	Intergenic	-	NA	-5.094	SINE	-
Chr7:106669858G>A (SNP1)	rs17424561	Intergenic	3.04	NA	-1.806	-	-
Chr7:106690778CTTTT>T	NA	Intronic (PPKAR2B)	-	0.01	0.556	-	-
Chr7:106736863C>T	rs149440050	Intronic (PPKAR2B)	3.07	0.01	0.135	LINE	-
Chr7:106741374T>C (SNP2)	rs79579403	Intronic (PPKAR2B)	3.03	0.00	0.8	LINE	GeneHancer
Chr7:106741580ATT>A	NA	Intronic (PPKAR2B)	-	0.01	0	LINE	GeneHancer
Chr7:106764419T>A (SNP3)	rs17425867	Intronic (PPKAR2B)	3.05	0.00	0.852	-	-
Chr7:106807591TAAAA>T	NA	Intergenic	-	NA	0.621	-	-
Chr7:106812322A>A	NA	Intronic (HBP1)	-	0.00	-2.377	SINE	-
Chr7:106815154T>C (SNP4)	rs117113959	Intronic (HBP1)	2.93	0.05	-0.481	-	-
Chr7:106837681G>A (SNP5)	rs17349280	Intronic (HBP1)	2.90	0.01	0.275	-	-
Chr7:106930234C>T (SNP6)	rs117386523	Intronic (COG5)	2.92	0.00	0.641	-	-
Chr7:106967931A>G (SNP7)	rs80149210	Intronic (COG5)	2.91	0.00	0.838	LINE	-



Table S7. (continued)

Genome	RefSNP	Location	gnomAD AF (%)	SpliceAI	PhyloP	Repeatmasker	Regulatory element
<u>Chr7:106993159A>T</u> (SNP8)	rs199667576	Intronic (COG5)	2.96	0.00	-100	-	-
<u>Chr7:107014419A>G</u> (SNP9)	rs9649298	Intronic (COG5)	2.90	0.00	2.769	-	-
Chr7:107081658G>A	rs188905420	Intronic (COG5)	2.31	0.00	-2.019	SINE	-
<u>Chr7:107147622T>C</u> (SNP10)	rs117714350	Intronic (COG5)	2.32	0.00	0.238	LINE	-
<u>Chr7:107242636C>T</u> (SNP11)	rs199915614	Intronic (BCAP29)	1.91	NA	-100	-	-
<u>Chr7:107282469A>C</u> (SNP12)	rs150942317	Intergenic	2.31	NA	0.241	LTR	-
Chr7:107316164G>A	rs185507318	Intronic (SLC26A4)	2.01	0.00	0.089	SINE	-

Rare genetic variants (allele frequency $\leq 5\%$ gnomAD) that are shared between two individuals that harbor the CEVA allele. SNPs that are part of the previously described CEVA (SNP 1-12) or the V1-CEVA haplotype (SNP 4-12) are underlined. Genome, Genomic position according to GRCh37/hg19; RefSNP, dbSNP reference SNP number; GnomAD AF, allele frequency (%) in gnomAD database V.2.1.1; spliceAI, highest splicing prediction score; RepeatMasker, the interspersed repeats or low complexity DNA sequence at the genomic position according to RepeatMasker; Regulatory element, overlap of the genomic position with a predicted *cis* regulatory element according to GeneHancer V5 or EnhancerAtlas 2.0; NA, not available.

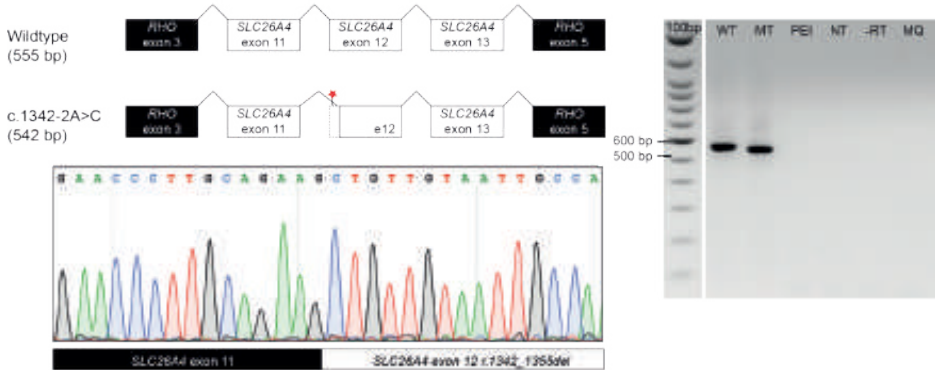
Table S8. Analyzed ears of affected individuals

Class	Number of subjects (male/female)	Number of EVA ears (male/female)	Number of analyzed ears (male/female)	Average age of subjects and analyzed ears (years)	Average age of analyzed ears (years), amount of analyzed ears between brackets
M2	11 (5/6)	22 (10/12)	21 (10/11)	13.2	18.4 (n = 48)
M1/CEVA	10 (6/4)	17 (10/7)	16 (9/7)	12.8	7.5 (n = 20)
M1	4 (1/3)	8 (2/6)	8 (2/6)	25 (7, 16, 18 and 59)	15.8 (n = 5)
M0/CEVA	2 (0/2)	3 (0/4)	3 (0/4)	15 (6 and 24)	10.1 (n = 6)
M0	10 (5/5)	17 (9/8)	17 (9/8)	14.6	12.9 (n = 94)

Table adapted from Chao et al. 2019.⁷ Only ears with sufficient audiometric data were used in the analysis.

SUPPLEMENTARY FIGURES

A SLC048



B SLC085

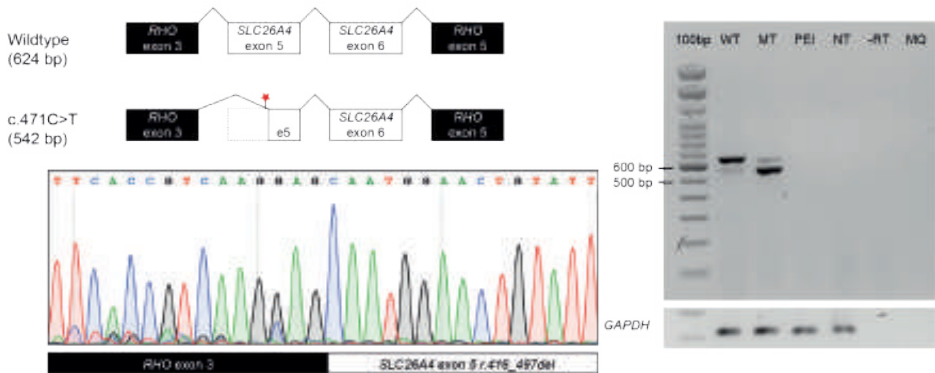


Figure S1. Results of *in vitro* splice assays for variants in SLC048 and SLC085. *In vitro* splice assays were performed in HEK293T cells to validate predicted splice defects. **(A)** In SLC048, a canonical splice site SLC26A4 variant (c.1342-2A>C) was detected. According to SpliceAI predictions, the splice variant (MT) weakens the canonical splice acceptor site. Splice assay results revealed usage of an alternative splice acceptor site located 13 nucleotides downstream. This leads to the formation of a truncated out-of-frame exon 12 (NM_000441.1:r.1342_1355del; p.Ser448Leufs*3). **(B)** In SLC085, a synonymous variant was detected (c.471C>T, p.(Pro157=)). According to SpliceAI, the variant (MT) potentially strengthens an alternative splice acceptor site. The *in vitro* splice assay confirmed that the alternative splice acceptor site (located 27 nucleotides downstream of the variant) is used, which leads to partial exon 5 skipping (NM_000441.1:r.416_497del; p.Gly139Alafs*6,=). Bp, base pair; wt, wildtype; mt, mutant; PEI, transfection reagent-only; RT, reverse transcriptase control; MQ, water control.

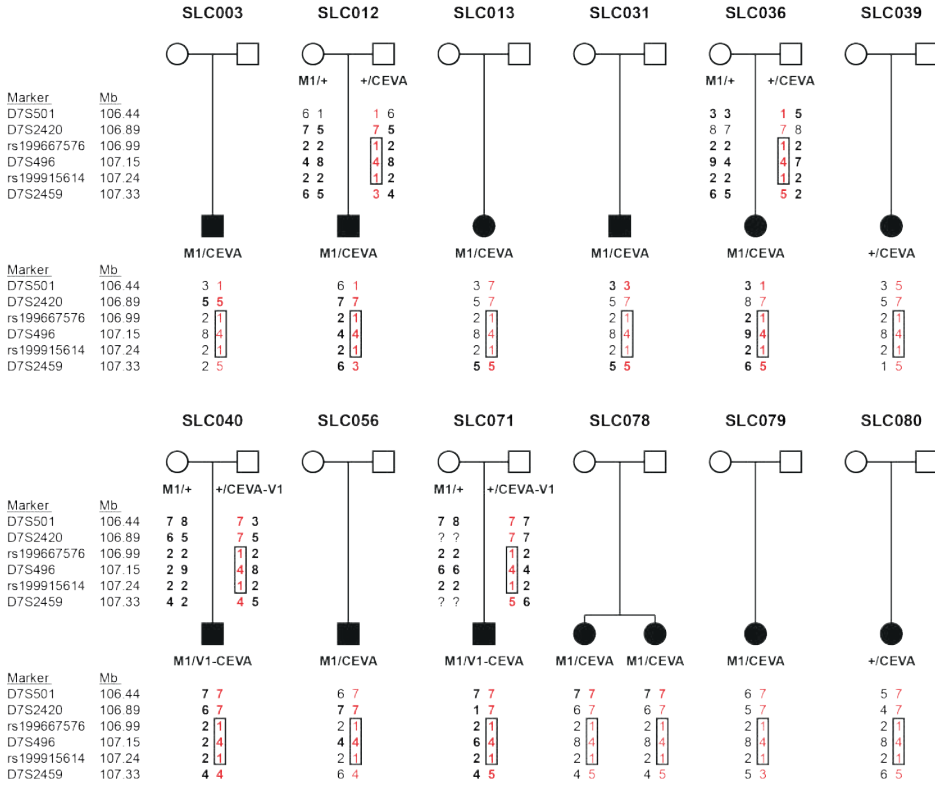


Figure S2. Family pedigrees with haplotypes of VNTR markers. The allele carrying the CEVA haplotype is marked in red. VNTR markers for which the phase of the alleles could be conclusively determined via segregation in the family are marked in bold. Genomic positions (Mb) on chromosome 7 are according to the UCSC genome browser (GRCh37/hg19). VNTR markers of the CEVA haplotype are marked in red. A shared haplotype of 0.89 Mb delimited by the markers D7S501 and D7S2459 was identified. A different repeat length was determined for marker D7S2420 in individual SLC003, the marker is still considered to be potentially part of the shared haplotype as a change of repeat length cannot be excluded. +, wildtype allele; M1, (likely) pathogenic *SLC26A4* variant.

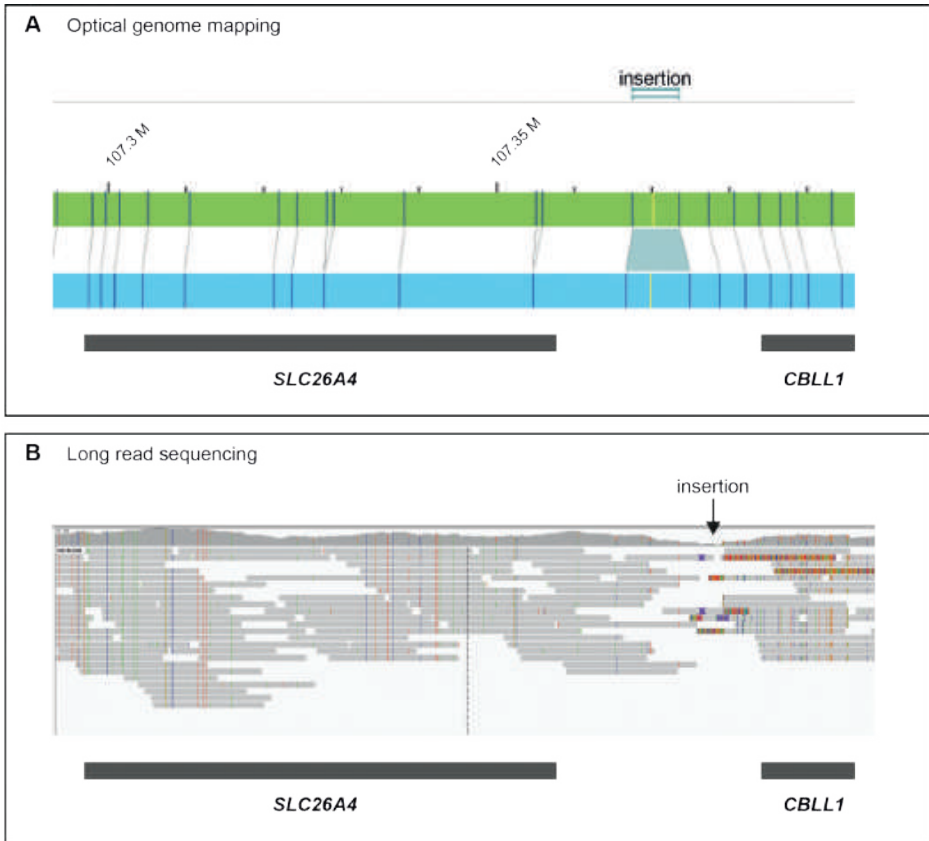


Figure S3. Optical genome mapping and long-read sequencing. Optical genome mapping (Bionano Genomics) and long-read sequencing (PacBio) were performed to detect potential structural variants (SVs) that could be present on the CEVA allele. **(A)** Optical genome mapping was performed using ultra-high molecular weight DNA isolated from peripheral blood cells from individual SLC012 (M1/CEVA). No SVs within the CEVA region or *SLC26A4* were called. One insertion event was called just telomeric from the CEVA-haplotype, but was also called in 100% of the control samples. **(B)** Hi-Fi sequencing reads visualized in IGV software. PacBio long-read sequencing was performed on genomic DNA isolated from peripheral blood from individual SLC079 (M1/CEVA). After sequencing analyses, no SVs remained that were present within the CEVA region or *SLC26A4*. The same insertion event as depicted in A was detected using PacBio sequencing, but was also present in control data. The insertion event is therefore considered a reference problem and not a true SV.

M0

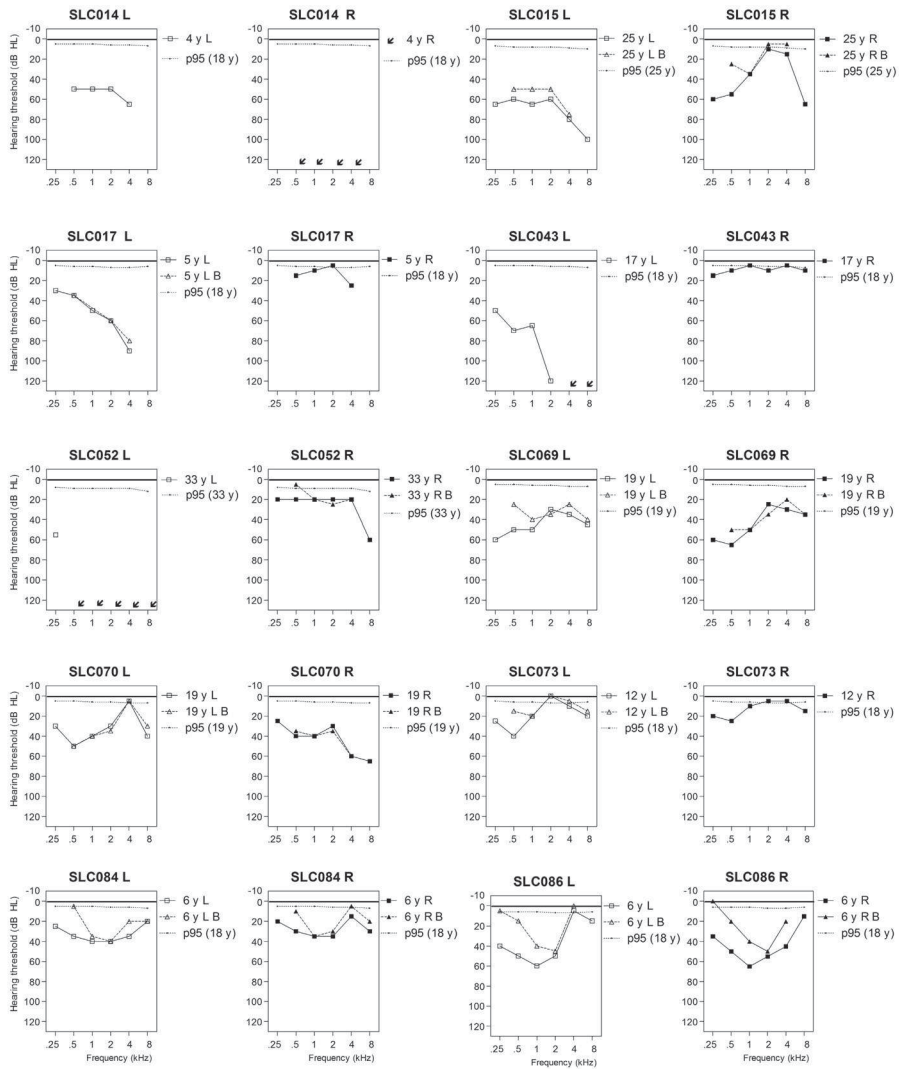
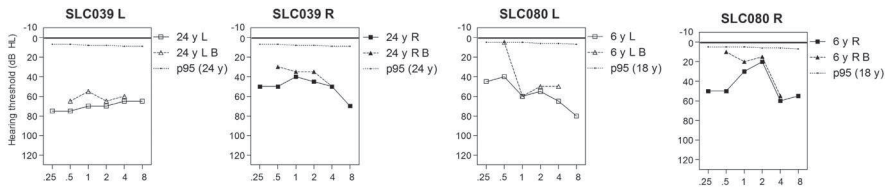
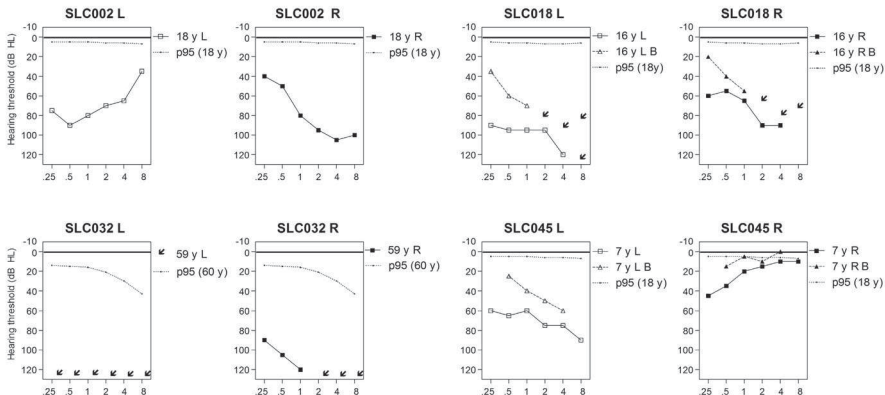


Figure continues on next page

M0/CEVA



M1



M1/(V1)-CEVA

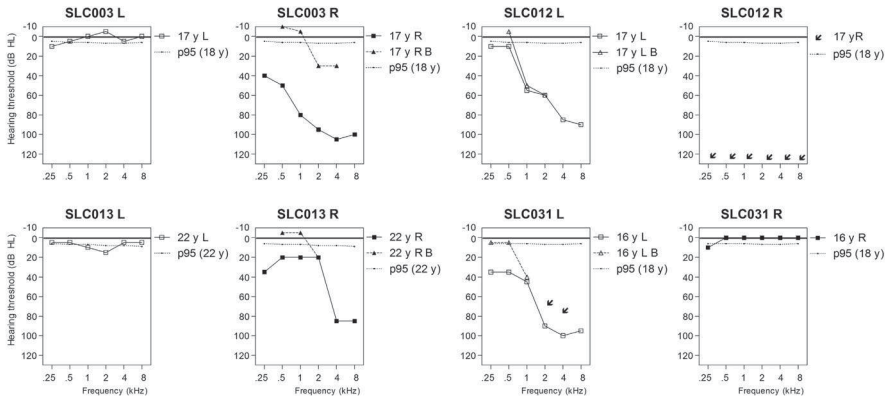
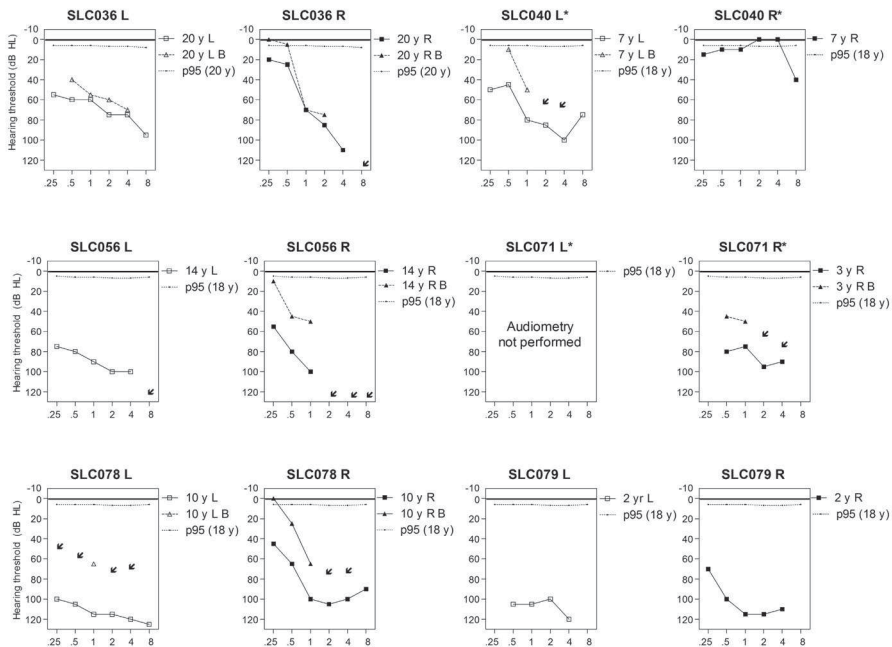


Figure continues on next page

M1/(V1)-CEVA (continued)



M2

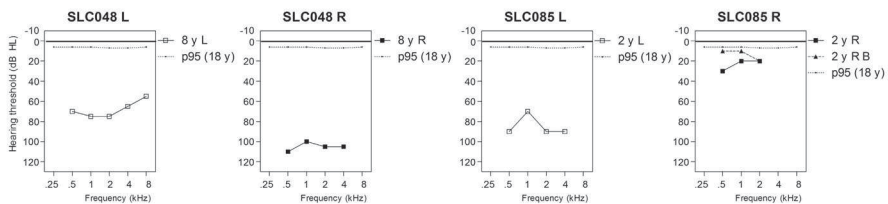


Figure S4. Pure tone audiometry of affected individuals. Air, and if available, bone conduction thresholds of all subjects are depicted, except for subjects of the M2 reference cohort. The p95 values are matched to the individuals' sex and age at the most recent audiometry, according to the ISO 7029:2017 standard. The age range for which the ISO 7029:2017 can be applied is 18 to 70 years. Black arrows: threshold could not be measured. The CEVA haplotype was detected in 8 individuals, in an additional 2 individuals (SLC040 and SLC071, indicated with *), a smaller haplotype was found, termed V1-CEVA. y, age in years; R, right; L, left; B, bone conduction; dB HL, decibel hearing level; kHz, kiloHertz.

SUPPLEMENTARY REFERENCES

1. Oza, A.M., DiStefano, M.T., Hemphill, S.E., Cushman, B.J., Grant, A.R., Siegert, R.K. *et al.* Expert specification of the ACMG/AMP variant interpretation guidelines for genetic hearing loss. *Human Mutation* 39, 1593-1613 (2018).
2. Fishilevich, S., Nudel, R., Rappaport, N., Hadar, R., Plaschkes, I., Iry Stein, T. *et al.* GeneHancer: genome-wide integration of enhancers and target genes in GeneCards. *Database (Oxford)* 2017, bax028 (2017).
3. Gao, T. & Qian, J. EnhancerAtlas 2.0: an updated resource with enhancer annotation in 586 tissue/cell types across nine species. *Nucleic Acids Research* 48, d58-d64 (2020).
4. Fornes, O., Castro-Mondragon, J.A., Khan, A., van der Lee, R., Zhang, X., Richmond, P.A. *et al.* JASPAR 2020: update of the open-access database of transcription factor binding profiles. *Nucleic Acids Research* 48, d87-d92 (2020).
5. Stelzer, G., Rosen, N., Plaschkes, I., Zimmerman, S., Twik, M., Fishilevich, S. *et al.* The GeneCards suite: from gene data mining to disease genome sequence analyses. *Current Protocols in Bioinformatics* 54, 1.30.1-1.30.33 (2016).
6. Pollard, K.S., Hubisz, M.J., Rosenbloom, K.R. & Siepel, A. Detection of nonneutral substitution rates on mammalian phylogenies. *Genome Research* 20, 110-121 (2010).
7. Chao, J.R., Chattaraj, P., Munjal, T., Honda, K., King, K.A., Zalewski, C.K. *et al.* SLC26A4-linked CEVA haplotype correlates with phenotype in patients with enlargement of the vestibular aqueduct. *BMC Medical Genetics* 20, 118 (2019).



Chapter 4.1

De novo and inherited loss-of-function variants of *ATP2B2* are associated with rapidly progressive hearing impairment

Jeroen J. Smits, Jaap Oostrik, Andy J. Beynon, Sarina G. Kant, Pia A.M. de Koning Gans, Liselotte J.C. Rotteveel, Jolien S. Klein Wassink-Ruiter, Rolien H. Free, Saskia M. Maas, Jiddeke van de Kamp, Paul Merkus, DOOFNL Consortium, Wouter Koole, Ilse Feenstra, Ronald J.C. Admiraal, Cornelis P. Lanting, Margit Schraders, Helger G. Yntema, Ronald J.E. Pennings and Hannie Kremer

Human Genetics 138, 61–72 (2019)

ABSTRACT

ATP2B2 encodes the PMCA2 Ca^{2+} pump, that plays an important role in maintaining ion homeostasis in hair cells among others by extrusion of Ca^{2+} from the stereocilia to the endolymph. Several mouse models have been described for this gene; mice heterozygous for loss-of-function defects display a rapidly progressive high frequency hearing impairment. Up to now *ATP2B2* has only been reported as a modifier, or in a digenic mechanism with *CDH23* for hearing impairment in humans.

Whole exome sequencing in hearing impaired index cases of Dutch and Polish origin revealed five novel heterozygous (predicted to be) loss-of-function variants of *ATP2B2*. Two variants, c.1963G>T (p.Glu655*) and c.955delG (p.Ala319fs), occurred *de novo*. Three variants; c.397+1G>A (p.?), c.1998C>A (p.Cys666*), c.2329C>T (p.Arg777*) were identified in families with an autosomal dominant inheritance pattern of hearing impairment. After normal newborn hearing screening, a rapidly progressive high frequency hearing impairment was diagnosed at the age of about three to six years. Subjects had no balance complaints and vestibular testing did not yield abnormalities. There was no evidence for retro-cochlear pathology or structural inner ear abnormalities. Although a digenic inheritance pattern of hearing impairment has been reported for heterozygous missense variants of *ATP2B2* and *CDH23*, our findings indicate a monogenic cause of hearing impairment in cases with loss-of-function variants of *ATP2B2*.

INTRODUCTION

Hearing loss (HL) is an important cause of social burden worldwide.¹ The reported incidence in early childhood varies from 1-3/1000.² It is estimated that early-onset sensorineural HL (SNHL) is hereditary in about 50% of the cases and in 20% of the cases nonsyndromic SNHL is inherited in an autosomal dominant pattern.³ Until now, more than 60 loci and 37 genes have been identified for autosomal dominant nonsyndromic SNHL (Hereditary Hearing loss Homepage). Still, for many subjects with congenital or childhood-onset HL, a genetic diagnosis cannot be provided.⁴ For several of the genes (recently) described to be associated with early-onset HL, defects have so far been found in only a few or one single family. To confirm association of such genes with HL, additional supportive data are required. Mouse models have contributed such evidence for several genes and have been of great significance by providing candidate genes for HL in humans.⁵⁻⁷

The plasma membrane Ca^{2+} ATPase 2 (PMCA2), encoded by *Atp2b2*, has already been known for two decades to be essential for hearing and balance in mouse (e.g. the *deafwaddler* mouse).⁸ It is one of the two PMCA2s with a tissue-specific expression; PMCA2 is mainly expressed in the inner ear, the cerebellum and the mammary gland. Alternative splicing of *Atp2b2* transcripts results in several PMCA2 isoforms, e.g. PMCA2 w/a, or z/a (for review⁹). Isoform PMCA2 w/a is the major PMCA2 isoform in the organ of Corti and is encoded by a transcript with three alternatively spliced exons at the first alternative splice site, site A.^{10,11} Given the structural and functional homology of the inner ear in mice, rat and human, PMCA2 was anticipated to be critical for hearing in humans as well, and indications for that have already been reported. A hypofunctional variant of PMCA2 (p.Val586Met) was found to aggravate HL in a family with a homozygous *CDH23* variant.¹² Moreover, digenic inheritance of SNHL was suggested in an isolated case with heterozygous missense variants in both *ATP2B2* and *CDH23*.¹³ Furthermore, SNHL in cases with the 3p deletion syndrome was suggested to be correlated with haploinsufficiency of *ATP2B2*.¹⁴ A heterozygous missense variant in *ATP2B2* has recently been associated with ataxia but without HL; the identified variant functionally affected a PMCA2 isoform that is expressed in the cerebellum but not prominently in the inner ear.¹⁵ Finally, two *de novo* truncating variants in *ATP2B2* have been reported in a study on autism.¹⁶ These studies, however, do not provide evidence for a causative association of *ATP2B2* with monogenic SNHL.

Here, we report four different heterozygous truncating variants and one canonical splice site variant in *ATP2B2* in families with nonsyndromic progressive SNHL. In two of the families, the variants are *de novo*. All variants affect exons, or their splice sites, that encode

the ortholog of the rat PMCA2 w/a isoform. This isoform is highly abundant in stereocilia of outer hair cells (OHC) and to a lesser extent at the apical surface of inner hair cells (IHC).¹¹

MATERIALS AND METHODS

Clinical examination

This study was approved by the medical ethics committee of the Radboud University Medical Center in Nijmegen, the Netherlands and was carried out according to the Declaration of Helsinki. Written informed consent was obtained from all participants or their legal representatives. Medical history was taken from all participants, with special attention paid to (acquired) HL and vestibular symptoms.

Affected individuals underwent general ear, nose and throat (ENT) examinations in the Radboud University Medical Center or findings of ENT examination were taken from their medical history. Pure tone audiometry (PTA) was performed according to current standards in a sound-attenuating booth, where air conduction hearing thresholds for the frequencies from 250 Hz to 8 kHz were measured. Bone conduction thresholds were measured for the frequencies 500 Hz to 8 kHz. The age- and gender-specific 95th percentile thresholds for individual hearing levels for each frequency were derived from the International Organization for Standardization; ISO 7029:2017. Individuals were considered affected when pure tone thresholds for at least three frequencies were below the 95th percentile (P_{95}) for the better hearing ear. The GENDEAF guidelines for description of audiological data were applied in this study.¹⁷ GraphPad Prism 6.0 was used to calculate an Age-Related Typical Audiogram (ARTA), based on linear regression, for the ages of 10 to 70 years as described.¹⁸ Speech perception was assessed in a sound-attenuating booth with standard monosyllabic consonant-vowel-consonant Dutch word lists.¹⁹ Otoacoustic emissions and click-evoked brainstem evoked response audiometric (BERA) measurements were performed according to current standards. In the Netherlands, the first step of newborn hearing screening is carried out by detection of transient evoked otoacoustic emissions (TEOAE).²⁰ If applicable, results of newborn hearing screening were assessed by hetero-anamnesis of parents.

Vestibular function was assessed by electronystagmography (ENG), caloric irrigation testing, rotary chair stimulation and video head impulse tests (vHIT), as described previously.²¹ Additionally, cervical and ocular vestibular-evoked myogenic potentials (cVEMP/oVEMP) were measured to assess saccular and utricular function, respectively, as described.^{22,23} When responses were seen at ≤ 100 dB hearing level in cVEMP testing, saccular function was considered as present, otherwise absent.²³ For oVEMPs, this normal value is ≤ 140 dB force level.²²

Subjects V.2 of family W18-0139 and I.1 of family W17-0883 were not able to participate in clinical evaluations, but retrospective data were analyzed. Subjects IV.3, IV.4 and V.1 of family W18-0139 did not consent for the study.

Genetic analyses

DNA was extracted from peripheral blood samples according to standard procedures. Exomes were enriched with the Agilent SureSelectXT Human AllExon v4 or v5 kit and sequencing was performed on an Illumina HiSeq4000 system by BGI Europe. Read alignment to the human reference genome (GrCH37/hg19) and variant calling was performed using BWA²⁴ and GATK software, respectively. Variant annotation was performed using a custom designed in-house annotation and variant evaluation pipeline. First, Whole Exome Sequence (WES) data were analyzed for variants in a panel of 142 genes known to be associated with nonsyndromic HL and relatively common syndromic forms of HL (gene list version DG 2.5; Hereditary Hearing Loss Exome Panel Genome Diagnostics Nijmegen-Maastricht, see **Table S1**) in a diagnostic setting. Variants in the 142 deafness-associated genes were classified according to guidelines from the Association for Clinical Genetic Science and the Dutch Society of Clinical Genetic Laboratory Specialists.²⁵ To address other recently published deafness genes, WES data of all subjects was reanalyzed with the most recent version of the gene panel; version DG 2.11, which consists of 159 deafness genes, see **Table S1**. Variants of the complete exome were evaluated according to the criteria described in the supplemental methods section.

Mean 20x coverage of the enriched regions in WES ranged between 93,5 – 98,0%. Copy number variation (CNV) was addressed by depth of coverage analysis with CoNIFER as described.^{26,27} Segregation analysis of selected variants was carried out by Sanger Sequencing, as described.⁷ Primer sequences are available upon request. Confirmation of parental identities in the cases with *de novo* variants was performed with the AmpFLSTR™ Identifiler™ kit, according to the manufacturer's protocol. Sequencing of *CDH23* for individuals I.1 and II.1 of family W17-0883 and III.3 of family W18-0139 was performed by massive parallel ion semiconductor sequencing as described.²⁸

RESULTS

Loss-of-function variants in *ATP2B2* are associated with hearing impairment

An otherwise healthy subject of Dutch origin with childhood-onset, rapidly progressive nonsyndromic SNHL (family W18-0138, III.1, **Figure 1**) was referred to our out-patient clinic for etiologic consultation. First, *GJB2* was screened in routine diagnostics, which revealed a heterozygous variant of uncertain significance c.647G>T (NM_004004; p.Arg216Ile) (DFNA3A;

DFNB1). This variant was not associated with autosomal dominant HL as it was inherited from the unaffected mother. In addition, no variant was identified in the second *GJB2* allele by Sanger sequencing. Therefore defects in *GJB2* were not considered to underlie the HL in the presented case. Subsequently, WES was performed, which revealed neither other (likely) pathogenic variants in genes of the deafness gene panel (version DG 2.5), nor CNVs of these genes. Finally, analysis of the complete WES data (beyond the gene panel for deafness) was carried out. Truncating variants and variants of canonical splice sites were considered potentially deleterious. Furthermore, other potentially pathogenic variants, that met the criteria as provided in the supplemental methods section, were considered. This analysis revealed a truncating variant in *ATP2B2*: c.955delG (NM_001001331.2, p.Ala319fs), which was neither present in our in-house database (~20,000 exomes) nor in gnomAD (version r2.02).²⁹ Importantly, the *ATP2B2* variant was not found in the parents and as both parental identities were confirmed, the variant was considered to be *de novo* (Figure 1). Several heterozygous missense and truncating defects of the mouse ortholog of *ATP2B2* were associated with early-onset, progressive high frequency HL.^{8,30-38} Therefore we regarded the *ATP2B2* variant to be an excellent candidate cause of the HL in this subject.

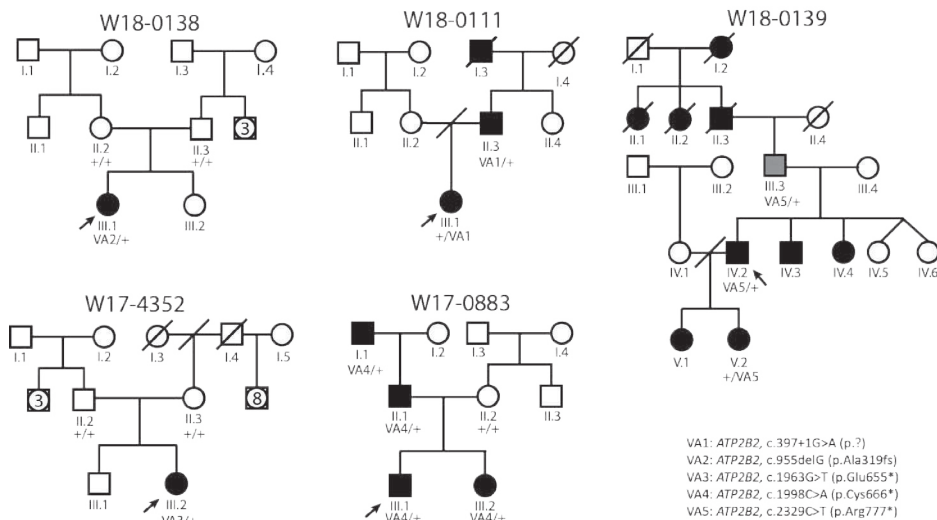


Figure 1. Pedigrees and segregation of *ATP2B2* variants VA1-VA5, variants in *ATP2B2*, as listed in table 1 and in this figure. Nomenclature of variants VA1-VA5 is according to transcript NM_001001331.2. The subject marked in grey (III.3, W18-0139) has late-onset hearing impairment, in contrast to all other affected individuals. Subjects IV.3, IV.4 and V.1 of family W18-0139 did not participate in this study. Deceased individuals are considered affected or unaffected by heteroanamnesis. Index cases are indicated by arrows. +, reference sequence

To confirm the association of *ATP2B2* defects with SNHL in humans, WES data of about 700 index cases were analyzed for truncating variants and variants in canonical splice sites in this gene. In 110 of these cases a dominant inheritance pattern of HL was indicated by the referring clinician. Defects of known genes associated with HL were previously excluded for these cases in routine diagnostics, as indicated in the methods section. Three cases were found to have nonsense variants in *ATP2B2*, and one case a variant in a canonical splice site (**Table 1**). All four cases had a reported onset of HL in the first decade (**Table 2**). Segregation analysis of the *ATP2B2* variants in the respective families demonstrated that the c.1963G>T variant in subject III.2 of family W17-4352 was *de novo*, as it was not detected in the parents (**Figure 1**) while both parental identities were confirmed. In families W17-0883 and W18-0111, the identified *ATP2B2* variants co-segregated with the HL in three and one affected family members, respectively. In family W18-0139, the *ATP2B2* variant was present in two participating family members with early-onset HL (IV.2 and V2) but also in individual III.3 who reported a late onset of HL, at the age of 55 years.

Table 1. *ATP2B2* variants identified in this study

Family code	Variant code	Genome	cDNA	Protein	Number of segregations
W18-0111	VA1	Chr3:10452301C>T	c.397+1G>A	p.?	1
W18-0138	VA2	Chr3:10426997delG	c.955delG	p.(Ala319fs)	<i>de novo</i>
W17-4352	VA3	Chr3:10400548C>A	c.1963G>T	p.(Glu655*)	<i>de novo</i>
W17-0883	VA4	Chr3:10400513G>T	c.1998C>A	p.(Cys666*)	3
W18-0139	VA5	Chr3:10391871G>A	c.2329C>T	p.(Arg777*)	2

VA1-VA5, variants in *ATP2B2*, as shown in the pedigrees in Figure 1. The indicated genomic positions are according to GRCh37/hg19. The cDNA and amino acid positions are based on transcript NM_001001331.2. None of the variants are present in gnomAD version r2.02 or in our in-house WES database of ~20.000 exomes.

Other variants that could potentially be causative for HL in the families were addressed (**Table S2 and S3**). For families W18-0138 and W17-4352, both a dominant and recessive inheritance pattern were addressed. Eleven variants met the described criteria and their segregation in the respective families was determined (**Figure S1 and Table S2**). In families W18-0138 and W17-4352, identified variants with a potentially dominant effect were not *de novo* but derived from a normal hearing parent and therefore considered unlikely to be pathogenic. Variants with a potentially recessive effect were only found in *DNM1* (family W17-4352), a gene that is associated with deafness in mouse.³⁹ However, the variant of one of the alleles was predicted to be synonymous and to have no effect on splicing. In the families with dominantly inherited HL, only one candidate variant, c.3226G>C (p.Asp1076His) in *MYO6*, co-segregated with the HL in family W18-0111.

Since digenic and modifier mechanisms have been described for the combination of *CDH23* and *ATP2B2* variants,^{12,13} we evaluated all rare variants in *CDH23* in the index cases. *CDH23* was completely covered in WES by at least 10 reads for all coding exons. Six rare variants, named VC1-VC6, were identified and segregation analysis was performed (**Figure S1 and Table S3**). Four variants (VC1-VC4), are missense variants predicted to have a deleterious effect by at least two of the employed pathogenicity prediction tools. VC2 and VC3 are located *in cis* on the paternal allele and are co-inherited with the *ATP2B2* variant in family W18-0111. VC1 and VC4 co-occurred with the *de novo* variants in families W18-0138 and W17-4352, respectively. Therefore, no segregation analysis was carried out. For an intronic (VC5) and a synonymous (VC6) variant, no effects on splicing or protein function were predicted. Also, VC5 does not co-segregate with the *ATP2B2* variant (and HL) in family W17-0883. Sequencing of *CDH23* was performed in individuals I.1 and II.1 (W17-0883) to identify other variants in this gene that might contribute the HL. This revealed only common variants. VC6 co-occurred with the *ATP2B2* variant in subjects IV.2 and V.2 of family W18-0139, but not in individual III.3. The latter reported to have developed HL around the age of 55 years. Sequencing of *CDH23* in this individual revealed that he carries the VC1 variant heterozygously.

Characteristics of ATP2B2-associated HL

None of the affected subjects or their parents reported exposure to excessive noise, long-term usage of antibiotics, history of head trauma or meningitis. Subjects III.3 and IV.2 of family W18-0139 reported complaints of tinnitus. All four subjects who underwent newborn hearing screening passed the first screening (**Table 2**). HL in all except two participating affected subjects was bilateral, sensorineural, symmetric, and mild-to-profound. For individual IV.2 of family W18-139, who repeatedly underwent ear surgery of the left ear, and I.1 of family W17-0883 who had a conductive HL on his left ear due to previous cholesteatoma surgery, only data of the right ears are depicted and included in further evaluations. For the other subjects mean air conduction threshold values are depicted in **Figure 2** and employed in further analyses. Audiogram configurations were (steeply) downsloping (**Figure 2**) and the age of onset was in the first decade with one exception (**Table 2**). Subject III.3 of family W18-0139 reported an onset age of 55 years, but no audiometry was performed before the age of 64 years. His hearing is clearly below the P95 for presbycusis for the higher frequencies. Other affected subjects (IV.3, IV.4 and V.1) in this family did not participate in the clinical and genetic evaluations, but on hetero-anamnesis they had an early childhood onset of HL. Subject III.3 reported that his father, paternal aunts and grandmother, had HL early in life and that they were wearing hearing aids. Speech reception thresholds in general were lower than or comparable to pure tone average thresholds (0,5 to 2 kHz), indicating absence of retrocochlear pathology. This was confirmed by BERA measurements in four subjects (**Table S4**).

Table 2. Individual results of otoscopy, pure-tone audiometry, newborn hearing screening, imaging, and speech discrimination tests

Family	Subject	Newborn screening	Age of onset (y)	Age during study (y)	Otosopic examination	CT		MRI		PTA ^b		SRT ^b		Maximum SRS (%) ^b	
						CT	MRI	R	L	R	L	R	L	R	L
W18-0111	III.1	pass	2-5	11	L myringo-sclerosis	N	N	22	37	27	47	85	88		
	II.3	NT	cong.	45	N			62	62	65	70	92	70		
W18-0138	III.1	NT	3	24	N	N	N	105	82	95	57	50	69		
	III.2	pass	2	6	N			70	75	60	60	70	65		
W17-4352	III.1	pass	4	9	N			33	40	36	40	82	74		
	III.2	pass	6	6	N			17	22	15	19	100	100		
W17-0883	II.1	NT	2-5	32	N	N	N	62	57	70	72	NT	NT		
	I.1 ^a	NT	2-5	67	NT			103 ^a	NA	NT	NA	NT	NA		
W18-0139	V.2	NT	4	17	NT			23	22	10	10	95	100		
	IV.2 ^a	NT	5	48	N ^a	N	N	60	NA	67	NA	93	NA		
	III.3	NT	55	68	N			13	20	13	21	95	95		

Age of onset is the reported age of onset in years. Age during study is the age at which subjects had clinical testing for this study. y, years; PTA, pure tone average, mean of 0.5, 1 and 2 kHz air conduction thresholds; R, right; L, left; SRT, speech reception threshold; SRS, speech recognition score; NT, not tested; N, normal; NA, not applicable; cong., congenital. ^aonly right ear was assessed; ^blatest audiogram, made at the age indicated in the fifth column. An exception is individual W18-0138 III.1, for whom the penultimate audiogram at the age of 22 was used because of cochlear implantation in her right ear at the age of 24 years.

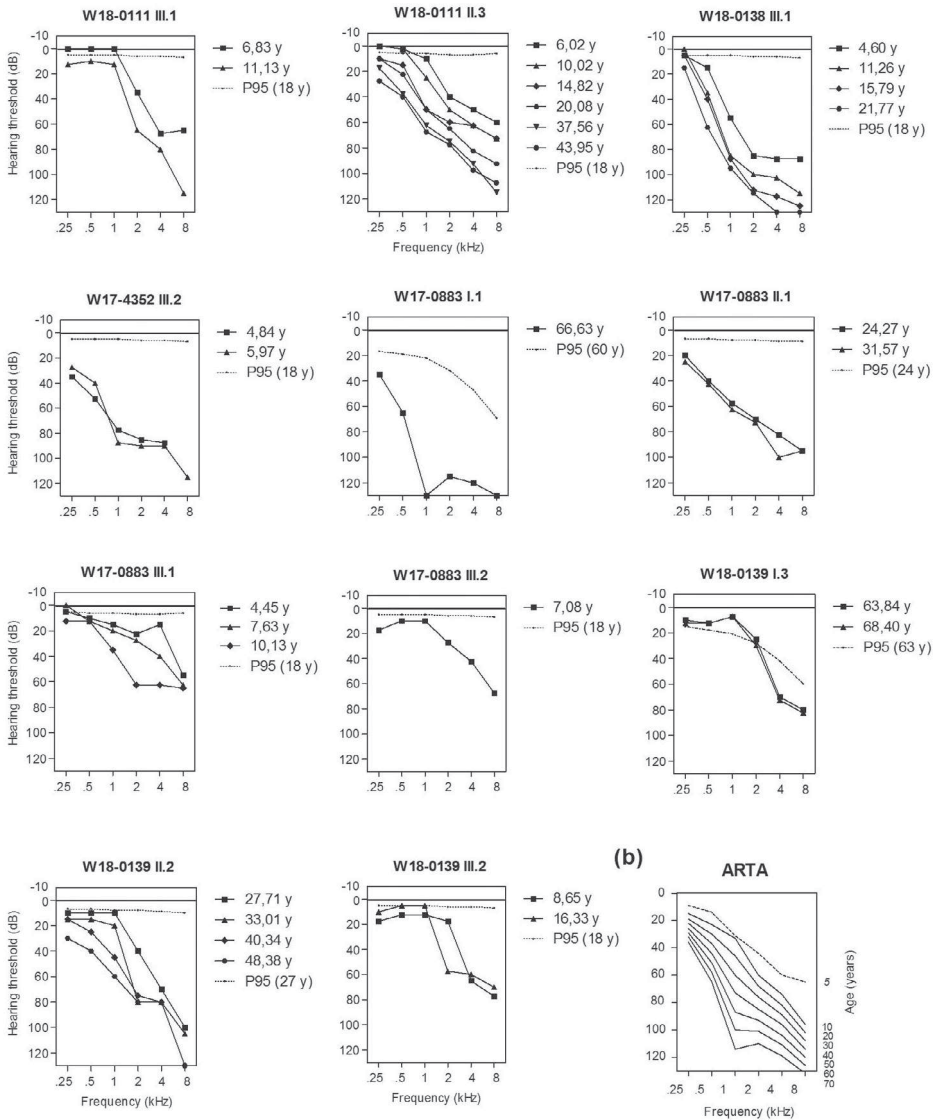


Figure 2 Audiograms of individuals with heterozygous deleterious *ATP2B2* variants (A) Air conduction thresholds of all participating individuals with a deleterious *ATP2B2* variant are depicted. For subjects I.1 of family W17-0883 and IV.2 of family W18-0139 only data of their right ears are displayed. For all other subjects, average of left and right ear thresholds are shown. The P95 values are matched to the individuals' sex and age at first audiometry, according to the ISO 7029:2017 standard. The lowest age for which the ISO 7029:2017 can be applied is 18 years. y, age in years. **(B)** ARTA (Age Related Typical Audiogram) representing cross-sectional linear regression analysis of last visit audiograms of all subjects with a deleterious *ATP2B2* variant (N = 11). The dashed line represents the average air conduction thresholds at the age of five.

An ARTA was calculated to provide insight in the progression of the HL per decade (**Figure 2B**). The average annual threshold deterioration (ATD) for the ages 10 to 70 was 0.5 dB/y for the low frequencies (250-500Hz), 1.1 dB/y for middle frequencies (1-2kHz) and 0.7 dB/y for the high frequencies (4-8kHz). Under the age of 10 years, audiograms tend to be less reliable due to more prevalent otitis media with effusion or less co-operation or cognitive capabilities of the young subjects. To give insight in the HL at this age, we calculated the average thresholds of all subjects with a hearing test at about 5 years of age (**Figure 2B**, dashed line).

Five subjects underwent computed tomography (CT) and/or Magnetic Resonance Imaging (MRI) of the bilateral temporal bones/cochlea and cerebellopontine angle, which revealed normal inner and middle ear anatomy, except for the left ear of subject IV.2 of family W18-0139 for reasons already indicated (**Table 2**).

Results of vestibular testing

Vestibular history was obtained from all subjects and extensive vestibular testing of at least one affected subject per family (except for family W17-4352) revealed only minor vestibular abnormalities (see **Table S4**). Two subjects reported vestibular complaints; one was diagnosed with benign paroxysmal position vertigo (BPPV) and the second had complaints due to a perilymph leakage at cholesteatoma surgery. Sacculus function could not be measured in subjects III.1 of family W18-0138 (bilaterally), III.1 (left ear) of W18-0111, IV.2 of W18-0139 (left ear), whereas utricular function was not measurable in III.1 of family W18-0138. Maximum stimulus levels were reached in all these subjects.

DISCUSSION

In this study, five families were presented, in which four mono-allelic truncating variants and one canonical splice site variant in *ATP2B2* co-segregated with early-onset progressive nonsyndromic SNHL and with late-onset SNHL in one subject. All five variants affected the (predicted) ortholog of the *w/a* isoform of *PMCA2*, which is the predominant Ca^{2+} ATPase in rodent hair cells and specifically localizes to stereocilia.^{10,11} In man, transcripts encoding the *w/a* isoform of *PMCA2* have so far not been identified but the *w* splicing pattern has been shown (ENSEMBL, UCSC genome browser). See **Figure S2** for a schematic representation of the different isoforms and positions of the variants. The truncating variants can be predicted to have a loss-of-function effect. This might also be the case for the splice site variant by inducing skipping of exon 3, retention of intron 3 or the use of an alternative exonic or intronic splice site. Skipping of exon 3 (198 nucleotides) is predicted to result in depletion of 66 amino acids from the N-terminal part of the protein, including the first transmembrane

region (**Figure S3** for splice prediction). Two of the truncating variants occurred *de novo*, which supports pathogenicity of the variants. A causal association with disease is further strengthened by a pLI score of 1.00 reported for *ATP2B2*. This score is an indication of extreme loss of function intolerance of *ATP2B2*.²⁹ The DOMINO variant effect prediction tool, predicts *ATP2B2* to be very likely associated with a dominantly inherited disorder⁴⁰ which is in agreement with the inheritance pattern of HL in the described families.

As digenic inheritance of HL was proposed for mono-allelic missense variants in *ATP2B2* and *CDH23*,¹³ we addressed this type of inheritance in the families in our study. Although rare *CDH23* variants co-occurred with *ATP2B2* variants in all five index cases, our findings indicate that mono-allelic loss-of-function variants of *ATP2B2* are the underlying cause HL. Firstly, the *CDH23* variant VC5 in individuals III.1 and III.2 of family W17-0883 is intronic and predicted not to affect splicing. Furthermore, this variant was not found in the affected family members I.1 and II.1, who also did not carry any other rare *CDH23* variants in the coding sequences or flanking intronic regions. Secondly, the synonymous *CDH23* variant VC6 in family W18-0139 is predicted not to affect the existing splice sites nor to introduce such sites. Although this variant did co-segregate with early-onset HL in the family, subject III.3 with late-onset HL carried a different *CDH23* variant, namely missense variant VC1 that is also seen in the index case of family W18-0138. Thirdly, none of the variants has been classified as (likely) pathogenic in Clinvar (VC1-VC3, (likely) benign; VC4, uncertain significance; VC6, conflicting, UV1/UV2/UV3) and all but one (VC4) occur relatively frequently in gnomAD. Only variants in deep intronic regions or promoter regions were not addressed and can therefore not be excluded. CNVs of *CDH23* can be excluded for the index cases only. Finally, the affected individual in the family reported by Ficarella et al. was pre-screened only for mutations in *GJB6*, *MYO6*, *CDH23*, and the most common mutations in *GJB2*.¹³ As many of the known genes associated with recessive HL were not tested, several of which are commonly involved (e.g. *MYO15A*), defects in other deafness genes cannot be excluded in the reported case. We cannot exclude a modifying effect of the *CDH23* variants on HL in the affected subjects in our study, as has been reported for mouse mutants of *Atp2b2*.³²

As indicated by the pLI score of 1.00, loss-of-function variants in *ATP2B2* are rare. In gnomAD, eight such variants are reported heterozygously, representing 26 alleles. Three of these variants, representing 21 alleles, affect canonical splice sites of the alternatively spliced exons 7-9 at site A and all three are in frame (see **Figure S2**). One of these three variants, c.1001-1G>A (NM_001001331.2), was identified in 19 non-Finnish Europeans and is predicted to result in the loss of the splice acceptor site of exon 9. This loss potentially results in skipping of this exon and thereby to a shift from splicing pattern w to y at site A (**Figure**

S2). Alternative splicing at site A determines apical targeting of the encoded PMCA2 in hair cells. When alternative splicing at site A resulted in insertion of at least 31 amino acids, the encoded PMCA2 exclusively targeted to the hair bundle.¹⁰ As exons 7, 8, and 9 encode 11, 20, and 14 amino acids respectively, skipping of exon 9 results in 31 amino acids encoded at site A (pattern y) and exclusively apical targeting of the protein.¹⁰ This suggests that the c.1001-1G>A might have no or a milder phenotypic effect as compared to *ATP2B2* variants identified in the present study.

The other two canonical splice site variants in gnomAD, each representing a single allele, are predicted to result in the loss of the splice donor site of exon 7 and the splice acceptor site of exon 8, respectively. Skipping of exon 7 would lead to a PMCA2 protein with 34 amino acids encoded by exons inserted at site A and thus apical targeting according to Grati et al.¹⁰ Skipping of exon 8 would result in a PMCA2 protein with both apical and basolateral distribution in hair cells.¹⁰ In conclusion, 21 of 26 loss-of-function alleles reported in gnomAD might well lead to no or a mild phenotype.

Two *de novo* truncating variants in *ATP2B2* have been identified in a study on autism spectrum disorders (ASD), which is a complex disorder.¹⁶ These variants, c.2268C>A (p.Cys756*) and c.3191G>G (p.Trp1064*) according to transcript NM_001001331.2, affect exons 15 and 20 of the transcript, respectively (**Figure S2**). Therefore, these variants are predicted to affect all known PMCA2 isoforms and to lead to nonsense mediated decay. Based on our findings, the *de novo ATP2B2* variants identified in the ASD cases are expected to cause HL but this was not reported by the authors. The age of the subjects was not specified but indicated to be more than two years. This suggests that these subjects might not yet have developed HL. Alternatively, if they are toddlers, the HL may have mimicked or contributed to symptoms of ASD due to communication problems as has been reported previously.⁴¹ The subjects in our study did not display signs of ASD and this condition was neither indicated by themselves nor by their parents.

The type of mutations and their distribution in the gene suggest haploinsufficiency as disease mechanism. Four of five presented *ATP2B2* variants potentially lead to nonsense mediated decay (NMD). A haploinsufficiency mechanism is further supported by the findings of McCullough et al. (2007) who demonstrated that SNHL in cases with the 3p-syndrome is associated with loss of *ATP2B2*.¹⁴ They reported a high-frequency HL with a steeply downsloping audiogram configuration, similar to that in the cases in our study. Malmgren et al. suggested that deletion of *ATP2B2* is not sufficient to cause HL.⁴² However, the HL in the cases they reported is not sufficiently characterized to support SNHL in all them. For example, HL of one of the included subjects was indicated to be conductive in the original publication.^{14,42,43}

WES data of index cases were analyzed for other variants in known mouse and/or human deafness genes that could potentially be causative for HL. This revealed only one candidate variant, c.3226G>C (p.Asp1076His) in *MYO6*, that co-segregated with the HL in family W18-0111. Although a phenotypic effect of this variant cannot be excluded, *MYO6* variants with a dominant effect are known to be associated with progressive HL with a different audiogram configuration and in the majority of cases an onset after childhood.⁴⁴⁻⁴⁷ Therefore, the identified variant is unlikely to fully explain the HL in family W18-0111. Also, the HL in family W18-0111 is comparable to that in the other families reported in this study.

Thirteen mouse mutants (*deafwaddler*) have been described for *Atp2b2*, 12 of which have been described to display congenital severe-to-profound HL accompanied by a severe vestibular/ataxic phenotype when the mutation is in the homozygous state. The mutations in all 12 affect the w/a isoform of PMCA2. Mice with loss of function *Atp2b2* mutations in the heterozygous state display a rapidly progressive early-onset HL (before the age of 3-5 weeks) with high frequency hearing being most severely affected.^{30-32,48} The type of HL in these mice is highly similar to that in the presented affected subjects.

Based on the findings in the presented families it cannot be determined whether hearing of the affected subjects was abnormal at birth, as all four subjects who underwent newborn hearing screening passed the first test. The TEOAE devices employed in the screening are calibrated to detect thresholds of 35 dB HL or more, for the frequencies between 1 and 4kHz.²⁰ This means that in case the tested newborns with *ATP2B2* defects had elevated thresholds, these were below 35 dB HL for the tested frequencies. Alternatively, only the thresholds for higher frequencies (>4 kHz) surpassed 35dB, which might have well been the case based on audiogram configuration (**Figure 2B**) and the findings in mouse models. Delayed speech development and difficulties at school, were the reasons for the parents to have their children's hearing tested leading to a diagnosis of HL around the age of 2-5 years.

One individual (W18-0139, III.3, **Figure 1**) in our study displayed HL with a late onset rather than an early onset. This suggests the existence of modifying (genetic) factors. For mouse, it has been described that small (15%) increases in PMCA2 activity can account for large differences in hearing phenotype.³² Therefore, it is tempting to speculate that the late onset of HL in this case might be due to a relatively high inner ear expression of the second *ATP2B2* copy. As subject II.3 was indicated to be severely hearing impaired at the age of 30 years, mosaic presence of the *ATP2B2* variant in subject III.3 seems unlikely to explain the late onset of his HL. However, as HL is genetically highly heterogeneous the deceased family members I.2, II.1, II.2 and II.3 may have had HL with a different genetic aetiology.

Identification of additional families with deletions or truncating variants of *ATP2B2* will shed light on the variability of onset age of *ATP2B2*-associated HL.

In hair cells and endolymph, Ca^{2+} is important for maintaining the endocochlear potential, contributes to the mechanotransduction (MET) current, affects MET channel activity, tip-link structure, and, although under debate now, it is thought to play a role in the process of fast adaptation (for review see⁴⁹⁻⁵¹). PMCA2 is the Ca^{2+} pump in OHC stereocilia and therefore important for Ca^{2+} homeostasis in these structures. As has been demonstrated for several of the *Atp2b2* mutant mice, HL and OHC dysfunction precedes hair cell degeneration and Ca^{2+} cytotoxicity has been hypothesized to underlie the latter.^{34,36,52} Degeneration of both OHCs and IHCs was demonstrated to be most severe at the cochlear base in heterozygous as well as homozygous *Atp2b2* mutant mice.^{34,36} This is in agreement with high-frequency hearing being most severely affected in the presented families. Analogous to what has been described in mice with a heterozygous *Atp2b2* mutation, degeneration of OHCs, IHCs and supporting cells is likely to cause progression of HL to severe-to-profound in humans.

PMCA2 is also expressed in the stereocilia of vestibular hair cells.^{8,10} A vestibular phenotype was only seen in homozygous or compound heterozygous and not in heterozygous *Atp2b2* mutant mouse models.^{8,30-32,34-36,53} This is histologically supported by studies of Takahashi and Kitamura on the “*wri*” mouse model; in *wri/wri* homozygotes severe degeneration is seen in both the cochlea and saccule within three months. In heterozygotes, degeneration was only seen in the cochlea.³⁷ Vestibular complaints were found in only two patients in this study, but can be attributed to other factors than defects in *ATP2B2* (**Table S4**). Oculomotor, vHIT, caloric and rotational chair testing yielded no abnormalities, as expected from previous studies in mouse models. In four subjects, we could not determine whether saccular or utricular function was present. Firstly, we measured until 100dB HL (cVEMP) and 140 dB FL (oVEMP), according to protocol. Higher stimulus levels are too uncomfortable for subjects. The contralateral measurements were close to maximum stimulus levels in subjects III.1 of family W18-0111 and IV.2 of W18-0139. It is therefore possible that ipsilateral levels could have been measured with stimuli just above the maximum stimulus levels. Secondly, in about half of all patients who underwent vestibular examination in our clinic prior to cochlear implantation, it was impossible to measure c- and oVEMPs (A.J. Beynon, unpublished data). This relates to subject III.1 of W18-0138, who was the only subject with a cochlear implant. Based on the present findings, we concluded that heterozygous loss-of function variants in *ATP2B2* are unlikely to be associated with vestibular dysfunction.

In conclusion, we presented heterozygous *ATP2B2* defects to be associated with dominantly inherited nonsyndromic SNHL. All but one subject displayed a rapidly progressive high-frequency HL with a congenital or early-childhood onset. Four and possibly all five identified variants have a truncating effect. As amino acid substitutions in mouse PMCA2 can lead to loss of function (e.g.^{34,36}), missense variants in *ATP2B2* are to be expected as a cause of HL in humans as well. Variants resulting in reduced PMCA2 function might lead to recessive HL, analogous to the deafwaddler (*dfw*) allele.³²

ACKNOWLEDGEMENTS

We thank Ilse de Wijs, Genome Diagnostics Radboudumc, for her contribution to DNA-analysis. This work was financially supported by a grant from the Heinsius Houbolt foundation [to H.K. and R.J.E.P.].

COLLABORATORS

The DOOFNL consortium is a Dutch nationwide collaboration on hereditary hearing loss and consists of M.F. van Dooren, S.G. Kant, H.H.W. de Gier, E.H. Hoefsloot, M.P. van der Schroeff (ErasmusMC, Rotterdam, the Netherlands), L.J.C. Rotteveel, F.G. Ropers (LUMC, Leiden, the Netherlands), J.C.C. Widdershoven, J.R. Hof, E.K. Vanhoutte (MUMC+, Maastricht, the Netherlands), R.J.C. Admiraal, I. Feenstra, H. Kremer, C.P. Lanting, R.J.E. Pennings, H.G. Yntema (Radboudumc, Nijmegen, the Netherlands), R.H. Free and J.S. Klein Wassink-Ruiter (UMCG, Groningen, the Netherlands), R.J. Stokroos, A.L. Smit, M.J. van den Boogaard (UMC, Utrecht, the Netherlands) and F.A. Ebbens, S.M. Maas, A. Plomp, T.P.M. Goderie, P. Merkus and J. van de Kamp (Amsterdam UMC, Amsterdam, the Netherlands).

REFERENCES

1. WHO. The global burden of disease: 2004 update. (Geneva: World Health Organization, 2008).
2. Wroblewska-Seniuk, K.E., Dabrowski, P., Szyfter, W. & Mazela, J. Universal newborn hearing screening: methods and results, obstacles, and benefits. *Pediatr Res* 81, 415-422 (2017).
3. Smith, R.J., Bale, J.F., Jr. & White, K.R. Sensorineural hearing loss in children. *Lancet* 365, 879-90 (2005).
4. Zazo Seco, C. *et al.* The diagnostic yield of whole-exome sequencing targeting a gene panel for hearing impairment in The Netherlands. *Eur J Hum Genet* 25, 308-314 (2017).
5. Friedman, L.M., Dror, A.A. & Avraham, K.B. Mouse models to study inner ear development and hereditary hearing loss. *Int J Dev Biol* 51, 609-31 (2007).
6. Brown, S.D., Hardisty-Hughes, R.E. & Mburu, P. Quiet as a mouse: dissecting the molecular and genetic basis of hearing. *Nat Rev Genet* 9, 277-90 (2008).
7. Wesdorp, M. *et al.* MPZL2, Encoding the Epithelial Junctional Protein Myelin Protein Zero-like 2, Is Essential for Hearing in Man and Mouse. *Am J Hum Genet* 103, 74-88 (2018).
8. Street, V.A., McKee-Johnson, J.W., Fonseca, R.C., Tempel, B.L. & Noben-Trauth, K. Mutations in a plasma membrane Ca²⁺-ATPase gene cause deafness in deafwaddler mice. *Nat Genet* 19, 390-4 (1998).
9. Strehler, E.E. & Zacharias, D.A. Role of alternative splicing in generating isoform diversity among plasma membrane calcium pumps. *Physiol Rev* 81, 21-50 (2001).
10. Grati, M., Aggarwal, N., Strehler, E.E. & Wenthold, R.J. Molecular determinants for differential membrane trafficking of PMCA1 and PMCA2 in mammalian hair cells. *J Cell Sci* 119, 2995-3007 (2006).
11. Hill, J.K. *et al.* Splice-site A choice targets plasma-membrane Ca²⁺-ATPase isoform 2 to hair bundles. *J Neurosci* 26, 6172-80 (2006).
12. Schultz, J.M. *et al.* Modification of human hearing loss by plasma-membrane calcium pump PMCA2. *N Engl J Med* 352, 1557-64 (2005).
13. Ficarella, R. *et al.* A functional study of plasma-membrane calcium-pump isoform 2 mutants causing digenic deafness. *Proc Natl Acad Sci U S A* 104, 1516-21 (2007).
14. McCullough, B.J. *et al.* 3p-- syndrome defines a hearing loss locus in 3p25.3. *Hear Res* 224, 51-60 (2007).
15. Vicario, M. *et al.* A V1143F mutation in the neuronal-enriched isoform 2 of the PMCA pump is linked with ataxia. *Neurobiol Dis* 115, 157-166 (2018).
16. Takata, A. *et al.* Integrative Analyses of De Novo Mutations Provide Deeper Biological Insights into Autism Spectrum Disorder. *Cell Rep* 22, 734-747 (2018).
17. Mazzoli, M. *et al.* Recommendations for the description of genetic and audiological data for families with nonsyndromic hereditary hearing impairment. (2003).
18. Huygen, P.L.M., Pennings, R.J.E. & Cremers, C.W. Characterizing and distinguishing progressive phenotypes in nonsyndromic autosomal dominant hearing impairment. in *audiological medicine 1* Vol. 1 37-46 (2003).
19. Bosman, A.J. & Smoorenburg, G.F. Intelligibility of Dutch CVC syllables and sentences for listeners with normal hearing and with three types of hearing impairment. *Audiology* 34, 260-84 (1995).

20. van der Ploeg, C.P., Uilenburg, N.N., Kauffman-de Boer, M.A., Oudesluys-Murphy, A.M. & Verkerk, P.H. Newborn hearing screening in youth health care in the Netherlands: National results of implementation and follow-up. *Int J Audiol* 51, 584-90 (2012).
21. Oonk, A.M. *et al.* Vestibular function and temporal bone imaging in DFNB1. *Hear Res* 327, 227-34 (2015).
22. Vanspauwen, R., Wuyts, F.L., Krijger, S. & Maes, L.K. Comparison of Different Electrode Configurations for the oVEMP With Bone-Conducted Vibration. *Ear Hear* 38, 205-211 (2017).
23. Papathanasiou, E.S., Murofushi, T., Akin, F.W. & Colebatch, J.G. International guidelines for the clinical application of cervical vestibular evoked myogenic potentials: an expert consensus report. *Clin Neurophysiol* 125, 658-666 (2014).
24. Li, H. & Durbin, R. Fast and accurate short read alignment with Burrows-Wheeler transform. *Bioinformatics* 25, 1754-1760 (2009).
25. Wallis, Y. *et al.* Practice Guidelines for the Evaluation of Pathogenicity and the Reporting of Sequence Variants in Clinical Molecular Genetics. . *ACGS/VGKL* (2013).
26. Krumm, N. *et al.* Copy number variation detection and genotyping from exome sequence data. *Genome Res* 22, 1525-32 (2012).
27. Pfundt, R. *et al.* Detection of clinically relevant copy-number variants by exome sequencing in a large cohort of genetic disorders. *Genet Med* 19, 667-675 (2017).
28. Diekstra, A. *et al.* Translating sanger-based routine DNA diagnostics into generic massive parallel ion semiconductor sequencing. *Clin Chem* 61, 154-62 (2015).
29. Lek, M. *et al.* Analysis of protein-coding genetic variation in 60,706 humans. *Nature* 536, 285-91 (2016).
30. Watson, C.J. & Tempel, B.L. A new Atp2b2 deafwaddler allele, dfw(i5), interacts strongly with Cdh23 and other auditory modifiers. *Hear Res* 304, 41-8 (2013).
31. Carpinelli, M.R., Manning, M.G., Kile, B.T. & Burt, R.A. Two ENU-induced alleles of Atp2b2 cause deafness in mice. *PLoS One* 8, e67479 (2013).
32. McCullough, B.J. & Tempel, B.L. Haplo-insufficiency revealed in deafwaddler mice when tested for hearing loss and ataxia. *Hear Res* 195, 90-102 (2004).
33. Tsai, Y.S. *et al.* A de novo deafwaddler mutation of Pmca2 arising in ES cells and hitchhiking with a targeted modification of the Pparg gene. *Mamm Genome* 17, 716-22 (2006).
34. Spiden, S.L. *et al.* The novel mouse mutation Oblivion inactivates the PMCA2 pump and causes progressive hearing loss. *PLoS Genet* 4, e1000238 (2008).
35. Kozel, P. *et al.* Balance and hearing deficits in mice with a null mutation in the gene encoding plasma membrane Ca²⁺-ATPase isoform 2. *J Biol Chem.* (1998).
36. Bortolozzi, M. *et al.* The novel PMCA2 pump mutation Tommy impairs cytosolic calcium clearance in hair cells and links to deafness in mice. *J Biol Chem* 285, 37693-703 (2010).
37. Takahashi, K. & Kitamura, K. A point mutation in a plasma membrane Ca(2+)-ATPase gene causes deafness in Wrinkle Mouse Sagami. *Biochem Biophys Res Commun* 261, 773-8 (1999).
38. Xu, L. *et al.* Identification of a novel point mutation of mouse Atp2b2 induced by N-ethyl-N-nitrosourea mutagenesis. *Exp Anim* 60, 71-8 (2011).
39. Boumil, R.M. *et al.* A missense mutation in a highly conserved alternate exon of dynamin-1 causes epilepsy in fitful mice. *PLoS Genet* 6(2010).

40. Quinodoz, M. *et al.* DOMINO: Using Machine Learning to Predict Genes Associated with Dominant Disorders. *Am J Hum Genet* 101, 623-629 (2017).
41. Worley, J.A., Matson, J.L. & Kozlowski, A.M. The effects of hearing impairment on symptoms of autism in toddlers. *Dev Neurorehabil* 14, 171-6 (2011).
42. Malmgren, H., Sahlen, S., Wide, K., Lundvall, M. & Blennow, E. Distal 3p deletion syndrome: detailed molecular cytogenetic and clinical characterization of three small distal deletions and review. *Am J Med Genet A* 143A, 2143-9 (2007).
43. Angeloni, D. *et al.* CALL gene is haploinsufficient in a 3p- syndrome patient. *Am J Med Genet* 86, 482-5 (1999).
44. Oonk, A.M. *et al.* Progressive hereditary hearing impairment caused by a MYO6 mutation resembles presbycusis. *Hear Res* 299, 88-98 (2013).
45. Sampaio-Silva, J. *et al.* Exome Sequencing Identifies a Novel Nonsense Mutation of MYO6 as the Cause of Deafness in a Brazilian Family. *Ann Hum Genet* 82, 23-34 (2018).
46. Miyagawa, M., Nishio, S.Y., Kumakawa, K. & Usami, S. Massively parallel DNA sequencing successfully identified seven families with deafness-associated MYO6 mutations: the mutational spectrum and clinical characteristics. *Ann Otol Rhinol Laryngol* 124 Suppl 1, 148S-57S (2015).
47. Topsakal, V. *et al.* Genotype-phenotype correlation for DFNA22: characterization of non-syndromic, autosomal dominant, progressive sensorineural hearing loss due to MYO6 mutations. *Audiol Neurootol* 15, 211-20 (2010).
48. Noben-Trauth, K., Zheng, Q.Y., Johnson, K.R. & Nishina, P.M. mdfw: a deafness susceptibility locus that interacts with deaf waddler (dfw). *Genomics* 44, 266-72 (1997).
49. Qiu, X. & Muller, U. Mechanically Gated Ion Channels in Mammalian Hair Cells. *Front Cell Neurosci* 12, 100 (2018).
50. Bortolozzi, M. & Mammano, F. PMCA2 pump mutations and hereditary deafness. *Neurosci Lett* 663, 18-24 (2018).
51. Cali, T., Brini, M. & Carafoli, E. The PMCA pumps in genetically determined neuronal pathologies. *Neurosci Lett* (2017).
52. Konrad-Martin, D., Norton, S.J., Mascher, K.E. & Tempel, B.L. Effects of PMCA2 mutation on DPOAE amplitudes and latencies in deafwaddler mice. *Hear Res* 151, 205-220 (2001).
53. Sun, X.Y. *et al.* Insertion of an intracisternal A particle retrotransposon element in plasma membrane calcium ATPase 2 gene attenuates its expression and produces an ataxic phenotype in joggle mutant mice. *Gene* 411, 94-102 (2008).

SUPPLEMENTARY METHODS

The following criteria have been applied to select candidate variants with a dominant effect detected in WES: allele frequency $\leq 0.05\%$ in GnomAD (version r2.02) and in the in-house database (~20,000 exomes), ≥ 5 variant reads, % variant reads ≥ 20 and ≤ 90 , located in exonic regions and canonical splice sites of genes known to be associated with hearing loss in humans and/or mice. Synonymous variants were excluded, except those in *CDH23*.

For families W17-4352 and W18-0138, also candidate variants compliant with recessive inheritance have been selected as follows: ≥ 2 variants in a gene, allele frequency $\leq 1\%$ in GnomAD (version r2.02) and in the in-house database (~20,000 exomes), ≥ 5 variant reads, located in exonic regions and canonical splice sites of genes known to be associated with hearing loss in humans and/or mice considered. For homozygous variants % variant reads had to be ≥ 80 and for compound heterozygous variants ≥ 20 and ≤ 90 . Synonymous variants were excluded, except those in *CDH23*.

Prediction of a potential pathogenic effects of missense variants was performed with CADD PHRED (≥ 15), SIFT (≤ 0.05), PolyPhen-2 (PPH2, ≥ 0.450) and Mutation Taster (deleterious). Values for predicted pathogenicity are indicated between brackets. Segregation analysis was performed if at least two of the tools predicted a pathogenic effect of the variant. In the evaluation of candidate variants for recessive inheritance, segregation analysis was performed if the pathogenicity criteria were met for one of the variants. Segregation analysis was performed for all rare *CDH23* variants. A potential effect on splicing was predicted with the tools SpliceSiteFinder-like, MaxEntScan, NNSPLICE, GeneSplicer, and Human Splicing Finder as available in Alamut Visual (version 2.10). A change of at least 30% of splice site scores in at least two of the tools was regarded significant. Also PPH2 and SIFT were employed via Alamut Visual.

SUPPLEMENTARY TABLES

Table S1. Hearing impairment gene panel DG 2.11

Gene name	Gene name (continued)	Gene name (continued)	Gene name (continued)	Gene name (continued)
<i>ACTB</i>	<i>DIAPH1</i>	<i>KITLG</i>	<i>PRPS1</i>	<i>WBP2</i>
<i>ACTG1</i>	<i>DIAPH3</i>	<i>LARS2</i>	<i>PTPRO</i>	<i>WFS1</i>
<i>ADCY1</i>	<i>DMXL2^a</i>	<i>LHFPL5</i>	<i>RAI1^a</i>	<i>YAP1</i>
<i>AIFM1</i>	<i>DSPP</i>	<i>LMX1A^a</i>	<i>RDX</i>	
<i>APOPT1</i>	<i>EDN3</i>	<i>LOXHD1</i>	<i>ROR1^a</i>	
<i>ATP2B2^a</i>	<i>EDNRB</i>	<i>LRP5^a</i>	<i>S1PR2</i>	
<i>ATP6V1B1</i>	<i>ELMOD3</i>	<i>LRTOMT</i>	<i>SERPINB6</i>	
<i>BCS1L^a</i>	<i>EPS8</i>	<i>MARVELD2</i>	<i>SIX1</i>	
<i>BDP1</i>	<i>EPS8L2^a</i>	<i>MCM2</i>	<i>SIX5</i>	
<i>BSND</i>	<i>ESPN</i>	<i>MET^a</i>	<i>SLC17A8</i>	
<i>CABP2</i>	<i>ESRP1^a</i>	<i>MIR96</i>	<i>SLC22A4^a</i>	
<i>CACNA1D</i>	<i>ESRRB</i>	<i>MITE</i>	<i>SLC26A4</i>	
<i>CCDC50</i>	<i>EYA1</i>	<i>MPZL2^a</i>	<i>SLC26A5</i>	
<i>CD164</i>	<i>EYA4</i>	<i>MSRB3</i>	<i>SLC29A3^a</i>	
<i>CDC14A^a</i>	<i>FAM65B</i>	<i>MYH14</i>	<i>SLC33A1</i>	
<i>CDH23</i>	<i>FGF3</i>	<i>MYH9</i>	<i>SLC44A4^a</i>	
<i>CEACAM16</i>	<i>FOX11</i>	<i>MYO15A</i>	<i>SLITRK6</i>	
<i>CEP78^a</i>	<i>GAB1^a</i>	<i>MYO3A</i>	<i>SMPX</i>	
<i>CIB2</i>	<i>GATA3^a</i>	<i>MYO6</i>	<i>SNAI2</i>	
<i>CLDN14</i>	<i>GIPC3</i>	<i>MYO7A</i>	<i>SOX10</i>	
<i>CLIC5</i>	<i>GJB2</i>	<i>NARS2</i>	<i>STRC</i>	
<i>CLPP</i>	<i>GJB3</i>	<i>NLRP3</i>	<i>SYNE4</i>	
<i>CLRN1</i>	<i>GJB6</i>	<i>OPA1</i>	<i>TBC1D24</i>	
<i>COCH</i>	<i>GPR98</i>	<i>OSBPL2</i>	<i>TECTA</i>	
<i>COL11A1</i>	<i>GPSM2</i>	<i>OTOA</i>	<i>TIMM8A</i>	
<i>COL11A2</i>	<i>GRHL2</i>	<i>OTOF</i>	<i>TJP2</i>	
<i>COL2A1</i>	<i>GRXCR1</i>	<i>OTOG</i>	<i>TMC1</i>	
<i>COL4A3</i>	<i>GRXCR2</i>	<i>OTOGL</i>	<i>TMEM132E</i>	
<i>COL4A4</i>	<i>HARS</i>	<i>P2RX2</i>	<i>TMIE</i>	
<i>COL4A5</i>	<i>HARS2</i>	<i>PAX3</i>	<i>TMPRSS3</i>	
<i>COL4A6</i>	<i>HGF</i>	<i>PCDH15</i>	<i>TMTC2^a</i>	
<i>COL9A1</i>	<i>HOMER2</i>	<i>PDZD7</i>	<i>TNC</i>	
<i>COL9A2</i>	<i>HSD17B4</i>	<i>PET100</i>	<i>TPRN</i>	
<i>CRYM</i>	<i>ILDR1</i>	<i>PEX1^a</i>	<i>TRIOBP</i>	
<i>DCDC2</i>	<i>KARS</i>	<i>PEX6^a</i>	<i>TSPEAR</i>	
<i>DFNA5</i>	<i>KCNE1</i>	<i>PNPT1</i>	<i>TYR</i>	
<i>DFNB31</i>	<i>KCNJ10</i>	<i>POU3F4</i>	<i>USH1C</i>	
<i>DFNB59</i>	<i>KCNQ1</i>	<i>POU4E3</i>	<i>USH1G</i>	
<i>DIABLO</i>	<i>KCNQ4</i>	<i>PRKCB^a</i>	<i>USH2A</i>	

Hereditary hearing impairment gene panel version DG-2.11, as used by Genome Diagnostics Nijmegen-Maastricht. The panel consists of 159 genes, both syndromic and non-syndromic forms of hereditary hearing impairment. Underlined genes are associated with HI in an autosomal dominant inheritance pattern. ^aGenes that have been added to the list since gene panel version DG-2.5, including *ATP2B2*.

Table S2. Rare variants in known human and mouse deafness genes in the index cases

Family code	Variant code ^a	Gene name	transcript	Genome	cDNA	Protein	CADD-PHREDD ^b	SIFT ^c	PPH2 ^d	Mutation Taster ^e	In house frequency (%)	gnomAD-E EAS (%)	gnomAD-E NFE (%)
W18-0138	V1	<i>WFS1</i>	NM_006005.3	Chr4: 6293021G>C	c.558G>C	p.Lys186Asn	18.4	0.48	0.725	Disease causing	0.012	NA	0.002
	V2	<i>SLC17A8</i>	NM_139319.2	Chr12: 100796485_100796486delinsAA	c.1015_1016delinsAA	p.Ala339Asn	33	0.04	0.940	NA	0.049	NA	0.029
	V3	<i>GJB2</i>	NM_004004.5	Chr13: 20763074C>A	c.647G>T	p.Arg216Ile	13.4	0.01	0.155	Disease causing	0.037	NA	0.007
	V4	<i>SLC26A5</i>	NM_198999.2	Chr7: 103032076T>C	c.1226A>T	p.Lys409Met	24	0.09	0.997	Disease causing	0.004	NA	0.005
W18-0111	V5	<i>WFS1</i>	NM_006005.3	Chr4: 6303168T>C	c.1646T>C	p.Leu549Pro	11.97	0.13	0.331	Disease causing	0.008	NA	0.003
	V6	<i>MYO6</i>	NM_004999.3	Chr6: 76617371G>C	c.3226G>C	p.Asp1076His	20.4	0.00	0.997	Disease causing	0.008	NA	0.001
W17-4352 ^f	V7	<i>MYO7A</i>	NM_000260.3	Chr11: 76903126G>A	c.3955G>A	p.Val1319Ile	31	0.25	0.926	Disease causing	0.004	0.000	0.002
	V8	<i>DNM1</i>	NM_004408.3	Chr9: 130984483C>T	c.857C>T	p.Thr286Met	21	0.08	1.000	Polymorphism	0.004	0.000	0.000
	V9	<i>DNM1</i>	NM_004408.3	Chr9: 130965899T>C	c.150T>C	p.=	9	NA	NA	NA	0.004	0.000	-
	V10	<i>IRF6</i>	NM_006147.3	Chr1: 209968743A>G	c.400T>C	p.Trp1344Arg	15.4	0.01	NA	Disease causing	0.004	0.000	0.000
W17-0883	V11	<i>PTGER1</i>	NM_000955.2	Chr19: 14583633_14583635del	c.946_948del	p.Leu316del	36	NA	NA	NA	0	NA	0.002

In family W17-4352 GnomAD East Asian was also assessed due to ancestry. Genomic positions are according to GRCh37/hg19. cDNA positions are according to transcript NM_022124.5. For none of the variants an effect on transcript splicing is predicted. V1-V11, variants in other (mouse) deafness genes than candidate gene *ATP2B2* as depicted in **Figure S1**; in house frequency is based on WES of ~20 000 individuals; GnomAD E EAS, allele frequency (%) in gnomAD, exomes of East-Asians; GnomAD E NFE, allele frequency (%) in gnomAD, exomes of non-Finnish Europeans; NA, not applicable. ^aVariant code used in **Figure S1**; None of the variants were predicted to have an effect on splicing. Scores that meet the thresholds for pathogenicity are indicated in red. V, variant.

Table S3. Rare *CDH23* variants in the index cases.

Family code (index case)	Variant code ^a	Genome	cDNA	Protein	CADD _{-PHREDD} ¹	SIFT ²	PPH2 ³	Mutation Taster ⁴	Pathogenicity Classification ACGS/VKGL ^b	Pathogenicity Classification ClinVar ^c	In house frequency (%)	gnomAD-E EAS (%)	gnomAD-E NFE (%)
W18- (III.1)	VC1	g.73491873A>G	c.3845A>G	p.Asn1282Ser	14.17	0.00	0.796	Disease causing	UV1/UV2	UV1/UV2	0.694	NA	0.523
W18- (III.1)	VC2	g.73377112G>A	c.1096G>A	p.Ala366Thr	34.00	0.00	0.993	Disease causing	UV1/UV2	UV1/UV2	0.996	NA	0.902
W17- (III.1)	VC3	g.73472494A>G	c.3293A>G	p.Asn1098Ser	16.95	0.00	0.018	Disease causing	UV1	UV1/UV2	0.400	NA	0.386
W17- (III.2)	VC4	g.73558192G>A	c.6911G>A	p.Arg2304Gln	16.21	0.05	0.060	Polymorphism	UV3	UV1/UV23	0.016	0.026	0.004
W17- (III.1)	VC5	g.73434968G>A	c.1514+35G>T	p.?	0.14	NA	NA	NA	NA	-	-	NA	-
W18- (III.3)	VC6	g.73565712G>A	c.8022G>A	p.=	11.12	NA	NA	NA	UV1/UV3	UV1-UV3	0.849	NA	0.851

In family W17-4352 GnomAD East Asian was also assessed due to ancestry. Genomic positions are according to GRCh37/hg19. cDNA positions are according to transcript NM_022124.5. For none of the variants an effect on transcript splicing is predicted. Amino acids changed in VC1-VC4 are located in cadherin domains 12, 4, 10 and 22, respectively. VC1-VC6, variants in *CDH23*, as listed in **Figure S1**, in house frequency is based on WES of ~20 000 individuals; GnomAD EAS, allele frequency (%) in gnomAD, exomes of East-Asians; GnomAD E NFE, allele frequency (%) in gnomAD, exomes of non-Finnish Europeans; NA, not applicable. ^aVariant code used in **Figure S1**; ^bPathogenicity classification is based on guidelines from the Association for Clinical Genetic Science and the Dutch Society of Clinical Genetic Laboratory Specialists⁵; ^cClassification according to ClinVar. None of the variants were predicted to have an effect on splicing. Scores that meet the thresholds for pathogenicity are indicated in red.

Table S4. Individual results of ABR measurements, vestibular history and vestibular testing

Family	Subject (age)	Click-evoked ABR	Anamnesis and history of vestibular symptoms	Oculomotor testing	vHIT	Caloric measurement				Conclusion
						Warm (°/s)(10-52) ^a		Cold (°/s) 7-31) ^a		
						AD	AS	AD	AS	
W18-0111	III.1 (11)	NT	no	N	N	21	28	31	35	N
	II.3 (44)	NT	no	N	N	29	30	18	11	N
W18-0138	III.1 (24)	NT	no	N	N	19	11	NT	NT	N
W17-0883	III.1 (10)	symmetric, minor TWD related to HI	no	N	N	NT	NT	24	24	N
	II.1 (31)	symmetric, minor TWD related to HI	no	N	N	11	38	21	27	N
W18-0139	IV.2 (48) ^c	symmetric, minor TWD related to HI	Balance complaints when standing or walking after cholesteatoma surgery with perilymph leak in left ear.	N	N	20	4	16	3	Right N
	III.3 (68)	symmetric, minor TWD related to HI	Diagnosed with benign paroxysmal positional vertigo (BPPV)	N	N	31	29	24	19	N

Family	Subject	Rotating chair/pendular chair ²				cVEMP		oVEMP		Conclusion			
		Gain (%) (33-72) ^a	SPV (°/s) (30-65) ^a	Tau (s) (11-26) ^a	Conclusion	Threshold (dBHL)(<100) ^a	conclusion	Thresholds (dBFL)(<140) ^a	Conclusion				
		CW	CCW	CW	CCW	AD	AS	AD	AS				
W18-0111	III.1	45	69	40	62	14	10	100	>100	AD normal, AS no sacular function measured	124	126	Normal thresholds, no utricular lesions
		29	22	36	28	NA	NA	NT	NT	NA	NT	NT	NT
W18-0138	III.1	73	59	66	53	22	16	>100	>100	slightly hyperreactive to AD due to fear	>140	>140	No utricular function measured
W17-0883	III.1	70	76	64	69	25	21	87	87	slightly hyperreactive	NT	NT	NA
W18-0139	IV.2 ^c	64	58	58	52	31	26	90	87	slightly hyperreactive	NT	NT	NA
		31	46	30	47	11	10	92	>100	AD normal, AS no sacular function measured	135	132	Normal thresholds, no utricular lesions
III.3	III.3	82	65	74	58	7	10	87	92	CW slightly hyperreactive SPV and hypo-reactive Tau	130	130	Normal thresholds, no utricular lesions

ABR, auditory brainstem response; vHIT, video head impulse test; cVEMP, cervical vestibular evoked myogenic potentials; oVEMP, ocular vestibular evoked myogenic potentials; °, degree; s, seconds; SPV, slow phase velocity; Tau, time constant; dBHL, decibel hearing level; dBFL, decibel force level; AD, right ear; AS, left ear; CW, clock-wise; CCW, counter clock-wise; TWD, total wave delay; N, normal; NT, not tested; NA, not applicable. ^anormal values at our institute; ^bsubject W18-0111 II.3 had pendular chair testing instead of rotating chair testing. ^conly right ear results assessed.

SUPPLEMENTARY FIGURES

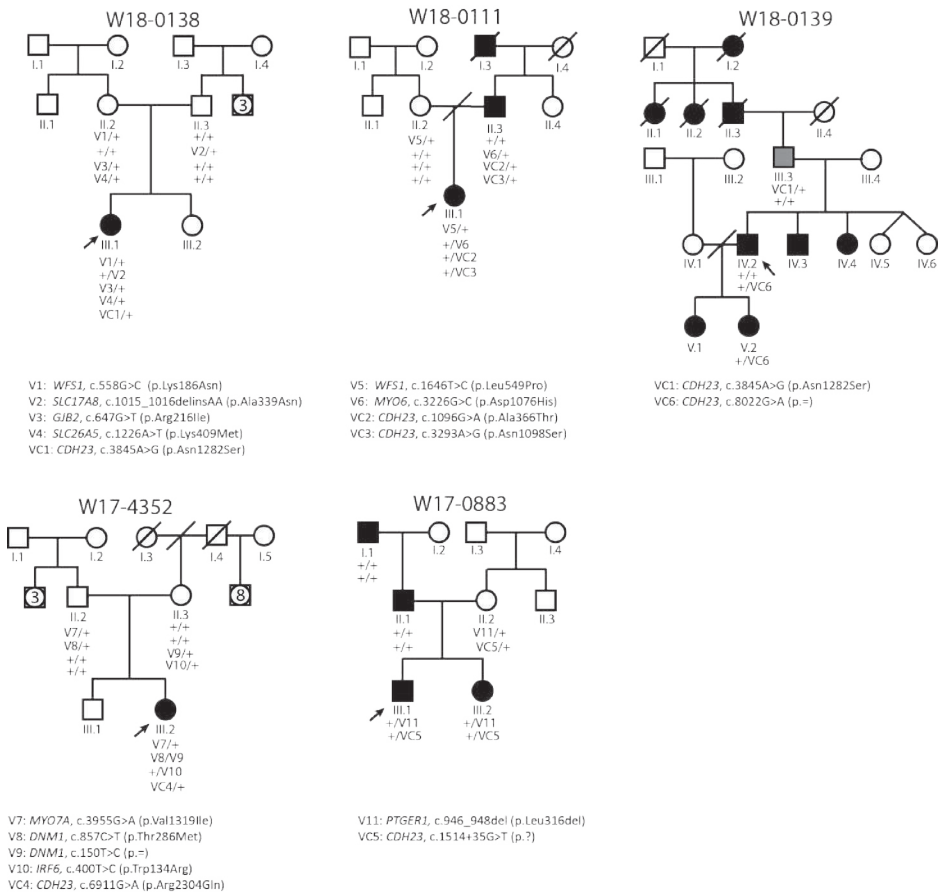


Figure S1. Segregation of variants identified in WES Segregation analysis of selected variants identified in WES. The subject marked in grey (III.3, W18-0139) has late onset hearing impairment, in contrast to the early onset of hearing impairment in all other affected individuals. Affected individuals IV.3, IV.4 and V.1 of family W18-0139 did not participate in this study. Deceased individuals are considered affected or unaffected by heteroanamnesis. Index cases are indicated by arrows. Full details of the variants are provided in **Tables S2 and S3**. +, reference sequence. V, variant; VC, variant in *CDH23*.

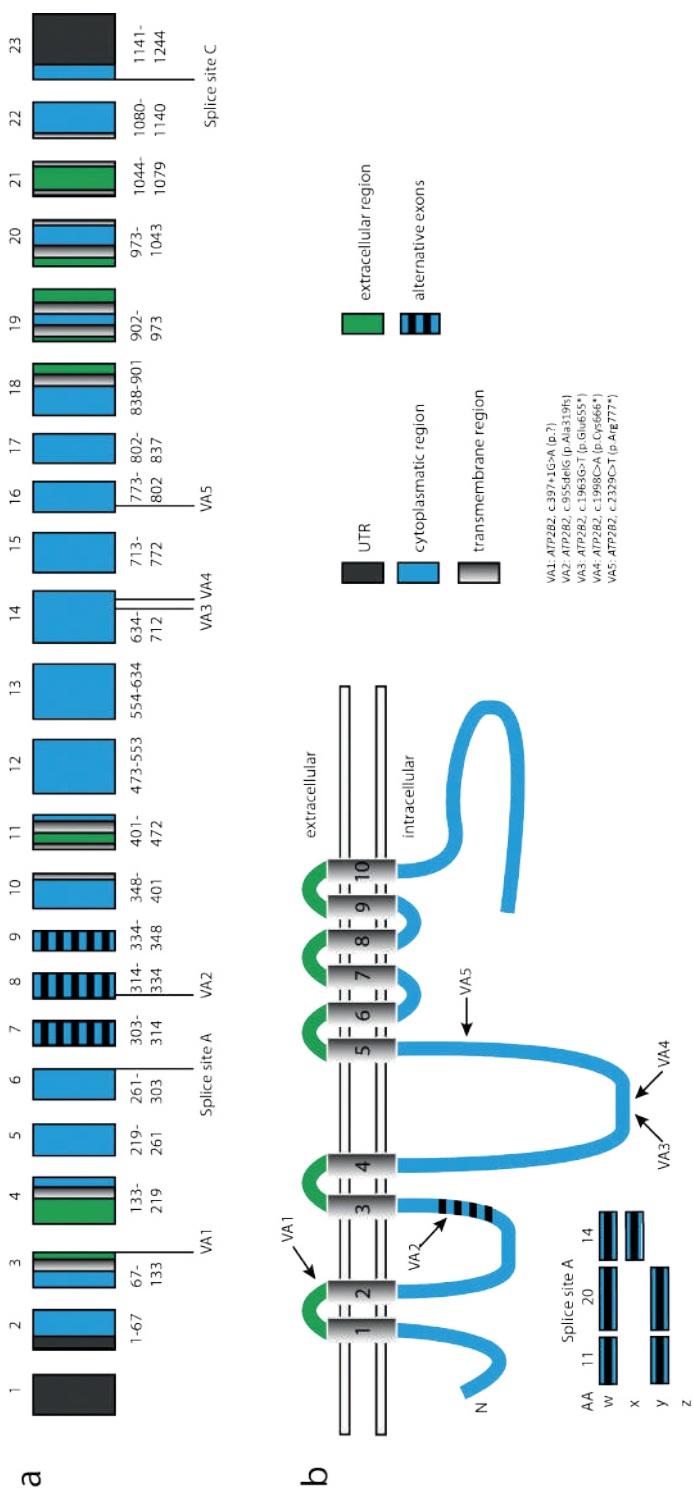


Figure S2. Exonic and protein structure of *ATP2B2*/PMCA2 (A) Schematic representation of the genomic structure of *ATP2B2* transcript NM_001001331.3. Exons are numbered and alternatively spliced exons are striped. Numbers 1 to 1243 represent the encoded amino acid residues. Colors represent the encoded protein domains as shown in b, domains were extracted from Uniprot. **(B)** Schematic representation of PMCA2 as encoded by transcript NM_001001331.3. This transcript contains alternatively spliced exons 7-9 at splice site A (w isoform), no alternatively spliced exons at splice site C. In man, the transcript orthologous to the *w/a* splice pattern in mouse has not been identified (UCSC and ENSEMBL Genome browsers). Splice variants at site A (w, x, y, z) are according to those described for mouse⁶. Variants identified in this study are indicated as VA1-VA5 (see also Table 1). AA, amino acids; C, C terminus; N, N terminus; UTR, untranslated region; VA, variant in *ATP2B2*.

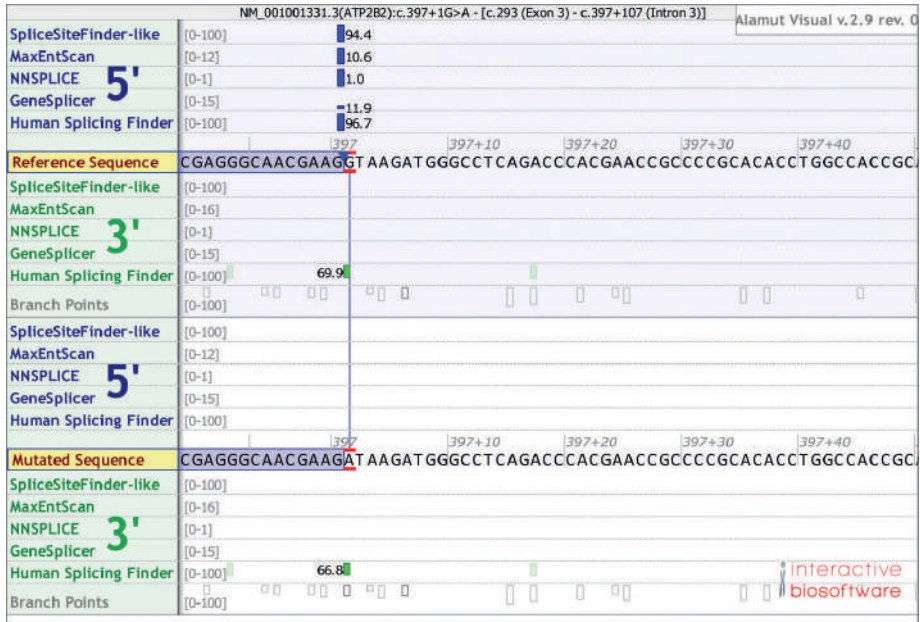


Figure S3. Splice prediction The variant c.397+1G>A (p.(?)) is predicted to cause loss of the splice donor site of exon 3. Splice site prediction scores and figure were obtained from AlamutVisual version 2.10.

SUPPLEMENTARY REFERENCES

1. Kircher, M. *et al.* A general framework for estimating the relative pathogenicity of human genetic variants. *Nat Genet* 46, 310-5 (2014).
2. Kumar, P., Henikoff, S. & Ng, P.C. Predicting the effects of coding non-synonymous variants on protein function using the SIFT algorithm. *Nat Protoc* 4, 1073-81 (2009).
3. Adzhubei, I.A. *et al.* A method and server for predicting damaging missense mutations. *Nat Methods* 7, 248-9 (2010).
4. Schwarz, J.M., Cooper, D.N., Schuelke, M. & Seelow, D. MutationTaster2: mutation prediction for the deep-sequencing age. *Nature Methods* 11, 361-362 (2014).
5. Wallis, Y. *et al.* Practice Guidelines for the Evaluation of Pathogenicity and the Reporting of Sequence Variants in Clinical Molecular Genetics. . *ACGS/VGKL* (2013).
6. Strehler, E.E. & Zacharias, D.A. Role of alternative splicing in generating isoform diversity among plasma membrane calcium pumps. *Physiol Rev* 81, 21-50 (2001).

URLs

ClinVar, <https://www.ncbi.nlm.nih.gov/clinvar/>

GnomAD, <http://gnomad.broadinstitute.org/>

Uniprot, <http://www.uniprot.org/uniprot/Q01814>

UCSC Genome browser, <https://genome.ucsc.edu/>

Ensemble Genome browser, <https://www.ensembl.org/index.html>



Chapter 4.2

A *RIPOR2* in-frame deletion is a frequent and highly penetrant cause of adult-onset hearing loss

Suzanne E. de Bruijn*, Jeroen J. Smits*, Chang Liu, Cornelis P. Lanting, Andy J. Beynon, Joëlle Blankevoort, Jaap Oostrik, Wouter Koole, Erik de Vrieze, DOOFNL Consortium, Cor W.R.J. Cremers, Frans P.M. Cremers, Susanne Roosing, Helger G. Yntema, Henricus P.M. Kunst, Bo Zhao, Ronald J.E. Pennings[†], and Hannie Kremer[‡]
(*, ~ gelijke bijdrage)

Journal of Medical Genetics 58, 96-104 (2021)

ABSTRACT

Hearing loss is one of the most prevalent disabilities worldwide, and has a significant impact on quality of life. The adult-onset type of the condition is highly heritable but the genetic causes are largely unknown, which is in contrast to childhood-onset hearing loss. An in-frame deletion of 12 nucleotides in *RIPOR2* was identified as a highly penetrant cause of adult-onset progressive hearing loss that segregated as an autosomal dominant trait in 12 families from the Netherlands. Hearing loss associated with the deletion in 63 subjects displayed variable audiometric characteristics and an average age of onset of 30.6 years (SD 14.9 years, range 0-70 years). A functional effect of the *RIPOR2* variant was demonstrated by aberrant localization of the mutant RIPOR2 in the stereocilia of cochlear hair cells and failure to rescue morphological defects in *RIPOR2*-deficient hair cells, in contrast to the wildtype protein. Strikingly, the *RIPOR2* variant is present in 18 of 22,952 individuals not selected for hearing loss in the Southeast Netherlands. Collectively, the presented data demonstrate that an inherited form of adult-onset hearing loss is relatively common, with potentially thousands of individuals at risk in the Netherlands and beyond, which makes it an attractive target for developing a (genetic) therapy.

INTRODUCTION

Hearing loss (HL) is one of the most prevalent disabilities worldwide¹ and genetic factors importantly contribute to this condition. So far, 118 genes have been associated with nonsyndromic forms of sensorineural HL and variants in these genes explain a significant part of subjects with an early onset of HL, i.e., congenital or in childhood.²⁻⁴ Our knowledge of the genetic architecture of adult-onset HL is limited despite a high heritability which is estimated to be 30-70%.⁵⁻⁷ Differences in phenotypic parameters that are used and age ranges of study participants may well contribute to the variation in the reported heritability. As summarized by Lewis et al.⁸, genome-wide association studies (GWAS) of hearing status in adults and genetic analyses of families with dominantly inherited post-lingual onset HL indicate that both common variants and rare variants contribute to adult-onset HL with a small and large effect size, respectively. Such variants may or may not affect genes that are already known to function in the auditory pathway.

Previously, we identified a 12.4-Mb locus for adult-onset HL on chromosome 6 (p24.1-22.3): DFNA21.^{9,10} However, the underlying pathogenic variant in the studied family (W97-056) remained elusive. Here, we present the identification of an in-frame deletion (c.1696_1707del; NM_014722.3) in *RIPOR2* (RHO Family Interacting Cell Polarization Regulator 2) to underlie autosomal dominant nonsyndromic HL (adNSHL) in this family and in 11 additional (large) families of Dutch origin. The allele frequency (AF) of this variant suggests that it potentially explains adult-onset HL in thousands of individuals in the Netherlands and Northwest Europe. Our study expands the phenotypic spectrum associated with *RIPOR2* defects which had so far only been described to underlie early-onset recessively inherited HL.¹¹

4.2

MATERIALS AND METHODS

Study approval

The study of human subjects was approved by the medical ethics committee of the Radboudumc (registration number: NL33648.091.10) and performed in accordance with the principles of the World Medical Association Declaration of Helsinki. Written informed consent was obtained from all participants or their legal representatives. All animal experiments were approved by the Institutional Animal Care and Use Committee of Indiana University School of Medicine (registration number: 19075).

DNA sequencing

Next generation sequencing was performed for identification of DNA variants. Details of employed sequencing techniques are provided in **Supplementary Methods**.

Variant interpretation

For exome sequencing and Molecular Inversion Probe (MIP) datasets, annotated variants were filtered based on a population AF of $\leq 0.5\%$ in the gnomAD database V.2.1, and our in-house exome database (~15,000 alleles). Variants in coding and splice site regions (-14/+14 nucleotides) were analyzed. Interpretation of missense variants was performed using the *in silico* tools CADD-PHRED (≥ 15),¹² SIFT (≤ 0.05),¹³ PolyPhen-2 (≥ 0.450)¹⁴ and MutationTaster (deleterious)¹⁵ to predict potential functional effects. Variants were considered if a pathogenic effect was predicted by at least two different tools. Potential effects on splicing of missense and synonymous variants were evaluated using the algorithms embedded in the AlamutVisual software (V.2.10, Interactive Biosoftware). A change of $\geq 5\%$ in splice site scores predicted by at least two algorithms was considered significant. For candidate variants, segregation analysis was performed by Sanger sequencing. PCR conditions are available upon request.

Clinical evaluation

Medical history was taken from all participants with special attention paid to acquired and noise-induced HL. Both affected and unaffected participants underwent general Ear Nose and Throat examinations, or this medical information was taken from previous examinations. Age of onset of HL was reported by subjects themselves. Only reports of a specific age of onset were used in calculations. The audiometric data in this study are described according to GENDEAF guidelines.¹⁶ Pure tone- and speech- audiometry and click-evoked auditory brainstem response (ABR) was performed in a sound-attenuated booth, according to current standards (International Organisation for Standardization; ISO 8253-1:2010, ISO 389-1, ISO 389-5 and ISO 389-6).¹⁷ Individuals were considered affected when pure tone thresholds for at least three individual frequencies were below the frequency-specific 95th percentile of age- and sex-specific thresholds (ISO7029:2017) for the best hearing ear. HL was considered asymmetric if pure tone audiometry showed a difference of more than 10 dB between both ears at two individual frequencies.¹⁶ Longitudinal (individual) progression of HL was calculated if there was a follow-up duration of at least 10 years, after onset of HL. The progression rate is defined as the mean increase pure tone average at 0.5-4 kHz ($PTA_{0.5-4kHz}$) in dB/year between first and last audiometry. For symmetric HL, the average of both ears was used to calculate progression; for asymmetric HL, the best-hearing ear at first audiometry was used. In case of profound HL at 0.5-4 kHz at the latest audiometry, the most recent audiometry at which all thresholds at 0.5-4 kHz could be measured, was selected. Cross-sectional linear regression analysis was applied on pure tone thresholds to calculate an Age Related Typical Audiogram (ARTA),¹⁸ using

Prism 6.0 software (GraphPad). A k-means clustering analysis was performed as described in **Supplementary Methods**.

Injctoporation of Ripor2-constructs and immunostaining

The generation of *Ripor2*^{LacZ/LacZ} mice has been described previously.¹⁹ For *Ripor2* DNA construct generation, *Ripor2* cDNA (NM_029679.2, without exon 13) was amplified from a mouse-cochlear cDNA library and cloned into a pEGFP-N3-derived vector from which the EGFP coding sequence was deleted. Procedures for injctoporation and immunostaining have been described previously,¹⁹ and are detailed in **Supplementary Methods**.

Immunoprecipitations and western blots

Cell culture, immunoprecipitations and western blots were carried out as described.^{19,20} Experiments were carried out at least three times. Antibodies used are listed in **Supplementary Methods**.

Methods and materials for VNTR marker analysis, vestibular testing and allele-specific expression analysis are provided in **Supplementary Methods**.

RESULTS

Exome sequencing revealed an in-frame deletion in RIPOR2

To identify the genetic defect underlying the HL in family W97-056 (**Figure 1**), exome sequencing was performed in three affected family members (III:22, IV:20 and IV:25). After applying the variant filtering and prioritization described above, two variants were shared between the three affected individuals (**Table S1**). A *SPATS1* variant (c.419G>A; p.(Gly140Glu); NM_145026.3), did not completely segregate with HL within the family as 7 out of 23 affected subjects did not harbor the variant (**Figure S1**). Also, *SPATS1* expression was not detected in the mammalian cochlea^{21,22} and *SPATS1* function has only been related to spermatogenesis.²³ Therefore, this variant was deemed non-causative.

Segregation analysis identified the *RIPOR2* variant in 20 of 23 affected subjects of family W97-056 (**Figure 1**). The variant was not found in subjects III:14, III:20, and III:21; a recombination event in subject III:14 previously delimited the centromeric border of the *DFNA21* locus.¹⁰ The *RIPOR2* c.1696_1707del variant was also found in three unaffected family members (V:2, age 23 years; IV:26, age 40 years and III:28, age 51 years). The strong association of the *RIPOR2* variant with HL in this family urged us to further address this and other variants in *RIPOR2* in families with (adult-onset) HL.

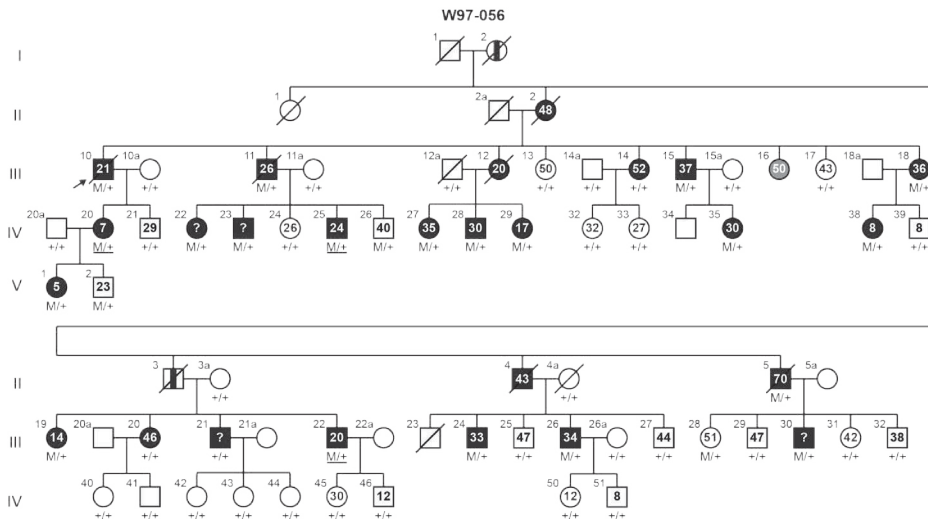
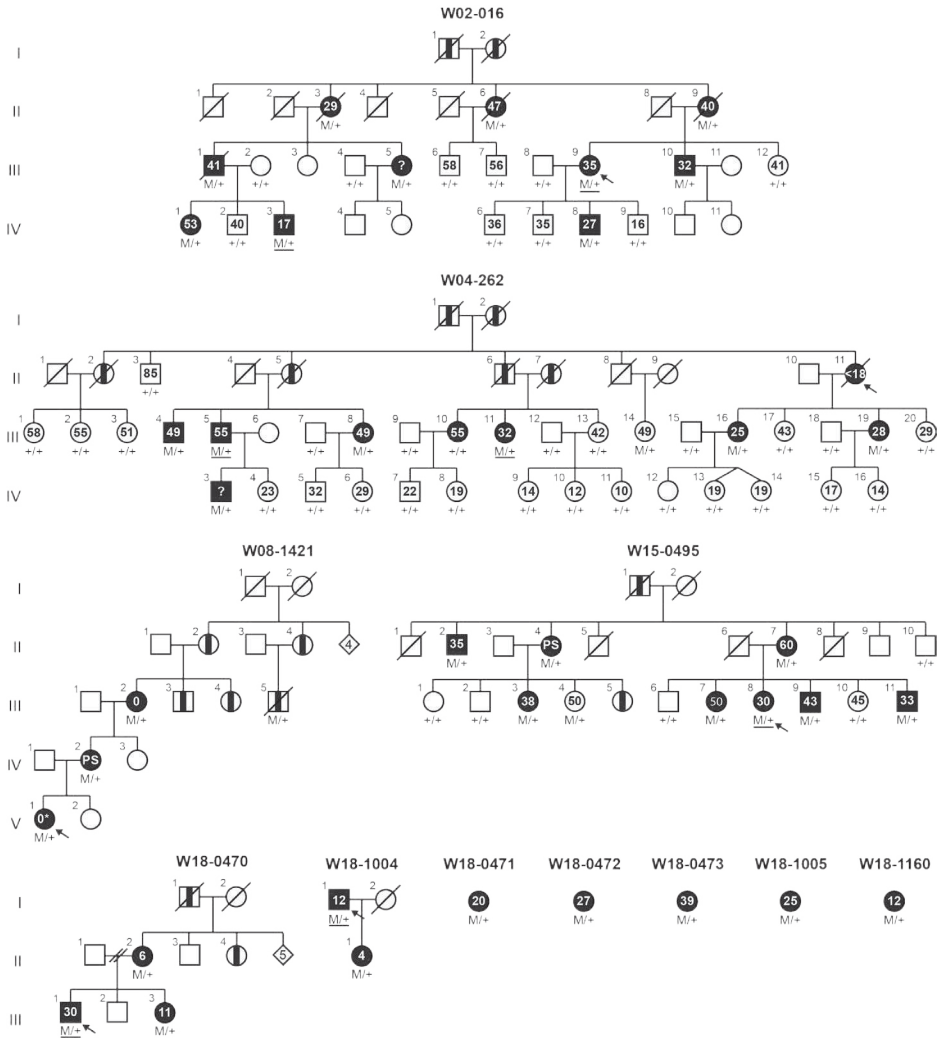


Figure 1. Pedigree of family W97-056 and segregation of *RIPOR2* variant c.1696_1707del For affected and unaffected family members, the age of onset of hearing loss or the age at the most recent audiometric evaluation are indicated in the pedigree symbols, respectively. Subjects who did not report an age of onset are indicated with a question mark. The index case is marked by an arrow. Exome sequencing was performed in subjects with an underlined genotype. Subjects determined to be affected by heteroanagnosis are indicated with a vertical black bar. The subject marked in grey is diagnosed with intellectual disability and excluded from further participation in this study. Subject identifiers correspond to those in de Brouwer et al., 2005. M, c.1696_1707del; +, wildtype.

The in-frame deletion was present in exon 14 of *RIPOR2* (c.1696_1707del; p.(Gln566_Lys569del); NM_014722.3; Chr6:g.24,843,303_24,843,314del; rs760676508). It affects a highly conserved protein region of *RIPOR2* which is present in all *RIPOR2* isoforms (**Figure S2**). *RIPOR2* has previously been associated with recessively inherited early-onset hearing loss and is positioned 0.9 Mb centromeric of the *DFNA21* locus.^{10,11} No copy number variants were detected that were shared by all three subjects.

The *RIPOR2* variant c.1696_1707del associates with adNSHL in eleven additional families

An exome sequencing dataset of 1,544 index cases with (presumed) hereditary HL was evaluated for rare *RIPOR2* variants. In these cases, (likely) pathogenic variants in known deafness genes were previously addressed in a clinical diagnostic setting. The c.1696_1707del variant was identified in 10 index cases, all diagnosed with adNSHL (**Figure 2**). Analysis of a dataset obtained through MIP sequencing of 89 HL-associated genes in 64 index cases with (presumed) adNSHL revealed another subject (V:1, W08-1421; **Figure 2**) with this variant. No other rare *RIPOR2* variants (AF \leq 0.5%) that met the variant filtering criteria were identified.



4.2

Figure 2. Family pedigrees and segregation of *RIPOR2* variant c.1696_1707del For affected and unaffected family members, the age of onset of hearing loss or the age at the most recent audiometric evaluation are indicated in the pedigree symbols, respectively. Subjects who did not report an age of onset are indicated with a question mark. Index cases are marked by arrows. Exome sequencing was performed in subjects with an underlined genotype. Subjects determined to be affected by heteroanamnesis are indicated with a vertical black bar. Based on the information provided in the questionnaires, an autosomal dominant inheritance pattern of hearing loss is likely for each of the single cases. M, c.1696_1707del; +, wildtype; PS, primary school.

For 6 of the 11 index cases with the c.1696_1707del *RIPOR2* variant, family members were included in the study and segregation analysis was performed (**Figure 2**). The variant was detected in 39 of 40 affected subjects, but not in subject III:10 of family W04-262. As observed in family W97-056, the *RIPOR2* variant was also found in unaffected subjects namely III:14 of family W04-262 and III:4 of family W15-1495, aged 49 and 50 years respectively.

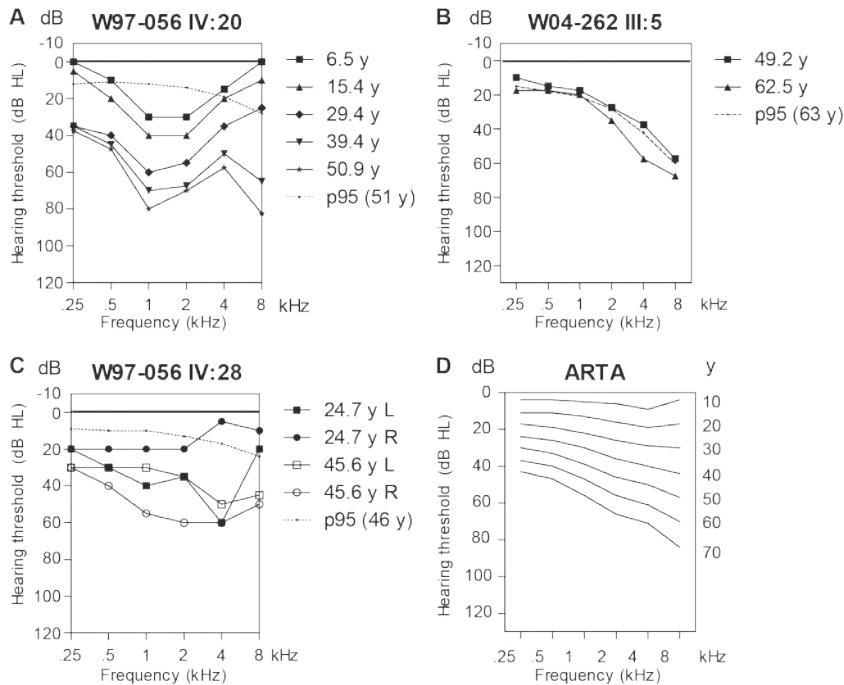


Figure 3. Selection of audiograms and the ARTA. (A-C) Air conduction thresholds of three selected individuals with the c.1696_1707del *RIPOR2* variant are depicted. For the individuals in panels A and B, hearing loss was symmetric and the average of left and right ear thresholds are depicted. For the individual in panel C, hearing loss was asymmetric and the thresholds for both right and left ears are depicted. The p95 values are matched to the individuals' sex and age at most recent audiometry, according to the ISO 7029:2017 standard. **(D)** Age Related Typical Audiogram (ARTA), cross-sectional linear regression analysis of last visit audiograms of affected subjects with the c.1696_1707del *RIPOR2* variant. y, age in years; R, right; L, left; dB HL, decibel hearing level; kHz; kiloHertz

For all 11 index cases, targeted reanalysis of sequencing data for known adNSHL-associated genes was performed to reveal other (likely) pathogenic variants.⁴ No rare variants were identified that both segregated with HL in the family and were classified as (likely) pathogenic in ClinVar²⁴ (Table S2). The presence of an identical *RIPOR2* variant in 12 families of Dutch origin is suggestive for a common ancestor. Indeed, a shared haplotype of ~0.71 Mb, flanking the variant (D6S2439-D6S1281), was observed in the seven families and potentially the five single cases (Supplementary Results, Figure S3).

Clinical evaluation of individuals with the c.1696_1707del variant and phenocopies

To characterize the HL associated with the c.1696_1707del *RIPOR2* variant, 200 affected and unaffected subjects from seven families and five single index cases were evaluated between 1997 and 2018. The *RIPOR2* variant was found to be present in 64 of the 200 subjects. Detailed clinical data per individual are provided in Table S3.

The mean reported age of onset is 30.6 years (standard deviation 14.9 years) with a wide range from congenital to 70 years (**Figure S4**). Evaluation of audiometric data showed that subjects with the *RIPOR2* variant have progressive sensorineural HL, ranging from mild to profound, with variable audiometric configurations (**Figure 3, Figure S5**).

In order to distinguish audiometric patterns, a k-means clustering algorithm, independent of subject age, was applied on the latest audiogram of each subject. This unbiased approach yielded four audiometric patterns, each with a distinct audiometric configuration (**Figure 4**). Asymmetry of HL was seen in 16 cases. Inter-aural differences in progression of HL were also seen (**Figure 3C**). For three subjects (III:30 of family W97-056, II:11 of family W04-262 and V:1 of W08-1421), an explanation for asymmetry was noted (**Table S3**).

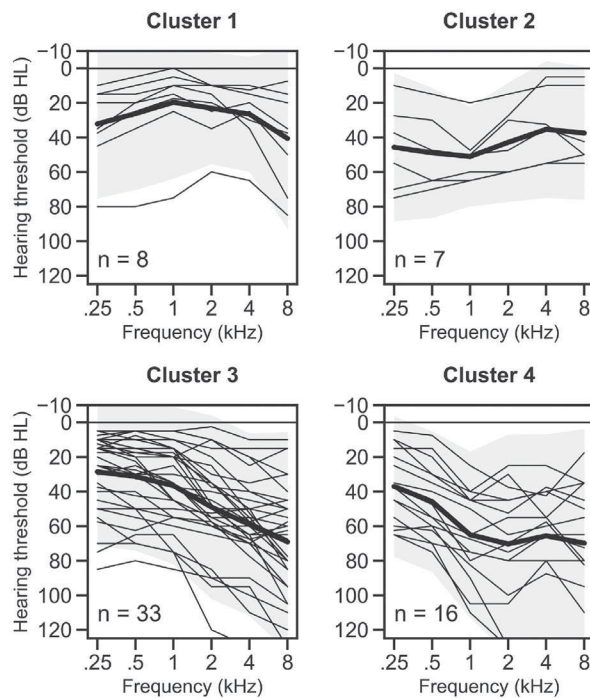


Figure 4. Four audiometric patterns of *RIPOR2*-associated hearing loss Air conduction thresholds of all subjects were analyzed with a k-means clustering protocol. The thick black lines depict the average of each cluster, the transparent grey areas represent the ± 2 standard deviations. Cluster 1: mild hearing loss (average (PTA_{0.5-4 kHz})) 23 dB hearing level (HL) with an inverse U-shape audiogram. Cluster 2: moderate hearing loss (average 48 dB HL), with relatively worse hearing in the lower frequencies. Cluster 3: moderate (average 39 dB HL) high-frequency hearing loss with a gently down sloping audiogram configuration (average of 28 dB HL difference between the mean of 0.5-1 and 4-8 kHz). Cluster 4: moderate (average 60 dB HL), mid-frequency hearing loss with a U-shape audiogram, individual audiometry (**Figure S5**) shows relatively faster deterioration of higher frequencies later in life, for example W97-056 IV:20. dB HL, decibel hearing level; kHz, kiloHertz.

Longitudinal analysis of HL in individual subjects revealed a large variation in progression of HL between subjects (**Table S3**). We could not identify a specific pattern, such as a certain progression (in dB/y) in certain decades. There was a median progression of 1.2 dB/y (range 0.5-2.7 dB/y), for the frequencies 0.5-4 kHz. Cross-sectional linear regression was applied to calculate ARTA (**Figure 3D**). Progression ranged from 0.7 dB/y (0.25 kHz) to 1.3 dB/y (8 kHz). Progression of HL was significant for all frequencies (*F*-test, *p*-value: <0.0001).

Speech reception thresholds were generally lower than, or comparable to, $PTA_{0.5-2\text{kHz}}$ (**Table S3**). This indicates absence of retrocochlear pathology and is in line with normal results of click-evoked ABR in four subjects (**Table S3**). CT and/or MRI of the bilateral temporal bones and cerebellopontine angle in six subjects revealed normal inner and middle ear anatomy (**Table S3**).

Vestibular testing, performed in 11 randomly selected subjects with the *RIPOR2* variant, aged 29 to 71 years, led to the conclusion that c.1696_1707del *RIPOR2* is not associated with vestibular dysfunction (**Table S4**). Further details are provided in the **Supplementary Results**.

Transcript levels of *RIPOR2* do not correlate with age of onset in affected subjects

We hypothesized that the variability in age of onset of the HL associated with the c.1696_1707del *RIPOR2* variant might be explained by differences in expression levels of the wildtype allele. Alternatively, variants in *cis* regulatory elements of the affected allele more distantly located from *RIPOR2*, could influence expression levels of the mutant allele and might thereby modulate the age of onset. To test these hypotheses, allele-specific transcript levels of *RIPOR2* were determined in peripheral blood cells of 33 subjects using quantitative RT-PCR. Subjects were divided into three groups based on self-reported age of onset: <20 years (*n*=7), 20-39 years (*n*=15) and >40 years (*n*=6). No significant differences were observed between the different subject groups, neither for the wildtype or c.1696_1707del variant *RIPOR2* alleles nor for total *RIPOR2* transcript levels (**Figure S7**). Also, no difference was observed between the ratios of *RIPOR2* mutant to wildtype relative transcript levels. A small difference was observed in total *RIPOR2* transcript levels between subjects with an early onset of HL and controls (*p*=0.0241). This could suggest a trend between low expression levels and an early onset of HL, however, considering the overall variability in transcript levels it is more likely that other factors play a role. A larger sample size would be required to confirm or negate the observed trend.

The in-frame deletion in *Ripor2* prevents correct localization of the protein in mouse cochlear hair cells

Previous studies have shown that RIPOR2 is specifically localized to the base of the stereocilia in mouse cochlear hair cells.¹⁹ RIPOR2 is highly conserved between mouse and human (87% amino acid identity). To study whether the localization of mouse RIPOR2 with a deletion of the orthologous four amino acid residues (p.584_587del) is altered, plasmids encoding wildtype- or mutant-RIPOR2 were injectoporated into cochlear outer hair cells of wildtype mice (P2). Interestingly, mutant-RIPOR2 was detected in the stereocilia but in none of the 12 evaluated cells it was retained at the stereocilia base where the wildtype protein was found to be localized in all 11 evaluated cells (**Figure 5A**). Morphology of the stereocilia was not significantly affected two days after injectoporation of the mutant *Ripor2* construct, suggesting the mutant protein did not visibly affect the stereocilia structure in the short term.

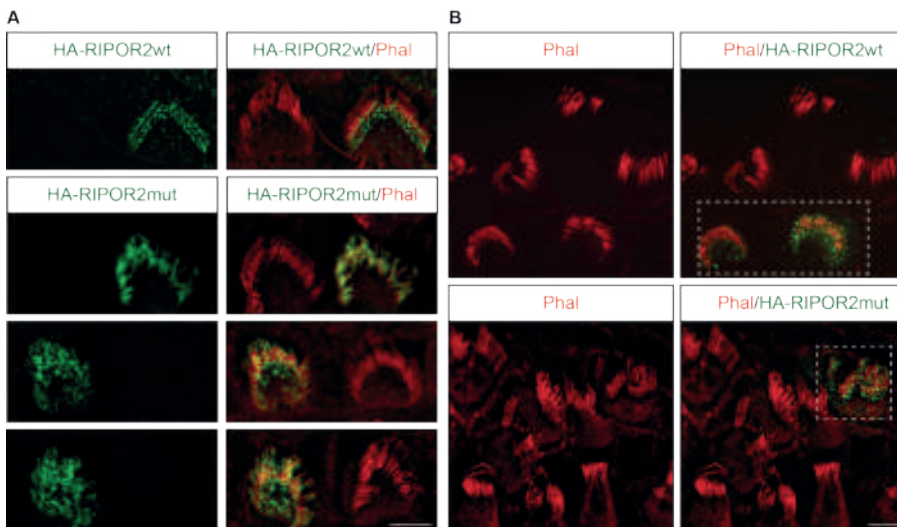


Figure 5. Functionality of mutant RIPOR2 is altered in mouse cochlear outer hair cells (A) Mutant RIPOR2 differed in localization from wildtype RIPOR2 in mouse cochlear outer hair cells. Outer hair cells of wildtype mice were injectoporated at P2 to express murine N-terminally HA-tagged wildtype RIPOR2 (RIPOR2wt) or mutant RIPOR2 (RIPOR2mut). Expression was evaluated after two days by immunohistochemistry and three representative images of cells expressing the mutant RIPOR2 are provided. Eleven cells expressing the wildtype construct and 12 cells expressing the mutant construct were evaluated. **(B)** Mutant RIPOR2 did not rescue stereocilia defects in RIPOR2-deficient hair cells. Cochlear explants of RIPOR2-deficient mice were prepared at P2 and injectoporated with constructs RIPOR2wt or RIPOR2mut. After culturing for two days, five out of six cells expressing the wildtype RIPOR2 construct demonstrated rescued hair bundle morphology but none of the 13 cells expressing the mutant RIPOR2 construct. Cells expressing the constructs are boxed. HA-tagged protein was stained in green, stereocilia were stained using phalloidin (phal) conjugated with Alex Fluor 568 (red). Scale bar represents 5 μm .

Potentially, the variant affects interactions of RIPOR2 that are essential for its localization. The four deleted amino acids are predicted to be part of a disorganized coiled coil structure (predicted using KMAD²⁵). Coiled coil regions are indicated to mediate protein-protein interactions, which supports the hypothesis that the variant affects RIPOR2 protein interactions.²⁶ Co-immunoprecipitation (Co-IP) assays demonstrated that both the dimerization ability (**Figure S8A**) and the interaction with RHOC (**Figure S8B**) of mutant RIPOR2 are intact.

Mutant RIPOR2 cannot rescue morphological defects in outer hair cells from *Ripor2* knockout mice

In *Ripor2* knockout mice, morphological defects were previously observed in hair cells, which included hair bundle polarity and cohesion and length of stereocilia.¹⁹ After injectoporation of the *Ripor2* mutant construct into outer hair cells of these mice, these defects could not be rescued in any of the 13 cells expressing mutant-RIPOR2. The typical V-shaped hair bundle was not formed, in contrast to the rescue effect observed in five out of six cells expressing wildtype-RIPOR2 (**Figure 5B**). This, together with the aberrant localization of mutant-RIPOR2, confirms an effect of the 4-amino acid deletion on RIPOR2 function in outer hair cells.

DISCUSSION

This study identified an in-frame 12 nucleotide deletion in *RIPOR2* as a prevalent and highly penetrant genetic factor for adult-onset HL in the Netherlands and beyond. HL associated with the deletion is highly variable in age of onset and audiometric characteristics. Our study exemplifies that an increasing contribution of environmental factors and of low-penetrance genetic factors to the hearing ability during life, complicates the identification of highly penetrant genetic factors in adult-onset HL. This is best illustrated by family W97-056 in which the linkage interval was falsely delimited by a phenocopy.

The *RIPOR2* variant was significantly enriched in an in-house dataset, previously coined “SE-NL” (Southeast Netherlands) with exomes of 22,952 unrelated individuals with unknown hearing abilities.²⁷ Eighteen individuals were heterozygotes for the variant (AF 0.0392%), as compared to 8 of 56,352 individuals (AF 0.0071%) and 5 of 32,287 individuals (AF 0.0077%) of non-Finnish European descent in the gnomAD exome database v2.1.1 and gnomAD genome database v3, respectively. As the variant was indicated to be inherited from a common ancestor, this individual might well be of Dutch origin or of neighboring regions.

Several lines of evidence indicate the association of the c.1696_1707del *RIPOR2* variant with HL. Firstly, the deletion affects four highly conserved amino acids of RIPOR2, which is

known to have a crucial role in murine and zebrafish hair cell development, function, and maintenance.^{11,19,28} *Ripor2* knockout mice are already found to be deaf at four weeks of age due to impaired mechanotransduction.¹⁹ Also, knockdown of *ripor2* in zebrafish induced loss of hair cells, and consequently profound hearing loss.¹¹ Secondly, aberrant localization of the mutant RIPOR2 in early postnatal mouse hair cells, *ex vivo*, and failure to rescue the stereocilia defects of *Ripor2* knockout mice indicate a functional effect of the variant. Thirdly, neither other rare potentially causative variants in protein coding regions and splice sites of the shared haplotype region, nor structural variants affecting this region were revealed in exome or genome sequencing.

RIPOR2 is localized at the taper region of the mechanically sensitive stereocilia of murine hair cells^{11,19,28} where it is organized in a ring-like fashion.¹⁹ The latter is thought to be achieved by homo-oligomerization in a head-to-head and tail-to-tail manner, regulated by RHOC.¹⁹ The oligomerization is essential for the structure of the taper region and for the morphology of the hair bundle as a whole, but the precise molecular mechanism is still elusive. The taper region is the specialized basal part of stereocilia that allows their deflection upon mechanical stimulation.²⁹ CLIC5, PTPRQ, MYO6, TPRN, RDX, GRXCR2, and RIPOR2 are described to concentrate and co-function in the taper region and to be crucial for its structure and/or for hair bundle development and maintenance in mice.^{19,30-35} Direct interactions of these proteins are indicated, e.g., of CLIC5, RDX and TPRN, but not RIPOR2.^{19,32} Also, interdependence for their concentration in the taper region was observed.^{19,31,32} In RIPOR2-deficient hair cells, for example, TPRN is no longer concentrated at the stereociliary base.^{19,30} Depletion of TPRN in *Tprn* knock-out mice leads to functional as well as (slowly) progressive morphological abnormalities of the stereocilia bundle.³⁰

Based on the above described molecular structure of the stereociliary taper, we hypothesize that p.(Gln566_Lys569)del RIPOR2 affects this taper region and thereby the durability of the hair bundle, potentially via an effect on TPRN. Additionally or alternatively, the *RIPOR2* variant might affect the amount of the RIPOR2-interaction partner MYH9 in stereocilia, as well as the abundance of phosphorylated MYH9 and acetylated α -tubulin in the kinocilia, as these proteins are reduced in RIPOR2-deficient mice.²⁸ Interestingly, *MYH9* defects in humans are also associated with progressive HL.³⁶

In light of developing therapeutic strategies, it is essential to determine whether the *RIPOR2* variant has a loss-of-function, a dominant negative or toxic gain-of-function effect. A haploinsufficiency effect of the variant seems to be the least plausible, as a loss-of-function *RIPOR2* variant in the heterozygous state was not indicated to be associated with HL.¹¹ Also, heterozygous *Ripor2* knockout mice displayed no significant hearing loss at four weeks¹⁹ and two months of age (Zhao, unpublished data). A dominant-negative effect of the p.(Gln566_Lys569del) variant cannot be excluded as an interaction between the mutant-

and wildtype-RIPOR2 was detected in Co-IP assays. However, a strong dominant negative effect would be expected to result in early-onset HL, comparable to that associated with the homozygous loss-of-function variant.¹¹ Therefore, we hypothesize that the variant has a toxic gain-of-function effect.

RIPOR2 is expressed in a wide-range of tissues and cell types.¹⁹ It is a known inhibitor of the small G-protein RHOA in neutrophils and T lymphocytes, where it regulates migration of these cells.³⁷ Additionally, *RIPOR2* is upregulated during muscle cell differentiation and induces the formation of filopodia.³⁸ We did not observe an effect of the four amino acid-deletion on filopodia formation (de Bruijn, unpublished data) which is in line with the fact that the deleted residues are not part of the RHOA-interaction domain.³⁸ This might, at least in part, explain that the *RIPOR2* variant leads to HL only. The variant could affect a cochlear-specific protein interaction that determines RIPOR2 localization in the hair bundle. Furthermore, in tissues other than the inner ear loss of RIPOR2 function might be compensated by RIPOR1 and RIPOR3 which are described to have redundant functions.^{39,40} Indeed, RNA levels of both *RIPOR1* and *RIPOR3* are low in hair cells (gEAR).⁴¹

The audiometric phenotype and age of onset of HL associated with c.1696_1707del *RIPOR2* displayed variation. Such intrafamilial phenotypic variation has also been reported for defects in several of the genes that can be associated with adult-onset adNSHL, e.g. *EYA4*, *MYO6* and *POU4F3*, and remains unexplained.⁴²⁻⁴⁴ Non-penetrance is an extreme of phenotypic variability. In our study, five subjects with the c.1696_1707del *RIPOR2* variant had normal hearing: V:2, IV:26, III:28, (W97-056), III:14 (W04-262), and III:4 (W15-1495). They are aged 23, 40, 51, 49, and 50 years, respectively, at the latest audiometric evaluation. The average reported age of onset in the studied families is 30 years (SD 14.9) and 70 years the highest reported onset age. Therefore, the unaffected subjects might develop HL in the future. However, incomplete penetrance of the variant cannot be excluded.

With a k-means cluster analysis, four distinct audiometric clusters could be distinguished. It is possible that subjects, due to increasing age, may go from one cluster to another cluster, which is not captured by the k-means clustering algorithm, since no longitudinal data are used. As no clear patterns of age of onset or audiometric configurations were observed within families or family branches with the *RIPOR2* variant, the phenotypic variability might well result from an interplay between environmental and genetic modifying factors. We have addressed differences in transcript levels of both wildtype and mutant *RIPOR2* alleles as potential modifiers of age of onset but no clear correlations were observed. As the analysis was performed on RNA extracted from peripheral blood, we cannot exclude that *RIPOR2* mRNA levels determined by cochlear-specific *cis* or *trans* regulatory elements modify the onset of HL. Other candidate genetic modifiers are variants in the genes that encode

proteins of the indicated complex of the stereocilia taper. As the taper region is thought to be essential for anchoring the mechanosensory stereocilia, noise exposure is an obvious candidate environmental modifying factor. Fourteen subjects with the *RIPOR2* variant reported noise exposure. However, we could not correlate onset or strong progression of HL with a preceding significant noise exposure.

Four subjects with HL who did not have the *RIPOR2* variant, are considered to be phenocopies. In the light of the heterogeneity in the etiology of HL, the occurrence of phenocopies is not unexpected. For individuals III:14 and III:20 (W97-056) a possible explanation for their HL is a Ménière-like disease and heavy smoking (COPD Gold III), respectively.^{45,46} Subject III:10 (W04-262) might have inherited a cause of HL associated with vestibular problems from her mother, who married into the family. HL in subject III:21 of family W97-056 remains unexplained.

The c.1696_1707del *RIPOR2* variant was only reported in non-Finnish Europeans, with the exception of a single individual of African origin (gnomAD v3 genomes). Assuming that the AF of 0.0392% determined in the SE-NL cohort is comparable throughout the Netherlands, the c.1696_1707del *RIPOR2* variant is estimated to be present in more than 13,000 individuals who are therefore at risk to develop HL or have developed HL already due to this variant. About 30,000 additional individuals can be calculated to be at risk, based on the AF of 0.0096% of the variant in Northwest Europe (gnomAD v2.1.1) with ~156 million inhabitants (United Nations Population Division estimates, 2019). This large number of individuals at risk to develop HL due to the c.1696_1707del *RIPOR2* variant illustrates the need to gain broader estimates of the penetrance of the variant which was ~90% at the age of 50 years in the studied families. However, this calculated penetrance cannot be excluded to be biased because these families were included based on index cases with HL. Further insight in the age-related penetrance of c.1696_1707del *RIPOR2* will pave the way for the identification of modifying factors which may convey handles for prevention.

In conclusion, we demonstrate that an adult-onset type of HL (DFNA21) is relatively common and associated with a “mild” variant in *RIPOR2*. Potentially, thousands of individuals in the Netherlands and beyond are at risk to develop HL. More such variants might well wait to be “unmasked” as (population-specific) frequent and highly penetrant causes of adult-onset HL. Because of the large number of subjects estimated to be at risk for HL due to the c.1696_1707del *RIPOR2* variant, it is an attractive target for the development of a genetic therapy. The great progress that is being made for this in hearing disorders is promising.⁴⁷

ACKNOWLEDGEMENTS

The authors thank José van den Broek, Herman Kok, Lisanne Schenk, Daniëlle Manders, Karin Krommenhoek and Jacquélien Jilissen for their contributions to clinical evaluations and Saskia van der Velde-Visser for her contributions in EBV transformations and cell culture. We would like to thank Sita Vermeulen, Galuh Astuti and Hanka Venselaar for their contribution to statistical and bioinformatic analyses. This study was financially supported by a DCMN Radboudumc grant, by a grant of the Heinsius-Houbolt foundation and an NIH/NIDCD (R01 DC017147) grant.

COLLABORATORS

The DOOFNL consortium is a Dutch nationwide collaboration on hereditary hearing loss and consists of M.F. van Dooren, H.H.W. de Gier, E.H. Hoefsloot, M.P. van der Schroeff (ErasmusMC, Rotterdam, the Netherlands), S.G. Kant, L.J.C. Rotteveel, F.G. Ropers (LUMC, Leiden, the Netherlands), J.C.C. Widdershoven, J.R. Hof, E.K. Vanhoutte (MUMC+, Maastricht, the Netherlands), R.J.C. Admiraal, I. Feenstra, H. Kremer, C.P. Lanting, R.J.E. Pennings, H.G. Yntema (Radboudumc, Nijmegen, the Netherlands), R.H. Free and J.S. Klein Wassink-Ruiter (UMCG, Groningen, the Netherlands), R.J. Stokroos, A.L. Smit, M.J. van den Boogaard (UMC, Utrecht, the Netherlands) and F.A. Ebbens, S.M. Maas, A. Plomp, T.P.M. Goderie, P. Merkus and J. van de Kamp (Amsterdam UMC, Amsterdam, the Netherlands).

REFERENCES

1. World Health Organisation. The global burden of disease: 2004 update. (Geneva: World Health Organization, 2008).
2. Sloan-Heggen, C.M. *et al.* Comprehensive genetic testing in the clinical evaluation of 1119 patients with hearing loss. *Human Genetics* 135, 441-450 (2016).
3. Zazo Seco, C. *et al.* The diagnostic yield of whole-exome sequencing targeting a gene panel for hearing impairment in The Netherlands. *European Journal of Human Genetics* 25, 308-314 (2017).
4. Van Camp, G. & Smith, R. Hereditary Hearing Loss Homepage. Available from: <https://hereditaryhearingloss.org>.
5. Gates, G.A., Couropmitree, N.N. & Myers, R.H. Genetic associations in age-related hearing thresholds. *Archives of Otolaryngology-Head & Neck Surgery* 125, 654-659 (1999).
6. Karlsson, K.K., Harris, J.R. & Svartengren, M. Description and primary results from an audiometric study of male twins. *Ear and Hearing* 18, 114-120 (1997).
7. Wolber, L.E., Steves, C.J., Spector, T.D. & Williams, F.M.K. Hearing ability with age in northern European women: a new web-based approach to genetic studies. *PLoS One* 7, e35500 (2012).
8. Lewis, M.A. *et al.* Whole exome sequencing in adult-onset hearing loss reveals a high load of predicted pathogenic variants in known deafness-associated genes and identifies new candidate genes. *BMC Medical Genomics* 11, 77 (2018).
9. Kunst, H. *et al.* Non-syndromic autosomal dominant progressive non-specific mid-frequency sensorineural hearing impairment with childhood to late adolescence onset (DFNA21). *Clinical Otolaryngology & Allied Sciences* 25, 45-54 (2000).
10. De Brouwer, A.P.M. *et al.* Fine mapping of autosomal dominant nonsyndromic hearing impairment DFNA21 to chromosome 6p24.1-22.3. *American Journal of Medical Genetics Part A* 137A, 41-46 (2005).
11. Diaz-Horta, O. *et al.* FAM65B is a membrane-associated protein of hair cell stereocilia required for hearing. *Proceedings of the National Academy of Sciences of the United States of America* 111, 9864-9868 (2014).
12. Kircher, M. *et al.* A general framework for estimating the relative pathogenicity of human genetic variants. *Nature genetics* 46, 310-315 (2014).
13. Vaser, R., Adusumalli, S., Leng, S.N., Sikic, M. & Ng, P.C. SIFT missense predictions for genomes. *Nature Protocols* 11, 1 (2015).
14. Adzhubei, I.A. *et al.* A method and server for predicting damaging missense mutations. *Nature Methods* 7, 248-249 (2010).
15. Schwarz, J.M., Cooper, D.N., Schuelke, M. & Seelow, D. MutationTaster2: mutation prediction for the deep-sequencing age. *Nature Methods* 11, 361 (2014).
16. M. Mazzoli, G.V.C., V. Newton, N. Giarbini, F. Declau, A. Parving. Recommendations for the description of genetic and audiological data for families with nonsyndromic hereditary hearing impairment. *GeneReviews* (2003).
17. Smits, J.J. *et al.* De novo and inherited loss-of-function variants of ATP2B2 are associated with rapidly progressive hearing impairment. *Human Genetics* 138, 61-72 (2019).

18. Huygen, P., Pennings, R. & Cremers, C. Characterizing and distinguishing progressive phenotypes in nonsyndromic autosomal dominant hearing impairment. *Audiological Medicine*, 37-46 (2003).
19. Zhao, B., Wu, Z. & Müller, U. Murine Fam65b forms ring-like structures at the base of stereocilia critical for mechanosensory hair cell function. *eLife* 5, e14222 (2016).
20. de Bruijn, S.E. *et al.* Homozygous variants in KIAA1549, encoding a ciliary protein, are associated with autosomal recessive retinitis pigmentosa. *Journal of Medical Genetics* 55, 705-712 (2018).
21. Schrauwen, I. *et al.* A comprehensive catalogue of the coding and non-coding transcripts of the human inner ear. *Hearing Research* 333, 266-274 (2016).
22. Scheffer, D.I., Shen, J., Corey, D.P. & Chen, Z.-Y. Gene expression by mouse inner ear hair cells during development. *Journal of Neuroscience* 35, 6366-6380 (2015).
23. Capoano, C.A., Wettstein, R., Kun, A. & Geisinger, A. Spats 1 (Srsp1) is differentially expressed during testis development of the rat. *Gene Expression Patterns* 10, 1-8 (2010).
24. Landrum, M.J. *et al.* ClinVar: public archive of relationships among sequence variation and human phenotype. *Nucleic Acids Research* 42, D980-D985 (2014).
25. Lange, J., Wyrwicz, L.S. & Vriend, G. KMAD: knowledge-based multiple sequence alignment for intrinsically disordered proteins. *Bioinformatics* 32, 932-936 (2016).
26. Rose, A. & Meier, I. Scaffolds, levers, rods and springs: diverse cellular functions of long coiled-coil proteins. *Cellular and Molecular Life Sciences CMLS* 61, 1996-2009 (2004).
27. Cremers, F.P.M., Cornelis, S.S., Runhart, E.H. & Astuti, G.D.N. Author response: penetrance of the ABCA4 p.Asn1868Ile allele in Stargardt disease. *Investigative Ophthalmology & Visual Science* 59, 5566-5568 (2018).
28. Diaz-Horta, O. *et al.* Ripor2 is involved in auditory hair cell stereociliary bundle structure and orientation. *Journal of Molecular Medicine* 96, 1227-1238 (2018).
29. Barr-Gillespie, P.-G. Assembly of hair bundles, an amazing problem for cell biology. *Molecular Biology of the Cell* 26, 2727-2732 (2015).
30. Men, Y. *et al.* Tprn is essential for the integrity of stereociliary rootlet in cochlear hair cells in mice. *Frontiers of Medicine* 13, 690-704 (2018).
31. Liu, C., Luo, N., Tung, C.-Y., Perrin, B.J. & Zhao, B. GRXCR2 regulates taperin localization critical for stereocilia morphology and hearing. *Cell Reports* 25, 1268-1280 (2018).
32. Salles, F.T. *et al.* CLIC5 stabilizes membrane-actin filament linkages at the base of hair cell stereocilia in a molecular complex with radixin, taperin, and myosin VI. *Cytoskeleton (Hoboken)* 71, 61-78 (2014).
33. Sakaguchi, H. *et al.* Dynamic compartmentalization of protein tyrosine phosphatase receptor Q at the proximal end of stereocilia: implication of myosin VI-based transport. *Cell Motil Cytoskeleton* 65, 528-38 (2008).
34. Pataky, F., Pironkova, R. & Hudspeth, A.J. Radixin is a constituent of stereocilia in hair cells. *Proceedings of the National Academy of Sciences* 101, 2601-2606 (2004).
35. Gagnon, L.H. *et al.* The chloride intracellular channel protein CLIC5 is expressed at high levels in hair cell stereocilia and is essential for normal inner ear function. *Journal of Neuroscience* 26, 10188-98 (2006).
36. Lalwani, A.K. *et al.* Human nonsyndromic hereditary deafness DFNA17 is due to a mutation in nonmuscle myosin MYH9. *American Journal of Human Genetics* 67, 1121-1128 (2000).

37. Gao, K. *et al.* Front-signal-dependent accumulation of the RHOA inhibitor FAM65B at leading edges polarizes neutrophils. *Journal of Cell Science* 128, 992-1000 (2015).
38. Yoon, S., Molloy, M.J., Wu, M.P., Cowan, D.B. & Gussoni, E. C6ORF32 is upregulated during muscle cell differentiation and induces the formation of cellular filopodia. *Developmental Biology* 301, 70-81 (2007).
39. Mardakheh, F.K., Self, A. & Marshall, C.J. RHO binding to FAM65A regulates Golgi reorientation during cell migration. *Journal of Cell Science* 129, 4466-4479 (2016).
40. Hermjakob, H. *et al.* IntAct: an open source molecular interaction database. *Nucleic Acids Research* 32, D452-D455 (2004).
41. Cremers, F.P.M. *et al.* Comprehensive registration of DNA sequence variants associated with inherited retinal diseases in Leiden Open Variation Databases. *Human Mutation* 35, 147-148 (2014).
42. Oonk, A.M.M. *et al.* Progressive hereditary hearing impairment caused by a MYO6 mutation resembles presbycusis. *Hearing Research* 299, 88-98 (2013).
43. Vahava, O. *et al.* Mutation in transcription factor POU4F3 associated with inherited progressive hearing loss in humans. *Science* 279, 1950-1954 (1998).
44. O'Neill, M.E. *et al.* A gene for autosomal dominant late-onset progressive non-syndromic hearing loss, DFNA10, maps to chromosome 6. *Human Molecular Genetics* 5, 853-6 (1996).
45. Bayat, A. *et al.* Is COPD associated with alterations in hearing? A systematic review and meta-analysis. *International Journal of Chronic Obstructive Pulmonary Disease* 14, 149-162 (2018).
46. Hu, H. *et al.* Smoking, smoking cessation, and the risk of hearing loss: Japan epidemiology collaboration on occupational health study. *Nicotine & Tobacco Research* 21, 481-488 (2018).
47. Omichi, R., Shibata, S.B., Morton, C.C. & Smith, R.J.H. Gene therapy for hearing loss. *Human Molecular Genetics* 28, R65-R79 (2019).

SUPPLEMENTARY MATERIALS AND METHODS

DNA sequencing and variant identification

Genomic DNA was isolated from peripheral blood lymphocytes following standard procedures. Subsequently, exome enrichment was performed using the Agilent SureSelect Human All Exome V5 kit according to the manufacturer's protocols. Exome sequencing was performed on an Illumina HiSeq system by BGI Europe (Copenhagen, Denmark). Read mapping along the hg19 reference genome (GRCh37/hg19) and variant calling were performed using BWA V.0.78¹ and GATK HaplotypeCaller V.3.3². A coverage of >20 reads was reached for 85.1% to 97.8% of the enriched regions. For variant annotation an in-house developed annotation and variant evaluation pipeline was used. For sequencing data of family W97-056, copy number variant (CNV) detection was performed using CoNIFER V.0.2.2.³ Genome sequencing was performed by BGI (Hong Kong, China) on a BGISeq500 using a 2x 100 bp paired end module, with a minimal median coverage of 30-fold per genome. Structural variants were called using Manta V.1.1.0⁴ and CNVs using Control-FREEC.⁵ Variants were validated and visualized using the IGV Software (V.2.4).⁶

In the index case of family W08-1421, targeted DNA sequencing was performed using MIP sequencing.⁷ MIPs were designed covering exons and exon-intron boundaries of a panel of 89 HL genes (**Table S6**). Sequencing and data analysis were performed as previously described.⁸ For each targeted region, an average coverage of 420 reads was obtained. A coverage of >20 reads was reached for 85.4% of the MIPs. Only those called variants were considered that had a quality-by-depth >200 and that were present in less than 10% of the samples that were analyzed in the same sequence run (n=150).

VNTR marker analysis

Genotyping of Variable Number of Tandem Repeats (VNTR) markers was performed by genomic DNA amplification using touchdown PCR and analysis on an ABI Prism 3730 Genetic Analyzer (Applied Biosystems). Genomic positions of markers were determined using the UCSC genome browser (human genome assembly GRCh37/hg19). Alleles were assigned with the GeneMarker software (V.2.6.7, SoftGenetics) according to the manufacturer's protocol.

Audiometric cluster analysis

A k-means clustering algorithm was applied on the last audiogram of affected subjects with the *RIPOR2* variant.⁹ Each audiogram was first normalized by subtracting the average hearing threshold across all frequencies from the data, preventing the algorithm to select clusters based on average hearing threshold, while retaining the overall shape of the audiogram.

Next, the optimal number of clusters in the data was obtained by using the Elbow method;¹⁰ for a number of $k=1$ to $k=15$ clusters. The distortion, i.e. the sum of squared distances from each point to its assigned center, was determined for each value of k . The smallest number of k clusters with the lowest distortion (i.e. the elbow) was then taken as the optimal number of clusters. Finally, the audiograms of all the patients within each cluster were visualized and an average cluster prototype was obtained by averaging all audiograms within a cluster.

Vestibular testing

Vestibular function was assessed by electronystagmography, caloric irrigation testing, rotary chair stimulation and video head impulse tests, as described previously.¹¹ Cervical and ocular vestibular-evoked myogenic potentials (cVEMP/oVEMP) were measured to assess saccular and utricular function, respectively.^{12,13} When responses were seen at or below 100 dB Hearing Level during (air conducted) cVEMP testing, saccular function was considered to be present, otherwise absent.¹² For (bone conducted) oVEMP stimulation, this normal value is ≤ 140 dB Force Level.¹³

Allele-specific expression analysis

Peripheral blood (2.5 ml) was collected in PAXgene Blood RNA tubes (BD Biosciences). RNA was isolated using the PAXgene blood RNA kit (Qiagen) following the manufacturer's protocol. Subsequently, cDNA was prepared using the iScript cDNA synthesis kit (Bio-Rad) with 500 ng RNA. Allele-specific primer sets were designed and validated; the design was based on a forward primer that specifically hybridizes to either the mutant or wildtype *RIPOR2* alleles. Additionally, primers were designed for exons 3-4 of *RIPOR2*, as well as for exons 2-3 of the reference gene *GUSB* (NM_000181). Primer sequences are provided in **Table S7**. All qPCR reaction mixtures were prepared with the GoTaq qPCR Master Mix (Promega) according to the manufacturer's protocol. Amplifications were performed with the Applied Biosystem Fast 7900 System (Applied Biosystems). For all RNA samples, cDNA was synthesized twice, and all qPCR reactions were performed in duplicate. Relative gene expression levels, as compared to the internal reference gene *GUSB*, were determined with the ΔC_t method.¹⁴ Statistical analyses were performed using a one-way ANOVA followed by Tukey's multiple comparison test to test for significance between the groups.

Injectoporation of *Ripor2*-constructs, immunostaining and antibodies

For injectoporation, the organ of Corti was isolated and placed in DMEM/F12 medium with 1.5 $\mu\text{g}/\text{ml}$ ampicillin. Glass electrodes (~ 2 μm diameter) were used to deliver the plasmid (500 ng/ μl in Hank's Balanced Salt Solution (HBSS)) to the sensory epithelium. A series of 3 pulses were applied at 1 sec intervals with a magnitude of 60V and duration of 15 msec

(ECM 830 square wave electroporator; BTX). Two days after injectoporation, samples were fixed in the fixative containing 4% paraformaldehyde in HBSS for 20 min. Tissues were then washed in HBSS and blocked for 20 min at room temperature in HBSS containing 5% BSA, 1% goat serum and 0.5% Triton X-100, and then incubated overnight at 4°C with primary antibodies in HBSS containing 1% BSA and 0.1% Triton X-100. Tissues were washed in HBSS and incubated 2 hours at room temperature with secondary antibodies. Tissues were mounted in ProLong® Antifade Reagents (ThermoFisher). Stacked images were then captured by fluorescence deconvolution microscope (Leica). Antibodies used were: anti-HA (mouse; 1:500; cat.#2367S; Cell Signaling), Alex Fluor 568-phalloidin (1:500; cat.#A12380; ThermoFisher) and Alexa Fluor 488 goat anti-mouse (1:1000; cat.#A11017; ThermoFisher). Antibodies used for co-immunoprecipitations were: anti-HA (mouse; 1:500; cat.#2367S; Cell Signaling), anti-Myc (rabbit; 1:500; cat.#2278S; Cell Signaling), anti-Myc (mouse; 1:500; cat.#9E10; Santa Cruz); anti-GFP (mouse; 1:1000; cat.#SC-9996; Santa Cruz).

SUPPLEMENTARY RESULTS

The *RIPOR2* c.1696_1707del variant is derived from a common ancestor

VNTR marker analysis was performed to determine whether a haplotype of the chromosomal region flanking the variant was shared by the different families. Indeed, a shared haplotype of ~1.0 Mb, delimited by markers D6S2439 and D6S1281, was found in the seven families for which segregation analysis of the marker alleles could be performed (**Figure S3**). This haplotype was also potentially shared by the five single cases. For marker D6S1545, a different CA-repeat length was determined on the variant-carrying allele of family W18-0470 whereas the alleles of two more centromeric markers were still shared. Since a rare event that caused a repeat length change of the D6S1545 allele may have occurred, this marker locus was still considered to be part of the shared haplotype. To further refine the shared haplotype, we extracted homozygous SNPs present in the region between D6S2439 and D6S1281 from the exome sequencing datasets. Subsequently, homozygous SNP genotypes were compared between all index cases and discordant alleles were seen for SNP rs6901322 (Chr6: 24,583,804) that is located between D6S2439 and D6S1554. This SNP was found in homozygous state in subject IV:20 (W97-056), but was absent in the index cases of families W02-016 (III:9) and W18-0473. Based on these results, the shared haplotype is delimited by SNP rs6901322 at the telomeric side and comprises a region of 0.713 Mb. Genome sequencing in two members of family W97-056 (IV:25 and III:22) excluded potentially causative CNVs or other structural variants that are present within the shared chromosomal region.

The c.1696_1707del *RIPOR2* variant is not associated with vestibular dysfunction

Four of 64 subjects with the *RIPOR2* variant had vestibular complaints. Subjects III:1, III:9, IV:1 (W02-016) and the index cases of family W18-0472 reported infrequent vertigo attacks, complaints after cochlear implant surgery, a diagnosis of benign paroxysmal positional vertigo and migrainous vertigo, respectively (**Table S3**). Vestibular testing was randomly performed in 9 subjects with the *RIPOR2* variant, aged 29 to 71 years, and included the abovementioned subjects III:1 and III:9 of family W02-016. No abnormalities were found, except for a mild hyporeflexia in subject III:1 of family W02-016 (**Table S4**), which is appropriate for the subject's age of 71 years. Based on these results, we conclude that c.1696_1707del *RIPOR2* is not associated with vestibular dysfunction. This is in line with the lack of vestibular dysfunction in *Ripor2*^{-/-} mice despite expression of the gene in the vestibular organ of wildtype mice.¹⁵ Also, humans with recessively inherited HL caused by a homozygous loss-of-function defect in *RIPOR2*, did not report balance problems, vertigo or dizziness but absence of a vestibular phenotype was not confirmed by objective vestibular testing.¹⁶

SUPPLEMENTARY TABLES

Table S1. Shared rare WES variants in family W97-056

Genome	Gene	Transcript	cDNA	Protein	In-house AF (%)	gnomAD_E AF (%)	gnomAD_G AF (%)	CADD_PPHRED	SIFT	PPH2	MutationTaster (prob)
Chr1: 248,059,798T>A	<i>OR2W3</i>	NM_001001957.2	c.910T>A	p.(Leu304Met)	0.07	0.02	0.03	6.504	0.1	0.032	Polymorphism (1.0)
Chr6: 15,501,310C>T	<i>JARID2</i>	NM_004973.3	c.2118C>T	p.(Leu706=)	0.18	0.03	0.04	NA	NA	NA	NA
Chr6: 16,146,884C>T	<i>MYLIP</i>	NM_013262.3	c.1249-9C>T	-	0.01	-	-	NA	NA	NA	NA
Chr6: 24,843,303_24,843,314del	<i>RIPOR2</i>	NM_014722.3	c.1696_1707del	p.(Gln566_Lys569del)	0.08	0.00	-	NA	NA	NA	NA
Chr6: 41,196,733C>T	<i>TREML4</i>	NM_198153.2	c.345C>T	p.(Ser115=)	0.47	0.31	0.30	NA	NA	NA	NA
Chr6: 44,329,574G>A	<i>SPATS1</i>	NM_145026.3	c.419G>A	p.(Gly140Glu)	0.18	0.11	0.12	19.16	0.02	1.0	Disease causing (0.98)

Variants identified by whole exome sequencing (WES) that are shared by all three index cases of family W97-057 and have an allele frequency of $\leq 0.5\%$ in gnomAD and the in-house database (~7,500 exomes). For none of the variants is an effect on transcript splicing predicted nor are any reported in the ClinVar database. Scores that meet the thresholds for pathogenicity as described in the methods section are indicated in red. Thresholds for pathogenicity: CADD-PPHRED (≥ 15), SIFT (≤ 0.05), PolyPhen-2 (≥ 0.450) and MutationTaster (disease causing). Genome, Genomic positions according to GRCh37/hg19; In-house AF, allele frequency (%) in the in-house database (~15,000 alleles); GnomAD_E AF and GnomAD_G AF, allele frequencies (%) in respectively gnomAD exome or genome databases; CADD_PPHRED, Combined Annotation Dependent Depletion PHRED score; SIFT, Scale-Invariant Feature Transform; PPH2, Poly-Phen-2 score; MutationTaster (prob), MutationTaster score with probability (0-1); -, frequency not available; NA, not applicable.

Table S2. Rare variants in the index cases in genes known to be associated with adHL

Family	Genome	Gene	Transcript	cDNA	Protein	In-house AF (%)	gnomAD_E AF (%)	gnomAD_G AF (%)	CADD_PHRD	SIFT	PPH2	MutationTaster (prob)	ClinVar
W18-0470	Chr22: 36681327T>C	<i>MYH9</i>	NM_002473.4	c.5323A>G	p.(Lys1775Glu)	0.18	0.15	0.19	22.2	0.03	0.120	Disease causing (1.0)	UV2
W18-0473	Chr4: 6303119C>T	<i>WFS1</i>	NM_006005.3	c.1597C>T	p.(Pro533Ser)	0.22	0.07	0.08	19.64	0.00	1.000	Disease causing (1.0)	UV1-UV3
	Chr22: 36700183G>A	<i>MYH9</i>	NM_002473.4	c.2248G>A	p.(Asp750Asn)	0.01	0.00	-	20.80	0.00	0.997	Disease causing (1.0)	NA
W18-1160	Chr11: 76873225A>G	<i>MYO7A</i>	NM_000260.3	c.1403A>G	p.(His468Arg)	0.10	0.01	0.02	19.61	0.01	0.993	Disease causing (1.0)	UV3

For none of the variants is an effect on transcript splicing predicted. Scores that meet the thresholds for pathogenicity as described in the methods section are indicated in red. Thresholds for pathogenicity: CADD-PHRD (≥ 15), SIFT (≤ 0.05), PolyPhen-2 (≥ 0.450) and MutationTaster (deleterious). Genome, Genomic positions according to GRCh37/hg19; In-house AF, allele frequency (%) in in-house database (~7,500 exomes); GnomAD_E AF and GnomAD_G AF, allele frequencies (%) in respectively gnomAD exome or genome databases; CADD_PHRD, Combined Annotation Dependent Depletion PHRED score; SIFT, Scale-Invariant Feature Transform; PPH2, Poly-Phen-2 score; MutationTaster (prob), MutationTaster score with probability (0-1); ClinVar, American College of Medical Genetics and Genomics (ACMG) classification of variants as in ClinVar; UV1, benign; UV2, likely benign; UV3, variant with unknown significance; NA, not available.

Table S3. Individual results of otoscopic examination, audiometry, imaging and progression of HL

Family	Subject	Age of onset (y)	Otoscopic examination	Clinical remarks	Imaging		Audiometry				Progression of HL		General remarks		
					CT	MRI	Subject age (y)	PTA	SRT	Maximum SRS (%)	Progression rate (dB/y)	YOF (y)			
						R	L	R	L	R	L				
W97-056	II:2	48	NT			81	72	63	70	72	87	65	0.6	53-82	
	II:4	43	NT	Ab, NE, T		72	93	90	NT	NT	NT	NT	NA	63-72	
	II:5	70	NT	NE		79	63	52	NT	NT	NT	NT	NA	0	Professional noise exposure
	III:10	21	NT	NE		41	47	48	61	70	95	95	0.5	21-56	
	III:11	26	NT	O, T		54	43	38	NT	NT	NT	NT	NA	0	
	III:12	20	NT	T		41	40	43	43	42	90	95	NA	32-40	
	III:15	37	N	NE, T		67	50	48	57	51	92	75	1.0	46-67	
	III:18	36	NT	T		62	50	51	50	NT	95	90	0.9	41-62	
	III:19	14	N	A		42	NA	73	NA	NA	NA	41	1.4	21-42	Rear profoundly deaf
	III:22	20	NT	T		62	75	80	70	70	75	88	0.8	42-62	
	III:24	33	N			43	62	60	63	67	93	93	1.8	36-48	
	III:26	34	N	O, T		45	50	52	NT	NT	NT	NT	NA	0	
	III:28	NOHL	NT			52	7	10	NT	NT	NT	NT	NA	47-51	
	III:30	NR	N	A		64	53	35	42	25	100	100	1.2	48-64	Otosclerosis, infrequent balance complaints
	IV:20	7	N	T		50	70	63	62	52	88	90	0.9	7-51	
	IV:22	NR	N	T		27	20	25	NT	NT	NT	NT	NA	0	
	IV:23	NR	NT			36	7	8	NT	NT	NT	NT	0.5	25-35	
	IV:25	24	NT			42	25	18	18	22	NT	NT	0.4	22-42	
	IV:26	NOHL	NT			41	7	7	NT	NT	NT	NT	NA	NA	

Table S3. (continued)

Family	Subject	Age of onset (y)	Otosopic examination	Clinical remarks	Imaging		Audiometry			SRT			Maximum SRS (%)			Progression of HL		General remarks
					CT	MRI	Subject age (y)	PTA	R	L	R	L	R	L	R	L	Progression rate (dB/y)	
IV:27		35	N				47	17	18	12	18	100	100	100	0.3	26-47		
IV:28		30	N	A, NE, T	N	N	45	32	52	37	55	100	92	1.8	25-46	Professional noise exposure		
IV:29		17	N	NE			26	5	10	NT	NT	NT	NT	NA	22-26			
IV:35		30	N	NE, T			37	15	15	10	10	100	100	NA	0	Recreational noise exposure		
IV:38		8	N	T			31	8	7	8	7	100	100	NA	NA			
V:1		5	N	NE, T			25	40	37	28	27	100	97	1.3	8-25			
V:2		NOHL	N				23	3	5	<10	<10	100	100	NA	NA			
W02-016																		
II:3		29	NT	T			82	68	68	65	70	100	93	0.9	82-92			
II:6		47	N				89	80	83	80	80	52	67	2	76-86			
II:9		40	N				73	NA	82	67	72	75	55	NA	69-73	R ear profoundly deaf above 2 kHz		
III:1		41	N	A, V			73	40	67	35	77	88	62	NA	66-73	Infrequent vertigo attacks since the age of 65 years		
III:5		NR	N				65	20	27	18	17	95	96	NA	0			
III:9		35	N	O, A, T, V	N	N	39	48	42	47	38	80	100	3	24-47	Balance complaints after CI surgery		
III:10		32	N	T			32	15	20	10	15	100	95	1.4	32-60			
IV:1		53	NT	V			42	12	10	NT	NT	NT	NT	NA	0	Benign paroxymal positional vertigo		
IV:3		17	N				47	27	25	25	17	100	100	1	34-47			

Table S3. (continued)

Family	Subject	Age of onset (y)	Otoscopic examination	Clinical remarks	Imaging		Audiometry				Progression of HL		General remarks
					CT	MRI	Subject age (y)	PTA	SRT	Maximum SRS (%)	Progression rate (dB/y)	YOF (y)	
					R	L	R	L	R	L			
	IV:8	27	N		38	37	32	30	100	95	2.7	17-30	
W04-262	II:11	<18	Rarectasis L sclerotic	A, T	70	85	87	>95	37	44	NA	0	Multiple ear surgeries, a.o. ear drum surgery
	III:4	49	N	T	67	40	47	28	35	100	NA	0	
	III:5	55	N	NE, T	63	32	23	NT	NT	NT	0.6	49-63	
	III:8	49	N	A	59	43	32	37	22	100	1.4	46-59	
	III:11	32	N	A, T	60	62	55	60	70	95	2	47-60	
	III:14	NOHL	N	Ab	49	7	7	NT	NT	NT	NA	NA	
	III:16	25	N	A, T	47	70	65	80	77	55	60	0.9	29-47
	III:19	28	N	A	49	83	92	NA	NA	42	42	2.1	33-49
	IV:3	NR	N		21	12	7	NT	NT	NT	NA	0	
W15-0495	II:2	35	NT	T	84	73	75	65	70	60	70	0.9	74-84
	II:4	PS	N		81	77	85	105	105	60	50	2.4	58-81
	II:7	60	NT	A	80	60	73	55	72	73	55	1.5	70-80
	III:3	38	N	T, A	55	22	15	19	14	100	97	NA	51-55
	III:4	NOHL	NT	NE	51	8	7	NT	NT	NT	NA	0	Noise trauma
	III:7	50	NT		52	22	20	NT	NT	NT	NA	0	
	III:8	30	N	A, T	48	62	58	52	48	92	92	NA	44-51
	III:9	43	N	NE	46	38	37	42	44	96	90	NA	0
	III:11	33	N	NE, T	38	38	37	40	40	100	95	NA	36-38
W08-1421	III:2	cong.	N	T	67	42	43	30	40	87	65	1.8	50-67

Table S3. (continued)

Family	Subject	Age of onset (y)	Otoscopy examination	Clinical remarks	Imaging		Audiometry			SRT			Maximum SRS (%)			Progression of HL		General remarks
					CT	MRI	Subject age (y)	PTA	R	L	R	L	R	L	R	L	Progression rate (dB/y)	
	IV:2	PS	N	A, Ns, O, T			34	27	28	27	32	95	93	NA	NA	6		
	V:1	0	Reardrum perforation	A, Ab, Ns, O, T			9	73	67	58	60	NT	NT	NA	NA	NA	Neonatal intensive care, surgeries, ototoxic antibiotics	
W18-0470	II:2	6	N				66	42	38	27	27	100	95	NA	NA	0		
	III:1	30	N	O			31	19	18	16	14	100	100	NA	NA	0		
	III:3	11	NT				23	23	22	15	13	100	100	NA	NA	5		
W18-1004	I:1	12	N				54	17	23	NT	NT	NT	NT	NA	NA	0		
	II:1	4	N				20	38	35	30	27	100	95	NA	NA	5		
W18-0471	I:1	20	N	A, T			47	72	117	64	NA	83	0	NA	NA	0		
W18-0472	I:1	27	N	T, V			31	35	37	18	22	100	100	NA	NA	0		Migrainous vertigo
W18-0473	I:1	39	NT				N	N	48	35	42	NT	NT	NT	NT	NA		
W18-1005	I:1	25	N				N	26	42	45	32	37	100	97	NA	NA	0	
W18-1160	I:1	12	N	T			50	47	48	42	43	100	100	NA	NA	7		

Age of onset is the age of onset in years as reported by the subjects. Subject age is the age at which the audiometric data of column 9 to 14 were obtained, in general the last audiogram. If no speech audiometry was performed during the latest pure tone audiometry, the latest audiogram in which both were measured, was selected. Progression rate of HL, calculated as described in the methods section, if there was at least a follow-up duration of 10 years. Y, years; PTA, pure tone average, mean of 0.5, 1 and 2 kHz air conduction thresholds; R, right; L, left; SRT, speech reception threshold; SRS, speech recognition score in %; YOF, years of follow up; NOHL, unaffected subject; NR, age of onset of HL not reported; PS, subject reported onset of HL during primary school; NT, not tested; N, no abnormalities; T, Tinnitus; NE, extensive exposure to noise; O, recurrent otitis; A, asymmetric HL; Ab, subject reported long-term antibiotics usage, but no details about duration and which antibiotics; V, vestibular complaints; NA, not applicable.

Table S4. Results of vestibular testing

Family	Subject (age)	Click-evoked ABR	Remarks and history of vestibular complaints	Oculo-motor testing	vHIT (gain)	SPV Caloric irrigation				Rotating chair				Conclusion			
						Warm (°/s) (10-52) ^a		Cold (°/s) (7-31) ^a		Gain (%) (33-72) ^a		SPV (°/s) (30-65) ^a			Tau (s)	Conclusion	
						R	L	R	L	CW	CCW	CW	CCW				
W97-056	III:24 (48)	NT	no	normal	NT	NT	12	13	normal	NA	NA	49	50	15	15	normal	
	III:11 (53)	NT	no	normal	NT	31	18	16	9	normal	NA	NA	28	30	14	14	Under-estimated ^b
W02-016	III:1 (71)	N	Infrequent vertigo attacks since the age of 65 years	normal	NT	NT	3	11	hyporeactive	NA	NA	51	33	10	11	11	Hypo-reactive
	III:9 (63) ^c	N	Balance complaints after CI surgery	normal	normal	NT	NT	19	24	normal	70	61	63	56	15	19	normal
	III:10 (60)	N	no	normal	normal	32	39	NT	NT	normal	46	57	42	52	12	12	normal
W04-262	III:16 (60)	NT	no	normal	normal	31	30	37	46	normal	NA	NA	42	65	22	15	normal
	III:19 (48)	NT	no	normal	NT	9	7	9	8	normal	65	78	59	71	21	15	normal
W18-1421	IV:2 (47)	NT	no	normal	normal	23	19	12	19	normal	75	80	68	72	11	11	normal
W18-0470	III:1 (32)	N	no	normal	normal	12	26	12	12	normal	82	60	75	55	10	12	normal

Auditory brainstem response; vHIT, video head impulse test; °/s, degrees per seconds; SPV, slow phase velocity; Tau, time constant; R, right ear; L, left ear; CW, clockwise; CCW, counter clockwise; N, no abnormalities; NT, not tested; NA, not applicable. ^a, normative values at our institute. ^b, nystagmus was suppressed due to stress. ^c, Subject was tested after CI surgery and also had c- and oVEMP testing, no abnormalities were objectified (data not shown).

Table S5. Individual results of age of onset, otoscopy, audiometry and progression of HL of the phenocopies

Family	Subject	Age of onset (y)	Otoscopy examination	Clinical remarks	Imaging		Subject age (y)	Audiometry				Progression of HL		General remarks		
					CT	MRI		PTA	SRT		Maximum SRS (%)	Progression rate (dB/y)	YOF (y)			
									R	L					R	L
W97-056	III:14	52	N	V			69	42	40	48	42	85	92	0.8	39-70	Ménière-like phenotype
	III:20	46	N	Ab, T			70	45	40	37	37	100	100	0.7	50-71	Smoking, COPD Gold III, often antibiotics
	III:21	NR	NT				68	38	37	20	25	NT	NT	0.8	45-68	
W04-262	III:10	55	N	T, V			60	33	38	33	41	100	95	NA	0	

Family members with HL that do not carry the *RIPOR2* variant are considered a phenocopy. Age of onset is the age of onset in years as reported by the subjects. Subject age is the age at which the audiometric data of column 9 to 14 were obtained. If no speech audiometry was performed during the latest audiometric testing, the penultimate audiogram was selected. Progression rate of HL was calculated if there was at least a follow-up duration of 10 years. Y, years; PTA, pure tone average, mean of 0.5, 1 and 2 kHz air conduction thresholds; R, right; L, left; SRT, speech reception threshold; SRS, speech recognition score in %; YOF, years of follow up; NR, age of onset of HL not reported; NT, not tested; N, no abnormalities; V, vestibular complaints; Ab, subject reported long-term antibiotics usage, but no details about duration and which antibiotics; T, Tinnitus; NA, not applicable.

Table S6. Genes analyzed by MIP sequencing

<i>ACTG1</i>	<i>ESPN</i>	<i>MYH14</i>	<i>SLC17A8</i>
<i>ADCY1</i>	<i>ESRRB</i>	<i>MYH9</i>	<i>SLC26A4</i>
<i>BDP1</i>	<i>EYA4</i>	<i>MYO15A</i>	<i>SLC26A5</i>
<i>BSND</i>	<i>GIPC3</i>	<i>MYO3A</i>	<i>SMPX</i>
<i>CABP2</i>	<i>GJB2</i>	<i>MYO6</i>	<i>STRC</i>
<i>CCDC50</i>	<i>GJB3</i>	<i>MYO7A</i>	<i>SYNE4</i>
<i>CDH23</i>	<i>GJB6</i>	<i>NAT2</i>	<i>TBC1D24</i>
<i>CEACAM16</i>	<i>GPSM2</i>	<i>OSBPL2</i>	<i>TECTA</i>
<i>CIB2</i>	<i>GRHL2</i>	<i>OTOA</i>	<i>TJP2</i>
<i>CLDN14</i>	<i>GRM7</i>	<i>OTOF</i>	<i>TMC1</i>
<i>CLIC5</i>	<i>GRM8</i>	<i>OTOG</i>	<i>TMEM132E</i>
<i>COCH</i>	<i>GRXCR1</i>	<i>OTOGL</i>	<i>TMIE</i>
<i>COL11A2</i>	<i>GRXCR2</i>	<i>P2RX2</i>	<i>TMPRSS3</i>
<i>COL4A6</i>	<i>HGF</i>	<i>PCDH15</i>	<i>TNC</i>
<i>CRYM</i>	<i>ILDR1</i>	<i>PNPT1</i>	<i>TPRN</i>
<i>DCDC2</i>	<i>KARS</i>	<i>POU3F4</i>	<i>TRIOBP</i>
<i>GSDME</i>	<i>KCNQ4</i>	<i>POU4F3</i>	<i>TSPEAR</i>
<i>DFNB31</i>	<i>LHFPL5</i>	<i>PRPS1</i>	<i>USH1C</i>
<i>DFNB59</i>	<i>LOXHD1</i>	<i>PTPRQ</i>	<i>USH1G</i>
<i>DIABLO</i>	<i>LRTOMT</i>	<i>RDX</i>	<i>WFS1</i>
<i>DIAPH1</i>	<i>MARVELD2</i>	<i>RIPOR2</i>	
<i>ELMOD3</i>	<i>MIR96</i>	<i>SERPINB6</i>	
<i>EPS8</i>	<i>MSRB3</i>	<i>SIX1</i>	

Table S7. Primer sequences

Target	Primer	Oligonucleotides (5'-3')
<i>RIPOR2</i> exon 14, wt allele	Forward	aagcagctgggtcaagagg
	Reverse	gcagccttcagattctcc
<i>RIPOR2</i> exon 14, mut allele	Forward	ggaaggaacatcacaagag
	Reverse	gcagccttcagattctcc
<i>RIPOR2</i> exons 3-4, mRNA	Forward	ggccttgaaaaatggacttg
	Reverse	ccaggcgagagtttcttttc
<i>GUSB</i> exons 2-3, mRNA	Forward	agagtggctgctgaggattgg
	Reverse	ccctcatgctctagcgtgtc

Primer sequences for *RIPOR2* are based on reference sequence NM_00147722.3 and for *GUSB* on NM_00181.3. wt, wildtype; mut, mutant.

SUPPLEMENTARY FIGURES

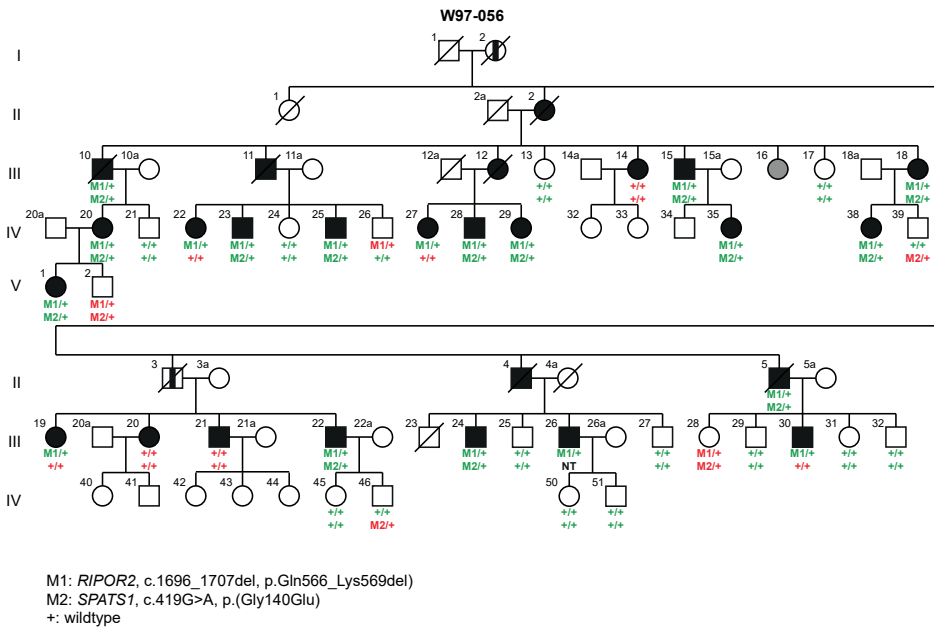


Figure S1. Segregation analysis of the *SPATS1* and *RIPOR2* variants in W97-056 Subjects determined to be affected by heteroanamnesis are indicated with a vertical black line. The subject marked in grey is diagnosed with intellectual disability and excluded from further participation in this study. Subject identifiers correspond to those in de Brouwer et al., 2005.¹⁷ Genotypes in green correspond to a co-occurrence of the variant and hearing impairment and those in red to lack of co-occurrence. NT, not tested.

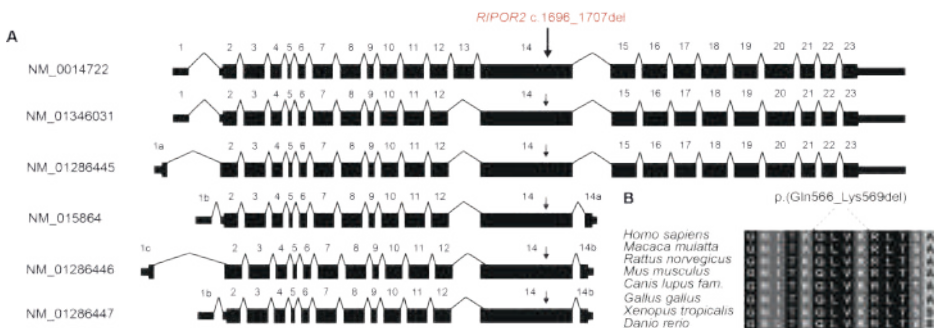


Figure S2. Schematic overview of major *RIPOR2* transcripts (A) Transcripts are extracted from the Ensembl genome browser. The position of the c.1696_1707del *RIPOR2* variant is indicated with an arrow. **(B)** Evolutionary conservation of the amino acids that are affected by the variant. Fully conserved amino acid residues are shown on a black background. A dark grey background marks chemical similarity of residues and a light grey background indicates chemical dissimilarity.

A

Position (bp)	Marker	W97-056: IV:25	W02-016: IV:3	W04-262: III:19	W08-1421: V:1	W15-0495: III:9	W18-0470: III:3	W18-1004: I:1	W18-0471	W18-0472	W18-0473	W18-1005	W18-1160
24,185,805	D6S276	5	9	10	8	5	8	5	10	5	8	5	5
24,306,692	D6S2439	1	6	6	3	1	7	1	6	2	3	3	3
24,843,752	D6S1554	1	1	1	1	1	1	1	1	1	1	1	1
24,964,249	D6S1571	1	1	1	1	1	1	1	1	1	1	1	1
24,983,204	D6S1545	4	4	4	4	4	3	4	4	4	4	4	4
25,296,948	D6S1281	2	2	2	1	2	2	2	2	2	1	2	1
25,495,470	D6S1621	1	1	1	1	1	1	1	1	1	3	2	2

B

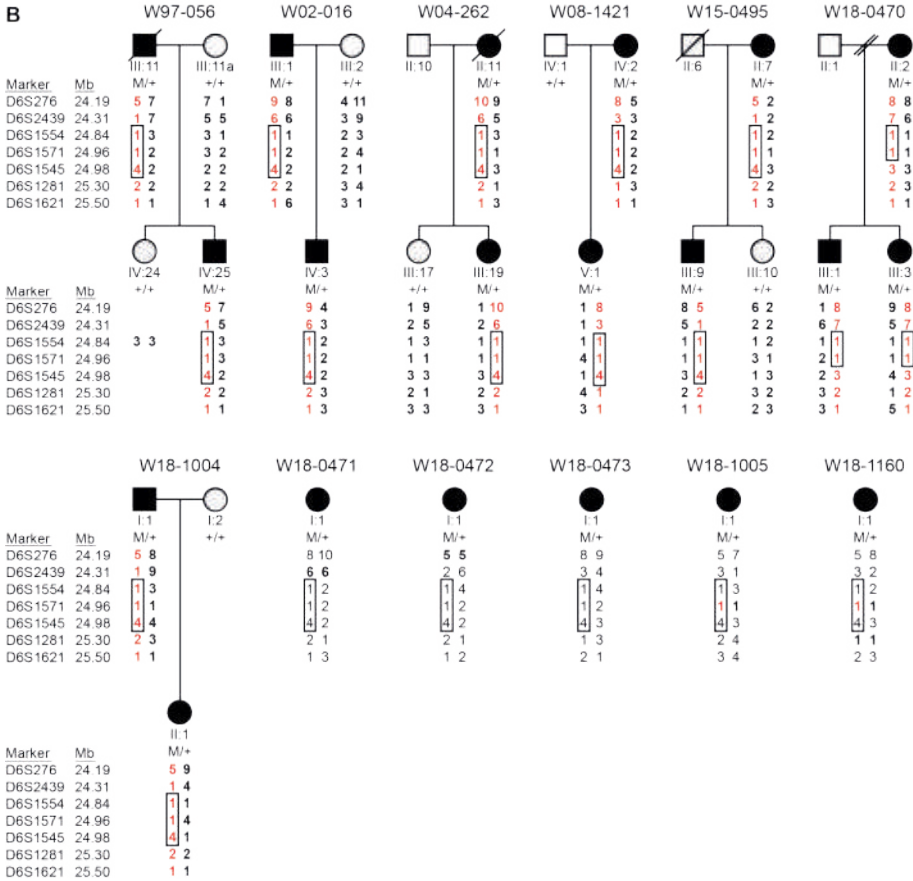


Figure S3. Family pedigrees with genotypes and haplotypes of VNTR markers (A) The shared haplotype is marked in grey. For marker D6S1545 (light-grey), a different CA-repeat length was determined in one family, but the marker is considered to be potentially part of the shared haplotype as a change of repeat length cannot be excluded. Markers for which the phase of the alleles could conclusively be determined via segregation in the family are marked in bold. The *RIPOR2* c.1696_1707del variant is located between the markers D6S2439 and D6S1554. Genomic positions (bp) are according to the UCSC Genome Browser (GRCh37/hg19). **(B)** The haplotypes carrying the *RIPOR2* c.1696_1707del variant are shown in red. A haplotype of 1.1 Mb was found to be shared (boxed) and is delimited by the markers D5S1554 and D6S1545. Alleles for which the parent of origin could conclusively be determined are marked in bold.

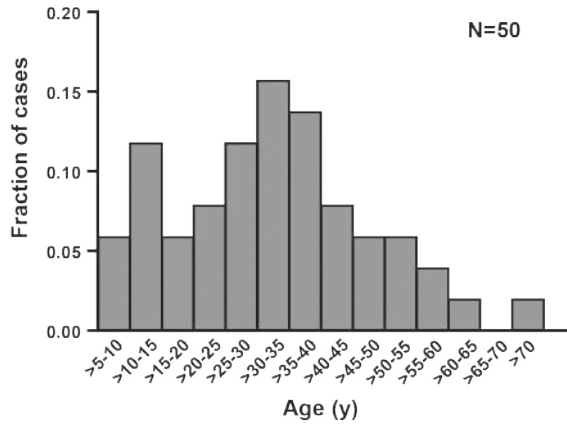
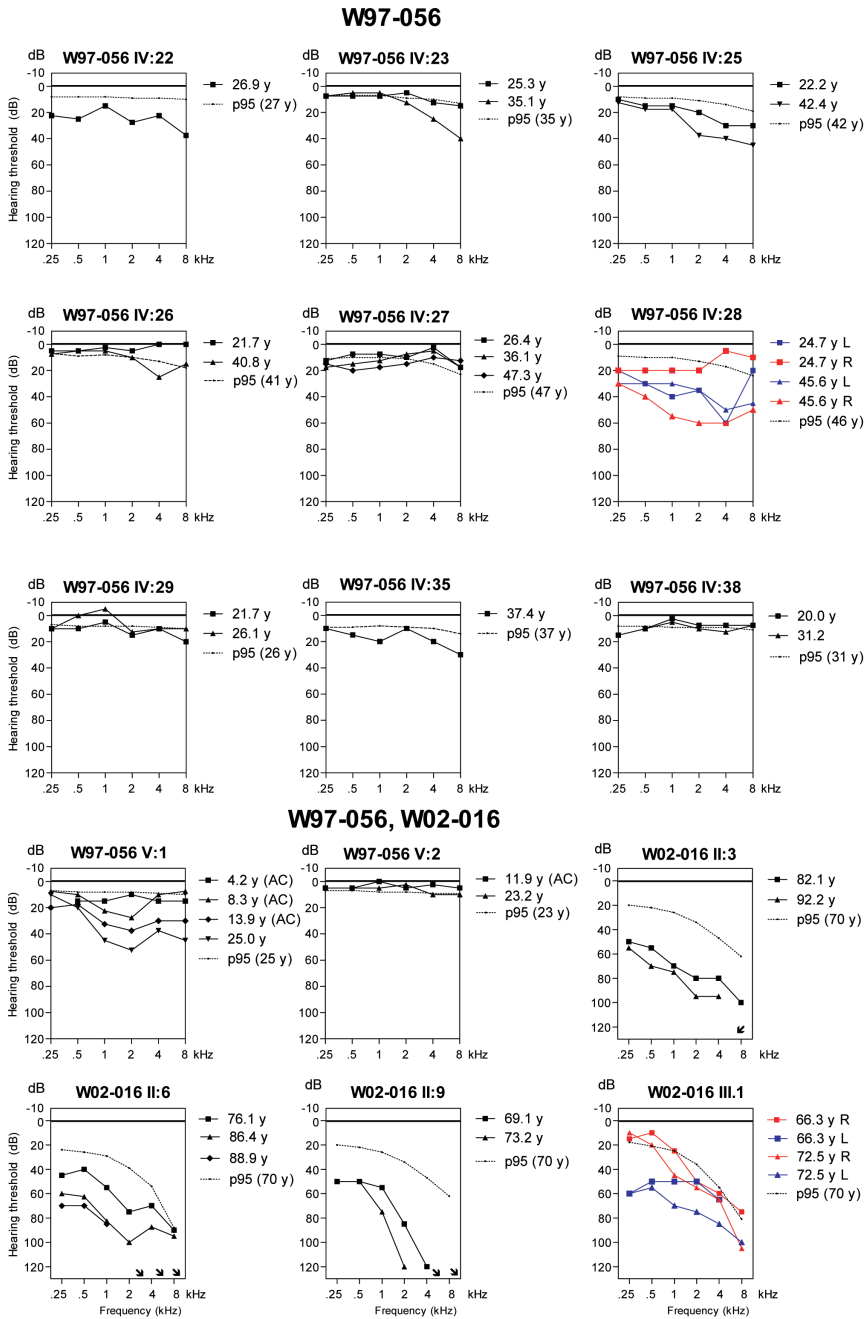
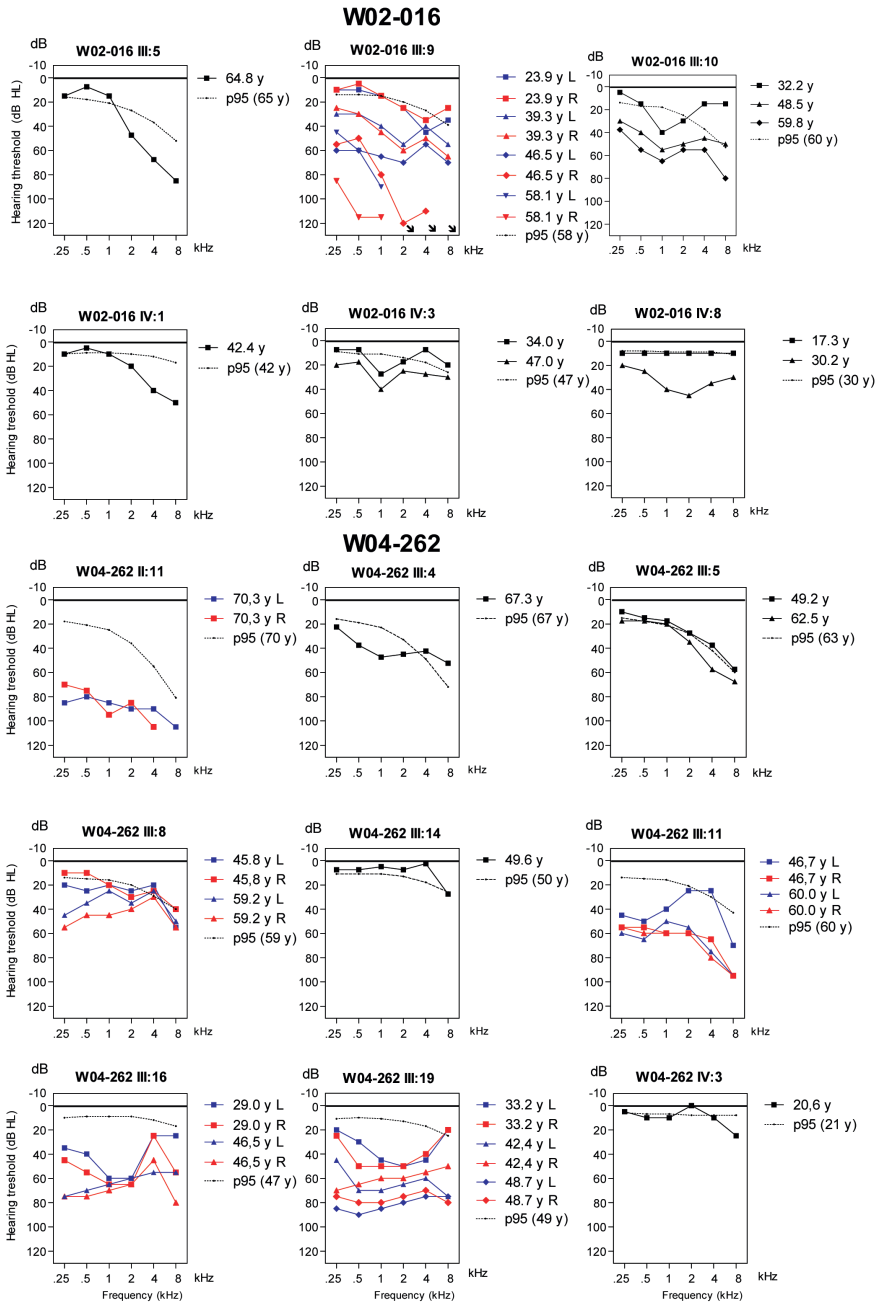
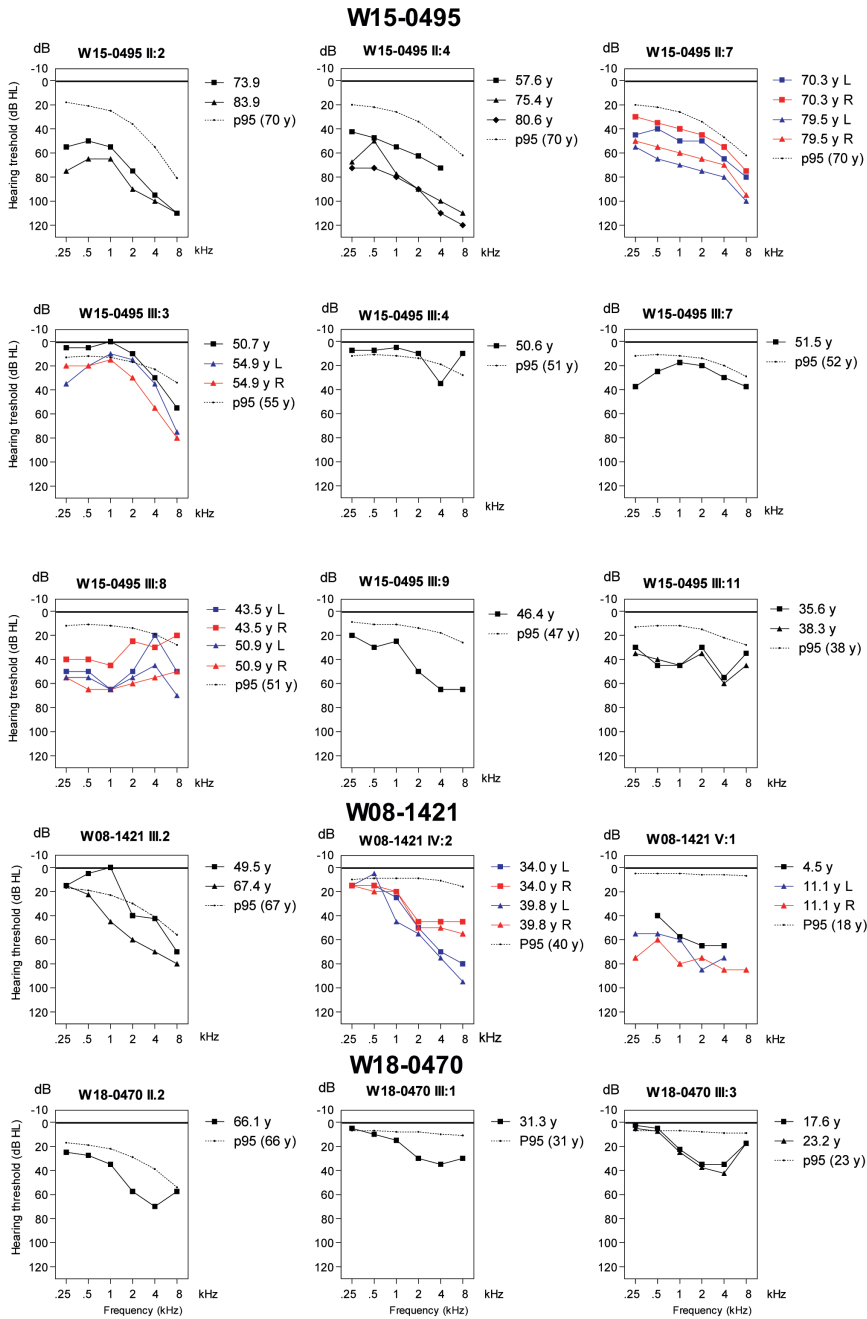


Figure S4. Reported age of onset of hearing loss of subjects with the *RIPOR2* c.1696_1707del variant
Distribution of the reported ages of onset of *RIPOR2*-associated hearing loss per 5 years for 52 subjects who reported a specific age of onset. y, years.







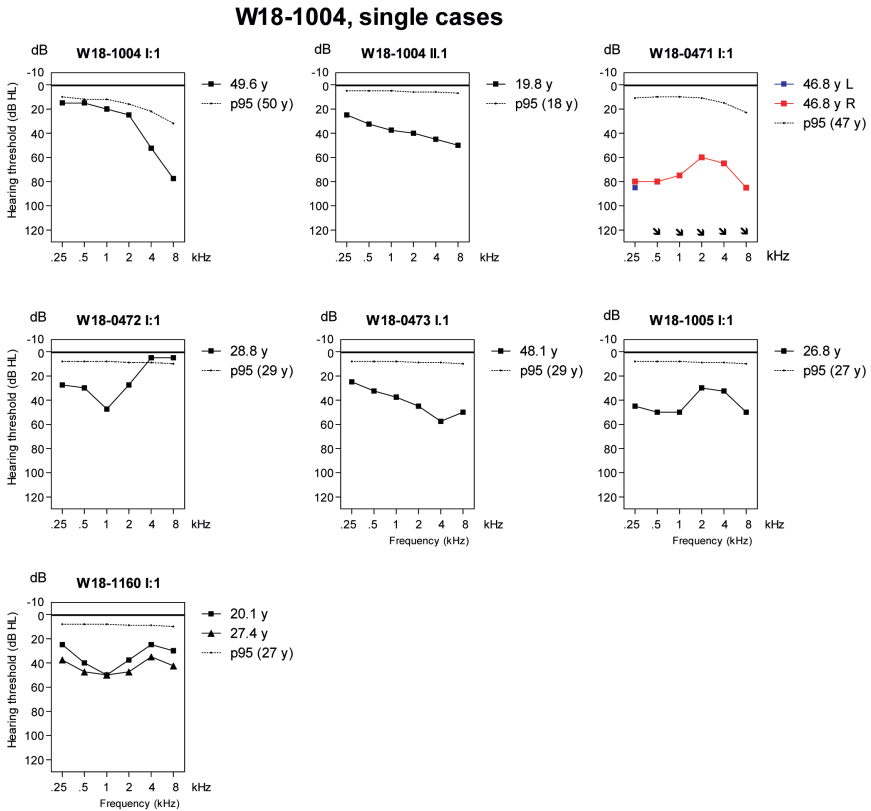


Figure S5. Pure tone audiometry Air conduction thresholds of all subjects (except III.5 of W08-1421) with the c.1696_1707del *RIPOR2* variant are depicted. In case of symmetry, the averages of left and right ear thresholds are shown. Otherwise, colored (right red, left blue) audiograms of both ears are depicted. The p95 values are matched to the individuals' sex and age at the most recent audiometry, according to the ISO 7029:2017 standard. The age range for which the ISO 7029:2017 can be applied is 18 to 70 years. Part of the pure tone audiometry for family W97-056 has been published previously by Kunst et al. 2000.¹⁸ y, age in years; R, right; L, left; dB HL, decibel hearing level; kHz, kiloHertz; AC, only air conduction levels available, no additional bone conduction thresholds have been measured.

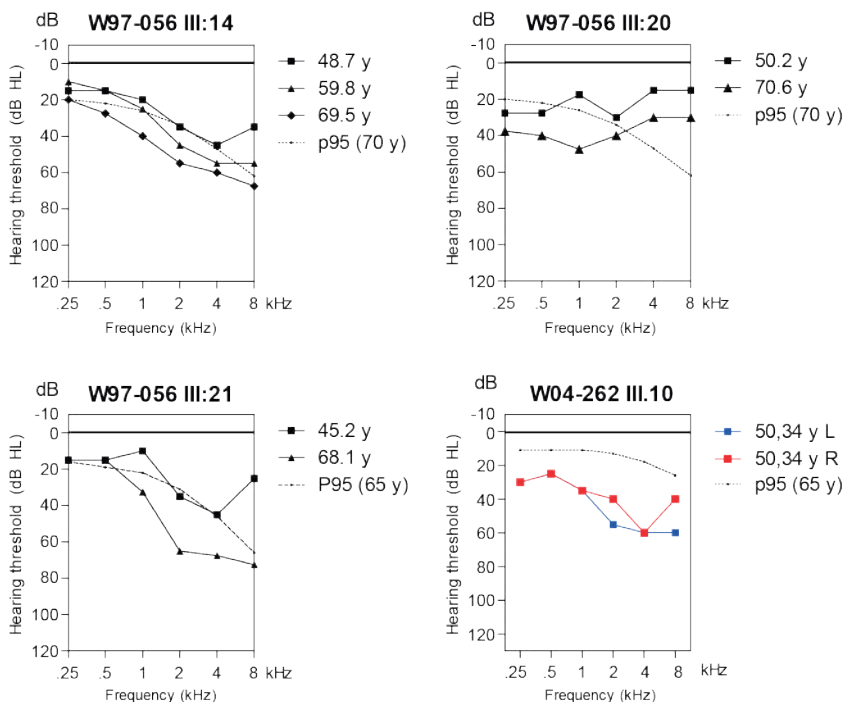


Figure S6. Audiograms of hearing impaired individuals without the *RIPOR2* c.1696_1707del variant Air conduction thresholds are depicted of all hearing impaired subjects who did not have the c1696_1707del *RIPOR2* variant. In **Table S5** information about possible explanations for their hearing impairment is provided. In case of symmetry, the averages of left and right ear thresholds are shown. Otherwise, colorized (right red, left blue) audiograms of both ears are depicted. The p95 values are matched to the individuals' sex and age at the most recent audiometry, according to the ISO 7029:2017 standard. The age range for which the ISO 7029:2017 can be applied is 18 to 70 years. y, age in years; R, right; L, left; dB HL, decibel hearing level; kHz, kiloHertz.

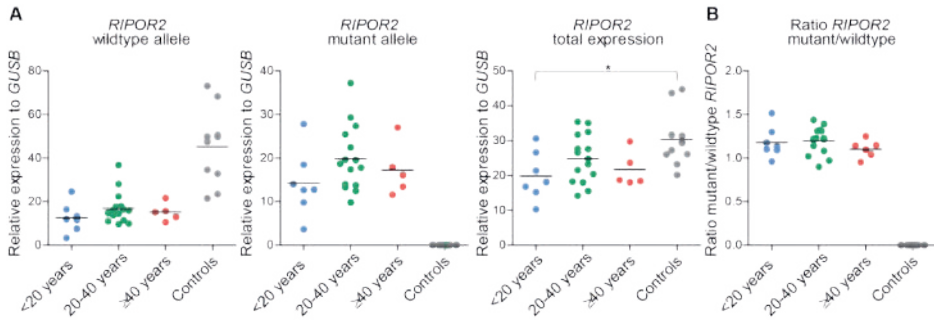


Figure S7. Transcript levels of *RIPOR2* alleles determined by RT-qPCR. (A) Subjects were divided in three groups based on the reported ages of onset: early onset (<20 years, n=7), middle onset, (20-39 years, n=15) and late onset (≥40, n=6) hearing impairment. RNA samples isolated from peripheral blood of individuals without the *RIPOR2* variant were used as controls (n=10). **(B)** Calculated ratio of *RIPOR2* mutant to wildtype relative expression analysis. A one-way ANOVA followed by Tukey's multiple comparison test was employed to identify potentially significant differences between the transcript levels of the groups. * p-value = 0.0214.

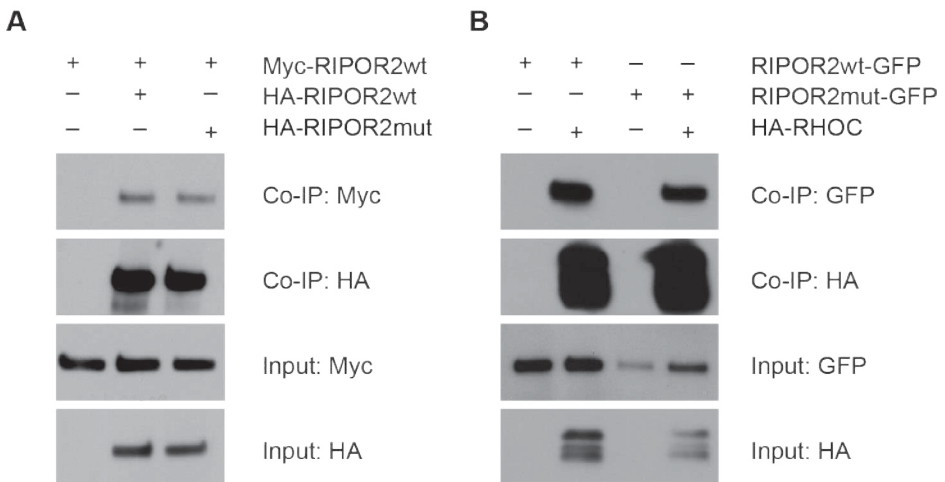


Figure S8. *RIPOR2* dimerization and interaction with RHOC (A) Interaction of murine *RIPOR2*-wildtype (*RIPOR2*wt) and -mutant (*RIPOR2*mut) was studied using CoIP assays. HEK293T cells were transfected with constructs encoding N-terminally tagged proteins as indicated above each panel. Immunoprecipitations were performed using anti-HA antibodies, followed by western blotting. **(B)** Interaction with RHOC was studied using C-terminally GFP-tagged *RIPOR2*-wildtype or -mutant and N-terminally HA-tagged RHOC. Immunoprecipitations were performed using anti-HA antibodies, followed by western blotting.

SUPPLEMENTARY REFERENCES

1. Li, H. & Durbin, R. Fast and accurate short read alignment with Burrows-Wheeler transform. *Bioinformatics* 25, 1754-1760 (2009).
2. McKenna, A. *et al.* The Genome Analysis Toolkit: a MapReduce framework for analyzing next-generation DNA sequencing data. *Genome research* 20, 1297-1303 (2010).
3. Krumm, N. *et al.* Copy number variation detection and genotyping from exome sequence data. *Genome Research* 22, 1525-1532 (2012).
4. Chen, X. *et al.* Manta: rapid detection of structural variants and indels for germline and cancer sequencing applications. *Bioinformatics* 32, 1220-1222 (2016).
5. Boeva, V. *et al.* Control-FREEC: a tool for assessing copy number and allelic content using next-generation sequencing data. *Bioinformatics* 28, 423-425 (2012).
6. Robinson, J.T. *et al.* Integrative genomics viewer. *Nature Biotechnology* 29, 24 (2011).
7. Hardenbol, P. *et al.* Multiplexed genotyping with sequence-tagged molecular inversion probes. *Nature Biotechnology* 21, 673 (2003).
8. Khandelwal, K.D. *et al.* Novel IRF6 Mutations Detected in Orofacial Cleft Patients by Targeted Massively Parallel Sequencing. *Journal of Dental Research* 96, 179-185 (2016).
9. Tarpey, T. Linear transformations and the k-means clustering algorithm: Applications to clustering curves. *Journal of the American Statistical Association* 61, 34-40 (2007).
10. Ketchen, D.J. & Shook, C.L. The application of cluster analysis in strategic management research: an analysis and critique. *Strategic Management Journal* 17, 441-458 (1996).
11. Oonk, A.M. *et al.* Vestibular function and temporal bone imaging in DFNB1. *Hearing Research* 327, 227-34 (2015).
12. Vanspauwen, R., Wuyts, F.L., Krijger, S. & Maes, L.K. Comparison of different electrode configurations for the oVEMP with bone-conducted vibration. *Ear and Hearing* 38, 205-211 (2017).
13. Papathanasiou, E.S., Murofushi, T., Akin, F.W. & Colebatch, J.G. International guidelines for the clinical application of cervical vestibular evoked myogenic potentials: an expert consensus report. *Clin Neurophysiol* 125, 658-666 (2014).
14. Pfaffl, M.W. A new mathematical model for relative quantification in real-time RT-PCR. *Nucleic Acids Research* 29, e45-e45 (2001).
15. Diaz-Horta, O. *et al.* Ripor2 is involved in auditory hair cell stereociliary bundle structure and orientation. *Journal of Molecular Medicine* 96, 1227-1238 (2018).
16. Diaz-Horta, O. *et al.* FAM65B is a membrane-associated protein of hair cell stereocilia required for hearing. *Proceedings of the National Academy of Sciences of the United States of America* 111, 9864-9868 (2014).
17. De Brouwer, A.P.M. *et al.* Fine mapping of autosomal dominant nonsyndromic hearing impairment DFNA21 to chromosome 6p24.1-22.3. *American Journal of Medical Genetics Part A* 137A, 41-46 (2005).
18. Kunst, H. *et al.* Non-syndromic autosomal dominant progressive non-specific mid-frequency sensorineural hearing impairment with childhood to late adolescence onset (DFNA21). *Clinical Otolaryngology & Allied Sciences* 25, 45-54 (2000).



Chapter 4.3

Cochlear supporting cells require GAS2 for cytoskeletal architecture and hearing

Tingfang Chen, Alex M. Rohacek, Matthew Caporizzo, Amir Nankali, Jeroen J. Smits, Jaap Oostrik, Cornelis P. Lanting, Erdi Küçük, Christian Gilissen, Jiddeke M. van de Kamp, Ronald J.E. Pennings, Staci M. Rakowiecki, Klaus H. Kaestner, Kevin K. Ohlemiller, John S. Oghalai, Hannie Kremer, Benjamin L. Prosser, and Douglas J. Epstein

Developmental Cell 56, 1526-1540 (2021)

ABSTRACT

In mammals, sound is detected by mechanosensory hair cells that are activated in response to vibrations at frequency dependent positions along the cochlear duct. We demonstrate that inner ear supporting cells provide a structural framework for transmitting sound energy through the cochlear partition. Humans and mice with mutations in *GAS2*, encoding a cytoskeletal regulatory protein, exhibit hearing loss due to disorganization and destabilization of microtubule bundles in pillar and Deiters' cells, two types of inner ear supporting cells with unique cytoskeletal specializations. Failure to maintain microtubule bundle integrity reduced supporting cell stiffness, which in turn, altered cochlear micromechanics in *Gas2* mutants. Vibratory responses to sound were measured in cochleae from live mice, revealing defects in the propagation and amplification of the traveling wave in *Gas2* mutants. We propose that the microtubule bundling activity of GAS2 imparts supporting cells with mechanical properties for transmitting sound energy through the cochlea.

INTRODUCTION

The organ of Corti is a specialized sensory epithelium unique to mammals that lines the length of the cochlear duct and is responsible for sound reception. It comprises a single row of inner hair cells (IHCs), three rows of outer hair cells (OHCs) and a variety of interspersed supporting cells that sit atop the basilar membrane. Sound waves propagate through the cochlear duct by way of fluid motion causing the basilar membrane to oscillate at frequency dependent positions.^{1,2} IHCs convert sound induced vibrations into electrochemical signals that are transmitted to the brain along auditory nerve fibers.²⁻⁴ OHCs enhance the detection and discrimination of sound frequencies by amplifying basilar membrane vibrations more than 1000-fold in a feedback loop driven by OHC electromotility.⁵ In comparison to hair cells, relatively little is known about the role that supporting cells play in the transmission of mechanical vibrations across the cochlear partition.

Computational models predict that the unique geometry and cytoskeletal composition of inner ear supporting cells provides a structural framework for the exchange of forces between the basilar membrane and the apical surface of the organ of Corti.⁶⁻¹² Nevertheless, experimental evidence in support of these models, especially from *in vivo* studies, is limited. It also remains unclear whether mutations in genes that selectively perturb supporting cell mechanical properties would cause hearing loss, and if so, by what means.

Pillar and Deiters' cells are two types of supporting cells with intricate morphologies and cytoskeletal specializations that form strategic connections with OHCs, in keeping with their putative structural role.¹³⁻¹⁵ Inner and outer pillar cells form the tunnel of Corti, which separates IHCs from OHCs. The head of each inner and outer pillar cell projects laterally to contact the first and second row of OHCs, respectively.¹⁶⁻¹⁸ Deiters' cells reside at the base of each OHC and extend a long phalangeal process to the reticular lamina at the apical surface of the organ of Corti into which OHCs insert their stereocilia.^{2,14,15} The arrangement of OHCs and Deiters' cells in a Y-shaped configuration resembles that of a braced frame used in building construction to withstand shearing forces, such as wind and seismic pressure.^{8,11,15}

A particularly striking aspect of pillar and Deiters' cells is their rigid cytoskeleton composed of hundreds to thousands of microtubules organized in tightly bundled arrays that are cross-linked to actin filaments.^{7,16,18-20} Pillar cells possess two densely packed microtubule bundles, one that runs across the pillar cell head and another that assembles parallel to the apicobasal axis.^{18,21} Deiters' cells contain microtubule bundles of lesser complexity.^{18,19} These cytoskeletal elements bestow pillar and Deiters' cells with stiff mechanical properties.^{7,18-20}

Microtubules are composed of polymerized α - and β -tubulin heterodimers and are generally required for cell shape, structural support and intracellular transport in differentiated cells.²²

Not all microtubules are equivalent with respect to subunit composition, post-translational modifications, dynamic turnover, subcellular arrangement, and interactions with microtubule associated proteins (MAPs), all of which may influence microtubule function. Previous studies have demonstrated that pillar cell microtubules are heavily de-tyrosinated and acetylated, which in other systems has been shown to confer stability and flexibility, respectively, in response to mechanical stresses.²³⁻²⁷ MAPs are also predicted to influence the mechanical properties of pillar and Deiters' cells by cross-linking microtubules to actin filaments.⁷ Several candidate proteins for this cytoskeletal cross-linking activity have been proposed, but none have been functionally validated and the identity of this factor remains elusive.²⁸⁻³¹

We show here that Growth arrest-specific 2 (GAS2), a protein with microtubule and actin binding domains, is expressed in pillar and Deiters' cells in a pattern that co-localizes with microtubule bundles. *Gas2* mutant mice display severe hearing loss due to the disorganization and destabilization of microtubule arrays in inner ear supporting cells, resulting in a decrease in pillar cell stiffness and a buckling of Deiters' cell phalangeal processes. The reduction in pillar and Deiters' cell elastic properties alters OHC micromechanics in *Gas2* mutants, causing defects in the propagation and amplification of the traveling wave, as assessed by volumetric optical coherence tomography and vibrometry (VOCTV) in live mice. Homozygous loss-of-function mutations in *GAS2* were also identified in affected family members with congenital sensorineural hearing loss. Taken together, our study identifies *Gas2* as a hearing loss gene required to maintain microtubule bundles in inner ear supporting cells, affording them with mechanical stiffness to transmit sound energy through the cochlea.

MATERIALS AND METHODS

Ethical statement

All mouse experiments were performed in accordance with the ethical guidelines of the National Institutes of Health and with the approval of the Institutional Animal Care and Use Committee of the University of Pennsylvania. The study of human subjects was approved by the medical ethics committee of the Radboudumc (registration number: NL33648.091.10) and performed in accordance with the principles of the Declaration of Helsinki. Written informed consent was obtained from all participants or their legal representatives.

Mouse lines

The *Gas2*^{tm1a/+} mouse line was generated from ES-cells obtained from the European Conditional Mouse Mutagenesis Program (Clone: HEPD0681_7_F03) (**Figure S2A**). ES-Cells were injected into albino C57B/6N-tac blastocysts at the Transgenic and Chimeric Mouse

Facility (Perelman School of Medicine, University of Pennsylvania). High percentage chimeras (>90% black/agouti coat) were bred to albino C57B/6N-tac mice and the resulting pups were screened for the *Gas2^{tm1a}* allele by coat color and PCR genotyping. Primers flanking the floxed *Gas2* exon 5 (F- TTGGATCATATGGAGAGGCCAT, R-GGGCATATCACAGGCCATA) amplified a 223 bp product from the wild type allele and a 257 bp product from the *Gas2^{tm1a}* allele using the following PCR conditions: 95°C for 5 min, 95°C for 30 sec, 58°C for 30 sec, 72°C for 18 sec, steps 2-4 repeated for 31 cycles, 72°C for 10 min. *Gas2^{tm1a/+}* mice were maintained on a C57B/6N-tac background for at least 10 generations. To generate mice with a floxed allele of *Gas2* (*Gas2^{tm1c}*), *Gas2^{tm1a/+}* mice were crossed to the *FLPo* deleter strain (*B6 ROSA26Flpo*, The Jackson Laboratory) to remove the lacZ-Neomycin cassette (**Figure S2B**). *Gas2^{tm1c/+}* mice were intercrossed after segregating away the *FLPo* transgene and maintained as homozygotes. To generate conditional knockout mice lacking GAS2 in supporting cells (*cGas2*), *Gas2^{tm1c/tm1c}* mice were crossed to the *Sox2^{CreER/+}* line (B6; 129S- *Sox2^{tm1cre/ERT2}Hoch/J*, The Jackson Laboratory) (**Figure S2C**). *Sox2^{CreER/+}*; *Gas2^{tm1c/+}* mice were then crossed to *Gas2^{tm1c/tm1c}* mice to generate *Sox2^{CreER/+}*; *Gas2^{tm1c/tm1c}* (*cGas2*) and control (*Sox2^{CreER/+}*; *Gas2^{tm1c/+}*) pups that were administered tamoxifen (4mg/30g body weight) once a day for two consecutive days starting at P1 to induce *Gas2* recombination (**Figure S6**). Genotyping primers for *Gas2* mutants are listed in **Table S1**.

In situ hybridization

Embryos were collected from timed pregnant females (vaginal plug = E0.5). Heads were dissected at the level of the posterior hindbrain and fixed for 2 hours in 4% paraformaldehyde at 4°C, then washed in PBS. Samples were cryoprotected overnight in 30% sucrose/PBS then snap frozen in OCT embedding compound. Samples were serially sectioned along the transverse plane. Sections were hybridized with digoxigenin-UTP-labeled riboprobes as previously described.³²

Inner ear paint fill

Paint fills were performed essentially as described³³ with the use of White-Out Plus as the contrast medium.

Whole mount cochlear preparations

Inner ears were dissected and fixed in 4% paraformaldehyde for 2 hours or overnight at 4°C, then washed in PBS. The inner ears were decalcified in 0.25M EDTA for several hours (P14), for 1 day (P25), for 2 days (P42) or for 3 days (P60) until the bone was completely soft. Cochleae were then microdissected in 0.1% PBST to expose the sensory epithelium, and incubated with antibodies found in Key Resources.

Immunohistochemistry

Inner ears were processed for immunohistochemistry in the same fashion as for in situ hybridization. Inner ear sections were stained with DAPI and antibodies Iis. Specimens were imaged on a Leica TCS SP8 MP system using 63× oil or 20× objectives. Stacks of confocal images were acquired with a Z step of 0.37 μm and processed using ImageJ software. Specimens in **Figure 1** (L-N) were imaged on a Zeiss LSM 880 confocal microscope with Airyscan using 63x/1.4 oil objectives and acquired using ZEN v2.3 software.

Western blot

The organ of Corti was isolated from two *Gas2^{tm1a/tm1a}* and control mice at P0 in RIPA buffer and protein extraction was performed by manual homogenization. Protein concentration was measured using a Bradford assay. Protein lysates were prepared for gel electrophoresis by adding 4X Laemmli Sample Buffer (BIO-RAD, 1610747) to a final concentration. Samples were heat-denatured at 100 °C for 5 min, and 30 μg of total protein was loaded into each well of a 4-15% mini-protein TGX gel (BIO-RAD 10-well, 1.5 mm; Cat. #456-1084). Protein gels were run for 30 min at 80V then 90 min at 110V at room temperature on a BIO-RAD mini-protein Tetra electrophoresis system (10025025) using BioRad Power Supply (Power/PAC 300), then transferred onto a PVDF membrane (0.2 μm, 7*8.5cm size; Cat. #16201745) for 10 min at 250mA then 60 min at 280mA with ice cold water. The membrane was blocked with Intercept (PBS) Blocking Buffers (P/N: 927-70001) for 1 hour at room temperature. Primary antibodies: anti-N-terminal GAS2 (ab109762; 1:500), and anti-GAPDH (Invitrogen, MA5-15738; 1:1000). Secondary antibodies (Licor) used: goat anti-rabbit IRDye 680RD, and goat anti-mouse IRDye 800CD at dilutions of 1:10,000 and incubated for 1 h at room temperature. Standard protocols were used for the Odyssey Infrared Imaging System (LI-COR) for visualization and quantification.

Auditory Brainstem Response

All recordings were from the left ear. ABR recording was carried out using Tucker-Davis Technologies (TDT) System II hardware and software. Animals were anesthetized using ketamine and xylazine (80/15 mg/kg, intraperitoneal injection) and positioned dorsally in a custom head holder. Subdermal platinum needle electrodes (Grass) were placed in the mid-back (ground), behind the right pinna (reference), and at the vertex (active). Body temperature was monitored throughout testing using a rectal probe, and maintained at 37.5 ± 1.0°C using a DC current-based isothermal pad (FHC). A TDT ES-1 speaker was placed 7 cm along the interaural axis. Stimuli were 5 ms tone bursts (1000 repetitions, 20/s, 1.0 ms rise/fall time) at frequencies of 5, 10, 20, 28.3, 40 and 56.6 kHz. Responses were amplified x100,000 and filtered at 100-10,000 Hz. Thresholds were taken to be the lowest sound level for which Wave I could be identified, using a 5dB minimum step size.

Distortion product otoacoustic emissions (DPOAE)

DPOAE (2f₁-f₂) recordings were obtained in a separate session from ABR recordings, but the animals were prepared similarly as for ABRs. DPOAE iso-input (DP-gram) responses were obtained using EMAV (S. Neely, Z. Liu, BTNRH) in conjunction with TDT and custom hardware using f₂ frequencies ranging from 5-40 kHz. F₁ frequencies were given by f₂/1.2. L₁ and L₂ levels were set at 75 and 65 dB SPL, respectively. Stimuli were delivered to the ear using a custom coupler inserted using an operating scope. Each channel was output to a TDT EC-1 speaker. DPOAE responses were recorded using a Knowles FC-23652-P16 microphone calibrated to 40 kHz.

Endocochlear potential recording

After ABR and DPOAE recording, animals underwent a single terminal EP measurement from the cochlear lower basal turn of the left ear. Animals were anesthetized (60 mg/kg sodium pentobarbital, IP) and positioned ventrally in a custom head holder. Core temperature was maintained at 37.5 ± 1.0 °C using a thermostatically-controlled heating pad in conjunction with a rectal probe (Yellow Springs Instruments Model 73A). An incision was made along the midline of the neck and soft tissues were bluntly dissected and displaced laterally to expose the trachea and left bulla. A tracheostomy was then made and the musculature over the bulla was cut posteriorly to expose the bone overlying the round window. Using a fine drill, a hole was made in the left cochlear capsule directly over scala media of the lower basal turn. Glass capillary pipettes (40-80 MW) filled with 0.15 M KCl were mounted on a hydraulic microdrive (Frederick Haer) and advanced until a stable positive potential was observed that did not change with increased electrode depth. The signal from the recording electrode was led to an AM Systems Model 1600 intracellular amplifier. A silver/silver chloride ball inserted into the neck muscles served as ground.

Scanning electron microscopy (SEM)

Gas2 mutant and control cochleae were harvested at P25 and fixed in 2.5% glutaraldehyde in 0.1 M cacodylate buffer for 2 hours at room temperature. The inner ears were decalcified in 0.25M EDTA for three days at 4°C. After decalcification, the inner ears were post-fixed in 1% OsO₄ for 60 minutes (2x). The sensory epithelia were then dissected in distilled water. Specimens were dehydrated in a graded ethanol series, dried at the critical point in liquid CO₂, sputter coated with platinum (5.0 nm, controlled by a film-thickness monitor), and imaged with a field-emission SEM (FEI Quanta 250).

Transmission electron microscopy (TEM)

Inner ears were dissected from postnatal animals after euthanasia with CO₂. The apical turn was opened by cutting a hole in the otic capsule and the cochlea was perfused through the round window every 15 minutes with a mixture of 2% glutaraldehyde and 1% tannic acid in PBS for 90 minutes. The inner ear was then decalcified in 0.25M EDTA overnight at 4°C. The otic capsule, spiral ganglia and stria vascularis were removed to expose the sensory epithelium, which was postfixed in 1% OsO₄ for 90 minutes. The samples were submitted to the Electron Microscopy Resources Lab (Perelman School of Medicine, University of Pennsylvania), dehydrated in ethanol, permeated in propylene oxide, and embedded in Epon resin. Sections were taken on a diamond wafer blade, stained with uranyl acetate and lead citrate and imaged on Jeol-1010 transmission electron microscope.

Cochlear explant culture

Mice were decapitated on P9, and the organs of Corti were dissected in Leibovitz's L-15 medium. The tissues were adhered to petri dishes coated with BD CellTak (BD Life Sciences) and filled with Dulbecco's modified eagle's medium (DMEM)/F12 (1:1), containing 97% DMEM, 1% fetal bovine serum (FBS), 1% N-2, and 1% ampicillin. Cultures were maintained at 37 °C in an atmosphere containing 5% CO₂ for 1 to 5 days. Microtubule (SiR-tubulin) and DNA (Hoechst) stains were added to cultures 60 minutes and 10 minutes, respectively, prior to AFM measurements and washed out before the start of each experiment.

Atomic Force Microscopy (AFM)

An Echo Revolve Microscope equipped with a standard fluorescence package and Olympus 4x, 10x, 20x and 40x APO objectives was mounted on a passively isolated optical table. A Chiaro Nanoindenter (Optics 11 Life) was affixed to the optical table via the provided pedestal and positioned such that the end of the AFM cantilever was centered in the microscope field of view. A single AFM probe was cleaned with deionized water and 70% EtOH and reused for each experiment to reduce potential probe-probe variability. The optical interference pattern of the probe and a calibration via an indentation on an uncoated glass substrate prior to each experiment was used as a confirmation of probe accuracy and integrity on each experimental day. The indenter was a sphere of 9 μm radius affixed to a cantilever and 0.05 N/m purchased from Optics 11 Life. The laptop, controller and interferometer hardware were operated from a table adjacent to the optical table. Autofluorescence of the bead in the Texas Red channel and SiR tubulin labelling (Cy5 channel) of the pillar and Deiters' cells was used to accurately position the AFM probe over the respective cells. Repeated measurements with 2 μm excursions for a total of 60 μm were used to determine the stiffness of each cell type for each cochlea. The AFM cantilever was positioned over the

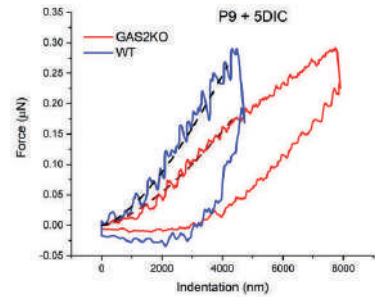
cochlea such that a total piezo travel distance of 15 μm at a speed of 10 $\mu\text{m/s}$ was sufficient to obtain 2–6 μm of indentation into the cells and the stiffness was determined by fitting the first 50% of the indentation curve to the Hertz equation for a spherical indenter, which assumes that the organ of Corti is a homogenous linearly elastic isotropic incompressible material, as previously applied.^{20,34} Fitting was conducted by the Piuma Software (Optics 11 Life).

Representative indentation curves are shown below for inner pillar cells from control and *Gas2^{tm1a/tm1a}* mice at P9 following 5DIC.

The slope of the indentation (top portion of the curve) is fitted to the Hertz equation (dashed lines):

$$F(\delta) = \frac{4}{3} \frac{E}{1 - \nu^2} R^{1/2} \delta^{3/2}.$$

Where F is the force, E is the Young's Modulus, R is the radius of the indenter, and δ is the depth of indentation.



Cochlear vibration measurements

Volumetric optical coherence tomography and vibrometry (VOCTV) was used to image and measure vibrations from the intact mouse cochlea, as described.³⁵ Mice (P42–P47) of either sex were anesthetized with ketamine (80–100 mg/kg) and xylazine (5–10 mg/kg), placed on a heating pad, and the skull was fixed to a custom head-holder with dental cement. A ventrolateral surgical approach was then used to access the left middle ear bulla, which was widely opened so that the otic capsule bone and middle ear ossicles could be visualized. To obtain cross-sectional images of the apical cochlear turn, the source beam was scanned across the otic capsule bone. Sound-evoked vibrations were then measured from one point on the basilar membrane with 100 ms pure-tones presented via a speaker (Fostex FT17H) positioned close to the eardrum. Displacement magnitudes and phases were obtained with stimulus frequencies ranging from 1–15 kHz in 0.5 kHz steps and stimulus levels from 10–80 dB SPL in 10 dB steps. After sacrificing the mouse via anesthetic overdose, the vibration measurements were repeated to collect postmortem data. All displacement responses included in this report were required to have magnitudes falling at least three standard deviations above the mean of the measurement noise floor at surrounding frequencies.³⁶ Significant differences between *Gas2* mutant and control mice were assessed using the non-paired, two-tailed t-test in MATLAB.

DNA sequencing and variant identification

DNA was extracted from peripheral blood samples according to standard procedures. For subjects V.2, V.5, and V.6 exomes were enriched with the Agilent SureSelect Human All Exon V5 kit (Agilent) and whole exome sequencing (WES) was performed on an Illumina HiSeq2000 or 4000 sequencer by BGI Europe. Read alignment, variant calling, variant annotation, and CNV analysis were performed as described.³⁷ Mean 20x coverage of the enriched regions in WES ranged between 95.5 – 97.1%. Initially, 173 genes associated with hearing loss were evaluated in a medical genetics setting, both on shared and individual level (gene list version DG-2.17; Hereditary Hearing Loss Exome Panel Genome Diagnostics Nijmegen-Maastricht). Subsequently, the complete exome was evaluated by selecting variants shared by all three subjects, according to the criteria described below. Segregation analysis of selected variants was carried out by Sanger sequencing, as described.³⁸ Primer sequences are provided in **Table S2**.

Genetic analyses in humans

Candidate variants compliant with recessive inheritance were selected as follows: ≥ 2 variants in a gene, allele frequency $\leq 1\%$ in gnomAD (version 2.1.1), both in combined and African/African American exome datasets, and our in-house WES database ($\sim 15,000$ alleles) and ≥ 5 variant reads, located in exonic regions and (canonical) splice sites. For homozygous variants, per cent variant reads had to be ≥ 80 and for (potentially) compound heterozygous variants ≥ 20 and ≤ 90 . Synonymous variants were evaluated when present in homozygous state or in canonical splice sites. Prediction of a potential deleterious effect of missense variants was performed with CADD PHRED (≥ 15)³⁹, SIFT (≤ 0.05)⁴⁰, PolyPhen-2 (PPH2, ≥ 0.450)⁴¹ and Mutation Taster (deleterious)⁴². Values for predicted deleteriousness are indicated between brackets. Segregation analysis was performed if at least two of the tools predicted a deleterious effect for a homozygous variant or for ≥ 2 potentially compound heterozygous variants in a certain gene. A potential effect on splicing was predicted using the four algorithms (SpliceSiteFinder, MaxEntScan, NNSPLICE, GeneSplicer) available in Alamut Visual (version 2.13, Interactive Biosoftware). A change of $\geq 5\%$ of splice site scores in at least two of the tools was regarded as significant. Also, PPH2 and SIFT scores were determined via Alamut Visual.

Clinical evaluation

Medical history was taken from all study participants and special attention was paid to non-genetic causes of hearing loss (HL) (e.g. perinatal issues or ototoxic medication). The age of onset of HL was congenital when identified at newborn hearing screening or determined by the age at diagnosis.⁴³ Affected subjects underwent general ear, nose and throat examination

and were evaluated for the presence of dysmorphic features by a clinical geneticist. Both affected and unaffected individuals underwent audiometric testing. Pure tone (conditioned play for subject V.7) audiometry, speech audiometry and click-evoked automated brainstem response measurements were performed in a sound-attenuating booth, according to current standards (International Organization for Standardization; ISO 8253-1:2010, ISO 389-1, ISO 389-5 and ISO 389-6).^{37,44} Individuals were considered affected when pure tone thresholds for at least three frequencies were above the frequency-specific 95th percentile of age- and sex-specific thresholds (ISO 7029:2017) for the best hearing ear. The lowest age for which this standard can be applied is 18 years. Audiometric data were described according to the GENDEAF guidelines.⁴⁵ Measurements of transient evoked otoacoustic emissions (TEOAEs) and distortion product (DPOAEs) were performed according to current standards. DPOAE input/output (I/O) functions were measured as described.⁴⁶ Vestibular function was assessed by electronystagmography, calorisation, rotary chair stimulation and video head impulse tests in subjects V.2 and V.5, as described previously.⁴⁷ Subjects V.6 and V.7 underwent video head impulse tests. Unaffected siblings also underwent a video head impulse test, as controls. Subject IV.1 did not participate in clinical evaluations and subject V.1 did not consent for the study.

RT-PCR

Aberrant splicing resulting from the *GAS2* c.723+1G>A variant was experimentally addressed by RT-PCR. For this, B-lymphoblast cells of subjects IV.1, IV.2, and V3-V5 were immortalized by transformation with the Epstein–Barr virus (EBV), as described.^{48,49} Total RNA was isolated from EBV-transformed cells with use of the NucleoSpin RNA II isolation kit (Machery Nagel). Treatment of cells with cycloheximide (CHX, cat. no. C4859, Sigma Aldrich) was performed at a final concentration of 1 µl/mL for 4 hours at 37°C. For cDNA synthesis with the SuperScript IV cDNA synthesis kit (Thermo Fisher), 1 µg RNA was used. RT-PCR was performed with primer combinations listed in **Table S2**, and followed by visualization using agarose gel electrophoresis. *GAPDH* (NM_002046.5) was used as cDNA input control. Sanger sequencing of amplicons was performed.

QPCR

Quantitative PCR (qPCR) was performed with primers designed to detect retention of intron 6 sequences and, for comparison, primers for *GAS2* exons 3-4 and for *GUSB* exons 2-3 (NM_000181) as reference gene (**Table S2**). Primer sets were validated using a dilution series of 4x, 8x, 16x, 32x and 64x of cDNA of individual V.5. The slopes of primer validation plots were between 0.99 and 1.04 with R² values > 0.99. Reaction mixtures were prepared with the GoTaq qPCR Master Mix (Promega) according to the manufacturer's protocol.

Amplifications were performed with the QuantStudio 3 System (Thermo Fisher). Three independent experiments were performed with qPCR reactions in triplicate. Experimental design and data analysis was performed using the QuantStudio Design & Analysis Software 1.4.3. Relative gene expression levels, as compared to *GUSB*, were determined with the ΔCt method.⁵⁰ A one-way ANOVA followed by a least significant difference t-test was employed to identify potentially significant differences.

Quantification and statistical analysis

Statistical analysis was performed using GraphPad Prism 8 software (Graphpad Software Inc.). Normality was assessed using Shapiro-Wilk and Kolmogorov-Smirnov tests. Relevant information for each experiment including sample size, statistical tests and p-values are described in the figure legends. In all cases $P < 0.05$ is considered statistically significant.

Quantification of pillar cell length and distance between hair cells was performed on phalloidin and α -tubulin stained transverse sections and whole mount images using ImageJ. At least two pillar cells were measured per sample from a minimum of three samples taken from the mid-basal turn of the cochlea.

Quantification of detyrosinated α -tubulin fluorescence was performed on binary thresholded images and total white (positive) pixels per unit area was calculated using ImageJ. Six inner and outer pillar cells were measured per sample from a minimum of three samples taken from the mid-basal turn of the cochlea.

Tortuosity measurements were calculated by dividing the actual length of the Deiters' cell phalangeal process by the shortest distance from beginning to end using ImageJ on scanning electron microscope images. Microtubule density was calculated by dividing the total number of microtubules on a given section by the total area of the section (μm^2) from transmission electron microscopy images using ImageJ. Measurements were performed on 3 cells per sample from a minimum of 3 samples taken from the mid-basal turn of the cochlea. Quantification of the area of organized microtubules in pillar and Deiters' cell was performed on transmission electron microscopy images using ImageJ. Microtubules were considered organized if one microtubule was surrounded by eight other equidistant microtubules. Measurements were performed on 3 cells per sample from a minimum of 3 samples taken from the mid-basal turn of the cochlea. Co-localization of GAS2 and dTyr α -tubulin was performed using Imaris 9.3.1 software. The Coloc package was utilized with thresholding and applied uniformly across all images. The data in **Figure 10** are presented as the percent volume B above threshold colocalized, where B is the volume of dTyr α -tubulin. All experiments were replicated in cochleae from at least three independent animals.

RESULTS

GAS2 localizes to supporting cell microtubules in the postnatal cochlea

We identified the *Gas2* gene in a screen for Sonic hedgehog dependent regulators of cochlear development.⁵¹ GAS2 is a member of a conserved family of cytoplasmic proteins that bind microtubules and actin through its GAS2 and Calponin homology domains, respectively (Figure S1A).⁵²⁻⁵⁴ A developmental time course analysis of *Gas2* expression in the inner ear of mouse embryos revealed prominent sites of staining along the medial and lateral walls of the otic vesicle and cochlear duct, marking progenitors of the sensory epithelium and stria vascularis, respectively (Figure S1B-F).

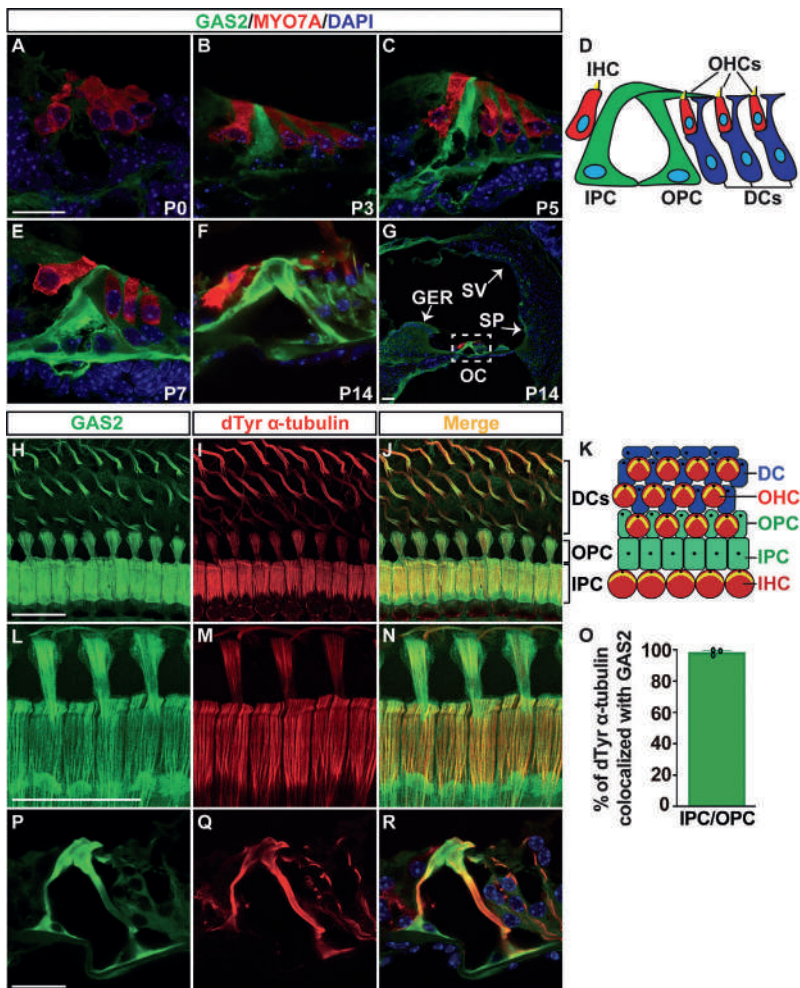


Figure 1. GAS2 localizes to supporting cell microtubules in the postnatal cochlea

Figure 1. (legend) (A-G) Transverse sections through the cochlea at postnatal stages stained for GAS2 (green), the unconventional Myosin VIIA protein (MYO7A), which labels hair cells (red), and the 4', 6-diamidino-2-phenylindole (DAPI) stain, which labels DNA (blue). Within the organ of Corti, GAS2 is expressed in pillar and Deiters' cells and is absent from hair cells. **(D)** Schematic illustration of cell types in the organ of Corti from a transverse view. **(H-Q)** Co-immunostaining of GAS2 and de-Tyrosinated α -tubulin (dTyr α -tubulin) on whole mount cochlear preparations at P14 **(H-J)**, P25 **(L-N)**, and transverse sections through the organ of Corti at P25 **(P-R)**. The high-resolution confocal images (Airyscan) in **(L-N)** show extensive co-localization of GAS2 and dTyr α -tubulin along the length of microtubule bundles in the heads of inner and outer pillar cells, as quantified in **(O)** (one sample T-test, three inner and outer pillar cells were analyzed per sample, from three mice). **(K)** Schematic illustration of cell types in the organ of Corti as viewed from the luminal surface. Scale bar = 20 μ m. Abbreviations: Deiters' cell (DC), greater epithelial ridge (GER), inner hair cell (IHC), inner pillar cell (IPC), organ of Corti (OC), outer hair cell (OHC), outer pillar cell (OPC), spiral prominence (SP), stria vascularis (SV).

Robust GAS2 expression was also detected in the organ of Corti at postnatal stages, including pillar cells at postnatal day 3 (P3), and Deiters' cells at P5 (**Figure 1A-D**). GAS2 staining persisted in inner and outer pillar cells as they separated from each other to form the tunnel of Corti at P7, and as they matured into adulthood (**Figure 1E,F,H,L**). GAS2 expression was also detected in the stria vascularis, spiral prominence, and greater epithelial ridge, and was notably absent from hair cells and spiral ganglion neurons (**Figure 1G**).

Given the presence of dense microtubule bundles in pillar and Deiters' cells, we sought to determine whether GAS2 associates with these cytoskeletal elements by performing co-immunolabeling experiments for GAS2 and α -tubulin on cochlear preparations at P14 and P25. At these stages, the majority of pillar and Deiters' cell microtubules are de-tyrosinated (dTyr) and acetylated (**Figure S1G-L**).^{23,24} Extensive co-localization of GAS2 and dTyr α -tubulin staining was evident along the length of microtubule bundles in the heads of inner and outer pillar cells, as well as Deiters' cell phalangeal processes extending between rows of OHCs (**Figure 1H-O**). Approximately, 98% of the dTyr α -tubulin staining co-localized with GAS2 on microtubule bundles at the apical surface (head) of inner and outer pillar cells (**Figure 1L-O**). Co-localization of GAS2 and dTyr α -tubulin persisted in the head, body and feet of inner and outer pillar cells into adulthood (**Figure 1P-R**). These data suggested a role for GAS2 in the organization of cytoskeletal specializations in cochlear supporting cells.

Gas2^{tm1a/tm1a} mice display hearing loss

To interrogate the function of GAS2 in the inner ear we generated *Gas2* mutant mice using targeted embryonic stem cells from the European Conditional Mouse Mutagenesis Program (**Figure S2A**).⁵⁵ *Gas2^{tm1a/tm1a}* mice are viable and born in the expected Mendelian ratio (**Figure S3F**). Loss of GAS2 expression was confirmed by immunostaining and RNA in situ hybridization on transverse sections through the cochlear duct at E11.5 (**Figure S3A-D**), as well as by western blot on protein extracts isolated from the cochlea at P0 (**Figure S3E**).

Gas2^{tm1a/tm1a} embryos showed no overt signs of inner ear dysmorphology (**Figure S3G,H**). Moreover, hair and supporting cells formed in the correct number and position and

expressed characteristic markers of their identity (**Figure S3K-P**). Spiral ganglion neurons also appeared to innervate appropriate sensory targets (**Figure S3I,J**). Cellular organization in the organ of Corti was maintained after birth in *Gas2^{tm1a/tm1a}* mice, with no deviations in the shape of the tunnel of Corti, length of pillar cells, or distance between inner and outer hair cells (**Figure S4A-L**). We conclude that GAS2 is not required for cochlear morphogenesis, or for the specification of principal inner ear cell types. We next determined whether GAS2 was necessary for hearing by measuring auditory brainstem responses (ABR) to pure tone stimuli in *Gas2^{tm1a/tm1a}* and control mice at two months of age (P56). *Gas2* mutant animals displayed significantly elevated ABR thresholds across all frequencies tested ($p < 0.001$, multiple t-test with Holm-Sidak method, $n = 6$), with the most pronounced threshold shifts (~50dB) detected at higher frequencies (**Figure 2A,B**). These results indicate that *Gas2^{tm1a/tm1a}* mice display severe hearing loss.

The expression of GAS2 in the marginal cell layer of the stria vascularis raised the possibility that defects in this tissue might be responsible for hearing loss in *Gas2* mutants. The stria vascularis is required to maintain the ionic composition of the endolymph and is frequently disrupted in genetic causes of hearing loss.⁵⁶ No differences in the morphology of the stria vascularis, or the expression of layer specific markers were observed between *Gas2^{tm1a/tm1a}* and control mice (**Figures S4M-T**). Moreover, the loss of GAS2 did not alter endocochlear potential, the driving voltage for the hair cell mechanotransduction current, suggesting that the cause of hearing loss in *Gas2^{tm1a/tm1a}* mice is not due to alterations in ion homeostasis (**Figure S4U**).

GAS2 regulates microtubule stability and organization

With no clear indication of alterations in ion transport in *Gas2^{tm1a/tm1a}* mice, we next examined the structure of the microtubule-rich support cells, which are another source of GAS2 expression in the postnatal cochlea. Pillar cell microtubules begin their assembly into bundles soon after birth and take approximately 14 days to fully mature. Pillar cell microtubules elongate from two organizing centers, one that forms at the lateral edge of the pillar cell head and runs parallel to the apical surface, and another that initiates more proximally in the pillar cell head and extends along the length of the body of the cell (**Figure 2C**).²¹

Microtubule growth initiated properly in pillar cells of *Gas2^{tm1a/tm1a}* mice as evaluated by dTyr α -tubulin staining at P5 (**Figure 2D,I,N**). The organization of microtubules into parallel fibers within the heads of inner and outer pillar cells was similar in *Gas2^{tm1a/tm1a}* and control mice at P12 (**Figure 2E,J,O**). In contrast, small gaps in dTyr α -tubulin staining began to appear in the center of inner pillar cell heads from *Gas2^{tm1a/tm1a}* mutants at P14 (**Figure 2F,K,P**). This cytoskeletal defect progressed with age, such that by P25, nearly 70% of microtubules were

depleted from the inner pillar cell heads of *Gas2^{tm1a/tm1a}* mutants, compared to controls (**Figure 2G,L,Q**). Almost all microtubules were lost from inner pillar cell heads at P60, with a small but significant reduction also observed in outer pillar cells (**Figure 2H,M,R**). Thus, GAS2 is required to maintain microtubule bundle stability in pillar cells beginning at P14, coinciding with the onset of hearing in mice. Deiters' cell microtubules were also severely disorganized and less tightly bundled in *Gas2^{tm1a/tm1a}* mice compared to controls, especially at P12 and P14 (**Figure 2E,F,J,K,S,V**). Further analysis by scanning electron microscopy (SEM) revealed that the Deiters' cell phalangeal processes in *Gas2^{tm1a/tm1a}* mutants were buckled and displayed increased tortuosity (**Figure 2T,U,W-Y**).

We further assessed the cytoskeletal ultrastructure of supporting cells by transmission electron microscopy at P25. Inner and outer pillar cells typically possess thousands of densely packed microtubules assembled in a grid like array with each microtubule surrounded by four actin filaments.¹⁸ The number, density and organization of pillar cell microtubules was greatly reduced in *Gas2^{tm1a/tm1a}* mice, and the cross links between microtubule and actin were mostly absent (**Figure 3A-D, A'-D', G-J, M-P, S-V**). Deiters' cell microtubules were also disorganized in *Gas2^{tm1a/tm1a}* mice but the total number did not differ from controls, and yet, microtubule density was still reduced due to the expanded area of the phalangeal process (**Figure 3E,F,E',F',K,L,Q,R,W,X**). These results demonstrate that GAS2 is required to organize the cytoskeletal ultrastructure of pillar and Deiters' cells likely through the formation of microtubule-actin cross links.

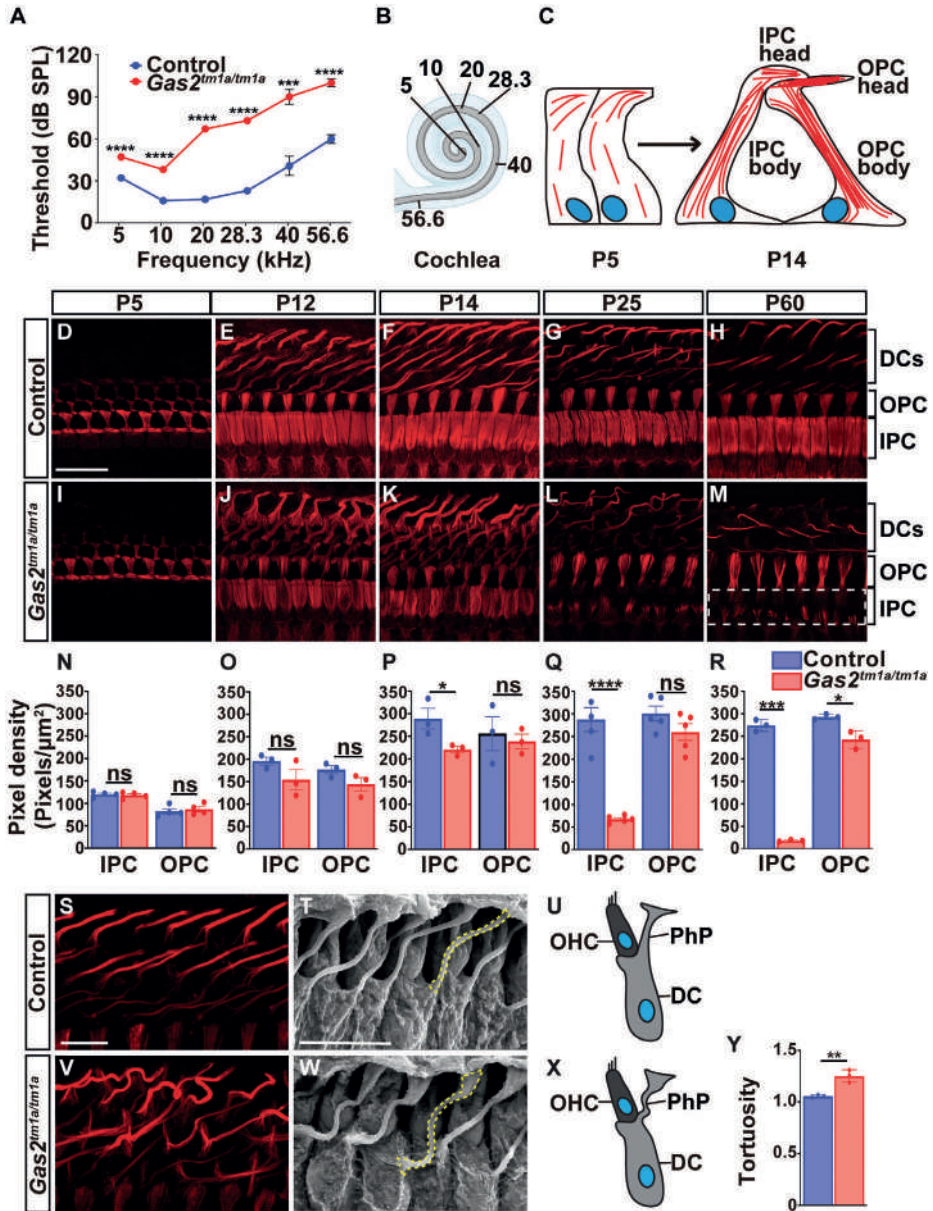


Figure 2. *Gas2^{tm1a/tm1a}* mice display hearing loss and defects in supporting cell microtubules (A) ABR thresholds are elevated in *Gas2^{tm1a/tm1a}* (n=6) compared to control (n=5) mice at P56 (***p<0.001, ****p<0.0001, multiple T-test with Holm-Sidak method). (B) Schematic representation of the tonotopic organization of the cochlear duct. (C) Illustration of microtubule bundle assembly at apical (head) and longitudinal (body) positions of inner and outer pillar cells. Microtubules are drawn in red and the nucleus in blue. (D-M) Time course analysis of dTyr α -tubulin immunostaining on whole mount cochlear preparations from control and *Gas2^{tm1a/tm1a}* mutants. The heads of inner pillar cells show a progressive destabilization of microtubule bundles that are almost completely absent at P60 (dotted white box). (N-R) Quantification of dTyr α -tubulin pixel density

in pillar cells from control and *Gas2^{tm1a/tm1a}* mice presented as mean \pm SEM (* p <0.05, **** p <0.0001, two-tailed t-test, six cells were analyzed per mouse, from a minimum of three mice, ns: not significant). (S,V) Whole mount dTyr α -tubulin immunostaining of cochlear preparations from control and *Gas2^{tm1a/tm1a}* mice at P25 showing microtubule disorganization in Deiters' cell phalangeal processes. SEM images (T,W) and schematic illustrations (U,X) of Deiters' cells from control and *Gas2^{tm1a/tm1a}* mice at P25 showing increased tortuosity of phalangeal processes (yellow dashed line) quantified in (Y) (** p <0.01, two-tailed t-test; four cells were analyzed per sample, n =3, error bars represent SEM). Scale bar = 20 μ m (D), 10 μ m (S), 10 μ m (T). Abbreviations: Deiters' cell (DC), inner pillar cell (IPC), outer pillar cell (OPC), outer hair cell (OHC), phalangeal process (PhP).

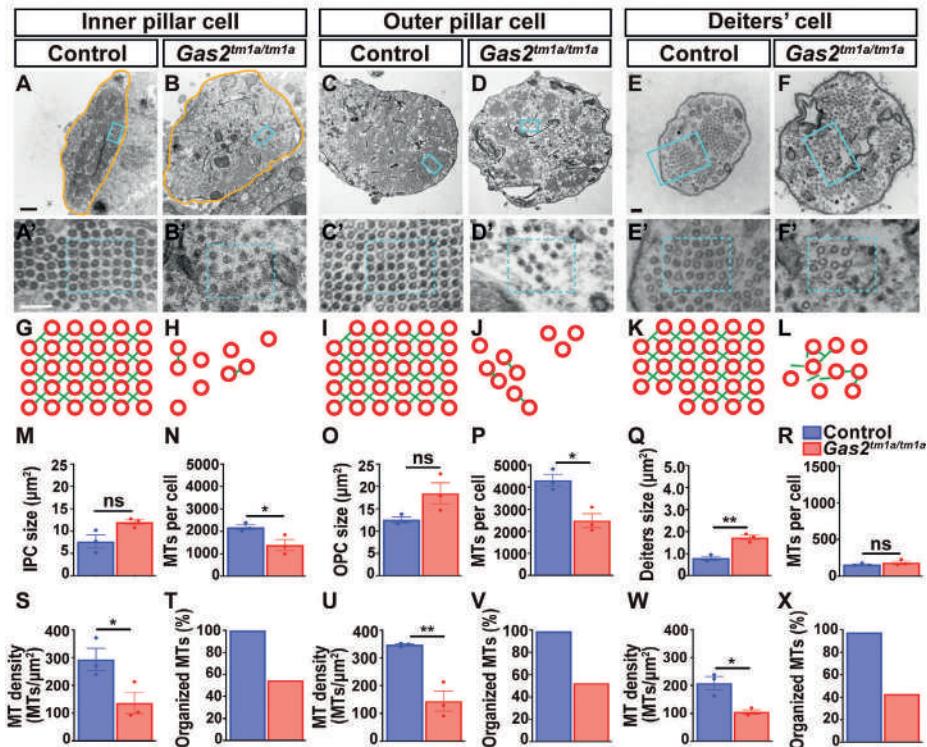


Figure 3. Cytoskeletal ultrastructure is dependent on GAS2 (A-F) Transmission electron micrographs through the body of inner and outer pillar cells, and a Deiters' cell phalangeal process from control and *Gas2^{tm1a/tm1a}* mice at P25. (A'- F') Enlargement of boxed areas from A-F. (G-L) Schematic illustration of cytoskeletal organization corresponding to boxed regions in A'-F'. Note the disorganization and destabilization of microtubule arrays and disruption of actin (green) and microtubule (red) cross-links in *Gas2^{tm1a/tm1a}* mice. (M-X) Quantification of cell size, microtubule number, density and organization in pillar and Deiters' cells presented as mean \pm SEM. (* p <0.05, ** p <0.01, two-tailed t-test, three cells were analyzed per sample, n =3 samples, ns: not significant). Scale bars = 500nm (A), 100nm (A', E, E').

Supporting cells are less stiff in the absence of GAS2

To assess the mechanical consequences of *Gas2* loss, we developed a cochlear explant assay that recapitulates the timing of microtubule destabilization and measured supporting cell stiffness by atomic force microscopy (Figure 4A-C).

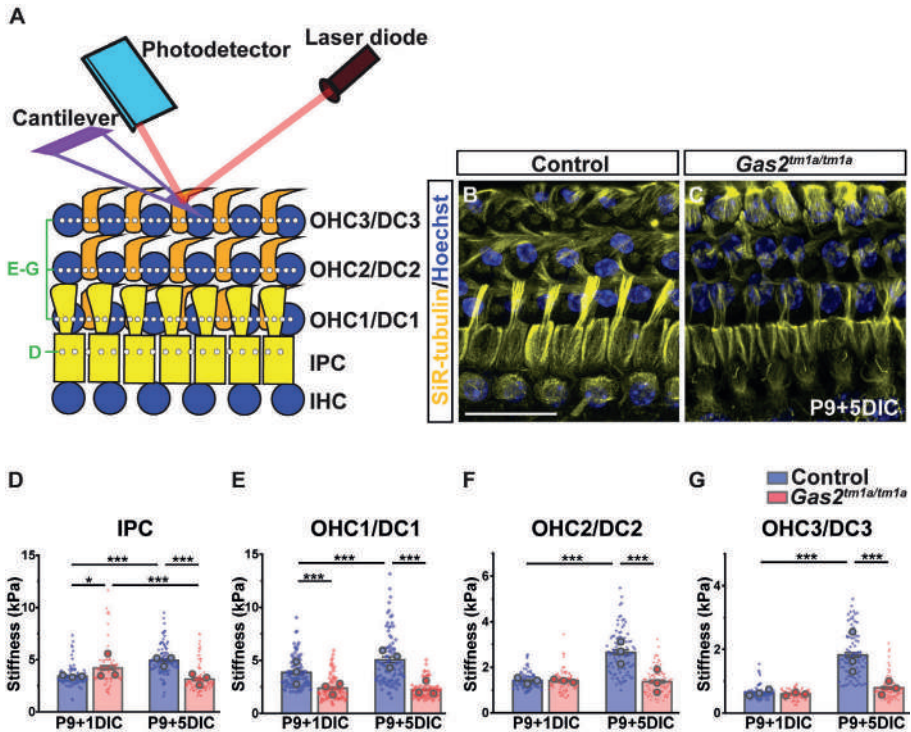


Figure 4. Supporting cells are less stiff in the absence of GAS2 (A) Illustration of experimental approach for measuring supporting cell mechanical properties by AFM. (B, C) Cochlear explants isolated from *Gas2^{tm1a/tm1a}* mice at P9 and grown for 5 days in culture (DIC) recapitulate supporting cell microtubule defects when compared to control mice as indicated by SiR tubulin (yellow) and Hoechst (blue) staining. Scale bar = 20µm (D-G) Quantification of stiffness in pillar cells (D) and individual OHC/Deiters' cell (DC) rows (E-G). The data are presented as mean ±SEM of 30 measurements (diamonds) at 2µm increments along each cell row, which was repeated for all rows in three independent cochlear samples (mean for each cochlea is shown as large circle) (* $p < 10^{-3}$, *** $p < 10^{-6}$, two-way ANOVA on cellular measurements with post hoc Bonferroni comparison, factors of genotype and DIC).

Cochlear explants isolated from control and *Gas2^{tm1a/tm1a}* mice at P9 and grown for one day in culture (P9+1DIC) showed little to no difference in stiffness properties across pillar cells and OHC rows, including regions between OHCs where Deiters' cell phalangeal processes contact the reticular lamina (Figure 4D-G). Whereas, stiffness measurements increased over time from P9+1DIC to P9+5DIC across pillar and OHC rows in control explants, consistent with the normal gain in microtubule density that occurs in postnatal animals, no such increase was observed in *Gas2^{tm1a/tm1a}* samples (Figure 4D-G). These data indicate a critical role for GAS2 in providing cochlear supporting cells with stiff mechanical properties.

OHC amplification is dependent on GAS2 in supporting cells

How might alterations in supporting cell stiffness impact auditory function? Given that both pillar and Deiters' cells provide mechanical support to OHCs and that amplification of basilar membrane vibrations by OHCs is required for hearing, we evaluated *Gas2^{tm1a/tm1a}* mice for defects in OHCs. A small but progressive loss of OHCs was observed in *Gas2^{tm1a/tm1a}* mice, resulting in a 10% decrease in OHC number by P60 (**Figure 5A-K**). This minor reduction in OHCs is unlikely to account for the hearing loss detected in *Gas2^{tm1a/tm1a}* mice.⁵⁷⁻⁵⁹ Moreover, SEM images of OHCs and IHCs showed no obvious differences in stereocilia bundle morphology between *Gas2^{tm1a/tm1a}* and control mice at P60 (**Figure 5L-O**).

Nevertheless, we did detect a significant upregulation in Caveolin 2 (CAV2) expression in OHCs from *Gas2^{tm1a/tm1a}* mice at P25 and P60 (**Figure S5A-I**). Caveolins are plasma membrane proteins and major constituents of lipid-rich caveolae that, among their many proposed roles, act as sensors of mechanical stress in a variety of cell types, including OHCs.⁶⁰⁻⁶² We suspect that the cytoskeletal defects in supporting cells may impose undue mechanical stress on OHCs, thus interfering with their ability to amplify basilar membrane vibrations in *Gas2^{tm1a/tm1a}* mice.

We next measured distortion product otoacoustic emissions (DPOAE), a sensitive readout of OHC amplification and organ of Corti mechanics.⁶³ DPOAEs from control mice showed amplitudes of 20 to 40 dB above the noise floor at f2 frequencies between 10 and 30 kHz, whereas DPOAEs were significantly reduced by 10 to 20 dB in *Gas2^{tm1a/tm1a}* mice (**Figure 5P**). This defect in cochlear function does not appear to be attributed to alterations in the OHC motor protein Prestin, which continues to be expressed in *Gas2^{tm1a/tm1a}* mice (**Figure S5J-O**). Based on these findings, we stipulate that the reduction in supporting cell stiffness in *Gas2^{tm1a/tm1a}* mice interferes with the OHC mediated active process, resulting in hearing loss.

To confirm that the change in cochlear mechanics was indeed attributed to the loss of GAS2 in supporting cells we generated conditional *Gas2* knock out mice (*cGas2*) by first converting the *Gas2^{tm1a}* allele into a *Gas2^{loxP}* allele, and then crossing these mice to an inducible *Sox2^{CreER/+}* line (**Figure S2A-C**). *cGas2* knockout mice (*Sox2^{CreER/+}; Gas2^{loxP/loxP}*) that were administered tamoxifen at early postnatal stages displayed selective loss of GAS2 expression in supporting cells and highly similar inner ear pathology and auditory dysfunction as the constitutive *Gas2^{tm1a/tm1a}* mutants (**Figure S6A-K**). *Sox2^{CreER/+}* is also active in hair cells at early postnatal stages.⁶⁴ However, GAS2 is not expressed in hair cells at any of the postnatal stages examined (**Figure 1 and S6**), alleviating concern that *Sox2^{CreER}* mediated recombination in hair cells might confound these results. Therefore, we conclude that the postnatal expression of GAS2 in supporting cells is required for OHC amplification.

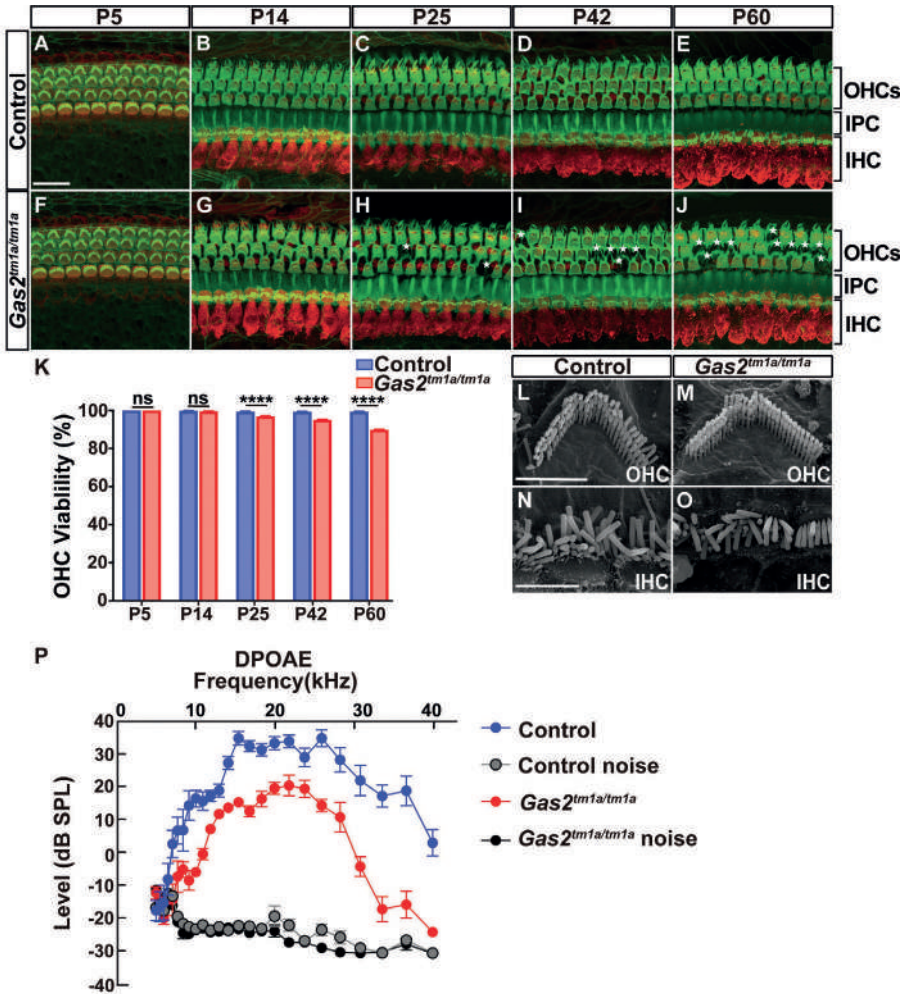


Figure 5. Outer hair cell function is compromised in *Gas2^{tm1a/tm1a}* mice (A-J) Time course analysis of MYO7A (red) and F-actin (green) immunostaining on whole mount cochlear preparations from control and *Gas2^{tm1a/tm1a}* mice (n=3 per timepoint). A small number of OHCs are lost over time (indicated by asterisk). Scale bar = 20µm. **(K)** Quantification of OHC viability (****P<0.001, Fisher’s Exact Test, ns: not significant). **(L-O)** SEM images of OHCs (L, M) and IHCs (N, O) from control and *Gas2^{tm1a/tm1a}* mice at P60, showing normal stereocilia morphology. Scale bars = 3µm (L) and 5µm (P). **(P)** DPOAEs are significantly reduced in *Gas2^{tm1a/tm1a}* (n=5) compared to control mice (n=6) at P56 (p<0.05, multiple T-test with Holm-Sidak method). Abbreviations: inner hair cell (IHC), inner pillar cell (IPC), outer hair cells (OHCs), and outer pillar cell (OPC). Abbreviations: inner hair cell (IHC), inner pillar cell (IPC), outer hair cells (OHCs), and outer pillar cell (OPC).

Transmission of sound evoked vibrations is impaired in *Gas2^{tm1a/tm1a}* mice

If pillar and Deiters’ cells act as structural scaffolds to support the mechanical properties of the organ of Corti, then destabilization of their cytoskeletal network should interfere with the transfer of mechanical vibrations through the cochlear partition. To formally test this

premise, we measured vibratory responses to sound in live mice using volumetric optical coherence tomography and vibrometry (VOCTV).³⁵ First, we imaged the apical turn of the mouse cochlea *in vivo*. The cochlear anatomy of wild type mice imaged using VOCTV has been thoroughly documented.^{35,65-68} We found that the cochlear anatomy of *Gas2^{tm1a/tm1a}* mice appeared grossly normal (**Figure 6A,B**). In particular, the morphology of the three cochlear scalae, Reissner's membrane (RM), the basilar membrane (BM), and the tectorial membrane (TM) were all indistinguishable from what is found in wild type mice.

Vibratory responses to sound stimuli were then measured from the basilar membrane within the apical turn to produce tuning curves. Data from one representative control and *Gas2^{tm1a/tm1a}* mouse are shown (**Figure 6C,D**). The sensitivity was calculated by dividing the displacement magnitude by the intensity of the sound stimulus. Control mice had the typical pattern of non-linear gain with sharper tuning and higher sensitivity for low intensity stimuli, termed cochlear amplification. While the same pattern was found in *Gas2^{tm1a/tm1a}* mice, the amount of gain was lower. In fact, vibratory responses to 10- and 20-dB sound pressure level (SPL) stimuli were below the noise floor in *Gas2^{tm1a/tm1a}* mutants, whereas they were easily measured in control mice. Postmortem, within each mouse, the sensitivity curves all overlapped, demonstrating the expected loss of cochlear amplification in both controls and mutants. In both live and dead mice, the vibration of the basilar membrane exhibited a progressive phase lag as the sound frequency was increased, consistent with traveling wave propagation (**Figure 6C,D**).

We then averaged the vibratory responses from nine control and eight *Gas2^{tm1a/tm1a}* mutant mice (**Figure 6E,F**). Within each cohort, the vibratory characteristics appeared quite similar as evidenced by the small SEM. The characteristic frequency (CF) of the measurement location, which is the frequency of maximal vibration to the lowest intensity stimuli, was similar between the cohorts (mean \pm SEM for the control and *Gas2^{tm1a/tm1a}* mutant were 8.8 ± 0.1 kHz and 8.4 ± 0.11 kHz, respectively; $p=0.21$). However, the reduced gain in the *Gas2^{tm1a/tm1a}* mutants was again notable by the lack of responses to 10- and 20-dB SPL stimuli. Next, we converted the averaged displacement data to sensitivity from the two cohorts, overlapped the responses, and assessed for differences between them (**Figure 6G,H**). Several notable features were observed. First, live *Gas2^{tm1a/tm1a}* mutants were found to have lower gain than live control mice. This was quantified as a difference in the change in sensitivity between 40-80 stimuli at the CF ($p=0.003$). Second, vibratory sensitivities to lower frequency stimuli were more level- and frequency-dependent for live control than live *Gas2^{tm1a/tm1a}* mice, such that the onset of the nonlinearity was at $\sim 0.5CF$ for the control whereas this was $\sim 0.7CF$ for the *Gas2^{tm1a/tm1a}* mutant.

We quantified this as a difference in the gain at 0.7 CF ($p=0.01$). Thus, the frequency range over which cochlear amplification occurs on the basilar membrane is reduced in *Gas2* mutants. Third, there was no difference in the sharpness of the tuning curves between the genotypes. We tested for this by calculating the Q_{10dB} , the frequency at the peak divided by the bandwidth

at 10 dB below the peak. We compared the $Q_{10\text{dB}}$ for live and dead mice to determine whether this was related to cochlear amplification, however the results demonstrated no significant differences (live: $p=0.44$; dead: $p=0.56$). Fourth, the phase slope at the CF was steeper in *Gas2^{tm1a/tm1a}* compared to control mice ($p=0.0013$). The rate of change of the phase with respect to the frequency corresponds to the travelling wave group delay. This result indicates that the traveling wave propagates more slowly near the CF in *Gas2^{tm1a/tm1a}* mutant mice and that there is less longitudinal coupling. This was found in both the live and dead conditions (Figure 6G).

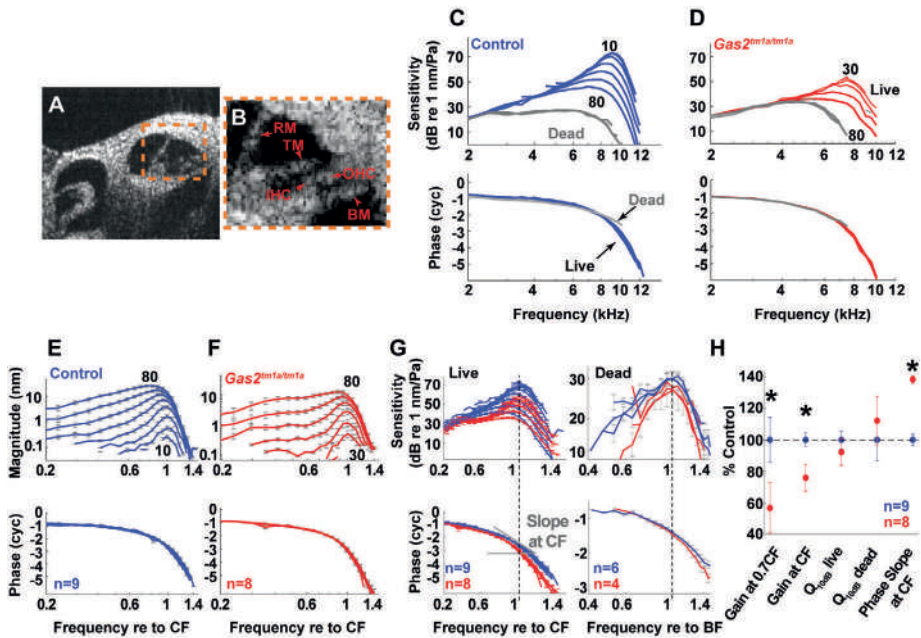


Figure 6. Vibratory responses to sound are impaired in live *Gas2^{tm1a/tm1a}* mice (A) Cross-sectional image of the apical cochlear duct of a mouse obtained with VOCTV. (B) Enlargement of organ of Corti (boxed region in A); BM, basilar membrane; IHC, inner hair cell; OHC, outer hair cell; RM, Reissner's membrane; TM, tectorial membrane. (C-D) BM sensitivity and phase for one control (blue) and one *Gas2^{tm1a/tm1a}* (red) mouse. The numbers indicate the highest and lowest stimulus intensities that produced measurable vibratory responses. Postmortem data (60-80 dB SPL) are in gray. (E-F) Average displacements and phases of the BM motions for control ($n=9$) and *Gas2^{tm1a/tm1a}* ($n=8$) mice. Frequencies are normalized to the CF of each individual mouse and error bars indicate the SEM. (G) The averaged vibratory sensitivity and phases of BM motion for live and dead mice are compared in control (blue) and *Gas2^{tm1a/tm1a}* (red) mice. The frequencies are normalized to the corresponding CF and best frequency (BF) for live and dead data, respectively. Data from live mice show that *Gas2^{tm1a/tm1a}* mutants have less amplification near CF and sharper phase change with increasing frequency. Data from dead mice (80 dB SPL) also show sharper phase change for *Gas2^{tm1a/tm1a}* mutants. (H) Mean values of sensitivity change from 40 to 80 dB SPL at 0.7CF, CF, and $Q_{10\text{dB}}$ for live (40 dB SPL stimuli) and dead (80 dB SPL stimuli) mice, and phase slope (for 40 dB SPL at the CF) as a percentage of the appropriate control mean. Asterisks denote $p<0.05$.

Whole exome sequencing (WES) identifies *GAS2* mutations in a family with hearing loss

To determine if *GAS2* is associated with hearing loss in humans, we screened families with unsolved cases of hereditary sensorineural hearing loss for mutations in *GAS2*. Four male siblings, born from consanguineous parents of Somalian descent, presented with early onset high frequency hearing loss at the Department of Clinical Genetics, Amsterdam University Medical Center (**Figure 7A**). Two brothers (V.6 and V.7) were diagnosed with hearing loss at birth and two others (V.2 and V.5) were diagnosed at one year of age. All affected subjects had delayed speech and language development. Medical history did not indicate any non-genetic causes of hearing impairment. Physical examinations did not reveal any abnormalities or dysmorphic characteristics.

Audiometry showed symmetrical bilateral (high frequency) hearing loss in subjects V.2 and V.5-V.7 (**Figure 7B and S7A**). Hearing in subject V.2 showed mild progression over time for the lower frequencies. Subjects IV.2, V.3, and V.4 had normal hearing for their age (**Table S3**). Oto-acoustic emissions were present in unaffected subjects and absent in affected subjects, except for transient evoked emissions in subject V.7 (**Table S3**). Click-evoked automated brainstem response and speech audiometry in affected subjects did not indicate retrocochlear pathology. Vestibular testing in the affected subjects V.2 and V.5-V.7 revealed normal vestibular function, comparable to that in the unaffected subjects V.3 and V.4.

Medical genetic testing revealed no pathogenic variants or copy number variants (CNVs) in 173 genes on the hereditary hearing loss gene panel. Subsequently, an 'open-the-exome' analysis was carried out to identify variants that were shared by subjects V.2, V.5 and V.6. This revealed a single rare homozygous variant, a nucleotide substitution in a canonical splice donor site in intron 6 of *GAS2* Chr11(GRCh37/hg19): g.22777500G>A; NM_005256.3:c.723+1G>A; p.? (**Figure 7C**). The *GAS2* variant segregated in the homozygous state with hearing loss in the family (**Figure 7A,D**). The unaffected parents were heterozygous for the *GAS2* variant. The variant is not reported in gnomAD (v.2.1.1) or the in-house WES dataset (>15,000 exomes) at Radboud University Medical Center. No further (likely) pathogenic *GAS2* variants were identified in WES data of ~800 index cases with hearing loss. Two compound heterozygous variants in *TMPRSS4* were also found to segregate with hearing loss in the family, however, *TMPRSS4* is not known to function in the inner ear and has very low expression in the cochlea (gEAR portal, <https://umgear.org/>), and was therefore not considered further.

The effect of the c.723+1G>A variant on *GAS2* splicing was evaluated by RT-PCR on RNA isolated from EBV-transformed cells from the parents (IV.1, IV.2), unaffected siblings (V.3, V.4) and affected subject (V.5) (**Figure S7B**). Almost no wild type splicing was observed between exons 6 and 7 in subject V.5, resulting in retention of intron 6 (**Figure S7B**). The

proportion of *GAS2* transcripts that retained intron 6 was significantly higher in affected compared to unaffected siblings, with intermediate levels observed in the heterozygous parents (Figure 7E).

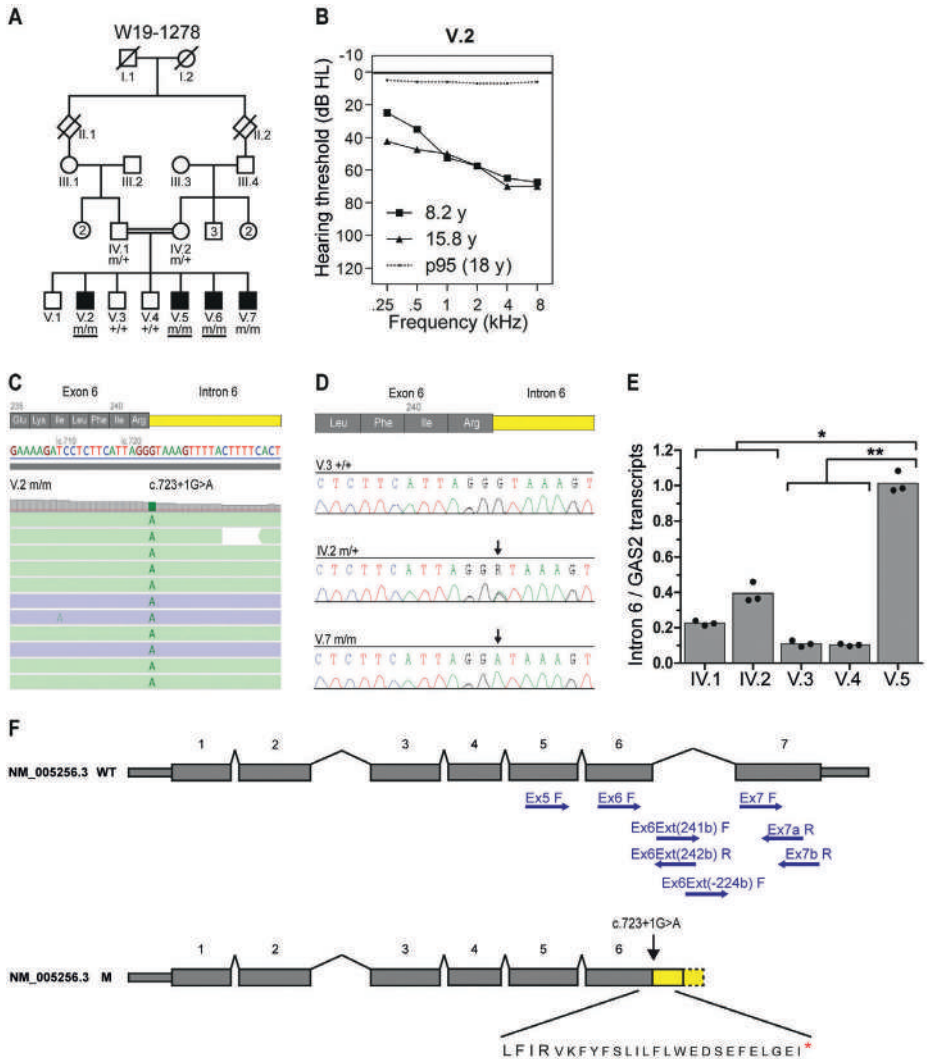


Figure 7. Human *GAS2* mutations associate with hearing loss (A) Pedigree of family W19-1278. Whole exome sequencing was performed in subjects with an underlined genotype. m, mutant *GAS2* c.723+1G>A; +, wild type (B) Average air conduction thresholds for both ears from subject V.2 measured at 8.2 and 15.8 years of age (y). The dotted line represents the 95th percentile of age- and sex-specific hearing level at the age of 18 years. This is the lowest age for which the ISO 7029:2017 standard can be applied. dB HL, decibel hearing level; kHz, kilohertz. (C) Analysis of WES paired-reads demonstrating a homozygous single nucleotide variant, *GAS2* c.723+1G>A, in subject V.2. (D) Sequences of exon6-intron6 boundaries amplified from genomic DNA of unaffected subjects V.3 and IV.2 and affected subject V.7. Arrows indicate the position of the c723+1G>A variant.

4.3

Figure 7. (legend continued) **(E)** Bar graph showing the genotype-dependence of intron 6 retention. Depicted are the ratios of relative levels of transcripts with intron 6 retention and relative levels of total GAS2 transcript. The dots represent the means of three independent experiments performed in triplicate (*p-value = 0.021; **p-value = 0.013). No statistically significant difference (p-value = 0.137) was observed between the parents and the unaffected offspring. **(F)** Schematic representation of GAS2 transcript NM_005256.3 and the effects of the c723+1G>A variant on exon 6 splicing. The positions of primers used in RT-PCR are indicated (see **Table S2** for primer combinations and sequences). Predicted amino acid sequence, including in frame stop codon (red asterisk), resulting from intron 6 retention is shown below the mutant transcript. Abbreviations: wild type (WT), mutant (M).

The mutant GAS2 transcripts are predicted to encode for a truncated GAS2 protein that terminates translation prematurely within the GAS2 domain due to the presence of an in-frame stop codon (TGA) at position c.723+67-69 (**Figure 7F**). These results, supported by our findings in mice, identify mutations in GAS2 as a cause of hearing loss.

DISCUSSION

Our study identifies GAS2 as a cytoskeletal regulatory protein that provides cochlear supporting cells with stiffness properties for transmitting mechanical forces through the cochlear partition in response to sound. We demonstrate that GAS2 is a structural MAP required for the organization and stabilization of microtubule bundles in pillar and Deiters' cells and the formation of cross-links with actin filaments. This GAS2 dependent microtubule bundling activity equips pillar and Deiters' cells with a rigid but flexible cytoskeletal framework for transferring forces from the basilar membrane to the reticular lamina, which are then amplified by OHCs. Consequently, *Gas2* mutations in mice and humans cause hearing loss through a mechanism that alters the way the traveling wave propagates along the cochlea.

Physiological role of GAS2 in hearing

OHCs generate force to selectively amplify basilar membrane traveling waves that peak at characteristic frequencies along the cochlear duct.⁵ Our work indicates that, in both the live and dead conditions, sound-induced vibration in one area of the basilar membrane causes the more apical regions to move less in *Gas2*^{tm1a/tm1a} compared to control mice. In other words, there is less longitudinal coupling in *Gas2* mutants. This conclusion stems mostly from the difference in the phase slopes between the two genotypes. The steeper phase slope in dead *Gas2* mutant compared to dead control mice means that the traveling wave is slower, a feature of reduced longitudinal coupling. In the live condition, this additionally manifests as a smaller frequency range over which cochlear amplification occurs (i.e. the 0.7CF vs 0.5CF difference). One feature of reduced longitudinal coupling that we did not detect was sharper tuning, which would have been indicated by a larger $Q_{10\text{dB}}$ in *Gas2*^{tm1a/tm1a} mutants. This is not surprising given that cochlear tuning includes multiple components beyond supporting cell

stiffness, such as the degree of amplification and the mechanical properties of the basilar membrane, tectorial membrane, and surrounding cochlear fluids.^{65,66,69-73}

Nevertheless, compared to *Prestin*^{-/-} mutants that lack OHC electromotility, the fundamental mechanism of power production continues to exist in *Gas2*^{tm1a/tm1a} mice, albeit at reduced capacity (**Figure 6C-F**).^{65,74,75} Thus, our data show that the supporting cell dysfunction in *Gas2* mutant mice reduces longitudinal coupling so that less OHCs are involved in amplifying the traveling wave. An additional explanation for the defects in cochlear amplification is that the reduced stiffness of Deiters' cell phalangeal processes fails to buffer OHCs from compressive forces. This premise is consistent with our observation that OHCs from *Gas2*^{tm1a/tm1a} mice display increased mechanical stress (**Figure S5A-I**). Similarly, the altered mechanical impedance of the organ of Corti may reduce power transfer from the OHC to the cochlear partition, thus impeding the feedback loop that drives cochlear amplification.⁵ Finally, another possibility is that the reduced stiffness of the Deiters' cell phalangeal processes impacts the feed-forward mechanism, a hypothetical role for these cells.^{6,9} These pathogenic mechanisms are not mutually exclusive and either one or all might explain the reduction in DPOAEs in mice with constitutive or conditional mutations in *Gas2*.

Our data also provide experimental evidence in favor of predictions made from mathematical models of cochlear micromechanics.⁸⁻¹² These models emphasize the importance of the organ of Corti cytoarchitecture, including the Y shaped configuration of Deiters' cells and OHCs for cochlear amplification. Taken together, these data lend further support to our conclusion that the distortion of Deiters' cells hinders cochlear amplification in *Gas2* mutant mice and contributes to hearing loss.

GAS2 is required for cytoskeletal cross-links in cochlear supporting cells

In addition to demonstrating the physiological importance of the supporting cell cytoskeleton for hearing, our data reveal that the organization and stabilization of the dense microtubule networks in pillar and Deiters' cells are dependent on GAS2 mediated cross-linking activity. In the absence of GAS2, supporting cell microtubules are no longer tethered to actin, resulting in their disarray over time. Our finding that stiffness was reduced in pillar and Deiters' cells from *Gas2* mutants prior to the exacerbation of the cytoskeletal phenotype emphasizes the importance of this cross-linking activity for supporting cell mechanical properties, in agreement with theoretical models.⁷

Similar cytoskeletal disorganization has been described in neurons upon the loss of MAPs, especially those with cross-linking activity.⁷⁶⁻⁷⁹ Interestingly, the GAS2 family member, GAS2L1, also regulates actin – microtubule crosstalk during axonal maturation.⁸⁰ Association of the GAS2 domain with microtubules causes disinhibition of the CH domain, allowing GAS2L1 to simultaneously interact with actin filaments. The GAS2L1 dependent stabilization

of F-actin filaments in rat hippocampal neurons was shown to promote axon branching, while restricting outgrowth. Thus, GAS2 family members constitute a group of structural MAPs with cytoskeletal organizing properties that influence diverse cellular and physiological processes.

While pillar and Deiters' cells are both dependent on GAS2 for the organization of microtubules into grid like arrays, only pillar cell microtubules break down over time. It is unclear what accounts for this difference. MAPs regulate microtubule dynamics through a variety of means, including the stimulation of microtubule growth, the inhibition of microtubule depolymerization, or the shielding of microtubules from severing enzymes.⁷⁹ It is conceivable that the differential expression or activity of factors regulating microtubule dynamics accounts for the cell type specific differences in microtubule stability. Interestingly, the pillar and Deiters' cell microtubules that persist in *Gas2* mutants remain detyrosinated and acetylated. Therefore, not only are these α -tubulin post translational modifications not dependent on GAS2 for their deposition, but they do not appear to be responsible for the loss of pillar cell microtubules, despite their known roles in microtubule stability and flexibility.²⁵⁻²⁷ It is also possible that since pillar cells serve as a hinge point during basilar membrane vibrations they are subject to deformation, causing microtubules to break in the absence of GAS2.⁸¹⁻⁸⁴

Human GAS2 mutations associate with hearing loss

The significance of our study is further heightened by the discovery that *GAS2* mutations segregate with hearing loss in a human pedigree. It is intriguing that hearing loss was more pronounced at higher frequencies in both humans and mice with *GAS2* mutations, suggesting a common pathogenic mechanism. In addition to hearing loss, female *Gas2* mutant mice also exhibit reduced fertility.⁸⁵ The combination of hearing loss in both sexes and reduced fertility in females has been described in humans with Perrault syndrome, a rare recessive disorder with a genetically heterogeneous etiology.⁸⁶⁻⁸⁸ The cause of Perrault syndrome remains unidentified in 60% of cases, suggesting the likely involvement of additional genes.⁸⁷ *GAS2* is a plausible candidate given the phenotypic overlap between *Gas2* mutant mice and Perrault syndrome patients. However, since no affected females were present in the pedigree in our study, further investigation of exomes from genetically unconfirmed cases of Perrault syndrome will be needed to determine if mutations in *GAS2* are linked to this condition.

Limitations of the study

While the body of evidence provided in this study supports our principle conclusion that supporting cell stiffness is required for cochlear mechanics, the precise mechanism by which *GAS2* mediates cytoskeletal cross-linking activity in pillar and Deiters' cells remains

uncertain. Further experimentation will be needed to determine if microtubule arrays are directly cross-linked to actin by GAS2, or whether they occur through interactions with additional MAPs. Furthermore, we cannot rule out the possibility that GAS2 expression in other inner ear cell types may also play a role in auditory function. For instance, interrogation of single cell RNA-seq datasets in the gEAR portal (<https://umgear.org/>) indicates that *Gas2* is also expressed in cochlear hair cells, albeit at a level that falls below our detection by immunostaining or in situ hybridization. The generation of conditional mutants that selectively delete *Gas2* in hair cells will be needed to determine if sensory cell types also require GAS2 for hearing.

ACKNOWLEDGEMENTS

We thank Dr. Jean Richa and his staff at the Transgenic and Chimeric Mouse Facility (Perelman School of Medicine, University of Pennsylvania) for assistance with transgenic mouse production. We also thank Biao Zuo and Yuri Veklich at the Electron Microscopy Resources Lab (Perelman School of Medicine, University of Pennsylvania) for assistance with TEM and SEM preparations. Use of confocal microscopes (CDB microscopy core, Perelman School of Medicine, University of Pennsylvania) under the supervision of Dr. Andrea Stout, is greatly appreciated.

The contributions of Thadé P.M. Goderie for collection and analysis of human audiometric data, Helger G. Yntema for medical genetic testing of patients, Saskia van der Velde-Visser for EBV transformation and cell culture, and Jailynn Harke for protein co-localization analysis are greatly appreciated.

COLLABORATORS

The DOOFNL consortium is a Dutch nationwide collaboration on hereditary hearing loss and consists of M.F. van Dooren, S.G. Kant, H.H.W. de Gier, E.H. Hoefsloot, M.P. van der Schroeff (ErasmusMC, Rotterdam, the Netherlands), L.J.C. Rotteveel, F.G. Ropers (LUMC, Leiden, the Netherlands), J.C.C. Widdershoven, J.R. Hof, E.K. Vanhoutte (MUMC+, Maastricht, the Netherlands), I. Feenstra, H. Kremer, C.P. Lanting, R.J.E. Pennings, H.G. Yntema (Radboudumc, Nijmegen, the Netherlands), R.H. Free and J.S. Klein Wassink-Ruiter (UMCG, Groningen, the Netherlands), R.J. Stokroos, A.L. Smit, M.J. van den Boogaard (UMC, Utrecht, the Netherlands) and F.A. Ebbens, S.M. Maas, A. Plomp, T.P.M. Goderie, P. Merkus and J. van de Kamp (Amsterdam UMC, Amsterdam, the Netherlands). The consortium contributed to the clinical evaluation and medical genetic testing of ~800 unsolved index cases of hearing loss.

REFERENCES

1. Bekesy, G. *Experiments in Hearing*, (McGraw-Hill, New York, 1960).
2. Fettiplace, R. Hair Cell Transduction, Tuning, and Synaptic Transmission in the Mammalian Cochlea. *Compr Physiol* 7, 1197-1227 (2017).
3. Yu, W.M. & Goodrich, L.V. Morphological and physiological development of auditory synapses. *Hear Res* 311, 3-16 (2014).
4. O. Maoileidigh D & Ricci, A.J. A Bundle of Mechanisms: Inner-Ear Hair-Cell Mechanotransduction. *Trends Neurosci* 42, 221-236 (2019).
5. Fisher, J.A., Nin, F., Reichenbach, T., Uthaiiah, R.C. & Hudspeth, A.J. The spatial pattern of cochlear amplification. *Neuron* 76, 989-97 (2012).
6. Geisler, C.D. & Sang, C. A cochlear model using feed-forward outer-hair-cell forces. *Hear Res* 86, 132-46 (1995).
7. Tolomeo, J.A. & Holley, M.C. Mechanics of microtubule bundles in pillar cells from the inner ear. *Biophys J* 73, 2241-7 (1997).
8. Nam, J.H. & Fettiplace, R. Force transmission in the organ of Corti micromachine. *Biophys J* 98, 2813-21 (2010).
9. Yoon, Y.J., Steele, C.R. & Puria, S. Feed-forward and feed-backward amplification model from cochlear cytoarchitecture: an interspecies comparison. *Biophys J* 100, 1-10 (2011).
10. Liu, Y., Gracewski, S.M. & Nam, J.H. Consequences of Location-Dependent Organ of Corti Micro-Mechanics. *PLoS One* 10, e0133284 (2015).
11. Motallebzadeh, H., Soons, J.A.M. & Puria, S. Cochlear amplification and tuning depend on the cellular arrangement within the organ of Corti. *Proc Natl Acad Sci U S A* 115, 5762-5767 (2018).
12. Sasmal, A. & Grosh, K. Unified cochlear model for low- and high-frequency mammalian hearing. *Proc Natl Acad Sci U S A* 116, 13983-13988 (2019).
13. Pritchard, U. The Development of the Organ of Corti. *J Anat Physiol* 13, 99-103 (1878).
14. Slepecky, N.B. Structure of the mammalian cochlea. in *The Cochlea* (eds. Dallos PJ, Popper AN & Fay RR) 44-129 (Springer-Verlag, New York, 1996).
15. Soons, J.A., Ricci, A.J., Steele, C.R. & Puria, S. Cytoarchitecture of the mouse organ of corti from base to apex, determined using in situ two-photon imaging. *J Assoc Res Otolaryngol* 16, 47-66 (2015).
16. Angelborg, C. & Engstrom, H. Supporting elements in the organ of Corti. I. Fibrillar structures in the supporting cells of the organ of Corti of mammals. *Acta Otolaryngol Suppl* 301, 49-6 (1972).
17. Slepecky, N. & Chamberlain, S.C. Distribution and polarity of actin in inner ear supporting cells. *Hear Res* 10, 359-70 (1983).
18. Zetes, D.E., Tolomeo, J.A. & Holley, M.C. Structure and mechanics of supporting cells in the guinea pig organ of Corti. *PLoS One* 7, e49338 (2012).
19. Sugawara, M., Ishida, Y. & Wada, H. Mechanical properties of sensory and supporting cells in the organ of Corti of the guinea pig cochlea--study by atomic force microscopy. *Hear Res* 192, 57-64 (2004).

20. Szarama, K.B., Gavara, N., Petralia, R.S., Kelley, M.W. & Chadwick, R.S. Cytoskeletal changes in actin and microtubules underlie the developing surface mechanical properties of sensory and supporting cells in the mouse cochlea. *Development* 139, 2187-97 (2012).
21. Tucker, J.B. *et al.* Formation of two microtubule-nucleating sites which perform differently during centrosomal reorganization in a mouse cochlear epithelial cell. *J Cell Sci* 108 (Pt 4), 1333-45 (1995).
22. Muroyama, A. & Lechler, T. Microtubule organization, dynamics and functions in differentiated cells. *Development* 144, 3012-3021 (2017).
23. Slepecky, N.B., Henderson, C.G. & Saha, S. Post-translational modifications of tubulin suggest that dynamic microtubules are present in sensory cells and stable microtubules are present in supporting cells of the mammalian cochlea. *Hear Res* 91, 136-47 (1995).
24. Saha, S. & Slepecky, N.B. Age-related changes in microtubules in the guinea pig organ of Corti. Tubulin isoform shifts with increasing age suggest changes in micromechanical properties of the sensory epithelium. *Cell Tissue Res* 300, 29-46 (2000).
25. Robison, P. *et al.* Detyrosinated microtubules buckle and bear load in contracting cardiomyocytes. *Science* 352, aaf0659 (2016).
26. Portran, D., Schaedel, L., Xu, Z., Thery, M. & Nachury, M.V. Tubulin acetylation protects long-lived microtubules against mechanical ageing. *Nat Cell Biol* 19, 391-398 (2017).
27. Xu, Z. *et al.* Microtubules acquire resistance from mechanical breakage through intraluminal acetylation. *Science* 356, 328-332 (2017).
28. Arima, T., Uemura, T. & Yamamoto, T. Cytoskeletal organization in the supporting cell of the guinea pig organ of Corti. *Hear Res* 24, 169-75 (1986).
29. Oshima, T., Okabe, S. & Hirokawa, N. Immunocytochemical localization of 205 kDa microtubule-associated protein (205 kDa MAP) in the guinea pig organ of Corti. *Brain Res* 590, 53-65 (1992).
30. Dougherty, G.W. *et al.* CLAMP, a novel microtubule-associated protein with EB-type calponin homology. *Cell Motil Cytoskeleton* 62, 141-56 (2005).
31. Zheng, J. *et al.* Marshalin, a microtubule minus-end binding protein, regulates cytoskeletal structure in the organ of Corti. *Biol Open* 2, 1192-202 (2013).
32. Nissim, S., Allard, P., Bandyopadhyay, A., Harfe, B.D. & Tabin, C.J. Characterization of a novel ectodermal signaling center regulating Tbx2 and Shh in the vertebrate limb. *Dev Biol* 304, 9-21 (2007).
33. Martin, P. & Swanson, G.J. Descriptive and experimental analysis of the epithelial remodellings that control semicircular canal formation in the developing mouse inner ear. *Dev Biol* 159, 549-58 (1993).
34. Katsuno, T. *et al.* TRIOBP-5 sculpts stereocilia rootlets and stiffens supporting cells enabling hearing. *JCI Insight* 4(2019).
35. Lee, H.Y. *et al.* Noninvasive in vivo imaging reveals differences between tectorial membrane and basilar membrane traveling waves in the mouse cochlea. *Proc Natl Acad Sci U S A* 112, 3128-33 (2015).
36. Kim, S., Oghalai, J.S. & Applegate, B.E. Noise and sensitivity in optical coherence tomography based vibrometry. *Opt Express* 27, 33333-33350 (2019).
37. Smits, J.J. *et al.* De novo and inherited loss-of-function variants of ATP2B2 are associated with rapidly progressive hearing impairment. *Hum Genet* 138, 61-72 (2019).
38. Wesdorp, M. *et al.* MPZL2, Encoding the Epithelial Junctional Protein Myelin Protein Zero-like 2, Is Essential for Hearing in Man and Mouse. *Am J Hum Genet* 103, 74-88 (2018).

39. Kircher, M. *et al.* A general framework for estimating the relative pathogenicity of human genetic variants. *Nat Genet* 46, 310-5 (2014).
40. Vaser, R., Adusumalli, S., Leng, S.N., Sikic, M. & Ng, P.C. SIFT missense predictions for genomes. *Nat Protoc* 11, 1-9 (2016).
41. Adzhubei, I.A. *et al.* A method and server for predicting damaging missense mutations. *Nat Methods* 7, 248-9 (2010).
42. Schwarz, J.M., Cooper, D.N., Schuelke, M. & Seelow, D. MutationTaster2: mutation prediction for the deep-sequencing age. *Nature Methods* 11, 361-362 (2014).
43. van der Ploeg, C.P., Uilenburg, N.N., Kauffman-de Boer, M.A., Oudesluys-Murphy, A.M. & Verkerk, P.H. Newborn hearing screening in youth health care in the Netherlands: National results of implementation and follow-up. *Int J Audiol* 51, 584-90 (2012).
44. Bosman, A.J. & Smoorenburg, G.F. Intelligibility of Dutch CVC syllables and sentences for listeners with normal hearing and with three types of hearing impairment. *Audiology* 34, 260-84 (1995).
45. M. Mazzoli, G.V.C., V. Newton, N. Giarbini, F. Declau, A. Parving. Recommendations for the description of genetic and audiological data for families with nonsyndromic hereditary hearing impairment. (2003).
46. Neely, S.T., Johnson, T.A., Kopun, J., Dierking, D.M. & Gorga, M.P. Distortion-product otoacoustic emission input/output characteristics in normal-hearing and hearing-impaired human ears. *J Acoust Soc Am* 126, 728-38 (2009).
47. Oonk, A.M. *et al.* Vestibular function and temporal bone imaging in DFNB1. *Hear Res* 327, 227-34 (2015).
48. Collin, R.W. *et al.* Antisense Oligonucleotide (AON)-based Therapy for Leber Congenital Amaurosis Caused by a Frequent Mutation in CEP290. *Mol Ther Nucleic Acids* 1, e14 (2012).
49. Wall, F.E., Henkel, R.D., Stern, M.P., Jenson, H.B. & Moyer, M.P. An efficient method for routine Epstein-Barr virus immortalization of human B lymphocytes. *In Vitro Cell Dev Biol Anim* 31, 156-9 (1995).
50. Pfaffl, M.W. A new mathematical model for relative quantification in real-time RT-PCR. *Nucleic Acids Res* 29, e45 (2001).
51. Muthu, V. *et al.* Genomic architecture of Shh-dependent cochlear morphogenesis. *Development* 146(2019).
52. Brancolini, C., Bottega, S. & Schneider, C. Gas2, a growth arrest-specific protein, is a component of the microfilament network system. *J Cell Biol* 117, 1251-61 (1992).
53. Zhang, T., Dayanandan, B., Rouiller, I., Lawrence, E.J. & Mandato, C.A. Growth-arrest-specific protein 2 inhibits cell division in *Xenopus* embryos. *PLoS One* 6, e24698 (2011).
54. Stroud, M.J. *et al.* GAS2-like proteins mediate communication between microtubules and actin through interactions with end-binding proteins. *J Cell Sci* 127, 2672-82 (2014).
55. Testa, G. *et al.* A reliable lacZ expression reporter cassette for multipurpose, knockout-first alleles. *Genesis* 38, 151-8 (2004).
56. Locher, H. *et al.* Development of the stria vascularis and potassium regulation in the human fetal cochlea: Insights into hereditary sensorineural hearing loss. *Dev Neurobiol* 75, 1219-40 (2015).
57. Hamernik, R.P., Patterson, J.H., Turrentine, G.A. & Ahroon, W.A. The quantitative relation between sensory cell loss and hearing thresholds. *Hear Res* 38, 199-211 (1989).
58. Chen, G.D. & Fechter, L.D. The relationship between noise-induced hearing loss and hair cell loss in rats. *Hear Res* 177, 81-90 (2003).

59. Chen, G.D., Tanaka, C. & Henderson, D. Relation between outer hair cell loss and hearing loss in rats exposed to styrene. *Hear Res* 243, 28-34 (2008).
60. Sinha, B. *et al.* Cells respond to mechanical stress by rapid disassembly of caveolae. *Cell* 144, 402-13 (2011).
61. Anzai, T. *et al.* Deformation of the Outer Hair Cells and the Accumulation of Caveolin-2 in Connexin 26 Deficient Mice. *PLoS One* 10, e0141258 (2015).
62. Echarri, A. *et al.* An Abl-FBP17 mechanosensing system couples local plasma membrane curvature and stress fiber remodeling during mechanoadaptation. *Nat Commun* 10, 5828 (2019).
63. Kemp, D.T. Otoacoustic emissions, their origin in cochlear function, and use. *Br Med Bull* 63, 223-41 (2002).
64. Walters, B.J., Yamashita, T. & Zuo, J. Sox2-CreER mice are useful for fate mapping of mature, but not neonatal, cochlear supporting cells in hair cell regeneration studies. *Sci Rep* 5, 11621 (2015).
65. Gao, S.S. *et al.* Vibration of the organ of Corti within the cochlear apex in mice. *J Neurophysiol* 112, 1192-204 (2014).
66. Dewey, J.B. *et al.* Mammalian Auditory Hair Cell Bundle Stiffness Affects Frequency Tuning by Increasing Coupling along the Length of the Cochlea. *Cell Rep* 23, 2915-2927 (2018).
67. Kim, J., Xia, A., Grillet, N., Applegate, B.E. & Oghalai, J.S. Osmotic stabilization prevents cochlear synaptopathy after blast trauma. *Proc Natl Acad Sci U S A* 115, E4853-E4860 (2018).
68. Dewey, J.B., Applegate, B.E. & Oghalai, J.S. Amplification and Suppression of Traveling Waves along the Mouse Organ of Corti: Evidence for Spatial Variation in the Longitudinal Coupling of Outer Hair Cell-Generated Forces. *J Neurosci* 39, 1805-1816 (2019).
69. Legan, P.K. *et al.* A targeted deletion in alpha-tectorin reveals that the tectorial membrane is required for the gain and timing of cochlear feedback. *Neuron* 28, 273-85 (2000).
70. Robles, L. & Ruggero, M.A. Mechanics of the mammalian cochlea. *Physiol Rev* 81, 1305-52 (2001).
71. Russell, I.J. *et al.* Sharpened cochlear tuning in a mouse with a genetically modified tectorial membrane. *Nat Neurosci* 10, 215-23 (2007).
72. Karavitaki, K.D. & Mountain, D.C. Evidence for outer hair cell driven oscillatory fluid flow in the tunnel of corti. *Biophys J* 92, 3284-93 (2007).
73. Nankali, A., Wang, Y., Strimbu, C.E., Olson, E.S. & Grosh, K. A role for tectorial membrane mechanics in activating the cochlear amplifier. *Sci Rep* 10, 17620 (2020).
74. Liberman, M.C. *et al.* Prestin is required for electromotility of the outer hair cell and for the cochlear amplifier. *Nature* 419, 300-4 (2002).
75. Dallos, P. *et al.* Prestin-based outer hair cell motility is necessary for mammalian cochlear amplification. *Neuron* 58, 333-9 (2008).
76. Sanchez-Soriano, N. *et al.* Mouse ACF7 and drosophila short stop modulate filopodia formation and microtubule organisation during neuronal growth. *J Cell Sci* 122, 2534-42 (2009).
77. Ka, M. & Kim, W.Y. Microtubule-Actin Crosslinking Factor 1 Is Required for Dendritic Arborization and Axon Outgrowth in the Developing Brain. *Mol Neurobiol* 53, 6018-6032 (2016).
78. Hahn, I., Voelzmann, A., Liew, Y.T., Costa-Gomes, B. & Prokop, A. The model of local axon homeostasis - explaining the role and regulation of microtubule bundles in axon maintenance and pathology. *Neural Dev* 14, 11 (2019).

79. Bodakuntla, S., Jijumon, A.S., Villablanca, C., Gonzalez-Billault, C. & Janke, C. Microtubule-Associated Proteins: Structuring the Cytoskeleton. *Trends Cell Biol* 29, 804-819 (2019).
80. van de Willige, D. *et al.* Cytolinker Gas2L1 regulates axon morphology through microtubule-modulated actin stabilization. *EMBO Rep* 20, e47732 (2019).
81. Nilsen, K.E. & Russell, I.J. The spatial and temporal representation of a tone on the guinea pig basilar membrane. *Proc Natl Acad Sci U S A* 97, 11751-8 (2000).
82. Fridberger, A., Boutet de Monvel, J. & Ulfendahl, M. Internal shearing within the hearing organ evoked by basilar membrane motion. *J Neurosci* 22, 9850-7 (2002).
83. Chan, D.K. & Hudspeth, A.J. Mechanical responses of the organ of corti to acoustic and electrical stimulation in vitro. *Biophys J* 89, 4382-95 (2005).
84. Ni, G., Elliott, S.J. & Baumgart, J. Finite-element model of the active organ of Corti. *J R Soc Interface* 13, 20150913 (2016).
85. York, J.P. *et al.* Growth Arrest Specific 2 (GAS2) is a Critical Mediator of Germ Cell Cyst Breakdown and Folliculogenesis in Mice. *Sci Rep* 6, 34956 (2016).
86. Chatzispayrou, I.A. *et al.* A homozygous missense mutation in ERAL1, encoding a mitochondrial rRNA chaperone, causes Perrault syndrome. *Hum Mol Genet* 26, 2541-2550 (2017).
87. Newman, W.G., Friedman, T.B., Conway, G.S. & Demain, L.A.M. Perrault Syndrome. in *GeneReviews* (eds. Adam, M.P. *et al.*) (University of Washington, Seattle, Seattle (WA), 2018).
88. Tucker, E.J. *et al.* Genomic sequencing highlights the diverse molecular causes of Perrault syndrome: a peroxisomal disorder (PEX6), metabolic disorders (CLPP, GGPS1), and mtDNA maintenance/translation disorders (LARS2, TFAM). *Hum Genet* 139, 1325-1343 (2020).

SUPPLEMENTARY METHODS

KEY RESOURCES TABLE

REAGENT or RESOURCE	SOURCE	IDENTIFIER
Antibodies(dilution)		
Mouse monoclonal anti-GAS2(F12) (1:400)	Santa Cruz	Cat#sc-398669
Rabbit anti-GAS2 (1:1000)	Abcam	Cat#b109762
Rabbit anti-MYO7A (1:350)	Proteus Biosc.	Cat#25-6790
Rabbit anti Detyrosinated-tubulin (1:200)	Abcam	Cat#ab48389
Mouse anti-Alpha-tubulin (1:400)	Cell Signaling	3873
Mouse anti-Acetylated-tubulin (1:400)	Sigma	Cat#T6793
Rabbit anti-SOX2 (1:200)	Chemicon	Cat#AB5603
Mouse anti-Neurofilament (1:400)	DSHB	Cat#2H3
Goat anti-KCNQ1 (1:300)	Santa Cruz	Cat#sc-10646
Mouse anti-ATP1A1 (1:250)	DSHB	Cat#A5
Rat anti-CD44 (1:200)	BD Pharmingen	Cat#sc-10646
Rabbit anti-Claudin-11 (1:100 + AR)	Novex	Cat#364500
Mouse anti-Connexin-26/GJB2 (1:200)	Thermo Fisher	Cat#710500
Mouse anti-CAV2 (1:800)	BD	Cat#610684
Mouse anti-Prestin (1:200)	Santa Cruz	Cat#sc-293212
Mouse anti-GAPDH(1:1000)	Invitrogen	Cat# MA5-15738
Hoechst (1:1000)	Thermo Fisher	Cat#62249
Rabbit anti-goat IGG Alexa488 (1:400)	Molecular probes	Cat#11078
Donkey anti-rat Alexa488 (1:400)	Molecular probes	Cat#21208
Goat anti-mouse Alexa488 (1:400)	Molecular probes	Cat#A28175
Goat anti-rabbit Alexa594 (1:400)	Molecular probes	Cat#A11037
IRDye® 680LT Goat anti-Mouse IgG (1:20000)	LI-COR	925-68020
IRDye® 800CW Goat anti-Rabbit IgG (1:20000)	LI-COR	925-32211
*AR, antigen retrieval – boil for 6 minutes in 10mM citric acid buffer (pH 6.0)		
Chemicals, Peptides, and Recombinant Proteins		
Phalloidin conjugated Alexa488 (1:400)	Molecular Probes	A-12379
Odyssey® Blocking Buffer	LI-COR	927-40000
Tamoxifen	Sigma	T5648
GoTaq qPCR MasterMix	Promega	A6002
SuperScript™ IV Reverse Transcriptase	Thermo Fisher	18090010
Critical Commercial Assays		
SiR-tubulin kit (1:1000)	Cytoskeleton, Inc	Cat#CY-SC002
Experimental Models: Cell Lines		
Mouse: Gas2tm1a(EUCOMM)Hmgu	https://www.eummc.org	HEPD0681_7_F03

Experimental Models: Organisms/Strains		
Mouse: Gas2tm1a/+	This paper	N/A
Mouse: B6.129S4-Gt(ROSA)26Sortm2(FLP*)Sor/J [FLPo (B6 ROSA26Flpo)]	The Jackson Labs	012930
Mouse: Gas2tm1c/tm1c	This paper	N/A
Mouse: Sox2creER	The Jackson Labs	017593
Oligonucleotides		
Genotyping primers for Gas2 alleles, see Table S1	This paper	N/A
Primers for qPCR of GAS2 cDNA, see Table S2	This paper	N/A
Software and Algorithms		
ImageJ	NIH	https://imagej.nih.gov/ij/
Prism 8	GraphPad	N/A
QuantStudio Design & Analysis Software 1.4.3	Thermo Fisher	N/A
Alamut Visual 2.13	Interactive Biosoftware	N/A
Other		
Leica TCS SP8 MP system	Leica	https://www.leica-microsystems.com/products/confocal-microscopes/p/leica-tcs-sp8-mp/downloads/
FEI Quanta 250 SEM	FEI	http://www.biotech.iastate.edu/wp_single/wp-content/uploads/2012/01/quanta.pdf
Jeol-1010 transmission electron microscope TEM	JEOL	https://iubemcenter.indiana.edu/equipment/microscopes/jeol-jem-1010/index.html
Zeiss LSM 880 with Fast Airyscan module	Zeiss	https://www.zeiss.com/microscopy/us/dynamic-content/news/2014/news-lsm-880.html

SUPPLEMENTARY TABLES

Table S1. Primer sets for genotyping mouse *Gas2* alleles

Fragment	Oligonucleotides	RT-PCR size wildtype (bp)	RT-PCR size mutant (bp)
5' arm	Reverse: GAAGTTCCTATTCCGAAGTTCCT	7076	-
	Reverse: CTGCCTGTGTTGAATGTTCTCAT		
3' arm	Forward: CCTGCTTGCCGAATATCATGG	6493	-
	Reverse: ACTTCTGTGGAGTCTCAGCTC		
Tm1a/Loxp	Forward: TTGGATCATATGGAGAGAGCCAT	223	257
	Reverse: GGGCATATCACAGGCCATA		
Tm1c	Forward: GGCGCATAACGATACCACGA	-	208
	Reverse: TATAAGCCGCCTACTGCGAC		
<i>Gas2</i> -LacZ	Forward: AGAACAAGCAACATGCGCTC	-	611
	Reverse: GACCTTGGGACCACCTCATC		
<i>Gas2</i> -Neo	Forward: CTCCCCCTGAACCTGAAACATA	-	360
	Reverse: TTATATAAGCCGCCTACTGCGA		
<i>cGas2</i> -Cre	Forward: GCGGCATGGTGCAAGTTGAAT	-	232
	Reverse: CGTTCACCGCATCAACGTTT		

Table S2. Primer sequences

Fragment	Primer name in Figure 7 and Supplementary Figure 1	Oligonucleotides	RT-PCR size wildtype (bp)	RT-PCR size mutant (bp)
Primers for amplification and sequence analysis of genomic DNA				
GAS2 exon 6	NA	Forward: GATGTCTTTGGGCCTGAAC	-	-
	NA	Reverse: GATCTCCATGGTGTCTTTGGTG		
Primers for RT-PCR and sequence analysis of GAS2 transcript				
GAS2 exon 5 - exon 7	Ex5 F	Forward: TTCTGCCCTTCTCCTTCAC	294	-
	Ex7a R	Reverse: ACACGGGAGATCTGCAGC		
GAS2 exon 6 - exon 7	Ex6 F	Forward: GTTCTGTGTGGAGCGGCTC	171	-
	Ex7a R	Reverse: ACACGGGAGATCTGCAGC		
GAS2 exon 5 - exon 6 extension c.723+242	Ex5 F	Forward: TTCTGCCCTTCTCCTTCAC	-	450
	Ex6Ext(242b) R	Reverse: TCACAAGTGGAAAGCCTTCTTC		
GAS2 exon 6 - exon 6 extension c.723+242	Ex 6 F	Forward: GTTCTGTGTGGAGCGGCTC	-	327
	Ex6Ext(242b) R	Reverse: TCACAAGTGGAAAGCCTTCTTC		
GAS2 exon 6 extension c.723+241 - exon 7	Ex6Ext(241b) F	Forward: TGAAGAAGGCTTCCACTTGTG	-	-
	Ex7a R	Reverse: ACACGGGAGATCTGCAGC		
GAS2 exon 6 extension c.724-224 - exon 7	Exon6Ext(- 224b) F	Forward: ACAGCAAAGCTGGGTTCTGG	-	331
	Ex7a R	Reverse: ACACGGGAGATCTGCAGC		
GAS2 exon 7 – exon 7	Ex7 F	Forward: TGCTGCACAACAAACATGTC	216	-
	Ex7b R	Reverse: GGCAGAGACCACCAAGTAG		
GAPDH exon 7 - 8 (NM_002046.5)	NA	Forward: CTGCACCACCACTGCTTAG	219	-
	NA	Reverse: AGCTCAGGGATGACCTTGC		
Primers for qPCR of GAS2 cDNA				
GAS2 exon 3 - 4	NA	Forward: ATCCTGGTGCCGAGATTTAGG	-	-
	NA	Reverse: CACACTTCTCTGGGTTGCTTG		
GAS2 exon 6 - exon 6Ext	NA	Forward: GTGGGAGAAAAGATCCTCTTC	-	-
	NA	Reverse: GAAGTTCCTGCTCTTATCTGTC		
GUSB exon 2 - 3 (NM_000181.4)	NA	Forward: AGAGTGGTGTGAGGATTGG	-	-
	NA	Reverse: CCCTCATGCTCTAGCGTGTC		

GAS2 reference sequence: NM_005256.3. (RT-)PCR was performed with annealing temperatures decreasing from 62.5 to 57.5 °C for 30 cycles. qPCR was performed with an annealing temperature of 60.0 °C.

Table S3. Individual results of newborn hearing screening, otoscopic examination, otoacoustic emissions and audiometry

Family	Subject	Newborn screening	Age of HL first detected (y)	Otoscopic examination	Otoacoustic emissions			PTA		SRT		Maximum SRS (%)	
					TEOA	DPOAE	I/O	R	L	R	L	R	L
W19-1278	IV.2	NA	NA	NT	present	present	present	8	5	NT	NT	NT	NT
	V.2	NT	1	N	absent	absent	absent	58	60	50	42	94	97
	V.3	NA	NA	NT	present	present	present	5	5	NT	NT	NT	NT
	V.4	NA	NA	NT	present	present	present	2	0	NT	NT	NT	NT
	V.5	P	1	N	absent	absent	absent	58	58	47	NT	93	98
	V.6	F	0	N	absent	absent	absent	60	62	45	50	95	95
	V.7	F	0	N	present	absent	absent	52	55	NT	NT	NT	NT

Age of onset (AoO), age of onset in years as reported by the subjects. Age at hearing test, the age at which the audiometric data of column 9 to 14 were obtained, in general the last audiogram. If no speech audiometry was performed during the latest pure tone audiometry, the latest audiogram in which both were measured, was selected. TEOAE, transient evoked otoacoustic emissions; DPOAE, distortion product otoacoustic emissions; I/O, DPOAE input/output functions; y, years; PTA, pure tone average, mean of 0.5, 1 and 2 kHz air conduction thresholds; SRT, speech reception threshold; SRS, speech recognition score in %; R, right; L, left; NA, not applicable; NT, not tested; N, normal; P, pass; F, fail.

4.3

SUPPLEMENTARY FIGURES

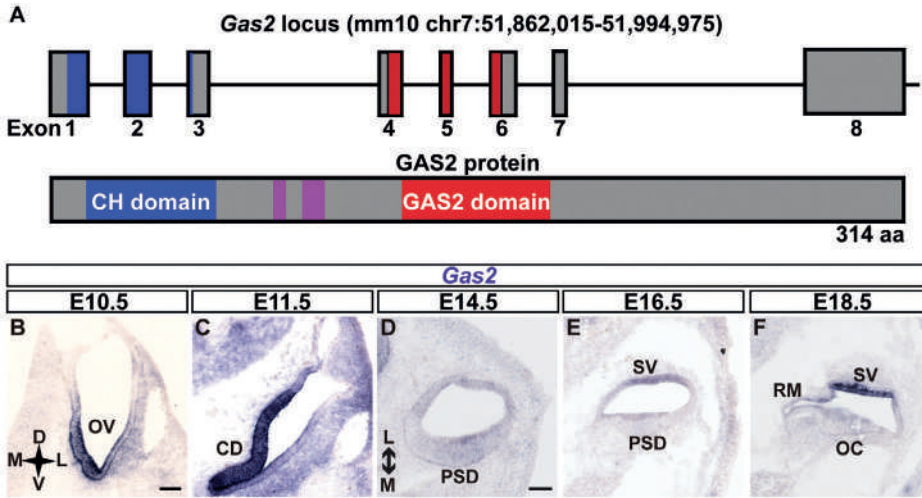


Figure S1. *Gas2* is expressed in the developing cochlea (A) Schematic of the mouse *Gas2* gene and encoded protein highlighting the positions of the calponin homology (CH) and *Gas2* domains. (B-F) Transverse sections through the inner ear showing the spatial and temporal patterns of *Gas2* expression during mouse embryonic development. Scale bar = 100 μ m (B, C), 50 μ m (D-F). Abbreviations: CD, cochlear duct; D, dorsal, L, lateral; M, medial; PSD, prosensory domain; OC, organ of Corti; OV, otic vesicle; RM, Reissner's membrane; SV, stria vascularis; V, ventral.

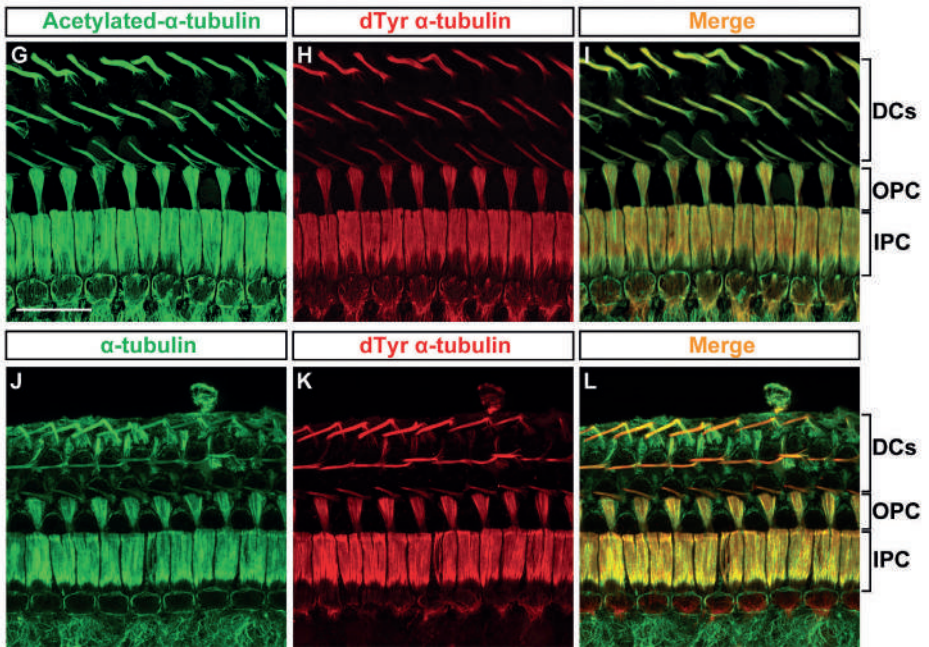


Figure S2. Pillar and Deiters' cell microtubules are extensively acetylated and detyrosinated (A-F) Whole mount immunostaining of cochlear preparations (P14) with antibodies against acetylated α -tubulin and dTyr α -tubulin (A-C), and pan α -tubulin and dTyr α -tubulin (D-F). The majority of microtubules in support cells are both acetylated and detyrosinated. Scale bar = 20 μ m.

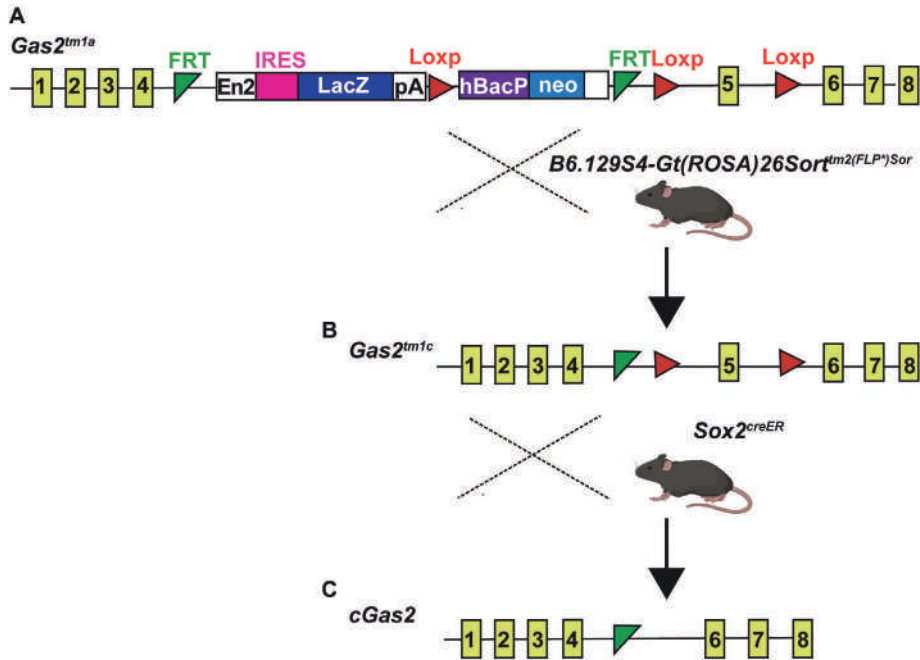


Figure S3. Breeding scheme to generate *Gas2* mutant alleles (A) Schematic of the *Gas2* knockout first allele (*Gas2*^{tm1a}) generated by the European Conditional Mouse Mutagenesis Program. (B) The *Gas2* floxed allele (*Gas2*^{tm1c}) was generated by crossing *Gas2*^{tm1a/+} mice with a FLPo deleter strain and selecting progeny with loxp sites surrounding exon 5. (C) Conditional *Gas2* knockout mice (*cGas2*) were generated by crossing *Gas2*^{tm1c/tm1c} mice with an inducible Sox2^{CreER} line, which selectively deletes *Gas2* in support cells upon tamoxifen administration.

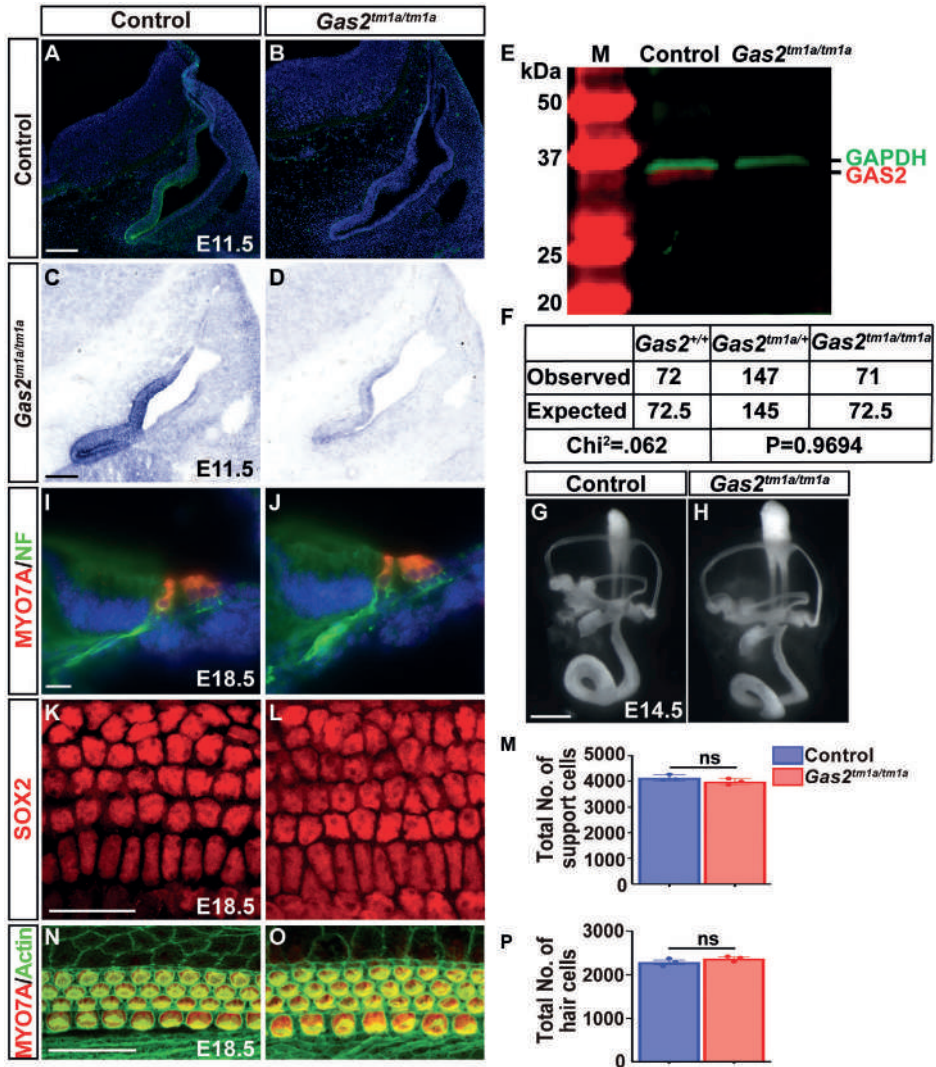


Figure S4. Inner ear development is unaffected by loss of Gas2 (A-D) Transverse sections through the otic vesicle showing the loss of Gas2 protein (A,B) and *Gas2* mRNA (C,D) in *Gas2*^{tm1a/tm1a} embryos compared to controls (n=3). (E) Western blot showing loss of Gas2 expression (red band) in relation to GAPDH (green band) in cochlea from *Gas2*^{tm1a/tm1a} embryos compared to controls (P0) (n=3). (F) Table displaying the observed genotypes of progeny from *Gas2*^{tm1a/+} intercrosses at the time of weaning, which fit the expected Mendelian ratios. (G-H) Paint fills of control and *Gas2*^{tm1a/tm1a} inner ears at E14.5 revealed no difference in morphology (n=3). (I-J) Transverse sections through the cochlea stained with markers of hair cells (Myo7a) and spiral ganglia (NF, neurofilament) show normal patterns of innervation between control and *Gas2*^{tm1a/tm1a} embryos at E18.5. (K-P) Whole mount immunostaining of cochlear preparations show no differences in the number of Sox2 positive support cells (K-M), or Myo7a, Phalloidin/F-actin positive hair cells (N-P) between control and *Gas2*^{tm1a/tm1a} embryos at E18.5. (M,P) Quantification of the total number of hair and support cells is represented as mean \pm SD [ns = not significant, $p=0.2373$ (M), $p=0.2156$ (P), two-sided t-test, n=3]. Scale bar = 100 μ m, (A-H), 10 μ m (I-J), 20 μ m (K-O).

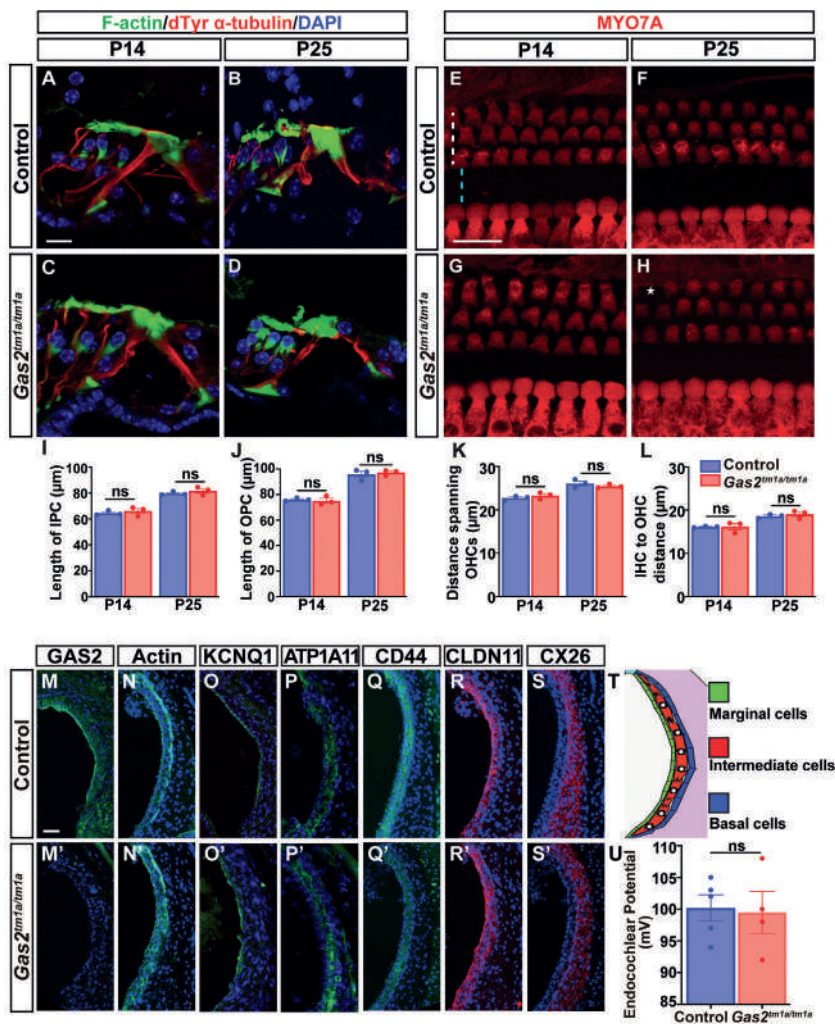


Figure S5. Cellular organization in the organ of Corti and stria vascularis is maintained in postnatal *Gas2^{tm1a/tm1a}* mice (A-D) Transverse sections through the cochlea of control and *Gas2^{tm1a/tm1a}* mice at P14 (A, E) and P25 (B, F) stained for F-actin (green), dTyr α -tubulin (red) and DAPI (blue) to reveal inner and outer pillar cell morphology. (E-H) Whole mount cochlear preparations from control and *Gas2^{tm1a/tm1a}* mice at P14 (E, G) and P25 (F, H) immunostained for Myo7a (red) to reveal inner and outer hair cell rows. (I-J) The length of IPCs and OPCs were not significantly different between control and *Gas2^{tm1a/tm1a}* mice (represented as mean \pm SEM, ns=not significant, Student's t-test, n=3). Scale bar = 20 μ m. (K-L) The distance between OHC rows (dashed white line in E) and the distance between inner and outer hair cell rows (dashed blue line in E) was not significantly different between control and *Gas2^{tm1a/tm1a}* mice (represented as mean \pm SEM, ns=not significant, Student's t-test, n=3). (M-S') Transverse sections through the stria vascularis of control (M-S) and *Gas2^{tm1a/tm1a}* (M'-S') mice at P25 stained with layer specific markers as schematized in (T). Despite the loss of Gas2 in the marginal cell layer, no other markers were differentially expressed between control and *Gas2^{tm1a/tm1a}* mice. (U) Endocochlear potential measurements between control (n=5) and *Gas2^{tm1a/tm1a}* (n=4) mice were not significantly different (represented as mean \pm SEM, ns=not significant, p=0.8556, two-tailed t-test). Scale bar = 25 μ m.

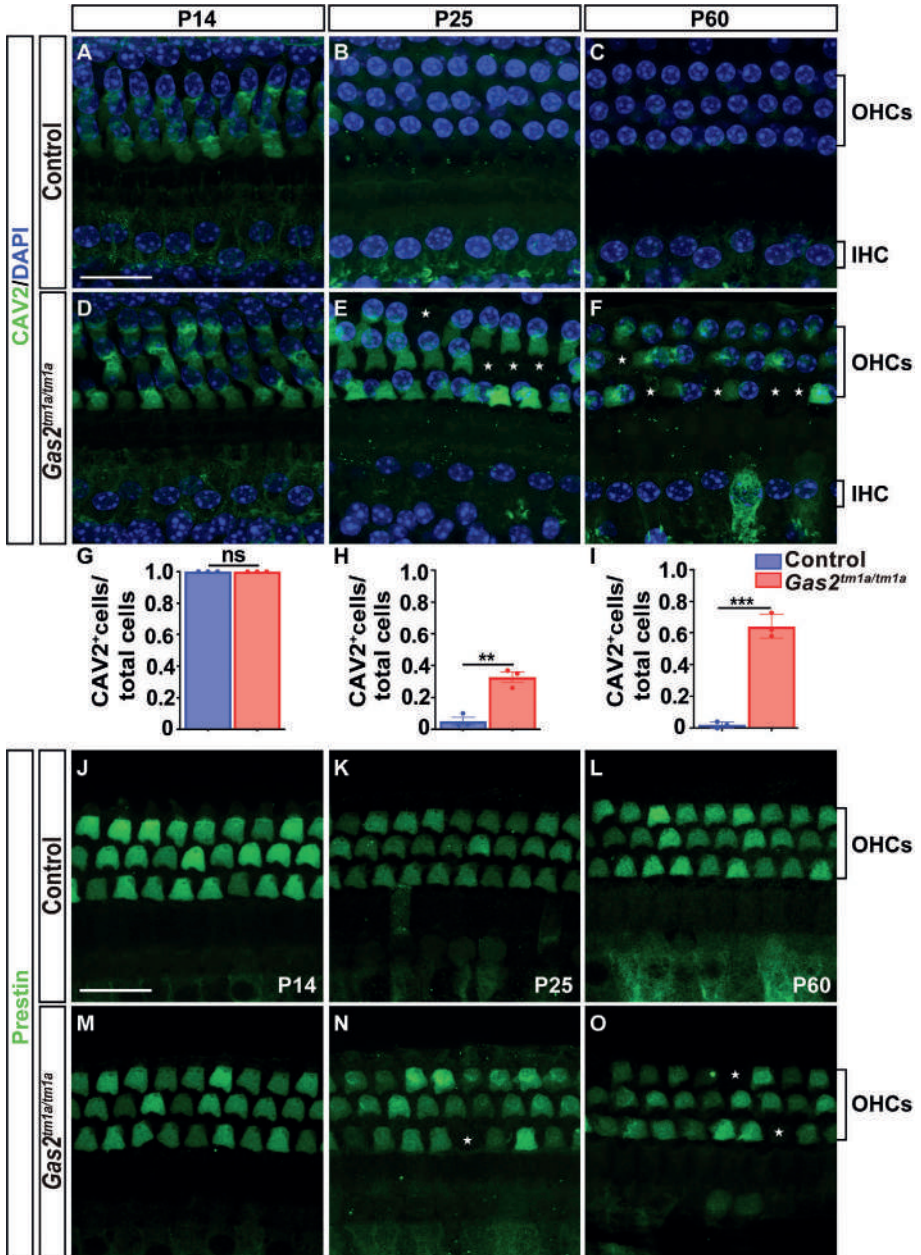


Figure S6. OHCs display increased mechanical stress but maintain Prestin expression in *Gas2^{tm1a/tm1a}* mice (A-F) Whole mount cochlear preparations from control and *Gas2^{tm1a/tm1a}* mice at P14 (A, D), P25 (B, E) and P60 (C, F) immunostained for Caveolin-2 (Cav2). (G-I) Quantification of the ratio of Cav2⁺ cells to the total number of hair cells at P14, P25, P60 represented as mean \pm SE (ns=not significant, ** $p < 0.01$, *** $p < 0.001$, two sided t-test, $n=3$). Whole mount cochlear preparations from control and *Gas2^{tm1a/tm1a}* mice at P14 (J, M), P25 (K, N) and P60 (L, O) showing no difference in the expression of Prestin.

4.3

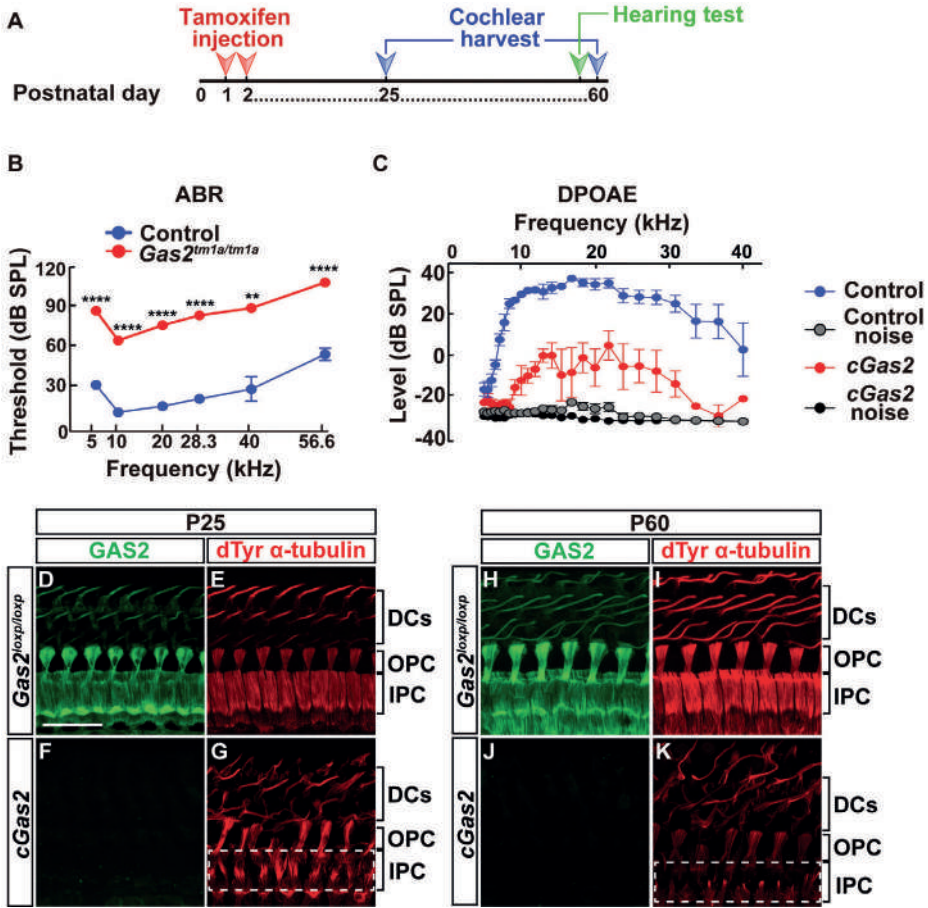


Figure S7. Gas2 is required postnatally in support cells for hearing (A) Timeline for the generation and analysis of *cGas2* knockout mice. (B) ABR thresholds from control (n=3) and *cGas2* (n=3) mice at P60 (**p<0.01, ****p<0.0001, multiple T-test with Holm-Sidak method). (C) Reduced DPOAE response in *cGas2* mice at P60 (p<0.05, multiple T-test with Holm-Sidak method, n=3). (D-K) Whole mount cochlear preparations from control and *cGas2* mice at P25 (D-G) and P60 (H-K) immunostained for Gas2 and detyrosinated α -tubulin. A progressive loss of pillar cell microtubules is observed with age, comparable to that described in *Gas2^{tm1a/tm1a}* mice (Fig. 2G,H,L,M).

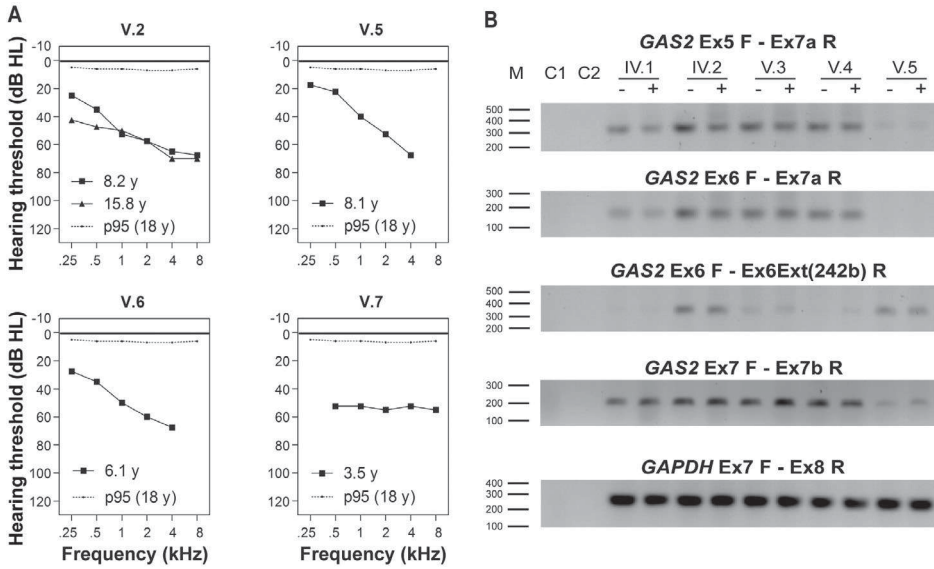


Figure S8. Hearing loss and splicing alterations in subjects with the c.723+1G>A GAS2 variant (A) Average air conduction thresholds of subjects V.5-7 with the c.723+1G>A GAS2 variant in the homozygous state. The dotted line represents the 95th percentile of age- and sex-specific hearing level at the age of 18 years. This is the lowest age for which the ISO 7029:2017 standard can be applied. Thresholds of subjects V5 and V6 are based on pure tone audiometry; thresholds of subject V7 are based on conditioned play audiometry. y, age in years; dB HL, decibel hearing level; kHz, kilohertz **(B)** RT-PCR using primer pairs in exon 6 and flanking exons and intronic sequences (referring to transcript NM_005256.3) was performed to detect aberrant splicing associated with the GAS2 c.723+1G>A variant. M, 100bp marker; C1, no reverse transcriptase in cDNA synthesis step; C2, PCR without cDNA input, +, cells treated with cycloheximide; -, no cycloheximide treatment.



GENERAL DISCUSSION

The research presented in this thesis aims to increase the knowledge of genes already known to be associated with hereditary hearing loss and to identify novel gene-disease associations. In **chapter 1**, an introduction to the presented work is given. In **chapter 2.1**, a family of Dutch origin with a novel pathogenic variant in *COCH* is described. The affected subjects showed a relatively mild audiovestibular phenotype compared to subjects with other *COCH* variants. In a systematic review and meta-analysis of audiometric data, the genotype-phenotype correlations of *DFNA9* were further explored (**chapter 2.2**). We reported distinct phenotypic differences in terms of progression of hearing loss and vestibular function, which could not strictly be associated with the affected cochlin domains. In **chapter 3**, we investigated a relatively common haplotype, termed CEVA, which was significantly enriched in a cohort of patients with an enlarged vestibular aqueduct (EVA) and a monoallelic *SLC26A4* variant. In **chapter 4**, we described two novel deafness genes, *ATP2B2* and *GAS2*, and we reported on the novel association of *RIPOR2* with dominantly inherited hearing loss.

In this general discussion of the thesis, the heterogeneity of audiovestibular phenotypes in hereditary hearing loss and the importance of and our view of thoroughly performed genotype-phenotype correlations are discussed. Subsequently, open research questions for known deafness genes are addressed as well as strategies for the identification of novel deafness genes. The importance of whole exome sequencing (WES)/whole genome sequencing (WGS), scientific collaborations, encountered difficulties, knowledge gaps, and ethical considerations will be highlighted. Finally, a glimpse into the future of research in hereditary hearing loss and therapeutic strategies is given.

Genotype-phenotype correlations in hereditary hearing loss

Patients (and/or their parents) pursue genetic diagnostics and counseling to be informed about (the possibility of) having a genetic condition. The information obtained from genetic testing is useful for gaining knowledge on the condition, starting an intervention, or initiating prevention strategies.¹ Patients with hereditary hearing loss want to be counseled in particular about options for intervention (54%), inheritance pattern and correlated recurrence risks (71%), and prognosis (81%).² To optimally counsel patients on these aspects, thoroughly performed genotype-phenotype correlation studies are essential. These studies may, for example, enable better differentiation between variants in a single gene (e.g., *CDH23*) that can either cause syndromic (Usher syndrome type Id) or non-syndromic hearing loss (*DFNB12*).³ This can especially be troublesome to parents of newborns diagnosed with hearing loss due to variants in this gene. Uncertainty about whether the identified variants will lead to retinitis pigmentosa later in life may dominate parents' life in the first decades

of the child's life, which may even be more burdensome than receiving the diagnosis of Usher syndrome right away. Furthermore, there may be other associations with specific types of hereditary hearing loss on which patients need to be counseled. For example, the contraindication of treatment with aminoglycoside antibiotics in the case of defects in *MT-RNR1*¹⁴ or increased susceptibility to noise-induced hearing loss associated with variants in *FOXO3* and *GRM7*.^{5,6} Another example is the occurrence of relatively frequent chromosome 15q15 deletions, which are in biallelic state causative of DFNB16 or deafness-male-infertility syndrome, depending on whether only *STRC* is deleted or both *STRC* (hearing loss) and *CATSPER2* (asthenoteratozoospermia).^{7,8} Knowledge of the underlying genetic condition and its associated comorbidities also can influence the rehabilitation of subjects with hearing aids or cochlear implants.^{9,10} Finally, thoroughly established genotype-phenotype correlations are indispensable for evaluating the effects of future (genetic) therapeutic interventions.¹¹

Phenotypic variability in hereditary hearing loss

The results described in this thesis (again) underline that hereditary hearing loss is a heterogeneous condition with a lot of variation in phenotypic expression.¹² This variation can be variant-specific and is, for example, reported for *COCH* (chapters 2.1 and 2.2), *GJB2*¹³, *MYO15A*¹⁴ and *EYA4*¹⁵. Furthermore, even the same pathogenic variant can display a large inter- and/or intrafamilial variation in phenotype, as was demonstrated for *COCH* (chapters 2.1 and 2.2) and *RIPOR2* (chapter 4.2). This variation is visible in different aspects of the condition. The reported age of onset of hearing loss for the family with the c.1312C>T p.(Arg438Cys) *COCH* variant (chapter 2.1) ranges from 18 to 49 years. Even more so, the reported age of onset in 12 families with the c.1696_1707del; p.(Gln566_Lys569del) *RIPOR2* in-frame deletion (chapter 4.2) ranges from 0 to 70 years. This variation in age of onset is not limited to the genes and variants presented in this thesis but is also seen in dominantly inherited hearing loss associated with several other genes, e.g., *MYO6*, *POU4F3*, and *OSBPL2*.¹⁶⁻¹⁹ Variation in audiometric configuration is also common; in 63 affected persons with the same deletion in *RIPOR2* (chapter 4.2), several different audiometric configurations were seen, which could be grouped into four main clusters.²⁰ Concerning vestibular symptoms, we describe a variable severity of the vestibular phenotype in *DFNA9*, depending on the specific variant in *COCH* (chapter 2.2).

There are, of course, also forms of hereditary hearing loss that seem to display a limited inter/intrafamilial phenotypic variability. Examples in this thesis are loss-of-function variants of *ATP2B2* and *GAS2*, which, so far, are known to cause a congenital/early-onset (progressive) high-frequency hearing loss (chapters 4.1 and 4.3).²¹ A single subject with late-onset hearing loss and a heterozygous truncating variant in *ATP2B2* is, however, an exception to the identified phenotypic pattern. Furthermore, as only a single human family is known with defects of *GAS2*, it may well be that other (types of) variants in this gene lead to a different phenotype.

Phenotypic variability – modifying factors

There are several explanations for phenotypic variability in hereditary hearing loss. First of all, hearing loss may not only be determined by genetic factors but also by other inborn, acquired, and environmental factors. Examples of these are anatomic malformations of the inner ear, recurrent or chronic otitis media, noise exposure, skull base trauma, autoimmune disorders, etcetera.^{22,23} The influence of these factors may differ from person to person and can lead to a bias in the described phenotype, especially in studies of only a few affected subjects. It goes without saying that one must also remain critical that not everyone's hearing loss has a genetic etiology. Large differences in hearing status due to environmental factors can also be seen at the general population level. This is illustrated by Rosen et al. (1964) in a study on the difference in the degree of presbycusis between a rural African tribe versus urban Americans in an industrialized society, although genetic factors can also play a role in this.²⁴ Secondly, the effect of a specific variant on the protein also plays a role in the severity of the phenotype, as was discussed for *COCH* (chapter 2.2) and reported for other genes such as *GJB2*, *TECTA*, *EYA4*, and *USH2A* as well.^{13,15,25,26} However, despite advancements in technology and knowledge, we often cannot yet fully predict, understand, or evaluate the functional consequences of a variant on the transcript and subsequently on the structure, stability, localization, and function of the encoded proteins and thus the effect on the phenotype. Thirdly, more attention is being paid to modifying factors as explanations for phenotypic differences.²⁷ Genetic modifiers have, for example, been shown to play a role in suppressing (*GAB1* and *METTL13*^{28,29}) or worsening (*ATP2B2* and *CDH23*³⁰) the severity of the hearing loss, or the retinal phenotype in Usher syndrome (*USH2A* and *PDZD7*³¹).

Phenotype reporting in hereditary hearing loss studies

The variable phenotype in hereditary hearing loss, as discussed above, has consequences for counseling, as the expected (audiovestibular) phenotype is often difficult to predict at an individual level. For this reason, it is crucial that there are comprehensive genotype-phenotype correlation studies that describe as completely as possible the variation in the phenotype associated with a specific type of hereditary hearing loss. Still, it is often challenging to obtain a clear picture of the phenotype associated with a certain gene or variant. There are numerous examples of incomplete descriptions of genotype-phenotype correlations in the literature (as described in chapter 2.2). Often, genotyping and/or phenotyping of only a few subjects in a family is performed, merely focusing on the (more severely) affected cases, which may cause a biased phenotype description. In addition, auditory and vestibular phenotypes are often described without reporting raw data, e.g., the inclusion of audiograms or vestibular test results. Another, often overlooked, form of bias is to present a genotype-phenotype correlation without adequately taking other explanations

for the hearing loss into account, for example, by not reporting environmental confounders or by not addressing other possible genetic causes for hearing loss. To address other possible genetic causes of hearing loss in affected subjects, we have developed a protocol to evaluate variants in genes associated with hearing loss in humans or animal models or that otherwise may be linked to hearing (chapters 2.1, 4.1-4.3). The identified potentially pathogenic variants were evaluated by segregation-analysis in accordance with this protocol.

Once the causal genetic defect in a family suspected of hereditary hearing loss has been identified, a thorough genotype-phenotype correlation study needs to be performed, including both subjects affected by hearing loss and, if possible, normal hearing subjects. Audiometric testing should at least include pure tone and speech audiometry and, if applicable, report the degree of progression of hearing loss (in dB/y), preferably demonstrated via ARTA (age-related typical audiograms).³² On indication, speech-in-noise audiometry, measurements of otoacoustic emissions, brainstem evoked response audiometry and/or psychophysical testing can be performed to identify a gene- or variant-specific audiometric profile.³³ Furthermore, it should be investigated whether a vestibular phenotype is associated with the hearing loss. Preferably, the vestibular examination consists of electronystagmography, caloric irrigation testing, rotary chair stimulation, video head impulse test, and cervical and ocular vestibular-evoked myogenic potentials (cVEMP/oVEMP) measurements. It is important to evaluate as many subjects as possible for vestibular dysfunction, independent of whether or not they report vestibular complaints, although this is hampered by the amount of time needed for a full vestibular examination. In the first place, to get a complete picture of (the variation of) the vestibular phenotype, but in addition, subjects can easily compensate for mild vestibular dysfunction and therefore not or under-report related complaints.³⁴⁻³⁷ If such subjects are not included in vestibular testing, this can lead to an incomplete description of vestibular (dys)function. To achieve complete genotype-phenotype descriptions, we endorse the use of 1. GENDEAF criteria when describing the audiovestibular phenotype³⁸, 2. the human phenotype ontology in case of a syndromic type of hearing loss³⁹, and 3. to report as much clinical and genetic data as possible, whether or not in online supplemental files.

Combining the described (variable) phenotypes associated with a certain gene in a (systematic) review is an informative way of providing a complete picture. A systematic review, according to the HuGE criteria, can provide a single overview of the prevalence, genotype, and expected (non-)syndromic phenotype of a genetic disorder.⁴⁰ Currently, only a handful of systematic reviews for hereditary hearing loss have been performed, primarily focusing on *GJB2*^{41,42}, *COCH* (chapter 2.2, or Janssens de Varebeke et al.⁴³), and syndromic

hearing loss (e.g., Usher⁴⁴, Stickler⁴⁵, and Waardenburg⁴⁶ syndrome). An alternative is to present a summary of the literature when reporting on novel variants, as was done, for example, in reports on *P2RX2*⁴⁷, *EYA4*¹⁵ and *LOXHD1*⁴⁸. To circumvent the efforts of composing publications, a website to which a variant, segregation analysis, audiogram, and basic additional data can be uploaded by registered clinicians or other professionals could already be helpful in clinical practice. The AudioGene website is an example that provides a selection of audioprofiles of mostly dominantly inherited types of hearing loss.⁴⁹

All these efforts together will ultimately lead to a better description of the characteristics of different types of hereditary hearing loss and subsequently to better patient care.

Open research questions on known and to-be-identified deafness genes

Known deafness genes

To date, most pathogenic variants that have been reported for hereditary hearing loss are highly penetrant and have straightforward consequences for the amino acid sequence of the encoded protein.^{50,51} Such variants are currently most frequently identified in regular care.^{52,53} There are presumably many patients whose hearing loss is caused by elusive or unrecognized defects of known deafness genes.^{54,55} Sometimes the phenotype can point towards an association with a specific deafness gene. This is, for example, the case with the strong association of an enlarged vestibular aqueduct and biallelic defects of *SLC26A4*.⁵⁶⁻⁵⁸ However, in ~25% of the subjects, only a monoallelic defect can be identified in the protein-coding and splice-site regions of *SLC26A4*.⁵⁹ Further research into these monoallelic subjects led to the identification of the CEVA haplotype.⁶⁰ Although the true causal defect has not yet been pinpointed, this was a starting point for further investigations, as described in Chapter 3. There are several other examples of the integration of phenotypic and genetic data to identify unknown variants in known deafness genes. Collin et al. (2008) revealed the pathogenic effect on transcript splicing of a silent variant in *TECTA* in subjects with a characteristic midfrequency hearing loss, although aided by linkage analysis.⁶¹ Furthermore, the phenotype associated with *DFNX2* aided Naranjo et al. (2010) in identifying a defect of an enhancer element of *POU3F4*.⁶²

Due to the considerable phenotypic and genetic heterogeneity in deafness, the phenotype-first approach often cannot provide a direct clue to the underlying genetic defect. An approach using a broad genetic test such as WES can overcome this obstacle. Still, the exome contains only approximately 85% of known disease-associated variants. Thus, attention also needs to be paid to variants that are not revealed by WES as noncoding DNA is not sequenced. Variants, such as small copy number variations, which can have a deleterious effect on protein structure, (ectopic) gene expression or dosage levels^{63,64}, and pathogenic

variants in non-coding DNA, such as defects of the basal promotor⁶⁵, (*cis*-regulatory) enhancers^{62,66,67}, and introns⁶⁸⁻⁷⁰, are missed in WES and thus largely elusive. Introducing WGS into clinical practice will facilitate the identification of such variants, although the currently applied short read WGS also has its limitations, namely in detection of inversions and translocations. Another point of attention is incomplete coverage of genomic regions in WES and WGS; a low or incomplete coverage means that variants in several thousand exons can be missed in these analyses. As coverage has improved over the past years, one should consider resequencing for cases that remained unsolved in the past.

The next challenge is the interpretation of identified variants. At present, our knowledge of the transcriptome, proteome, and metabolome of cell types of the inner ear is incomplete. The organ of Corti consists of two types of hair cells and several types of supporting cells.⁵⁵ In addition, there are other unique and indispensable cellular regions of the inner ear, e.g., the stria vascularis and the spiral ganglion, harboring different types of cells. All these cell types have a unique function in the inner ear, and when affected, this may lead to different types of inner ear dysfunction. Although insight is increasing in the cell-type-specific gene expression patterns during development and thereafter, we still lack detailed knowledge of gene regulation as well as alternative RNA-splicing for many of the cell types in the inner ear. This impairs the interpretation of newly identified variants. In addition, knowledge of gene structure and protein isoforms is important. For example, identifying novel exons of known deafness genes can reveal novel pathogenic variants⁷¹, or variants affecting a specific isoform of a protein that cause hearing loss, as we demonstrated in the study on *ATP2B2* (chapter 4.1). On the other hand, one can be misguided by seemingly deleterious variants that affect isoforms that are not expressed in the inner ear. Furthermore, variants that affect different protein domains can cause a different phenotype (chapter 2.2), let alone completely different disorders, as demonstrated for *TRIO*-associated neurodevelopmental disorders.⁷² To conclude, increased knowledge of the molecular structure of the inner ear is needed to improve the interpretation of variants identified in WES and especially those in WGS.

Even if a gene-disease relationship is already known, it is vital that this is critically assessed and validated in further studies. This not only relates to questioning possibly invalid genotype-disease associations, such as reported for *MYO1A* and *TSPEAR*⁷³⁻⁷⁶, but also to indicating gene-disease associations for which the evidence needs to be strengthened. The ClinGen Hearing Loss Gene Curation Expert Panel (HL GCEP) curates genes associated with hereditary hearing loss.⁷⁷

Modifiers and di- and oligogenic inheritance patterns in hereditary hearing loss

Despite all efforts, the genetic basis of more than half of all identified Mendelian diseases and associated phenotypes remains elusive. The existence of genetic modifiers and digenic and oligogenic inheritance patterns may well play a major role in this.^{27,78-81}

Significant phenotypic differences between affected persons in a family with hereditary hearing loss caused by a particular genetic defect could be an indication for the occurrence of genetic modifiers. As addressed above, some modifiers have been reported for hereditary hearing loss.²⁸⁻³⁰ Nevertheless, by analyzing WES or WGS data sets from patients with the same pathogenic variant, more attention should be paid to genetic modifiers as an explanation of the variation in the phenotype. A complicating factor is that a large number of well-phenotyped patients are required to identify modifiers with statistical significance, which is a problem in rare forms of hereditary hearing loss.⁸² Environmental factors and the magnitude of the modifying effect on the (audiometric) phenotype are also likely to play a role.⁸²

Digenic and oligogenic inheritance may be important reasons why no genetic cause of hearing loss is found in a significant percentage of patients in routine genetic diagnostics. The identification of digenic and oligogenic types of hereditary hearing loss is hindered by factors such as small family size, and technical (e.g., computational) limitations and costs. Despite this, several digenic combinations of genetic variants have been reported but mostly shown to be (highly) unlikely in further studies (^{31,66,83-88}, chapter 4.1).

The insufficient knowledge of modifiers and di- and oligogenic forms of hereditary hearing loss has caused an underestimation of the total genetic variation in hereditary hearing loss and is also likely to partially explain the inter- and intrafamilial variation of the associated phenotype.⁸⁹ The use of WES and WGS in (large) cohorts of well-phenotyped patients, the use of curated databases of genetic data, and the application of novel computational algorithms might reveal di- and oligogenic explanations for hearing loss in the (near) future as well as modifier genes.^{27,90,91}

Novel deafness-associated genes and novel associated inheritance patterns

The fourth chapter of this thesis focuses on identifying novel deafness genes and novel inheritance patterns associated with known deafness genes. As was mentioned in the introduction of this thesis, it is estimated that defects in up to 1,000 genes could be associated with hearing loss, and many remain to be identified in humans.⁹² Studies to identify such genes often follow a *family-first* approach: a single family with several hearing-impaired members, for which no causative genetic defect was identified in regular diagnostic care. Depending on anamnesis, clinical examination, the number of available family members, presumed inheritance pattern, and potential consanguinity, different research

strategies can be applied to identify the genetic cause, as summarized by Gillissen et al.⁹³ If a candidate variant is identified, the association of the defect and gene with hearing loss needs to be confirmed. An important aspect is to investigate the candidate gene in a cohort of index cases with presumed hereditary hearing loss in order to identify additional families with defects of the same gene. Examples of this approach are described in chapters 4.1 and 4.2. It may, however, happen that no additional families are identified in the same institute and/or partner institutes, which limits evidence for the gene-disease association, as exemplified in chapter 4.3. In that case, GeneMatcher is an option as this connects investigators with an interest in a specific gene.⁹⁴ Another opportunity to obtain sufficient evidence for a novel deafness gene in the absence of additional affected families is to study (existing) animal models or to perform functional assays.

Due to recent advancements in computational power, developments in bioinformatics, and next-generation sequencing techniques (WES/WGS), the *family-first* approach can be replaced by a *genotype-first* approach. In the latter approach, WES/WGS datasets can be analyzed by algorithms, with different strategies aimed to identify the 'interesting needles in the haystack'. A comparison of deleterious variants in different patient cohorts in a meta-analysis to identify genes with statistically significant enrichment of such variants in the hearing loss cohort is an example of such an approach.^{95,96} Another option is to search for genes with (identical) deleterious variants in multiple patients in a cohort. In such a strategy, one can choose to target a set of candidate genes for deafness derived from studies on animal models such as mice^{92,97-99} or from the human inner ear transcriptome.¹⁰⁰ Algorithms can also aid in this candidate gene selection.¹⁰¹⁻¹⁰³ The above-indicated strategies have in common that their success mainly depends on the size of the datasets to generate sufficient statistical power. This is especially important for hereditary hearing loss as this is a heterogeneous condition for which variants in a certain gene often explain <1% of the cases.^{104,105} The required size of data sets are often not present in a single institute but can be obtained through (inter)national collaborations. Such collaborations have been successful in identifying novel hereditary conditions for intellectual disability.^{95,96} An international collaboration to combine WES/WGS data of subjects with hereditary hearing loss could greatly enhance the identification of novel deafness genes and also holds promise to identify non-monogenic types of inheritance and modifier genes. However, this is hampered by the use of targeted sequencing of deafness gene panels in regular care in many diagnostic centers.¹⁰⁶ Regardless of the approach or algorithm used, it is important that subjects are thoroughly phenotyped and that subjects suspected of an acquired cause of hearing loss are excluded. The technical and knowledge gaps of WES/WGS, as discussed in the section on known deafness genes, also apply to identifying novel deafness genes. Furthermore, due

to the huge amount of data, filtering and prioritization of variants is essential (as applied in chapters 2.1, 3, and 4). However, the applied criteria may be too stringent, the used *in silico* prediction tools are not flawless^{107,108}, or a pathogenic variant may occur in a database derived from (alleged) healthy controls¹⁰⁹ which allows causal variants to be excluded from the datasets. Finally, solely focusing on certain genes, for example, because they are at the time of analysis associated with the phenotype of interest in other organisms (e.g., mice or zebrafish), can also limit the scope. For the latter two points, a re-evaluation of the applied criteria and tools and a broad selection of up-to-date animal and population databases may reveal missed variants in both known and novel deafness-associated genes.

Ethical considerations in genetic research

Ethical aspects should also be considered in research involving (large scale) WES/WGS data sets as these provide access to the complete exome/genome of subjects. Although the identification of risk factors or pathogenic variants in genes that are associated with (predisposition) for, e.g., cancer or heart diseases can be avoided by excluding such genes from the data sets prior to analysis, there is always a (low) risk of incidental findings.¹¹⁰ Subjects need to be thoroughly counseled on these risks, the measures that will be taken and which findings will be reported to study participants¹¹¹⁻¹¹³ and which not. In (inter)national collaborations in which WES/WGS data is shared, subjects should be informed about this and should be asked whether they consent to sharing their genetic data. Results of research should always be reported to the participants, although subjects should be offered the option not to receive this information.¹¹⁴

A glimpse of the future

The recent advancements in genetics, audiology, and imaging, and especially the integration of these, will have a major impact on care and research of hereditary hearing loss in the future.¹¹⁵ As discussed in detail in this thesis, WES has played a significant role in the presented research. WES is a less comprehensive type of next-generation sequencing compared to WGS and is associated with lower sequencing costs, less data storage, and less complex variant analysis.¹¹⁶ Although WES and short read WGS are currently less different from each other on a technical and quality level¹¹⁷, WGS allows for the analysis of the non-coding parts of the genome in health and disease. Also, other advanced techniques such as long read genome sequencing¹¹⁸⁻¹²⁰ and (single-cell) RNA sequencing^{121,122} will impact research and patient care. RNA sequencing and proteomics can be applied to study the functional effects of variants in both coding and non-coding genomic regions. It is preferred to perform these analyses on future inner ear cell models, as many deafness genes are not transcribed in commonly used patient-derived cell types such as blood cells or fibroblasts.¹²³

Unlike other organs (e.g., skin or blood) the inner ear is not routinely accessible for sampling as it is a difficult to reach and too vulnerable organ. Modeling the human inner ear *in vitro* is a solution for this.¹²⁴⁻¹²⁶ The data derived from the genome and inner ear epigenome, transcriptome, proteome, and metabolome can be integrated for multi-omics analyzes. This approach makes it possible to not only identify causative genomic defects, but also to investigate and understand their biological consequences.¹²⁷ In addition to obtaining more extensive insight into the function of the human genome, precise audiometric profiling will provide us with more detailed information about the exact (audiometric) consequences of a genetic defect at the level of the inner ear.³³ This kind of data can be important for natural history studies, for the evaluation of (genetic) therapies, and to differentiate between genetic and (additional) acquired causes of hearing loss. Current imaging techniques (CT, MRI, etc.) can be used to identify gross anatomical changes but provide insufficient resolution to determine the exact cause of hearing loss at a cellular or molecular scale. Developments in imaging and contrast agents, both for use *in vivo* and *ex vivo*, are promising and may lead to more insights into structural changes in an affected inner ear.¹²⁸ More post mortem research in subjects to visualize the pathology underlying hearing loss can also contribute to a better understanding of the disease, although the specific defect can be masked by end-stage degeneration of the organ of Corti.¹²⁹ All indicated developments in molecular genetics, audiology, and imaging and the integration of the obtained knowledge will lead to a better understanding of the precise (dys)function of the auditory system.

The advancing knowledge of the auditory system will also play an essential role in the development of inner ear therapies for hearing loss. Although hearing aids and cochlear implants still play a major role in treatment of hearing loss today and often provide adequate rehabilitation, they remain more or less 'one-size-fits-all' treatments. The diverse etiologies of deafness, diversity of target cells, and the various pathogenic processes require the development of specific (genetic) treatments.¹¹ Increasing numbers of studies are being performed to develop various (genetic) therapeutic strategies for hereditary hearing loss.^{11,130} While the first steps in developing therapies are promising, there are still major challenges in terms of time, high costs, efficacy, safety, and ethical considerations to overcome.^{11,130,131}

An often underexposed key factor is the patient's attitude towards these therapeutic developments. A recent survey performed by Levie et al. (2021) revealed that DFNA9 patients, in general, were positive towards participation in inner ear therapy trials. However, some had doubts about participating in studies with high-risk treatments or placebo-controlled study designs. And since these results are not directly translatable to other patient populations, it is important to investigate the attitude of different patient groups towards inner ear therapies. Finally, one patient group that should not be forgotten in such

studies is the Deaf community. Members of this community have long-standing concerns about the application of treatments for hearing loss on the grounds that it violates their autonomy and threatens the continuation of their Deaf culture. The same concerns were brought up for cochlear implants.¹³² Caution is needed when assuming that everyone is open to genetic therapy (or even conventional rehabilitation), or assuming that these are the best solution for every individual.

Conclusion of this thesis

In conclusion, we have definitely moved into a new direction with the strategies to identify novel genetic defects underlying hearing loss in both known and unknown deafness genes. The current and future knowledge and technical innovations, especially their combination, will further unveil yet unknown causes of deafness. Improvements in genetic diagnostics and thorough characterization of the genes associated with hereditary hearing loss will improve patient care and counseling. The development of (genetic) therapeutic strategies will add a new line of treatment options for hereditary hearing loss.

REFERENCES

1. *Understanding Genetics: A New York, Mid-Atlantic Guide for Patients and Health Professionals.*, (Washington (DC) 2009).
2. Oonk, A.M.M. *et al.* Psychological impact of a genetic diagnosis on hearing impairment-An exploratory study. *Clin Otolaryngol* 43, 47-54 (2018).
3. Bork, J.M. *et al.* Usher syndrome 1D and nonsyndromic autosomal recessive deafness DFNB12 are caused by allelic mutations of the novel cadherin-like gene CDH23. *Am J Hum Genet* 68, 26-37 (2001).
4. Jing, W. *et al.* Mitochondrial mutations associated with aminoglycoside ototoxicity and hearing loss susceptibility identified by meta-analysis. *J Med Genet* 52, 95-103 (2015).
5. Guo, H. *et al.* Association of genetic variations in FOXO3 gene with susceptibility to noise induced hearing loss in a Chinese population. *PLoS One* 12, e0189186 (2017).
6. Yu, P. *et al.* Effect of GRM7 polymorphisms on the development of noise-induced hearing loss in Chinese Han workers: a nested case-control study. *BMC Med Genet* 19, 4 (2018).
7. Verpy, E. *et al.* Mutations in a new gene encoding a protein of the hair bundle cause non-syndromic deafness at the DFNB16 locus. *Nat Genet* 29, 345-9 (2001).
8. Avidan, N. *et al.* CATSPER2, a human autosomal nonsyndromic male infertility gene. *Eur J Hum Genet* 11, 497-502 (2003).
9. Usami, S.I., Nishio, S.Y., Moteki, H., Miyagawa, M. & Yoshimura, H. Cochlear Implantation From the Perspective of Genetic Background. *Anat Rec (Hoboken)* 303, 563-593 (2020).
10. Hartel, B.P. *et al.* Hearing aid fitting for visual and hearing impaired patients with Usher syndrome type IIa. *Clin Otolaryngol* 42, 805-814 (2017).
11. Delmaghani, S. & El-Amraoui, A. Inner Ear Gene Therapies Take Off: Current Promises and Future Challenges. *J Clin Med* 9(2020).
12. Vona, B., Nanda, I., Hofrichter, M.A., Shehata-Dieler, W. & Haaf, T. Non-syndromic hearing loss gene identification: A brief history and glimpse into the future. *Mol Cell Probes* 29, 260-70 (2015).
13. Snoeckx, R.L. *et al.* GJB2 mutations and degree of hearing loss: a multicenter study. *Am J Hum Genet* 77, 945-57 (2005).
14. Zhang, J. *et al.* Genotype-phenotype correlation analysis of MYO15A variants in autosomal recessive non-syndromic hearing loss. *BMC Med Genet* 20, 60 (2019).
15. Shinagawa, J. *et al.* Prevalence and clinical features of hearing loss caused by EYA4 variants. *Sci Rep* 10, 3662 (2020).
16. Sampaio-Silva, J. *et al.* Exome Sequencing Identifies a Novel Nonsense Mutation of MYO6 as the Cause of Deafness in a Brazilian Family. *Ann Hum Genet* 82, 23-34 (2018).
17. Sanggaard, K.M. *et al.* A novel nonsense mutation in MYO6 is associated with progressive nonsyndromic hearing loss in a Danish DFNA22 family. *Am J Med Genet A* 146A, 1017-25 (2008).
18. Pauw, R.J. *et al.* Audiometric characteristics of a Dutch family linked to DFNA15 with a novel mutation (p.L289F) in POU4F3. *Arch Otolaryngol Head Neck Surg* 134, 294-300 (2008).
19. Thoenes, M. *et al.* OSBPL2 encodes a protein of inner and outer hair cell stereocilia and is mutated in autosomal dominant hearing loss (DFNA67). *Orphanet J Rare Dis* 10, 15 (2015).

20. Tarpey, T. Linear Transformations and the k-Means Clustering Algorithm: Applications to Clustering Curves. *Am Stat* 61, 34-40 (2007).
21. Morgan, A. *et al.* Lights and Shadows in the Genetics of Syndromic and Non-Syndromic Hearing Loss in the Italian Population. *Genes (Basel)* 11(2020).
22. Zahnert, T. The differential diagnosis of hearing loss. *Dtsch Arztebl Int* 108, 433-43; quiz 444 (2011).
23. Ascha, M.S. *et al.* Vestibular Aqueduct Midpoint Width and Hearing Loss in Patients With an Enlarged Vestibular Aqueduct. *JAMA Otolaryngol Head Neck Surg* 143, 601-608 (2017).
24. Rosen, S., Plester, D., El-Mofty, A. & Rosen, H.V. High Frequency Audiometry in Presbycusis. *Arch Otolaryngol* 79, 18-32 (1964).
25. Hartel, B.P. *et al.* A combination of two truncating mutations in USH2A causes more severe and progressive hearing impairment in Usher syndrome type IIa. *Hear Res* 339, 60-8 (2016).
26. Behloul, A. *et al.* A novel biallelic splice site mutation of TECTA causes moderate to severe hearing impairment in an Algerian family. *Int J Pediatr Otorhinolaryngol* 87, 28-33 (2016).
27. Rahit, K. & Tarailo-Graovac, M. Genetic Modifiers and Rare Mendelian Disease. *Genes (Basel)* 11(2020).
28. Yousaf, R. *et al.* Modifier variant of METTL13 suppresses human GAB1-associated profound deafness. *J Clin Invest* 128, 1509-1522 (2018).
29. Riazuddin, S. *et al.* Dominant modifier DFNM1 suppresses recessive deafness DFNB26. *Nat Genet* 26, 431-4 (2000).
30. Schultz, J.M. *et al.* Modification of human hearing loss by plasma-membrane calcium pump PMCA2. *N Engl J Med* 352, 1557-64 (2005).
31. Ebermann, I. *et al.* PDZD7 is a modifier of retinal disease and a contributor to digenic Usher syndrome. *J Clin Invest* 120, 1812-23 (2010).
32. Huygen, P., Pennings, R. & Cremers, C. Characterizing and distinguishing progressive phenotypes in nonsyndromic autosomal dominant hearing impairment. *Audiological Medicine*, p. 37-46. (2003).
33. Lanting CP, Snik A, Leijendeckers J, Bosman A & Pennings RJE. Genetic hearing impairment affects cochlear processing and, consequently, speech recognition in noise. *medRxiv* (2020).
34. Alberts, B., Selen, L.P.J., Verhagen, W.I.M., Pennings, R.J.E. & Medendorp, W.P. Bayesian quantification of sensory reweighting in a familial bilateral vestibular disorder (DFNA9). *J Neurophysiol* 119, 1209-1221 (2018).
35. Yuan, H.J. *et al.* Novel mutations in the vWFA2 domain of COCH in two Chinese DFNA9 families. *Clin Genet* 73, 391-4 (2008).
36. Street, V.A. *et al.* A novel DFNA9 mutation in the vWFA2 domain of COCH alters a conserved cysteine residue and intrachain disulfide bond formation resulting in progressive hearing loss and site-specific vestibular and central oculomotor dysfunction. *Am J Med Genet A* 139A, 86-95 (2005).
37. Lacour, M., Helmchen, C. & Vidal, P.P. Vestibular compensation: the neuro-otologist's best friend. *J Neuro* 263 Suppl 1, S54-64 (2016).
38. M. Mazzoli, G.V.C., V. Newton, N. Giarbini, F. Declau, A. Parving. Recommendations for the description of genetic and audiological data for families with nonsyndromic hereditary hearing impairment. (2003).
39. Kohler, S. *et al.* Expansion of the Human Phenotype Ontology (HPO) knowledge base and resources. *Nucleic Acids Res* 47, D1018-D1027 (2019).

40. J, L. & J, H. The HuGENet™ HuGE Review Handbook, version 1.0. (2006).
41. Chan, D.K. & Chang, K.W. GJB2-associated hearing loss: systematic review of worldwide prevalence, genotype, and auditory phenotype. *Laryngoscope* 124, E34-53 (2014).
42. Yao, J., Lu, Y., Wei, Q., Cao, X. & Xing, G. A systematic review and meta-analysis of 235delC mutation of GJB2 gene. *J Transl Med* 10, 136 (2012).
43. JanssensdeVarebeke, S., Topsakal, V., Van Camp, G. & Van Rompaey, V. A systematic review of hearing and vestibular function in carriers of the Pro51Ser mutation in the COCH gene. *Eur Arch Otorhinolaryngol* 276, 1251-1262 (2019).
44. Jouret, G. *et al.* Genetics of Usher Syndrome: New Insights From a Meta-analysis. *Otol Neurotol* 40, 121-129 (2019).
45. Acke, F.R., Dhooge, I.J., Malfait, F. & De Leenheer, E.M. Hearing impairment in Stickler syndrome: a systematic review. *Orphanet J Rare Dis* 7, 84 (2012).
46. Song, J. *et al.* Hearing loss in Waardenburg syndrome: a systematic review. *Clin Genet* 89, 416-425 (2016).
47. Liu, X.Z., Yan, D., Mittal, R., Ballard, M.E. & Feng, Y. Progressive Dominant Hearing Loss (Autosomal Dominant Deafness-41) and P2RX2 Gene Mutations: A Phenotype-Genotype Study. *Laryngoscope* 130, 1657-1663 (2020).
48. Wesdorp, M. *et al.* Further audiovestibular characterization of DFNB77, caused by deleterious variants in LOXHD1, and investigation into the involvement of Fuchs corneal dystrophy. *Clin Genet* 94, 221-231 (2018).
49. Taylor, K.R. *et al.* AudioGene: predicting hearing loss genotypes from phenotypes to guide genetic screening. *Hum Mutat* 34, 539-45 (2013).
50. Lu, J.T., Campeau, P.M. & Lee, B.H. Genotype-phenotype correlation--promiscuity in the era of next-generation sequencing. *N Engl J Med* 371, 593-6 (2014).
51. Azaiez, H. *et al.* Genomic Landscape and Mutational Signatures of Deafness-Associated Genes. *Am J Hum Genet* 103, 484-497 (2018).
52. Sloan-Heggen, C.M. *et al.* Comprehensive genetic testing in the clinical evaluation of 1119 patients with hearing loss. *Human genetics* 135, 441-450 (2016).
53. Zazo Seco, C. *et al.* The diagnostic yield of whole-exome sequencing targeting a gene panel for hearing impairment in The Netherlands. *Eur J Hum Genet* 25, 308-314 (2017).
54. Kremer, H. Hereditary hearing loss; about the known and the unknown. *Hear Res* 376, 58-68 (2019).
55. Booth, K.T., Azaiez, H., Jahan, I., Smith, R.J.H. & Fritzsche, B. Intracellular Regulome Variability Along the Organ of Corti: Evidence, Approaches, Challenges, and Perspective. *Front Genet* 9, 156 (2018).
56. Albert, S. *et al.* SLC26A4 gene is frequently involved in nonsyndromic hearing impairment with enlarged vestibular aqueduct in Caucasian populations. *Eur J Hum Genet* 14, 773-9 (2006).
57. Usami, S. *et al.* Non-syndromic hearing loss associated with enlarged vestibular aqueduct is caused by PDS mutations. *Hum Genet* 104, 188-92 (1999).
58. Everett, L.A. *et al.* Pendred syndrome is caused by mutations in a putative sulphate transporter gene (PDS). *Nat Genet* 17, 411-22 (1997).
59. Choi, B.Y. *et al.* Segregation of enlarged vestibular aqueducts in families with non-diagnostic SLC26A4 genotypes. *J Med Genet* 46, 856-61 (2009).

60. Chattaraj, P. *et al.* A common SLC26A4-linked haplotype underlying non-syndromic hearing loss with enlargement of the vestibular aqueduct. *J Med Genet* 54, 665-673 (2017).
61. Collin, R.W. *et al.* Mid-frequency DFNA8/12 hearing loss caused by a synonymous TECTA mutation that affects an exonic splice enhancer. *Eur J Hum Genet* 16, 1430-6 (2008).
62. Naranjo, S. *et al.* Multiple enhancers located in a 1-Mb region upstream of POU3F4 promote expression during inner ear development and may be required for hearing. *Hum Genet* 128, 411-9 (2010).
63. Weischenfeldt, J., Symmons, O., Spitz, F. & Korbel, J.O. Phenotypic impact of genomic structural variation: insights from and for human disease. *Nat Rev Genet* 14, 125-38 (2013).
64. de Bruijn, S.E. *et al.* Structural Variants Create New Topological-Associated Domains and Ectopic Retinal Enhancer-Gene Contact in Dominant Retinitis Pigmentosa. *Am J Hum Genet* 107, 802-814 (2020).
65. Matos, T.D. *et al.* A novel hearing-loss-related mutation occurring in the GJB2 basal promoter. *J Med Genet* 44, 721-5 (2007).
66. Del Castillo, F.J. & Del Castillo, I. DFNB1 Non-syndromic Hearing Impairment: Diversity of Mutations and Associated Phenotypes. *Front Mol Neurosci* 10, 428 (2017).
67. Moriguchi, T. *et al.* A Gata3 3' Distal Otic Vesicle Enhancer Directs Inner Ear-Specific Gata3 Expression. *Mol Cell Biol* 38(2018).
68. Van Laer, L. *et al.* DFNA5: hearing impairment exon instead of hearing impairment gene? *J Med Genet* 41, 401-6 (2004).
69. Vache, C. *et al.* Usher syndrome type 2 caused by activation of an USH2A pseudoexon: implications for diagnosis and therapy. *Hum Mutat* 33, 104-8 (2012).
70. Hilgert, N. *et al.* A splice-site mutation and overexpression of MYO6 cause a similar phenotype in two families with autosomal dominant hearing loss. *Eur J Hum Genet* 16, 593-602 (2008).
71. Rehman, A.U. *et al.* Mutational Spectrum of MYO15A and the Molecular Mechanisms of DFNB3 Human Deafness. *Hum Mutat* 37, 991-1003 (2016).
72. Barbosa, S. *et al.* Opposite Modulation of RAC1 by Mutations in TRIO Is Associated with Distinct, Domain-Specific Neurodevelopmental Disorders. *Am J Hum Genet* 106, 338-355 (2020).
73. Donaudy, F. *et al.* Multiple mutations of MYO1A, a cochlear-expressed gene, in sensorineural hearing loss. *Am J Hum Genet* 72, 1571-7 (2003).
74. Eisenberger, T. *et al.* Targeted and genomewide NGS data disqualify mutations in MYO1A, the "DFNA48 gene", as a cause of deafness. *Hum Mutat* 35, 565-70 (2014).
75. Delmaghani, S. *et al.* Defect in the gene encoding the EAR/EPTP domain-containing protein TSPEAR causes DFNB98 profound deafness. *Hum Mol Genet* 21, 3835-44 (2012).
76. Bowles, B. *et al.* TSPEAR variants are primarily associated with ectodermal dysplasia and tooth agenesis but not hearing loss: A novel cohort study. *Am J Med Genet A* (2021).
77. DiStefano, M.T. *et al.* ClinGen expert clinical validity curation of 164 hearing loss gene-disease pairs. *Genet Med* 21, 2239-2247 (2019).
78. Wright, C.F., FitzPatrick, D.R. & Firth, H.V. Paediatric genomics: diagnosing rare disease in children. *Nat Rev Genet* 19, 325 (2018).
79. Boycott, K.M. *et al.* International Cooperation to Enable the Diagnosis of All Rare Genetic Diseases. *Am J Hum Genet* 100, 695-705 (2017).

80. Chong, J.X. *et al.* The Genetic Basis of Mendelian Phenotypes: Discoveries, Challenges, and Opportunities. *Am J Hum Genet* 97, 199-215 (2015).
81. Boycott, K.M. *et al.* A Diagnosis for All Rare Genetic Diseases: The Horizon and the Next Frontiers. *Cell* 177, 32-37 (2019).
82. Kousi, M. & Katsanis, N. Genetic modifiers and oligogenic inheritance. *Cold Spring Harb Perspect Med* 5(2015).
83. Yang, T. *et al.* Mutations of KCNJ10 together with mutations of SLC26A4 cause digenic nonsyndromic hearing loss associated with enlarged vestibular aqueduct syndrome. *Am J Hum Genet* 84, 651-7 (2009).
84. Yang, T. *et al.* Transcriptional control of SLC26A4 is involved in Pendred syndrome and nonsyndromic enlargement of vestibular aqueduct (DFNB4). *Am J Hum Genet* 80, 1055-63 (2007).
85. Ficarella, R. *et al.* A functional study of plasma-membrane calcium-pump isoform 2 mutants causing digenic deafness. *Proc Natl Acad Sci U S A* 104, 1516-21 (2007).
86. del Castillo, I. *et al.* A deletion involving the connexin 30 gene in nonsyndromic hearing impairment. *N Engl J Med* 346, 243-9 (2002).
87. Hulander, M. *et al.* Lack of pendrin expression leads to deafness and expansion of the endolymphatic compartment in inner ears of Foxi1 null mutant mice. *Development* 130, 2013-25 (2003).
88. Wu, C.C. *et al.* Phenotypic analyses and mutation screening of the SLC26A4 and FOXI1 genes in 101 Taiwanese families with bilateral nonsyndromic enlarged vestibular aqueduct (DFNB4) or Pendred syndrome. *Audiol Neurootol* 15, 57-66 (2010).
89. Parsa, A. Genotype-phenotype correlations: filling the void. *Clin J Am Soc Nephrol* 5, 1542-3 (2010).
90. Rabbani, B., Tekin, M. & Mahdieh, N. The promise of whole-exome sequencing in medical genetics. *J Hum Genet* 59, 5-15 (2014).
91. Gazzo, A.M. *et al.* DIDA: A curated and annotated digenic diseases database. *Nucleic Acids Res* 44, D900-7 (2016).
92. Ingham, N.J. *et al.* Mouse screen reveals multiple new genes underlying mouse and human hearing loss. *PLoS Biol* 17, e3000194 (2019).
93. Gilissen, C., Hoischen, A., Brunner, H.G. & Veltman, J.A. Disease gene identification strategies for exome sequencing. *Eur J Hum Genet* 20, 490-7 (2012).
94. Sobreira, N., Schiettecatte, F., Valle, D. & Hamosh, A. GeneMatcher: a matching tool for connecting investigators with an interest in the same gene. *Hum Mutat* 36, 928-30 (2015).
95. Kaplanis, J. *et al.* Evidence for 28 genetic disorders discovered by combining healthcare and research data. *Nature* 586, 757-762 (2020).
96. Lelieveld, S.H. *et al.* Meta-analysis of 2,104 trios provides support for 10 new genes for intellectual disability. *Nat Neurosci* 19, 1194-6 (2016).
97. Friedman, L.M., Dror, A.A. & Avraham, K.B. Mouse models to study inner ear development and hereditary hearing loss. *Int J Dev Biol* 51, 609-31 (2007).
98. Bowl, M.R. *et al.* A large scale hearing loss screen reveals an extensive unexplored genetic landscape for auditory dysfunction. *Nat Commun* 8, 886 (2017).
99. Scheffer, D.I., Shen, J., Corey, D.P. & Chen, Z.Y. Gene Expression by Mouse Inner Ear Hair Cells during Development. *J Neurosci* 35, 6366-80 (2015).

100. Schrauwen, I. *et al.* A comprehensive catalogue of the coding and non-coding transcripts of the human inner ear. *Hear Res* 333, 266-274 (2016).
101. Pourreza, M.R. *et al.* Applying Two Different Bioinformatic Approaches to Discover Novel Genes Associated with Hereditary Hearing Loss via Whole-Exome Sequencing: ENDEAVOUR and HomozygosityMapper. *Adv Biomed Res* 7, 141 (2018).
102. Tranchevent, L.C. *et al.* Candidate gene prioritization with Endeavour. *Nucleic Acids Res* 44, W117-21 (2016).
103. Perl, K., Shamir, R. & Avraham, K.B. Computational analysis of mRNA expression profiling in the inner ear reveals candidate transcription factors associated with proliferation, differentiation, and deafness. *Hum Genomics* 12, 30 (2018).
104. Shearer, A.E., Hildebrand, M.S. & Smith, R.J.H. Hereditary Hearing Loss and Deafness Overview. in *GeneReviews((R))* (eds. Adam, M.P. *et al.*) (Seattle (WA), 1993).
105. Shearer, A.E. & Smith, R.J. Genetics: advances in genetic testing for deafness. *Curr Opin Pediatr* 24, 679-86 (2012).
106. Shearer, A.E. & Smith, R.J. Massively Parallel Sequencing for Genetic Diagnosis of Hearing Loss: The New Standard of Care. *Otolaryngol Head Neck Surg* 153, 175-82 (2015).
107. Ernst, C. *et al.* Performance of in silico prediction tools for the classification of rare BRCA1/2 missense variants in clinical diagnostics. *BMC Med Genomics* 11, 35 (2018).
108. Tian, Y. *et al.* REVEL and BayesDel outperform other in silico meta-predictors for clinical variant classification. *Sci Rep* 9, 12752 (2019).
109. Xue, Y. *et al.* Deleterious- and disease-allele prevalence in healthy individuals: insights from current predictions, mutation databases, and population-scale resequencing. *Am J Hum Genet* 91, 1022-32 (2012).
110. Kalia, S.S. *et al.* Recommendations for reporting of secondary findings in clinical exome and genome sequencing, 2016 update (ACMG SF v2.0): a policy statement of the American College of Medical Genetics and Genomics. *Genet Med* 19, 249-255 (2017).
111. Tindana, P. *et al.* Engaging research ethics committees to develop an ethics and governance framework for best practices in genomic research and biobanking in Africa: the H3Africa model. *BMC Med Ethics* 20, 69 (2019).
112. Mathaiyan, J., Chandrasekaran, A. & Davis, S. Ethics of genomic research. *Perspect Clin Res* 4, 100-4 (2013).
113. Caulfield, T. *et al.* Research ethics recommendations for whole-genome research: consensus statement. *PLoS Biol* 6, e73 (2008).
114. Heaney, C., Tindall, G., Lucas, J. & Haga, S.B. Researcher practices on returning genetic research results. *Genet Test Mol Biomarkers* 14, 821-7 (2010).
115. Horton, R.H. & Lucassen, A.M. Recent developments in genetic/genomic medicine. *Clin Sci (Lond)* 133, 697-708 (2019).
116. Wang, Z., Liu, X., Yang, B.Z. & Gelernter, J. The role and challenges of exome sequencing in studies of human diseases. *Front Genet* 4, 160 (2013).
117. Barbitoff, Y.A. *et al.* Systematic dissection of biases in whole-exome and whole-genome sequencing reveals major determinants of coding sequence coverage. *Sci Rep* 10, 2057 (2020).
118. Mantere, T., Kersten, S. & Hoischen, A. Long-Read Sequencing Emerging in Medical Genetics. *Front Genet* 10, 426 (2019).

119. van Dijk, E.L., Jaszczyszyn, Y., Naquin, D. & Thermes, C. The Third Revolution in Sequencing Technology. *Trends Genet* 34, 666-681 (2018).
120. de Bruijn, S.E., Fadaie, Z., Cremers, F.P.M., Kremer, H. & Roosing, S. The Impact of Modern Technologies on Molecular Diagnostic Success Rates, with a Focus on Inherited Retinal Dystrophy and Hearing Loss. *Int J Mol Sci* 22(2021).
121. Yizhar-Barnea, O. & Avraham, K.B. Single cell analysis of the inner ear sensory organs. *Int J Dev Biol* 61, 205-213 (2017).
122. Ranum, P.T. *et al.* Insights into the Biology of Hearing and Deafness Revealed by Single-Cell RNA Sequencing. *Cell Rep* 26, 3160-3171 e3 (2019).
123. GTEx-Consortium. The Genotype-Tissue Expression (GTEx) project. *Nat Genet* 45, 580-5 (2013).
124. van der Valk, W.H., Steinhart, M.R., Zhang, J. & Koehler, K.R. Building inner ears: recent advances and future challenges for in vitro organoid systems. *Cell Death Differ* 28, 24-34 (2021).
125. Menendez, L. *et al.* Generation of inner ear hair cells by direct lineage conversion of primary somatic cells. *Elife* 9(2020).
126. Romano, D.R., Hashino, E. & Nelson, R.F. Deafness-in-a-dish: modeling hereditary deafness with inner ear organoids. *Hum Genet* (2021).
127. Misra, B.B., Langefeld, C.D., Olivier, M. & Cox, L.A. Integrated Omics: Tools, Advances, and Future Approaches. *J Mol Endocrinol* (2018).
128. Kayyali, M.N. *et al.* Challenges and opportunities in developing targeted molecular imaging to determine inner ear defects of sensorineural hearing loss. *Nanomedicine* 14, 397-404 (2018).
129. Robertson, N.G. *et al.* Cochlin immunostaining of inner ear pathologic deposits and proteomic analysis in DFNA9 deafness and vestibular dysfunction. *Hum Mol Genet* 15, 1071-85 (2006).
130. Ren, Y., Landegger, L.D. & Stankovic, K.M. Gene Therapy for Human Sensorineural Hearing Loss. *Front Cell Neurosci* 13, 323 (2019).
131. Brokowski, C. & Adli, M. CRISPR Ethics: Moral Considerations for Applications of a Powerful Tool. *J Mol Biol* 431, 88-101 (2019).
132. Most, T., Wiesel, A. & Blitzer, T. Identity and attitudes towards cochlear implant among deaf and hard of hearing adolescents. *Deafness and Education International* 9(2), 68-82(2007).



English summary

The research presented in this thesis aims to provide more insights into known and novel genes for hereditary hearing loss and the associated phenotypes.

Chapter 1 is the introduction of this thesis. The anatomy and physiology of the audiovestibular organ are discussed and followed by a general introduction into hereditary hearing loss and diagnostic care. Finally, scientific research into hereditary hearing loss and the scope of this thesis are introduced.

In **Chapter 2**, two studies on dominantly inherited hearing loss type 9 (DFNA9) are presented. DFNA9 is caused by heterozygous pathogenic variants in *COCH* and is considered one of the most prevalent forms of dominantly inherited hearing loss in the Netherlands. In general, DFNA9 is characterized by an adult-onset progressive high-frequency hearing loss and often includes the deterioration of vestibular function.

Chapter 2.1 describes a novel variant in *COCH*, c.1312C>T p.(Arg438Cys), that co-segregates with hearing loss and a variable degree of vestibular (dys)function in a Dutch family. The variant affects the vWFA2 domain of cochlin. The reported mean age of onset of hearing loss is 33 years (range: 18-49 years), consistent with earlier reports. The hearing loss primarily affects higher frequencies, and its progression and the associated deterioration of speech perception are relatively mild compared to that in other DFNA9 families with different variants in *COCH*.

The variable phenotype of DFNA9 is evaluated in a systematic review and audiological meta-analysis in **chapter 2.2**. We identified 48 studies describing the audiovestibular phenotype associated with 27 *COCH* variants in 444 subjects. Significant differences in both age of onset and progression of HL and vestibular dysfunction were revealed in subjects with different pathogenic variants in *COCH*. In both studies on DFNA9, several hypotheses relating to pathophysiological mechanisms underlying DFNA9 were discussed and proposed. However, missing clinical data and concerns about the interpretation of previous research on the molecular effects of *COCH* variants limit mutual comparison.

Chapter 3 focuses on subjects with a unilateral or bilateral enlarged vestibular aqueduct (EVA) with or without an identified monoallelic pathogenic variant in *SLC26A4*. Despite strong genotype-phenotype correlations between *SLC26A4* defects and an EVA, 10-65% of these cases remains genetically unresolved. In this study, we investigated a cohort of 28 Dutch index cases diagnosed with hearing loss in combination with an EVA, lacking a genetic diagnosis after routine genetic testing. In 2017 an EVA-associated haplotype (Caucasian EVA,

CEVA) was reported to be significantly enriched in subjects with an EVA and with or without a pathogenic variant in *SLC26A4*. We hypothesized that this allele harbors a yet unidentified genetic defect and performed short- and long-read whole genome sequencing and optical genome mapping to identify this defect. Although we found that the CEVA haplotype was also significantly enriched in our patient cohort with monoallelic *SLC26A4* variants, we could not pinpoint a (likely) pathogenic defect on the allele. With the identification of two novel splice-altering *SLC26A4* variants, we were able to solve two monoallelic cases who did not have the CEVA-haplotype. Still, analyses addressing the defect(s) at the RNA, protein, or epigenetic level are required to finally solve the missing heritability in the unsolved cases.

Chapter 4 describes two novel deafness genes, and we report on the association of a known deafness gene with hearing loss that displays an autosomal dominant inheritance pattern. We address the genotype, functional role, and phenotype associated with these genes and identified variants.

In **Chapter 4.1**, we report on the identification of two *de novo* and three inherited loss-of-function variants in *ATP2B2* in eleven subjects of five families. A rapidly progressive high-frequency hearing loss was diagnosed in all but one affected subjects. In general, the age of onset of hearing loss was between three and six years. Subjects reported no balance complaints, and vestibular function was found to be normal. *ATP2B2* encodes the PMCA2 Ca^{2+} -pump, which plays an important role in maintaining ion homeostasis in hair cells, among others, by extrusion of Ca^{2+} from the stereocilia to the endolymph. Based on studies in mouse models, we hypothesize that *ATP2B2*-associated hearing loss in humans is caused by Ca^{2+} cytotoxicity and subsequent degeneration of hair cells and supporting cells. Although a digenic inheritance pattern of hearing impairment has been reported for heterozygous missense variants of *ATP2B2* and *CDH23*, our findings indicate a monogenic cause of hearing impairment in cases with loss-of-function variants of *ATP2B2*.

After more than 20 years of research, we present in **chapter 4.2** a heterozygous in-frame deletion of 12 nucleotides in *RIPOR2* as the cause of dominantly inherited hearing loss in twelve families. Up to now, *RIPOR2* was only associated with recessively inherited hearing loss. Clinical research in 63 affected subjects showed that hearing loss in the studied families had an average age of onset of 31 years, with a wide range of 0-70 years, and displayed variable audiometric characteristics. *Ex vivo* experiments confirmed a functional effect of the variant, as it resulted in aberrant localization of the mutant RIPOR2 protein throughout the stereocilia of mechanosensory hair cells. In contrast, the wildtype protein was concentrated at the stereocilia base. Moreover, mutant RIPOR2 could not rescue the morphological defects observed in *RIPOR2*-deficient hair cells, in contrast to the wildtype protein. The variant is indicated to be a founder mutation and is present in one per 1,275

individuals of a cohort from the South-East of the Netherlands. This suggests that this in-frame deletion is the most important cause of monogenic hearing impairment in the Netherlands, with potentially ~8,600 affected individuals aged 30 and over. It is possible that this genetic defect is also a significant cause of hearing loss in neighboring Northwestern European countries. This study demonstrates that specific and apparently 'mild' variants in genes associated with recessive early-onset hearing impairment can be an important cause of (late) adult-onset hearing impairment.

In **chapter 4.3**, we report on the association of *GAS2* with hearing loss in mice and humans. Extensive experiments in mouse models showed that variants in *Gas2*, encoding a cytoskeletal regulatory protein, cause high-frequency hearing loss, due to disorganization and destabilization of microtubule bundles in cochlear pillar and Deiters' cells. In a family of African origin, four male siblings, born from consanguineous parents, had a congenital or early-onset symmetrical, bilateral, and high-frequency hearing loss. The affected subjects displayed no vestibular dysfunction. Whole exome sequencing revealed a single homozygous nucleotide substitution in a canonical splice donor site in intron 6 of *GAS2*. Functional studies of this variant indicate that an aberrant *GAS2* protein is synthesized that is truncated within the *GAS2* domain.

This thesis is concluded by a general discussion in **chapter 5**. The heterogenous audiovestibular phenotype in hereditary hearing loss and the need for thorough genotype-phenotype correlation studies is addressed. Our view of genotype-phenotype correlation studies, the value of systematic reviews, and meta-analyses is discussed. Furthermore, open research questions on known and (yet) unidentified deafness genes are addressed in the current era of technological developments. The discussion ends with a glimpse into the future of research in hereditary hearing loss and the development of therapeutic strategies.

Nederlandse samenvatting

Het doel van het onderzoek, zoals beschreven in dit proefschrift, was om meer inzicht te verkrijgen in bekende en nieuwe genen voor erfelijk gehoorverlies en de bijbehorende fenotypen.

Hoofdstuk 1 is de inleiding van dit proefschrift. De anatomie en fysiologie van het binnenoer, het audiovestibulaire orgaan, worden beschreven. Dit wordt gevolgd door een algemene inleiding in erfelijk gehoorverlies en de bijbehorende zorg(organisatie). Ten slotte wordt wetenschappelijk onderzoek naar erfelijk gehoorverlies en de inhoud van dit proefschrift geïntroduceerd.

In **hoofdstuk 2** worden twee studies over dominant overervend gehoorverlies type 9 (DFNA9) beschreven. DFNA9 wordt veroorzaakt door heterozygote pathogene varianten in het *COCH*-gen. De aandoening is vermoedelijk een van de meest voorkomende vormen van dominant overervend gehoorverlies in Nederland. Over het algemeen wordt DFNA9 gekenmerkt door een op volwassen leeftijd beginnend progressief hoogfrequent gehoorverlies. Voorts is er vaak sprake van achteruitgang en uitval van de evenwichtsfunctie.

Hoofdstuk 2.1 beschrijft de identificatie van een nieuwe variant in het *COCH*-gen: c.1312C>T p.(Arg438Cys) in een familie van Nederlandse afkomst met een progressief gehoorverlies en een variabele mate van evenwichtsuitval. De *COCH*-variant ligt in een regio van het gen die codeert voor het vWFA-domein van het cochlin eiwit. De patiënten rapporteren een gemiddelde beginleeftijd voor het gehoorverlies van 33 jaar (variatie: 18-49 jaar). Dit komt overeen met eerdere studies over DFNA9. De patiënten hebben voornamelijk hoogfrequente gehoorverliezen. De progressie van het gehoorverlies en de bijbehorende verslechtering van het spraakverstaan zijn relatief mild vergeleken met die van DFNA9-families met andere varianten in het *COCH*-gen.

In **hoofdstuk 2.2** wordt het variabele fenotype van DFNA9 geëvalueerd in een systematische review en meta-analyse van de audiometrische data. Onze zoekstrategie leverde 48 studies op waarin het audiovestibulaire fenotype van 27 verschillende *COCH*-varianten bij in totaal 444 personen werd beschreven. Er werden significante verschillen in zowel de beginleeftijd, als de progressie van het gehoorverlies en de (mate) van vestibulaire disfunctie gezien tussen personen met verschillende *COCH*-varianten. In beide hierboven beschreven studies worden hypothesen omtrent het pathofysiologische mechanisme dat ten grondslag ligt aan DFNA9 bediscussieerd. Beperkt beschikbare klinische gegevens en twijfels over de interpretatie van eerder wetenschappelijk onderzoek naar de moleculaire effecten van de verschillende *COCH*-varianten beperken echter de onderlinge vergelijking.

Hoofdstuk 3 richt zich op patiënten met een unilateraal of bilateraal vergroot vestibulair aquaduct (EVA), met één of zonder een pathogene variant in het *SLC26A4*-gen. Ondanks een sterke genotype-fenotype correlatie tussen *SLC26A4*-gedefecten en een EVA, kan bij 10-65% van deze patiënten geen genetische diagnose worden gesteld. In 2017 werd een EVA-geassocieerd haplotype (Kaukasische EVA, CEVA) in de regio van het *SLC26A4*-gen geïdentificeerd. Dit haplotype kwam relatief frequent voor bij patiënten met een EVA en met één of geen pathogene variant in het *SLC26A4*-gen. We veronderstellen dat er op het allel met dit haplotype een onbekend genetisch defect aanwezig is, wat verklarend is voor de EVA en het bijbehorende gehoorverlies. In deze studie onderzochten we een cohort van 28 Nederlandse patiënten met gehoorverlies in combinatie met een bilaterale of unilaterale EVA, bij wie er in de reguliere zorg geen sluitende genetische diagnose gesteld kon worden. Om dit genetisch defect te identificeren, hebben we 'optical genome mapping' en 'short- en long-read whole genome sequencing' toegepast. Hoewel we ontdekten dat het CEVA-haplotype ook relatief frequent aanwezig was in ons patiëntencohort, hebben we het genetisch defect op dit allel niet kunnen identificeren. Met de identificatie van twee nieuwe splicing-modulerende *SLC26A4*-varianten waren we in staat om bij twee patiënten, ieder met één pathogene *SLC26A4*-variant *in trans*, wel een definitieve genetische diagnose vast te stellen.

Vervolgstudies, die gericht zijn op defecten op RNA-, eiwit- of epigenetisch niveau, zijn vereist om een onderliggende verklaring te vinden voor de EVA en het gehoorverlies die geassocieerd zijn met het CEVA-haplotype. En zodoende meer patiënten een definitieve genetische diagnose voor hun gehoorverlies te kunnen geven.

In **Hoofdstuk 4** beschrijven we de identificatie van twee nieuwe doofheidsgenen en de nieuwe associatie van een dominant overervingspatroon bij een derde gen, dat tot dusver alleen geassocieerd was met recessief overervend gehoorverlies. We gaan in op het genotype, de functionele rol van het eiwit en het fenotype behorende bij de genen en geïdentificeerde varianten.

Allereerst rapporteren we in **Hoofdstuk 4.1** over de identificatie van twee *de novo* en drie overgeërfde 'loss-of-function' varianten in het *ATP2B2*-gen bij elf patiënten uit vijf families. Bij op één na alle patiënten werd een progressief hoogfrequent gehoorverlies vastgesteld, met een beginleeftijd tussen de drie en zes jaar. De patiënten rapporteerden geen evenwichtsklachten en uit evenwichtsonderzoek bleek de vestibulaire functie normaal te zijn. Het *ATP2B2*-gen codeert voor de PMCA2 Ca^{2+} -pomp, die een belangrijke rol speelt bij het handhaven van de ion-homeostase in de cochleaire haarcellen, onder andere door het pompen van Ca^{2+} van de stereocilia naar de endolymfe. Op basis van studies in muismodellen veronderstellen we dat het *ATP2B2*-geassocieerd gehoorverlies bij mensen

wordt veroorzaakt door Ca^{2+} -cytotoxiciteit en hierdoor veroorzaakte degeneratie van haarcellen en steuncellen. Heterozygote missense varianten in het *ATP2B2*- en *CDH23*-gen waren in het verleden geassocieerd met een digeen overervingspatroon van gehoorverlies. Desondanks wijzen onze bevindingen op een monogene oorzaak van gehoorverlies bij patiënten met een 'loss-of-function' verandering in het *ATP2B2*-gen.

Vervolgens beschrijven we, na meer dan 20 jaar onderzoek, in **Hoofdstuk 4.2** een heterozygote 'in-frame' deletie van 12 nucleotiden in het *RIPOR2*-gen als de oorzaak van dominant overervend gehoorverlies in twaalf Nederlandse families. Tot dusver werden pathogene veranderingen in het *RIPOR2*-gen alleen in verband gebracht met recessief overervend gehoorverlies. Klinisch onderzoek bij 63 patiënten toonde aan dat zij een gemiddelde beginleeftijd van 31 jaar rapporteren voor het gehoorverlies, maar met een grote variatie van 0-70 jaar. Ook de audiogrammen vertoonden variabele kenmerken, waaronder hoogfrequente-, midfrequente- en laagfrequente patronen. *Ex vivo*-experimenten lieten zien dat het afwijkende RIPOR2-eiwit zich verspreidde in de stereocilia van de cochleaire haarcellen, in tegenstelling tot het wildtype-eiwit dat geconcentreerd bleef in de basis van de stereocilia. Hiermee kon een functioneel effect van de variant bevestigd worden. Bovendien kon het afwijkende RIPOR2-eiwit de morfologische defecten van RIPOR2-deficiënte haarcellen niet herstellen. Het wildtype-eiwit was wel in staat om deze morfologische defecten te herstellen. De 'in-frame' deletie wordt beschouwd als een 'founder' mutatie. Op basis van allelfrequenties wordt geschat dat de gevonden 'in-frame' deletie in het *RIPOR2*-gen de meest voorkomende oorzaak is van erfelijke slechthorendheid bij volwassenen in Nederland, met potentieel ~8.600 aangedane personen van 30 jaar en ouder. Mogelijk is dit genetische defect ook een belangrijke oorzaak van gehoorverlies in naburige Noordwest-Europese landen. Concluderend toont deze studie aan dat ogenschijnlijk 'milde' heterozygote veranderingen in genen die tot dusver geassocieerd zijn met recessief overervend congenitaal gehoorverlies, een belangrijke oorzaak kunnen zijn van dominant overervend gehoorverlies dat begint op volwassen leeftijd.

Tot slot presenteren we in **Hoofdstuk 4.3** de associatie van pathogene veranderingen in het *GAS2*-gen met gehoorverlies bij zowel muizen als mensen. Het gen codeert voor een cytoskelet-regulerend eiwit. Uitgebreide experimenten in muismodellen toonden aan dat een defect in het *Gas2*-gen en de bijbehorende afwezigheid van eiwitfunctie leiden tot een desorganisatie en destabilisatie van microtubulubundels in de pillar en Deiter's steuncellen, waardoor deze cellen hun functie in het orgaan van Corti verliezen. Dit gaat gepaard met een hoogfrequent gehoorverlies bij de gemuteerde muizen. Met betrekking tot de mens; in een gezin met consanguine ouders van Afrikaanse afkomst hebben vier broers gehoorverlies. Het gehoorverlies was reeds aanwezig bij de geboorte of begon in de eerste levensjaren. Er is sprake van een bilateraal, hoogfrequent gehoorverlies en evenwichtsonderzoek toonde

aan dat zij geen vestibulaire disfunctie hadden. Door middel van 'whole-exome-sequencing' werd een pathogene verandering in het *GAS2*-gen als oorzaak voor het gehoorverlies geïdentificeerd; een homozygote nucleotidesubstitutie in de 'canonical splice donor site' van het zesde intron. Functionele studies van deze variant laten zien dat er waarschijnlijk een verkort *GAS2*-eiwit wordt gesynthetiseerd. Dit verkorte eiwit heeft naar verwachting een vergelijkbaar effect op de organisatie en stabiliteit van microtubulibundels in de humane cochlea als de afwezigheid van het eiwit in de cochlea van de gemuteerde muizen.

Dit proefschrift wordt afgesloten met een algemene discussie in **hoofdstuk 5**. Het heterogene audiovestibulaire fenotype bij erfelijk gehoorverlies en de noodzaak van grondige studies naar genotype-fenotype correlaties komen aan de orde. Onze kijk op dergelijke studies, de waarde van systematische reviews en meta-analyses wordt bediscussieerd. Voorts komen onbeantwoorde onderzoeksvragen over bekende en (nog) onbekende doofheidsgenen aan bod, met nadruk op het de huidige technologische ontwikkelingen en mogelijkheden. De discussie eindigt met een blik op de toekomst van het onderzoek naar erfelijk gehoorverlies en de ontwikkeling van therapeutische strategieën.



LIST OF RELEVANT ABBREVIATIONS

Gene-, protein (domain)names and amino-acid abbreviations are not included

AA	amino acid
ABR	auditory brainstem response
ACMG	American College of Medical Genetics and Genomics
adHL	autosomal dominant hearing loss
adNSHL	autosomal dominant nonsyndromic hearing loss
AF	allele frequency
AFM	atomic force microscopy
ANOVA	analysis of variance
AoO	age of onset
arHL	autosomal recessive hearing loss
arNSHL	autosomal recessive nonsyndromic hearing loss
ARTA	age-related typical audiograms
ATD	annual threshold deterioration
BERA	brainstem evoked response audiometry
bp	base pair
BPPV	benign paroxysmal position vertigo
cDNA	complementary deoxyribonucleic acid
CEVA	caucasian EVA
CHX	cyclohexamide
cM	centiMorgan
CMV	cytomegalovirus
CNV	copy number variation
Co-IP	co-immunoprecipitation
CT	computed tomography
cVEMP	cervical vestibular evoked myogenic potentials
dB	decibel
dBHL	decibel hearing level
DNA	deoxyribonucleic acid
DFN	deafness
DFNA	autosomal dominantly inherited hearing loss
DFNB	autosomal recessively inherited hearing loss
DFNM	modifier of hereditary hearing loss
DFNX	x-linked inherited hearing loss

DFNY	y-linked inherited hearing loss
DPOAE	distortion product otoacoustic emissions
dTyr	detyrosinated
DVD	deafness variation database
EBV	Epstein-Barr virus
ENG	electronystagmography
ENT	ear-nose-throat
EVA	enlarged vestibular aqueduct
gnomAD	Genome Aggregation Database
GWAS	genome-wide association studies
HGMD	Human Gene Mutation Database
HL	hearing loss
Hz	hertz
IHC	inner hair cell
ISO	International Organization for Standardization
Kb	kilobase
kHz	kilo Hertz
LINE	long interspersed nuclear element
LOD	logarithm of odds
M	mutant
MAF	minor allele frequency
MAP	microtubule associated proteins
Mb	megabase
MIPs	molecular inversion probes
MRI	magnetic resonance imaging
mRNA	messenger ribonucleic acid
NGS	next generation sequencing
NMD	nonsense mediated decay
NSHL	nonsyndromic hearing loss
nt	nucleotide
OAE	otoacoustic emission
OHC	outer hair cell
oVEMP	ocular vestibular evoked myogenic potentials
PCR	polymerase chain reaction
PTA	pure tone average
qPCR	quantitative polymerase chain reaction
RNA	ribonucleic acid

SD	standard deviation
SEM	scanning electron microscopy
SE-NL	Southeast Netherlands
SNHL	sensorineural hearing loss
SNP	single-nucleotide polymorphism
SPL	sound pressure level
SRS	speech recognition score
SRT	speech reception threshold
SNV	single nucleotide variants
SV	structural variants
TEM	transmission electron microscopy
TEOAE	transient evoked otoacoustic emissions
vHIT	video head impulse test
VNTR	variable number tandem repeat
VOCTV	volumetric optical coherence tomography and vibrometry
WES	whole exome sequencing
WGS	whole genome sequencing
WHO	world health organization
WT	wildtype

DATA MANAGEMENT

The results of human studies were conducted in accordance with the principles of the Declaration of Helsinki. The medical and ethical review board Committee on Research Involving Human Subjects Region Arnhem Nijmegen, Nijmegen, the Netherlands has given approval to conduct these studies. Mouse studies described in Chapter 4 were approved by the Animal Ethics Boards of the associated universities.

In our studies, subjects received information on paper concerning the study they participated in and gave written informed consent. A part of the subjects were asked to complete questionnaires on paper. The paper data, including informed consents, requested clinical data and audiovestibular test results performed elsewhere, were stored in the department archive of the Ear Nose and Throat (ENT) department. Paper data were entered into the computer by use of Castor EDC. Data management and monitoring were also performed within Castor EDC. An audit trail was incorporated to provide evidence of the activities that has altered the original data. The privacy of the participants in this study is warranted by use of encrypted and unique individual subject codes. This code corresponds with the code on the informed consent forms. The code was stored separately from the study data. All participating subjects were registered in EPIC, the electronic patient file system of the Radboudumc. All DNA samples and cell lines were stored at the cell culture facility of the Department of Human Genetics. After registration at the cell culture facility, each DNA sample or cell line received a unique number. Lab experiments are recorded in Labguru, a digital lab book client which is centrally stored and daily backed-up on the local Radboudumc server. The identified variants in the studies published in this thesis, have been submitted to Leiden Open Variant Database.

The primary and secondary data that I have obtained during my PhD (including manuscripts, raw and analyzed sequencing data, patient data and other relevant files) have been stored on the ENT and Human Genetics department servers and are backed-up regularly:

T:\gen_gr\PIgroup-Hannie-Kremer\Deafness genetics

H:\KNdata\Otogenetica\Promovendi Otogenetica\Jeroen Smits 2017-2021

The data will be saved for 15 years after termination of each study. Using these patient data in future research is only possible after a renewed permission by the patient as recorded in the informed consent. Published data and datasets generated or analyzed in this thesis are part of published articles and its additional files are available from the associated corresponding authors on reasonable request.

PHD PORTFOLIO

Name PhD student:	<i>J.J. Smits</i>	PhD period:	1/3/2017-01-12-2020 (full and part-time appointment)
Department:	<i>Ear Nose and Throat, Human Genetics</i>	Promotor:	<i>Prof. dr. J.M.J. Kremer</i>
Graduate school:	<i>Donders Institute for Brain, Cognition and Behavior</i>	Co-promotores:	<i>Dr. R.J.E. Pennings Dr. C.P. Lanting</i>

COURSES AND WORKSHOPS	Year(s)	ECTS
Radboudumc introduction day	2017	0.5
Graduate school introduction day	2017	0.5
Scientific writing	2017	1.5
Clinical Genomics and NGS course (Bertinoro, IT)	2017	1.5
Management voor promovendi	2017	3.0
Audiometry and audiology course	2017	2.0
Endnote course	2017	0.5
Basiscursus Regelgeving en Organisatie voor Klinisch Onderzoekers (BROK)	2017	1.5
Scientific integrity course	2019	1.5
Graduate school day	2020, 2021	0.67

SEMINARS AND LECTURES	Year(s)	ECTS
Medical-clinical education and lectures at the ENT and Human Genetics departments	2017-2020	
Sensory disease meetings, Human Genetics department	2017-2020	
Theme discussions, Human Genetics department	2017-2020	
Radboud Research Round Sensory Disorders, Radboudumc	2017-2020	
Monthly Research Meeting Clinical Genetics	2018-2020	
International guest lectures, Radboudumc	2017-2020	
	total	12.0
OOR-ON seminar	2017	0.25

(INTER)NATIONAL SYMPOSIA & CONGRESSES	Year(s)	ECTS
Bi-annually meetings of Dutch ENT society (2017-2020) – <i>2x oral presentation</i>	2017-2020	4.0
Symposium Collegium Chirurgicum Neerlandicum – <i>poster presentation</i>	2018	0.5
Molecular Biology of Hearing and Deafness (Göttingen, DE) – <i>poster presentation</i>	2018	1.0
Refereeravond Klinische Genetica en KNO, ErasmusMC Rotterdam – <i>oral presentation</i>	2018	0.33
KNO onderwijsdag: wetenschappelijke integriteit	2018	0.25
NVHG Two-Day Annual Symposium – <i>poster presentation</i>	2018, 2019	1.0
DEAFSTEM European Congress (Groningen) – <i>oral presentation</i>	2019	0.5
Genetics Retreat - NVHG graduate meeting – <i>oral presentation</i>	2019	0.5
ESHG conference (virtual) – <i>poster presentation</i>	2021	0.5

TEACHING AND SUPERVISION	Year(s)	ECTS
Supervisor Meet the PhD (bachelor course Biomedical Sciences)	2019	0.5
Supervision scientific internship Medicine (K. Sezer)	2018	1.0
Teaching and supervision of medical students during their clinical rotations	2018-2020	0.5
Supervisor Meet the Expert (bachelor course Medical Sciences)	2020	0.5
Teaching in minor course "Dokter, het is toch niet erfelijk?"	2020, 2021	2.0
<hr/>		
PRIZES AND GRANTS	Year(s)	
Travel grant Simonsfonds	2017	
Sensory disease talent award (scientific quality and social impact), Radboudumc	2020	
Runner up "Beter Horen Wetenschapsprijs", Dutch ENT society	2021	
Runner up "ESHG Early Carreer Award (poster on conference)", European Society of Human Genetics.	2021	
<hr/>		
	Total	38.5

LIST OF PUBLICATIONS

Elke M.J. Devocht, Guido Dees, Remo A.G.J. Arts, **Jeroen J. Smits**, Erwin L.J. George, Marc van Hoof and Robert J. Stokroos, *Revisiting Place-Pitch Match in CI Listeners Using 3D Imaging Analysis*, *Annals of Otology, Rhinology & Laryngology* (2016) 125(5): 378-84.

Guido Dees, **Jeroen J. Smits**, Marc van Hoof, A. Miranda L. Janssen, Janny R. Hof, Dzamal Gazibegovic and Robert J. Stokroos, *A mid-scala Cochlear Implant electrode design achieves a stable post-surgical position in the cochlea of patients over time – a prospective observational study*, *Otology and Neurotology* (2018); 39(4): e231-e239.

Jeroen J. Smits, Jaap Oostrik, Andy J. Beynon, Sarina G. Kant, Pia A.M. de Koning Gans, Liselotte J.C. Rotteveel, Jolien S. Klein Wassink-Ruiter, Rolien H. Free, Saskia M. Maas, Jiddeke van de Kamp, Paul Merkus, DOOFNL Consortium, Wouter Koole, Ilse Feenstra, Ronald J.C. Admiraal, Cornelis P. Lanting, Margit Schraders, Helger G. Yntema, Ronald J.E. Pennings and Hannie Kremer, *De novo and inherited loss-of-function variants of ATP2B2 are associated with rapidly progressive hearing impairment*, *Human Genetics* (2019); 138: 61–72

Suzanne E. de Bruijn*, **Jeroen J. Smits***, Chang Liu, Cornelis P. Lanting, Andy J. Beynon, Joëlle Blankevoort, Jaap Oostrik, Wouter Koole, Erik de Vrieze, DOOFNL Consortium, Cor W.R.J. Cremers, Frans P.M. Cremers, Susanne Roosing, Helger G. Yntema, Henricus P.M. Kunst, Bo Zhao, Ronald J.E. Pennings~ and Hannie Kremer~, *A RIPOR2 in-frame deletion is a frequent and highly penetrant cause of adult-onset hearing loss*, *Journal of Medical Genetics* (2020); 58: 96-104 (*~gelijke bijdrage)

Jeroen J. Smits, E. van Beelen, Nicole J.D. Weegerink, Jaap Oostrik, Patrick L.M. Huygen, Andy J. Beynon, Cornelis P. Lanting, Henricus P.M. Kunst, Margit Schraders, Hannie Kremer, Erik de Vrieze and Ronald J.E. Pennings, *A Novel COCH Mutation Affects the vWFA2 Domain and Leads to a Relatively Mild DFNA9 Phenotype*, *Otology & Neurotology* (2020); 42(4): e399-e407

André S. Bueno, Kelly Nunes, Alex M.M. Dias, Leandro U. Alves, Beatriz C.A. Mendes, Juliana Sampaio-Silva, **Jeroen J. Smits**, Helger G. Yntema, Diogo Meyer, Karina Lezirovitz and Regina C. Mingroni-Netto, *Frequency and origin of the c.2090T>G p.(Leu697Trp) MYO3A variant associated with autosomal dominant hearing loss*, *European Journal of Human Genetics*, (2021); online ahead of print

Sissy Bassani, Edward Beelen, Mireille Rossel, Norine Voisin, Anna Morgan, Yoan Arribat, Nicolas Chatron, Jacqueline Chrast, Massimiliano Cocca, Benjamin Delprat, Flavio Faletra, Giuliana Giannuzzi, Nicolas Guex, Roxane Machavoine, Sylvain Pradervand, **Jeroen J. Smits**, Jiddeke M. van de Kamp, Alban Ziegler, Francesca Amati, Sandrine Marlin, Hannie Kremer, Heiko Locher, Tangui Maurice, Paolo Gasparini, Giorgia Giroto and Alexandre Reymond, *Variants in USP48 encoding ubiquitin hydrolase are associated with autosomal dominant non-syndromic hereditary hearing loss*, Human Molecular Genetics, (2021); 30(19): 1785–1796

Tingfang Chen, Alex M. Rohacek, Matthew Caporizzo, Amir Nankali, **Jeroen J. Smits**, Jaap Oostrik, Cornelis P. Lanting, Erdi Küçük, Christian Gilissen, Jiddeke M. van de Kamp, Ronald J.E. Pennings, Staci M. Rakowiecki, Klaus H. Kaestner, Kevin K. Ohlemiller, John S. Oghalai, Hannie Kremer, Benjamin L. Prosser and Douglas J. Epstein, *Cochlear supporting cells require GAS2 for cytoskeletal architecture and hearing*, Developmental Cell (2021); 56(10): 1526-1540.e7

Eveline A. van Beeck Calkoen, Ronald J.E. Pennings, **Jeroen J. Smits**, Sjoert A.H. Pegge, Liselotte J.C. Rotteveel, Paul Merkus, Berit M. Verbist, Esther Sanchez and Erik F. Hensen, *Contralateral hearing loss in children with a unilateral enlarged vestibular aqueduct*, International Journal of Pediatric Otorhinolaryngology (2021); 150:110891

Jeroen J. Smits*, Suzanne E. de Bruijn*, Cornelis P. Lanting, Jaap Oostrik, Luke O’Gorman, Tuomo Mantere, DOOFNL Consortium, Frans P.M. Cremers, Susanne Roosing, Helger G. Yntema, Erik de Vrieze, Ronny Derks, Alexander Hoischen, Sjoert A.H. Pegge, Kornelia Neveling, Ronald J.E. Pennings, and Hannie Kremer, *Exploring the missing heritability in subjects with hearing loss, enlarged vestibular aqueducts, and a single or no pathogenic SLC26A4 variant*, Human Genetics (2021); online ahead of print (*gelijke bijdrage)

Sybre M.M. Robijn, **Jeroen J. Smits***, Kadriye Sezer, Patrick L.M. Huygen, Andy J. Beynon, Erwin van Wyk, Hannie Kremer, Erik de Vrieze, Cornelis P. Lanting~ and Ronald J.E. Pennings~, *Genotype-phenotype correlations of pathogenic COCH variants in DFNA9: a HuGE systematic review and audiometric meta-analysis*, (2021); submitted (*~ gelijke bijdrage)

Carlijn M.A. van Kempen, Andy J. Beynon, **Jeroen J. Smits** and Mirian C.H. Janssen, *A retrospective cohort study exploring the association between different mitochondrial diseases and hearing loss* International Journal of Molecular Sciences, (2021); Submitted

CURRICULUM VITAE

Jeroen werd op 28 januari 1992 geboren te Zwolle. Aldaar groeide hij op in een warm gezin met zijn ouders en zusje Caroline. De middelbare school werd in eerste instantie aangevangen op het Gymnasium Celeanum. Na zijn brugklasjaar verhuisde het gezin naar Haren, alwaar de middelbareschooltijd werd vervolgd aan het Willem Lodewijk Gymnasium, te Groningen.



Direct na het behalen van het eindexamen in 2010 werd er gestart met de studie Geneeskunde aan de Universiteit van Maastricht. Naast zijn studie was hij actief in het studentenleven in Maastricht, (her)oprichtte hij een studentensportvereniging, was hij op lokaal, landelijk en internationaal niveau actief voor IFMSA (International Federation of Medical Student Associations) en werkte in een verpleeghuis. Tussen de bachelor en master Geneeskunde werd er een lange backpackreis door Nieuw-Zeeland ondernomen.

De coschappen werden onder meer gelopen in het Maastricht UMC+, het Steve Biko Academic Hospital, Pretoria, Zuid-Afrika en het NKI-Antoni van Leeuwenhoekziekenhuis, Amsterdam. Naast de coschappen verrichtte hij wetenschappelijk onderzoek naar cochleaire implantaten. De interesse voor de genetica werd gewekt tijdens een coschap kindergeneeskunde in het Maxima Medisch Centrum.

Na het *cum laude* afronden van de studie Geneeskunde werd gestart met het promotietraject naar de genetische oorzaken van slechthorendheid en correlaties tussen genetische oorzaak en fenotype. Dit traject vond plaats onder supervisie van prof dr. J.M.J. Kremer, dr. R.J.E. Pennings en dr. C.P. Lanting aan de afdelingen KNO en Humane Genetica van het Radboudumc. Gedurende dit promotietraject droeg hij bij aan de (uitbreiding van) het landelijke otogenetische samenwerkingsverband DOOFNL werd hij runner up bij de Beter Horen KNO-vereniging Wetenschapsprijs, runner up bij de ESHG Early Career Award posterprijs en werd hem de Sensory Disorders Talent award toegekend. In verband met het pensioneren van een medisch specialist, begon Jeroen naast zijn promotietraject met het verrichten van spreekuren voor otogenetica, alwaar de interesse in het vakgebied klinische genetica volledig tot bloei kwam. In september 2020 startte hij als ANIOS bij de afdeling klinische genetica van het Radboudumc. Deze aanstelling combineerde hij met het afronden van dit proefschrift. Voorts was hij werkzaam als arts op de COVID-19 afdeling gedurende de wereldwijde pandemie. Per 1 januari 2022 is Jeroen gestart als AIOS klinische genetica in het UMC Utrecht.

Dankwoord

Het dankwoord. Vaak het meest, misschien wel het enige gelezen deel van een proefschrift. En dat na al dat dat bloed, zweet en tranen. Het dankwoord is eigenlijk ook wel het moeilijkste om te schrijven. Want ondanks dat dit een individueel traject is om je te bekwamen als onafhankelijk onderzoeker, en alleen mijn naam op de voorkant staat, heb ik dit zeker niet alleen gedaan. Sterker nog, zonder de mensen die in dit stuk genoemd worden, was dit proefschrift er nooit gekomen.

Allereerst gaat mijn dank uit naar de patiënten die bereid waren om deel te nemen aan de verschillende studies die beschreven staan in dit proefschrift. Niets was onbespreekbaar, van het ondergaan van dagenlange extra onderzoeken tot geduldig wachten op de uitslag. En geduld is geen overbodige luxe, daar in wetenschappelijk onderzoek uitslagen soms lang op zich kunnen laten wachten (bijvoorbeeld meer dan 20 jaar in het *RIPOR2* project). Zonder de patiënten komt de wetenschap niet verder.

Van alle voorzieningen in het leven, is mijns inziens onderwijs een van de belangrijkste. Een gegeven dat niet vanzelfsprekend is in sommige delen van deze wereld. Mijn dank gaat uit naar de wijze lessen van leraren tot docenten en van coschapbegeleiders tot hoogleraren. Helaas teveel mensen om hier allemaal te noemen. Voor één persoon maak ik echter een uitzondering; juf **Rita** Jansen, bij jou begon het allemaal. Mijn ouders en ik zijn je ontzettend dankbaar, dat je mij als 4-jarig jochie een kans gaf.

Hooggeleerde Kremer en weledelzeergeleerden Pennings en Lanting, beste **Hannie**, **Ronald** en **Cris**: niet zonder reden noem ik jullie in een zin. Jullie vulden elkaar aan op inhoudelijk en persoonlijk vlak en versterkten elkaar als een team.

Hannie, dank voor je vertrouwen in mij en voor alles wat ik van je heb geleerd. De afgelopen jaren heb je mij bijgebracht wat het inhoudt om een wetenschapper te zijn. Ik ben onder de indruk van het hoge niveau van wetenschap dat jij nastreeft. Je nam nooit zomaar iets voor waar aan en je kritische blik en aandacht voor detail heeft menig artikel en presentatie naar een hoger niveau getild. Het feit dat je altijd meteen tijd vrij probeerde te maken voor mij en je andere promovendi, dat kenmerkt je. Je bleef ook altijd oog houden voor mijn ontwikkeling op andere domeinen; toen er (meermaals) op klinisch vlak een beroep op mij werd gedaan, heb je me hierin gesteund, ondanks dat dit voor het onderzoek wellicht niet de beste oplossing was. Ik bewaar fijne herinneringen aan onze goede gesprekken, je sinterklaasgedichten en de gezellige kaasfondue bij jullie thuis.

Ronald, ik had me geen betere copromotor kunnen wensen, je bent een gouden vent. Je vrolijkheid, energie, enthousiasme en gedrevenheid om de beste zorg voor de otogenetische/Usherpatiënt te leveren is bewonderenswaardig. Maar je mooiste eigenschap is wel dat je in staat bent om je eigen besognes meteen neer te leggen als een promovendus ergens mee zit en dat met je wil bespreken. Het lijkt zo simpel, maar de meesten hebben daar geen ruimte voor. En als de stress dan wat opliep, was jouw oplossing de promovendus uit te nodigen voor een (spontane) BBQ bij jou thuis. Onze overleggen waren meestal een mooie mix van serieuze zaken, kletspraat en elkaar jennen, wat een uitstekend recept was voor een fijne samenwerking.

Cris, je werd pas op een later moment officieel bij mijn promotie betrokken. Maar dat dit zou gebeuren, was volkomen logisch; vanaf het begin van je aanstelling was je al uit interesse betrokken. Bij elk manuscript had je een origineel idee voor een analyse, wat verrassende inzichten opleverde die waardevol waren voor het in perspectief plaatsen van de bevindingen. Een andere eigenschap is je vermogen om uit te zoomen en met een helicopterview te kijken naar het artikel als geheel en de rode draad in de kantlijn te benoemen. Ik hoop dat je je ideeën omtrent de psychofysica van het otogenetische oor tot uitvoering kan brengen; dit is wat het vak nodig heeft.

Beste **Jaap**, als ik een woord moet bedenken dat jou het beste omschrijft, dan is het engelengeduld, net zoals bij vele promovendi vóór mij. Of ik nou direct mijn eerste 'gelletje' verprutste door er doorheen te prikken, of wéér eens bij je navraag kwam doen naar de samenstelling voor de mastermix voor een PCR, je hielp me altijd geduldig. En op andere momenten was je de spreekwoordelijke reddende engel, want de combinatie van kliniek en promotie had soms nadelige gevolgen voor de continuïteit van het labwerk. En buiten het werk sprak ik graag met je af voor een biertje of een spelletjesavond. Wel moeten we echt weer een keer gaan winnen van de dames!

Beste **Andy**, je hebt een grote rol gespeeld in mijn proefschrift op het gebied van de vestibulogie. De afdeling mag ontzettend blij zijn met jou als vestibuloog, maar zeker ook met jou als onderzoeker en eeuwige optimist. Vrijwel aan het begin van mijn traject vertelde je vol passie over hoe jij keek naar je rol. Jouw kernwaarde was het *mogelijk* maken van onderzoek. En die kernwaarde heb je altijd nageleefd.

Lieve **Cindy** en **Suzanne**, ik ben blij dat jullie naast mij staan als paranimfen. Cindy, jarenlang hebben wij elkaar in de collegebanken en in de kroeg in Maastricht getroffen. Toen had ik nog niet kunnen bevroeden dat we allebei vanuit Maastricht naar Nijmegen zouden gaan om te promoveren. De afgelopen jaren hebben we samen op kantoor gezeten en lief en leed

gedeeld. En als ik eens een belangrijke dag had, liet je altijd een post-itje achter met een succeswens. Heel veel succes met de opleiding tot KNO-arts, dat gaat helemaal goedkomen! Suzanne, we zijn op dezelfde dag begonnen en we promoveren een maandje na elkaar. En dat is niet de enige parallel die ons verbindt. Want in onze samenwerking op meerdere projecten wisten we elkaar feilloos aan te vullen. Niet alleen de brug van lab naar kliniek, maar ook de wijze waarop we schreven: van 'te kort door de bocht' naar 'langdradig kluwen garen', we konden altijd op elkaar rekenen. Je hebt me meegenomen in de wonderde wereld van de moleculaire biologie en ervoor gezorgd dat ik even makkelijk praat over PacBio en Bionano als over audiogrammen. En we troffen elkaar graag naast het werk, van de vele spelletjesavonden tot drie uur wachten op de lekkerste pizza van Nijmegen. Ik ben blij dat je verder gaat in de wetenschap, mensen zoals jij hebben we nodig. Susanne en Cindy, ik hoop dat we nog lang vrienden blijven.

Beste **Helger**, ik waardeer het vertrouwen dat je me vanaf de eerste dag gaf. Ondanks dat je als hoofd van Genoomdiagnostiek vele prioriteiten had en mensen die iets van je wilden, maakte je altijd ruimte voor mijn projecten en verzoekjes. En hoe groot of complex mijn verzoek ook was, bij jou was het altijd "ja, tenzij". Ik hoop in de toekomst met je te mogen blijven samenwerken in de sterke verbintenis tussen wetenschap, diagnostiek en kliniek, zoals we in de afgelopen jaren hebben gekend.

Lieve **Ilse**, jouw rol binnen mijn proefschrift is groter dan je denkt. Niet zozeer op het gebied van het schrijven van de artikelen, maar als een hele fijne sparringpartner voor mij. Je nuchtere kijk op de wereld en het vermogen om dingen in perspectief te plaatsen, is heel fijn voor iemand die vol in de tunnel zit. In onze multidisciplinaire spreekuren gaf je me de kans om een kijkje te nemen in het vakgebied van de klinische genetica, waar ik de bevestiging vond dat dit het helemaal is voor mij.

De studies in dit proefschrift zouden er ook niet zijn geweest zonder het DOOFNL-consortium. **Astrid, Diane, Els, Fabienne, Fenna, Guus, Janny, Jet, Jiddeke, Jolien, Josine, Lies, Liselotte, Marc, Marjolein, Marie-José, Marieke, Paul, Robert, Rolien, Sarina, Saskia, Thadé** en **Vivian**, dank voor het warme welkom in jullie centra en de bereidheid om vele patiënten te benaderen en includeren. Samen hebben we een sterk en toonaangevend wetenschappelijk consortium op wereldniveau. Maar ook op klinisch vlak werpt onze samenwerking haar vruchten af. Het is hierbij mooi om te zien hoe we als professionals van verschillende disciplines elkaar weten te vinden en werken aan optimale otogenetische zorg in Nederland. **Marieke**, in het bijzonder dank aan jou voor het sparren en meedenken over mijn toekomst.

Hooggeleerden **Willemsen, Stokroos** en **Van Rompaey**, heel hartelijk dan voor uw bereidheid om mijn proefschrift te beoordelen en zitting te nemen in de manuscriptcommissie. **Robert**, we kennen elkaar niet alleen op professioneel vlak, maar ook in de arts-patiëntrelatie. Ik blijf je dankbaar; van je eerste zetje tot waar ik nu sta. Hooggeleerden **Van Zelst-Stams, Visser** en **Topsakal**, dank voor het willen plaatsnemen in de corona (what's in a name).

De afgelopen jaren heb ik niet op één afdeling gewerkt maar op drie; KNO, genomerecherche en klinische genetica. Ik voel me een enorme geluksvogel dat ik op elke afdeling te maken had met op-en-top professionals die ook nog eens ontzettend leuke collega's zijn.

Beste collega's van de afdeling KNO, de afdeling in Nijmegen is een hele fijne plek om te beginnen met de eerste 'volwassen' baan. De fijne en respectvolle sfeer zorgt voor een omgeving om te kunnen groeien. Lieve **arts-assistenten-en-PA**-groep, vanaf dag één voelde ik me onderdeel van de groep. Van geweldige assistentenweekendjes en wintersporten tot gewoon gezellig lunchen in de koepel en de week aftoppen bij Annie's. En daarbovenop kon ik me geen betere kantoorgenoten wensen. **Henriëke, Thijs, Luuk** en **Cindy**, wekelijks bespraken we de love-escapades van een van ons tijdens het foute muziekuurtje. Cindy, je vond het soms wel lastig met een poosje alleen mannen op de kamer. Ondanks dat je genoot van het bespreken van onze liefdeslevens, was er helaas niemand om de nieuwe documentaire over Beyoncé te bespreken met je. Gelukkig kwamen **Eveline, Emma** en **Hedwig** bij ons op de kamer om je te kunnen voorzien in deze behoefte. Eveline, samen hebben we lopen knallen aan de laatste loodjes voor ons proefschrift. Emma, ondanks dat ik nu de omgekeerde route bewandel, hoop ik je nog vaak te treffen. Hedwig, je bent samen met **Sybre**n, mijn opvolger, maar bovenal zijn jullie samen met **Sam en Emma** fijne vrienden geworden. Heel veel succes in de komende jaren, ik weet zeker dat jullie er iets moois van maken. Syb, er is altijd plaats op mijn bank voor jou. **Merle**, we raakten toevallig bij een koffietje aan de praat, wat de opmars was voor vele gezellige kopjes koffie binnen en buiten het ziekenhuis. Hooggeleerde Marres, beste **Henri**, dank voor uw interesse in mijn onderzoek en vooral ook in mij als mens. U maakte het daarnaast (financieel) mogelijk om nog een jaar extra onderzoek te doen, in combinatie met het opdoen van klinische ervaring in de otogenetica. Beste **Frank**, dank voor je rol als mentor. Ik kon altijd bij je binnenlopen om even te sparren en je voorzag me op een vaderlijke wijze van advies. Dank voor de mogelijkheid die je me bood om mijn eigen pad te ontdekken. Ik heb het gevonden.

Beste collega's van genomerecherche, ik heb grote bewondering voor jullie gedrevenheid om jullie onderzoek tot de wereldtop te laten behoren. Maar naast het harde werken was er genoeg ruimte voor leuke dingen buiten het werk om. **Erwin, Erik, Sanne, Janine, Jaap, Renske, Merel, Alex, Saskia, Frans** en **Susanne**, dank voor alle gezelligheid, wijze raad en

hulp bij de labexperimenten. **Galuh, Erdi** and **Christian**; thank you for assisting with the bio-informatical analyses. **Han**, de rol die jij wereldwijd speelt in de klinische genetica is ongeëvenaard. Desondanks ben en blij je je optimistische en toegankelijke jezelf. Of het nou even sparren is over mijn toekomstplannen in de genetica, of vele kilometers fietsen voor het goede doel.

Het warme welkom dat de afdeling Klinische Genetica van het Radboudumc mij gaf is een voorbeeld voor alle ziekenhuisafdelingen. **Ilja, Lot, Özlem, Thatjana, Lex, Erika, Femke, Inci, Nynke en Susanne**, het afgelopen jaar hebben we op en naast het werk veel plezier beleefd. Ik ga jullie (en de snoeptrommel) missen! **Wendy** en **Carlo**, ik kon me geen betere leidinggevendenden wensen. Dank voor jullie oog voor wat ik nodig had voor mijn persoonlijke ontwikkeling.

Dit proefschrift was er nooit gekomen zonder de ondersteuning van diverse secretariaten, geen agendapuzzel of bijzonder verzoekje was jullie te veel. In het bijzonder wil ik nog graag **Sandra** en **Patricia** van het KNO-patiëntensecretariaat noemen. Sandra, dank voor het regelen van alles rondom mijn patiënten, dat was in de combinatie van promoveren en klinische zorg een hele geruststelling. Patricia, jij hebt in luttele weken vele brievenpakketjes gemaakt en verstuurd naar deelnemers voor mijn studies.

Beste **Marc** en **Elke**, jullie hebben mij een aantal jaren begeleid bij de eerste stapjes in de wereld van de wetenschap. Hoewel ik uiteindelijk niet bij jullie ben gaan promoveren, koester ik de wijze lessen nog steeds.

Hooggeleerden Dubois, Erwich en Swinkels, beste **Ewout, Jan-Jaap** en **Dorine**. Dank voor het meedenken en geven van wijze raad bij alle hobbels onderweg. Ik heb veel geleerd van hoe jullie binnen jullie eigen vakgebied tot de top behoren en altijd het beste uit jullie zelf halen.

Eliane, een lang verblijf in Zuid-Afrika is de bron voor onze hechte vriendschap. Rondom een aantal gedeelde interesses, zoals kunst en lekker eten, bespreken wij het leven. Het is fijn om altijd met iemand open over de mooie en minder mooie dingen van het leven te kunnen praten. Maar bovenal kan ik heerlijk met je ouwehoeren. **Iris, Ruben**, ook bij jullie ligt de basis onder de evenaar. Dank voor de vriendschap, feestjes, gekkigheid en wijze raad rondom promoveren. **Janna**, in de filosofie hebben we elkaar gevonden; vele avondjes studium generale en dan onder het genot van een naborrel nog even de gedachten er overheen te laten gaan. Dank voor een hele fijne vriendschap. **Marlon**, je laat me met je positieve kijk op het leven inzien dat het leven komt zoals het komt en hoe belangrijk het is

om te genieten van het moment zelf. En op deze wijze heb je me door de laatste fase van het schrijven van dit proefschrift gesleept. Dank daarvoor.

Bassir, Ben-Max, David, Gijs, Maarten, Momme, Oscar, Ruben en **Wijnand**. Beste vrienden voor het leven. Geen betere omschrijving heb ik eigenlijk voor jullie. Een van onze vriendinnen gaf aan dat ze het bijzonder vond dat we zo'n hechte vriendengroep zijn, omdat we zo verschillend zijn. Maar ik denk dat we elkaar daarin zo goed vinden. Fijn dat jullie altijd voor mij klaar staan. Een leven zonder jullie zou niets waard zijn.

Lieve Omi **Gabique**, wat had je er nog graag bij willen zijn. Maar op het einde wist je dat mijn proefschrift nu écht bijna af was. Ik denk iedere dag aan je en mis je. Opi **Jules**, ik heb je nooit gekend, maar ik draag gelukkig je naam. Bonpa **Marcel**, ik vind het toch wel erg bijzonder dat meer dan 60 jaar nadat je promoveerde op het "*Familiair voorkomen van het phaeochromacytoma*" ik promoveer op het familiair voorkomen van gehoorverlies. Ik denk bij jou en Bonma **Joop** altijd terug aan ravotten in jullie huis, bos of de sneeuw van Savognin, mijn tweede thuis.

Lieve **papa, mama** en **Caroline**, bij jullie in Haren voel ik me altijd thuis. Caroline, je bent een ontzettend sterke vrouw geworden die zich nooit laat belemmeren door wie of wat dan ook. Je bent begaan met deze wereld en helpt ons er steeds aan te herinneren dat we er zuinig mee moeten omgaan. Ik heb er bewondering voor hoe je strijdt voor je idealen en voor hen wiens stem niet altijd gehoord wordt. Maar toch zul je altijd mijn kleine zusje blijven, met wie ik graag de pistes afa of een bordspelletje mee speel.

Papa en mama, dank voor de warme en lieve opvoeding. Ik zou het nergens beter hebben getroffen dan bij jullie. Jullie dachten altijd in mogelijkheden en ondersteunden mij en Caroline met het najagen van onze dromen. Maar ook als het even tegen zat, kunnen we altijd bij jullie terecht. En dat is een hele fijne en veilige gedachte. En ondanks dat we nu helaas verder weg van elkaar wonen dan ons lief is, blijft de band altijd even warm. Ik ben jullie oneindig dankbaar.

